THE GENERATION OF CARBON MONOXIDE IN COMPARTMENT FIRES

by
Daniel T. Gottuk

Dissertation submitted to the Faculty of the
Virginia Polytechnic Institute and State University
in partial fulfillment of the requirements for the degree of

DOCTOR OF PHILOSOPHY
in
Mechanical Engineering

APPROVED:

R. J. Roby, Chairman

C. L. Beyler

D. F. Cox

D. R. Jaasma

L. A. Roe

September, 1992
Blacksburg, Virginia

C.2

ABSTRACT

For the purpose of fire analysis and fire safety engineering, the development of empirical correlations for major species yields in compartment fires has become an important priority due to the inability to calculate these quantities from first principles. Studies of simplified upper layer environments have shown that major species production rates can be correlated with the equivalence ratio in what is known as the Global Equivalence Ratio concept (GER). Due to the simplification in these past experiments, it was not known if the GER concept was valid for compartment fires. Therefore, there was a need to determine if correlations existed between major species yields and the equivalence ratio for actual compartment fires. Since the flow of toxic gases from a room poses a hazard to building occupants, it was also important to determine if correlations for CO yield outside of a compartment on fire exist, particularly when external burning occurs.

A 2.2 m^3 test compartment was used to investigate the burning of four fuels (hexane, PMMA, spruce and flexible polyurethane foam) in compartment fires. The test compartment was specially designed with a two-ventilation path system which allowed the direct measurement of the plume equivalence ratio (the ratio of the fuel volatilization rate to the air entrainment rate normalized by the stoichiometric fuel-to-air ratio).

Empirical correlations between the upper layer yield of major species and the plume equivalence ratio were shown to exist. The results reveal that the production of CO is primarily dependent on the compartment flow dynamics (i.e., the equivalence ratio) and upper layer temperature. A chemical kinetics study indicated that increased compartment temperature affects upper layer species yields in two ways 1) the generation of species in the plume is changed and 2) oxidation of post-flame gases in the layer is

affected. The correlations developed in the compartment fires were qualitatively similar to those developed by Beyler for simplified upper layer environments. However, quantitative differences existed and are explained by the temperature effect.

The species yields downstream of hexane compartment fires were investigated and compared to upper layer yields. Results showed that downstream CO yields can be correlated to the plume equivalence ratio when taking into account the occurrence of external burning. When sustained external burning occurred for equivalence ratios greater than 1.7, downstream CO yields were reduced to 10 to 25 percent of the upper layer value. Results are very encouraging in indicating that an ignition criterion based on lean flammability limits is useful in predicting the flammability of upper layer gases in compartment fires. An ignition index value of 1.3 indicated the occurrence of sustained external burning and, thus, a reduction of CO, for the hexane fires studied.

ACKNOWLEDGEMENTS

I thank Dr. Rick Roby, my advisor, for the guidance he has given me over the last five years. He has provided me with many opportunities to grow not just as a student but as a professional in my field. He has not only been a mentor but has also become a friend.

Thanks also go to Dr. Craig Beyler, who was in many ways my co-advisor, Dr. Larry Roe, Dr. Dennis Jaasma and Dr. Dave Cox for serving on my committee.

I wish to express my appreciation for the friendships and laughs to all those who have come and gone in the office, Rik Johnsson, Linda Blevins, Jim Hunderup, James Reaney, Doug Wirth and Michelle Peatross. I especially, thank Doug and Linda for the many discussions we have had. I would also like to thank Michelle Peatross for her assistance as an undergraduate and later as a fellow graduate student. We worked closely together and benefitted from one another in tackling many of the common aspects of our projects.

My project would not have been accomplished without the help of the many undergraduate assistants and the technical support at Virginia Tech, especially Danny Lewis, Ben Poe and Frank Caldwell.

Support for this project was provided by the National Institute of Standards and Technology, Building and Fire Research Lab under grant number 60NANB8D0829. I am grateful for their support. I would like to acknowledge Bill Pitts of BFRL for the many discussions we had about the project. It is based on some of his ideas about CO formation that I discuss the temperature effect on fire plume chemistry.

I thank my parents for their continual encouragement and support through the years. I especially thank my wife, Ruth, who has helped me in so many ways, particularly, in the many midnight hours while completing this work. Her love and friendship are beyond words.

Finally, I thank God for the talents and opportunities He has given me to succeed and for the source of strength and comfort that He always provides.

TABLE OF CONTENTS

LIST OF FIGURES

LIST OF TABLES

CHAPTER 1

INTRODUCTION

1.1 Motivation

Fires in residential and commercial buildings kill approximately 6000 and injure 28,000 people annually [1]. A study done in the United Kingdom of fire victims showed that over 50 percent of the deaths were directly attributed to carbon monoxide poisoning and that in another 33 percent the gas contributed significantly to the cause of death [2]. The importance of the role of carbon monoxide as a fire hazard cannot be questioned [3,4].

As a chemical asphyxiant, carbon monoxide deprives the body of oxygen by forming carboxyhemoglobin. Hemoglobin in the blood usually combines with oxygen, however, it has an affinity for carbon monoxide 200-300 times greater than for oxygen [5]. Therefore, low levels of carbon monoxide can be hazardous. Concentrations of 2000-2500 ppm can produce unconsciousness in less than 30 minutes, and concentrations above 4000 ppm can be fatal in less than an hour [5]. Carbon monoxide levels of several percent are found in building fires. Some large scale fire tests have shown extremely high CO concentrations which would be lethal in a breath (e.g., 8 % in mobile homes [6,7]). It should be noted that what is of most importance is the levels of carbon monoxide that flow out of a burning room to adjacent spaces. This is because many people who die in fires are in rooms remote from the original room on fire.

Although carbon monoxide presents a severe threat to occupants of a building on fire, it is not well understood how this gas is generated in these complex environments. In the field of fire science, models continue to be developed to understand the growth,

spread and effects of fires. Models are typically used as either investigative or predictive tools: 1) to recreate a fire scenario in order to understand the causes of the fire or determine the reasons for hazardous outcomes and 2) to study varying fire scenarios in the design of building systems. In the second case, models can be used to predict safe egress times or used in the design of sprinkler systems and smoke ventilation systems, to name a few [e.g.,8,9,10]. Reference 11 provides an overview of current models and further references on the subject.

The advances in computers in the past twenty years, have allowed more complex and larger numerical models of building fires to be developed. However, the accuracy of these models is limited since much work is still required to understand the underlying physics and chemistry of fire. Although written six years ago, reference 12 by Emmons presents a good overview of the aspects of fire science which remain incomplete today. The continued relevance of Emmons' paper today is not an indication of the level of work being done in the area, but rather a sign of the complex nature of fire.

The incorporation of detailed chemistry in fire modeling is lacking. The complex fire environment cannot be characterized sufficiently for the application of chemical kinetics modeling, and equilibrium thermodynamics has also been shown to be inadequate at predicting species concentrations in compartment fire environments [13]. Since it is not possible to calculate species concentrations in compartment fires from first principles, experimental correlations need to be developed in order to incorporate the important aspect of carbon monoxide generation in compartment fire modeling.

1.2 Background

A typical compartment fire is illustrated in Figure 1.1. Typically, a two layer system is created in which the upper layer consists of hot products of combustion that collect below the ceiling and the lower layer consists of primarily ambient air which is entrained into the base of the fire. As a fire in a room develops, it initially burns in an overventilated mode similar to burning in the open. Due to the excess air, near complete combustion and little CO formation is expected in this mode. As the fire grows, ventilation paths in the room restrict air flow creating underventilated (fuel-rich) burning conditions. It is under these conditions that products of incomplete combustion are created, CO being of prime importance. In time, the upper layer descends and can spill below the top of a doorway or other opening into adjacent areas. As hot, vitiated fuel-rich gases flow into adjacent spaces, air with high O_2 concentrations can mix and create a secondary burning zone outside of the compartment. This is referred to as external burning. External burning can decrease human fire hazard through the oxidation of CO and smoke leaving the compartment, or increase the fire hazard by incompletely burning unburned fuel to CO.

The common parameters describing a compartment fire are the fuel burning rate, the air flow rate into the compartment and the temperature and gas composition of the upper and lower layer. The concept of an equivalence ratio has emerged as a useful tool in describing compartment fires by representing several of the common parameters. Due to the complex interaction between the plume and the upper and lower layers, a unique definition for the equivalence ratio does not exist. Two common definitions are presented below.

The upper layer equivalence ratio, ϕ_{ul}, is the ratio of the mass of the upper layer that originates from the fuel to the mass of the upper layer that originates from the air

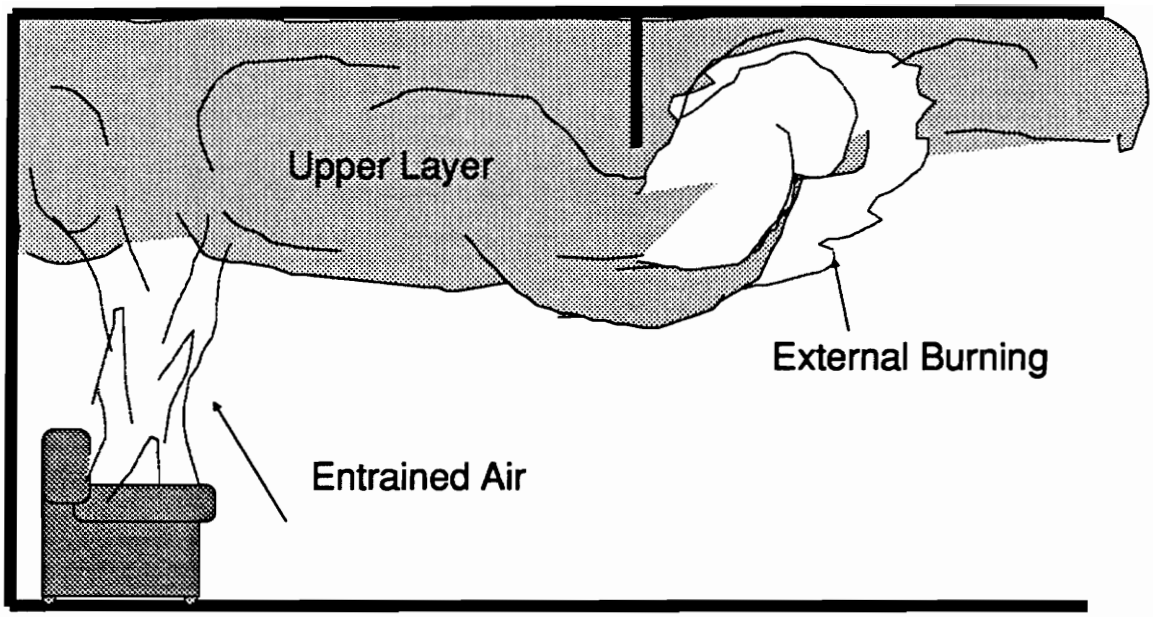

Figure 1.1 Development of a typical two layer compartment fire.

stream divided by the stoichiometric fuel-to-air ratio. The plume equivalence ratio, ϕ_p, is the ratio of the mass of fuel burning to the mass of air entrained into the fire plume normalized by the stoichiometric fuel to air ratio. The two equivalence ratios are not necessarily the same. As a fire grows, the upper layer composition represents a collective time history of products. In a typical fire, where all air enters the upper layer through the plume, ϕ_{ul} is the same as ϕ_p only during steady burning conditions. If the burning rate of the fire changes quickly compared to the residence time of the gases in the upper layer, the upper layer equivalence ratio lags behind the plume equivalence ratio. Another instance when ϕ_{ul} differs from ϕ_p is when additional fuel or air enters the upper layer directly. The two equivalence ratios are different for this case even for steady burning conditions.

1.3 Previous Work

Little work in the literature has been identified that systematically studies the generation of major species in compartment fires. No large scale studies have been done in which species measurements can be reasonably correlated to other fire parameters. However, Beyler [14,15], Toner [13] and Morehart [16] separately conducted similar experiments which showed that species composition measurements in simplified fire environments correlated well to the equivalence ratio. Tewarson expanded this work by studying major species production rates for wood crib enclosure fires [17]. He found that the species production rates were correlated by using the air-to-fuel stoichiometric fraction (the reciprocal of the equivalence ratio). Correlating the upper layer composition to a characteristic equivalence ratio has become known as the Global Equivalence Ratio concept (GER). This section briefly describes the work done to date on the GER concept and discusses the need for further study.

1.3.1 Hood Experiments

Beyler [14,15] was the first to measure major species production rates in a small-scale two layer environment. The experiments performed consisted of situating a burner under a one meter diameter, insulated collection hood as shown in Figure 1.2. The result was the formation of a layer of combustion products in the hood similar to that found in a two layer compartment fire. Except for wood, PMMA (polymethylmethacrylate) and polyethylene, continuous feed gas and liquid burners were used to study a range of fuels. Beyler's PMMA slab stock, 2.5 cm thick, was burned with fuel surface areas of 230 to 610 cm^2. Wood cribs consisted of 3.8 cm thick, 20 cm long ponderosa pine sticks with three to five layers each with three sticks per layer [15].

By varying the fuel supply rates and the distance between the burner and layer interface, and consequently the air entrainment rate, a range of equivalence ratios was obtained. Layer gases were exhausted at a constant, metered flow rate from the periphery of the hood at a depth of 15 cm below the ceiling. The general procedure was to allow steady-state burning conditions to develop so the layer maintained a constant depth below the 15 cm exhaust flow location. Gas samples were then taken from the exhaust stream. Using a hood-traversing, gas sampling probe with an aspirated thermocouple, Beyler observed reasonably well mixed uniform layers both in temperature and chemical composition during the steady conditions.

Beyler's results showed that species yields (grams of species produced per gram of fuel burned) correlated very well with the plume equivalence ratio. Beyler tested a variety of fuels to study the effect of chemical structure and found that carbon monoxide production for underventilated conditions ranked according to oxygenated hydrocarbons > hydrocarbons > aromatics. Although, different levels of CO were observed for various

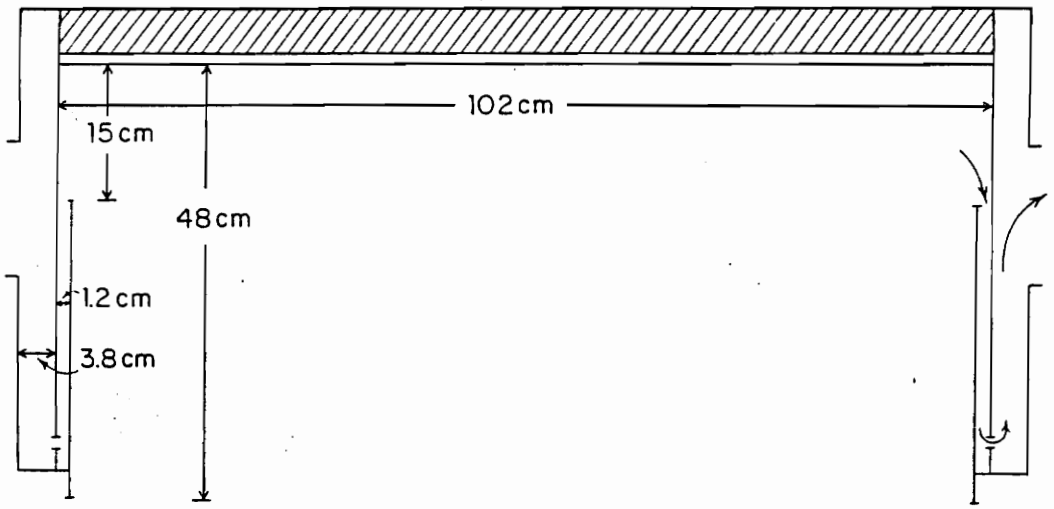

Figure 1.2 Cross section of cylindrical hood used by Beyler with dimensions shown on left and gas flows shown on right (figure taken from Beyler [14]).

fuels, the correlations were qualitatively similar. Below an equivalence ratio of 0.6 near zero CO production was observed. Above ϕ_p equal to 0.6, carbon monoxide yield increased with ϕ_p and, for most fuels, tended to level out at equivalence ratios greater than 1.2.

Toner performed similar hood-type experiments but using a different experimental setup [13]. The hood used was a 1.2 m cube insulated on the inside with ceramic fiber insulation board. The layer in the hood formed to the lower edges where layer gases were allowed to spill out. Gas sampling was done using an uncooled stainless steel probe inserted up into the layer. Detailed gas species measurements were made using a gas chromatograph system. The upper layer equivalence ratio was determined from conservation of atoms using the chemical species measurements, the composition of the fuel and the metered fuel flow rate. Twenty to 200 kW natural gas flames formed over a 19 cm diameter burner were studied. The layer in the hood was allowed to form and reach a steady condition before gas sampling was performed.

Toner concluded that species concentrations were well correlated to the upper layer equivalence ratio and insensitive to temperature for the range studied (490 to 870 K). Even though the equivalence ratios were defined differently, the correlations obtained were qualitatively similar to the correlations obtained by Beyler for different fuels. However, due to the steady-state nature of the fires, the plume equivalence ratio equalled the upper layer equivalence ratio for both Toner's and Beyler's experiments. The species concentrations were compared to the calculated equilibrium composition of the reactants at constant temperature and pressure. Toner found that the layer composition was modeled quite well by the chemical equilibrium composition for very overventilated conditions but not for underventilated conditions.

Morehart [16,18,19] studied similar methane hood experiments using much of the same apparatus as Toner [13] except for a different collection hood. The hood, 1.8 m square by 1.2 m high, was larger than that used by Toner and uninsulated. Morehart showed for his experiments that upper layer species concentrations were insensitive to the plume equivalence ratio but correlated well with the upper layer equivalence ratio. This was accomplished by burning a methane flame under the collection hood and obtaining a steady-state condition, thus, maintaining a given plume equivalence ratio. Air was then injected into the upper layer at a known flow rate to establish a steady-state ϕ_{ul} lower than the ϕ_p. By increasing the air supply rate to the upper layer, a range of ϕ_{ul} were established while maintaining a set ϕ_p. Morehart found that for a set plume equivalence ratio, species concentrations changed with the upper layer equivalence ratio in a well defined correlation. Figure 1.3 from reference [16] shows Morehart's measured CO mass fraction plotted against the upper layer equivalence ratio for a range of constant plume equivalence ratios. Toner's results are presented in the same Figure. Note that for Toner's experiments the plume and upper layer equivalence ratios were equal.

Although similar, the correlations obtained by Morehart deviated from those obtained by Toner. For underventilated methane fires ($\phi_p > 1.3$), Morehart observed lower CO, CO_2 and H_2O and higher CH_4 and O_2 concentrations than Toner. The only apparent differences between experiments was that Toner's layer temperatures were 120 to 200 K higher than those observed by Morehart (488 to 675 K). Due to the similarity in experimental apparatus except for the hood, Morehart concluded that the temperature difference resulted from having a larger uninsulated hood. The effect of temperature on the layer composition was investigated.

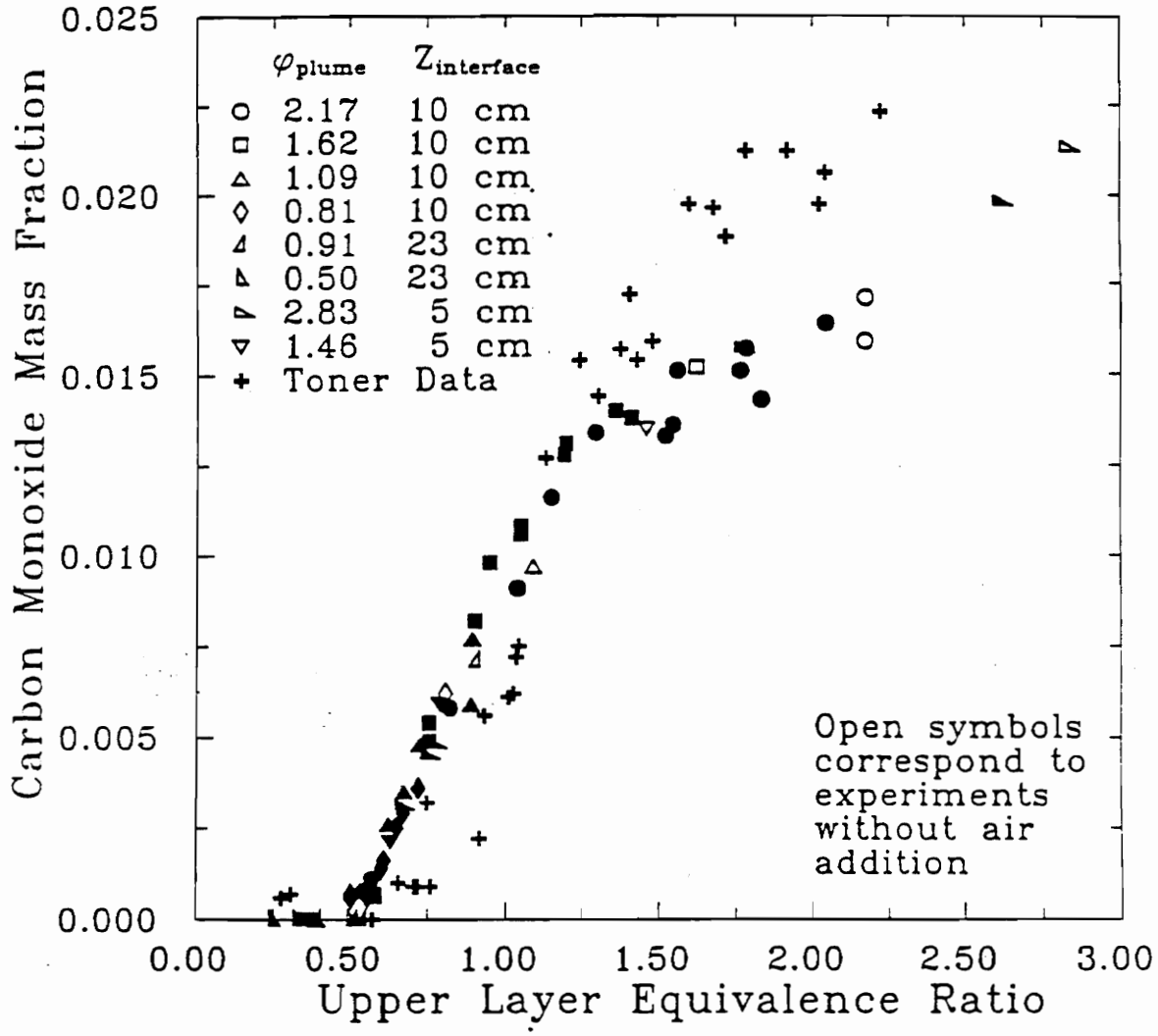

Figure 1.3 Measured CO mass fraction plotted against ϕ_{ul} for a range of constant ϕ_p methane fires under a hood. Figure taken from Morehart [16].

Morehart performed a set of experiments in which he repeated the same burning conditions (ϕ_{ul} = 1.45) with no air addition, but changed the insulation characteristics of his hood for each test. The results showed that with increasing insulation and, thus, increasing temperature, O_2 and CH_4 decreased with a balanced increase in H_2O and CO_2. For the range of temperatures observed (500 to 675 K) upper layer oxygen mass fraction decreased approximately 70 percent. As the temperature of Morehart's tests approached that of Toner's, the measured species concentrations approached those observed by Toner. Morehart claimed that CO concentrations remained nearly constant. However, study of his data shows an approximate 20% rise in CO which is the same magnitude of disparity between Toner and Morehart's data at the equivalence ratio tested. Since fires burn more inefficiently with increasing equivalence ratio, it is reasonable to expect that if higher equivalence ratio fires had been tested under the increasing temperature conditions, that even larger CO increases would have been realized, consistent with the discrepancy with Toner's results.

The hood experiments performed by the previous investigators differ from actual compartment fires in several ways. The hood setup allowed considerable radiation to the lab space below. Conversely, a real compartment would contain most of the radiation, thus, resulting in higher wall and upper layer temperatures. Consequently, higher fuel volatilization rates would be expected for an actual compartment fire. Also, the hood setup results in a lower layer which has an infinite supply of air which is neither vitiated nor heated. In a real compartment fire, the air supply is limited by the ventilation openings (doors, windows, etc.) and the depth of the upper layer. The air which is entrained into the lower layer of an actual compartment fire can be convectively heated by hot compartment surfaces prior to fire plume entrainment. Third, the hood

experiments did not include any significant ceiling and wall flame jets. These dynamic flame structures enhance mixing of the upper layer in actual compartment fires and extend the flame zone beyond the plume. Lastly, the hood experiment correlations were developed from sustained steady-state burning conditions. Actual fires of interest are usually in a continual growth stage, and, thus, quite transient in nature. It was not clear what the effect of more transient conditions would be on the correlations.

1.3.2 Compartment Fire Experiments

The only compartment fire study of the global equivalence ratio concept was performed by Tewarson [17]. Tewarson reported that CO, CO_2 and O_2 yields were correlated well by the air-to-fuel stoichiometric fraction (i.e., the reciprocal of the equivalence ratio). Enclosure fire data was taken from previous work in the literature for cellulosic-base fiberboard and pine wood cribs burned in various compartment geometries, 0.21 to 21.8 m^3 in volume with single and dual horizontal and vertical openings centered on the end walls. Additional data was obtained for pine wood cribs burned in a small scale flammability apparatus which exposed the sample to variable external radiant heat flux with either natural or forced air flow from below. All products were captured in a sampling duct where temperature and gas concentration measurements were made.

Tewarson plotted CO, CO_2 and O_2 yields versus mass air-to-fuel stoichiometric fractions (i.e., the reciprocal of the equivalence ratio) for wood crib compartment fires [17]. His results show distinct correlations with good agreement between data for CO_2 and O_2 from the varied experimental conditions. The CO_2 and O_2 yields are relatively constant for equivalence ratios up to about 1.7 and 1.4, respectively, and then decrease sharply as the equivalence ratio increases. The CO yield correlates with the equivalence

ratio but with a fair amount of scatter in the data. With increasing equivalence ratio, the CO yield increases and, similar to Beyler's correlation for ponderosa pine, appears to be leveling out to a value of about 1.4 for underventilated conditions.

However, the quality of Tewarson's correlations is compromised by the fact that the air entrainment rate used to calculate the mass air-to-fuel ratio was not measured directly, but rather was estimated from the ventilation parameter, $Ah^{1/2}$, where A is the cross sectional area and h is the height of the vent. Most enclosure fire work performed to date has consisted of compartments with a single ventilation opening through which both air flows in and upper layer gases flow out. The two-flow situation and the changing location of the layer interface makes accurate flow measurements difficult. It is also important to note that the elemental composition of the fuel volatiles used by Tewarson for the wood was not corrected for char yield. A correction of this sort would tend to decrease the calculated equivalence ratio.

1.3.3 External Burning Experiments

No studies have examined the effect of external flames on the levels of products of incomplete combustion flowing from a compartment fire. The majority of work that has been published on the phenomenon of external combustion has pertained to the physics of flame projection [20,21,22,23,24]. For example, Bullen and Thomas [24] report temperature and size measurements for external flames outside of compartment fires; however, they do not sufficiently describe the origin of the external flames nor their effect on species yields.

1.4 Scope of Thesis

In general, good progress has been made in the development of the global equivalence ratio concept. However, no systematic, instrumented compartment fires have been performed to examine the effects of actual compartment fire behavior on the species yield correlations with the equivalence ratio. Of equal importance, no studies have examined the effect of external burning on the levels of CO exiting a compartment fire.

The goals of this study were to 1) determine if correlations exist between species generation rates, primarily CO, and the equivalence ratio for compartment fires and 2) determine the efficiency of external flames in destroying downstream CO initially produced within the compartment.

Experiments performed examined the burning of four fuels in a 2.2 m^3 compartment. The compartment was specially designed to separate the entrained air flow into the fire plume and the outflow of upper layer gases. This allowed direct measurement of the entrained air rate. Thus, the plume equivalence ratio was calculated directly from the measured fuel burning rate and air entrainment rate. Varying the size of the fuel sample and the exhaust ventilation opening allowed a range of equivalence ratios to be obtained.

The production of species in compartment fires was examined by measuring species concentrations within the upper layer for a range of equivalence ratios. Four fuels (hexane, PMMA, spruce and polyurethane) were examined to assess the effect of fuel composition on CO production. A second set of hexane fires was performed in which species yields were measured downstream of the compartment to examine the effect of

external burning that occurred. The phenomenon of external burning was characterized and methods of predicting its occurrence were investigated.

The thesis is organized to first present the work of species generation in the upper layer and then the work of studying external burning, which builds on the first study. Chapter 2 describes the experimental apparatus used for all experiments, the selection and characterization of fuels and the test procedures used for both studies. The results for the upper layer chemical species production experiments are presented in Chapter 3 and discussed in Chapter 4. Chapter 5 presents and discusses the results for external burning experiments. Conclusions and future recommendations are included in Chapter 6.

CHAPTER 2

EXPERIMENTS

2.1 Introduction

This chapter describes the experimental apparatus and the test procedures used to investigate the generation of CO both within and downstream of the compartment. The chapter is organized in three main sections: 1) description of the experimental apparatus, 2) physical and chemical characterization of the test samples and 3) discussion of the test procedures and data reduction.

2.2 Apparatus

2.2.1 Compartment

The test compartment, Figure 2.1, was a two level structure consisting of a 1.2 m x 1.5 m x 1.2 m high fire compartment and a 1.2 m x 1.5 m x 0.3 m high air distribution plenum below this fire chamber. The compartment frame was constructed of 0.635-cm-thick 5.08 cm steel angle iron and 5.08 cm bar stock. Fire Master 2.54-cm-thick fire insulation board (Thermal Ceramics) completely covered the interior surfaces of the fire compartment. The air distribution chamber was enclosed with 0.3175-cm-thick sheet steel.

An inlet duct and an exhaust vent provide two ventilation paths in the compartment. A window style exhaust vent was horizontally centered in the front of the compartment with a 20.3 cm soffit. The vent size was varied to produce different

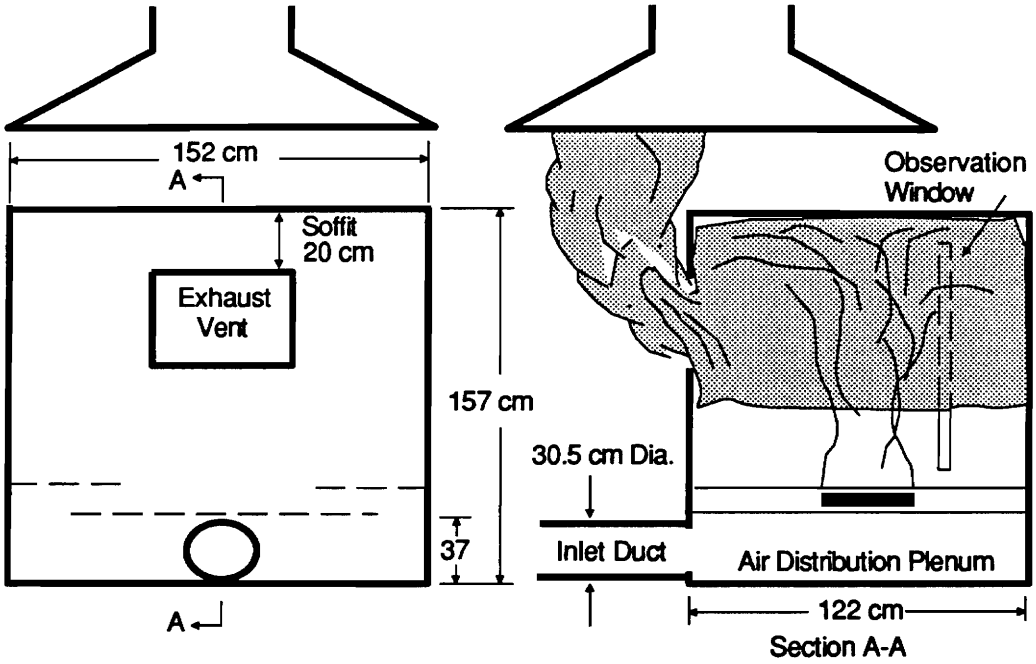

Figure 2.1 Schematic of the test compartment.

ventilation conditions while also assuring that there was only outflow of combustion products. Exhaust vent sizes ranged from 25.4-cm-wide by 15.9-cm-high (404 cm^2) to 50.8 x 31.8 cm (1615 cm^2).

Since there was only outflow through the exhaust vent, all the entrained air was naturally drawn into the compartment through a 4 m long, 30.5 cm diameter inlet duct which emptied into the air distribution plenum. The air in the plenum was drawn into the base of the fire compartment through thermally shielded vents on each side of the structure. Each vent shield was extended 28 cm in from the side wall and spanned from front to back of the compartment. The top surfaces were covered with fire insulation board. The entrained air rate was measured with a hot film, 0-2m/s linear velocity probe (Kurz model 415) with a claimed accuracy of $\pm$2.5 percent of the reading. The probe was positioned at the point of mean velocity based on measured velocity profiles. The flow was turbulent and, thus, the velocity profile was quite flat. The probe was calibrated in the experimental setup using a CO gas tracer method discussed in detail in Appendix A.

A 0.3175-cm-thick, 2.54-cm-wide Corning vycor glass window placed vertically down the side of the compartment allowed visual observation of the developing fire. Vycor glass is rated for continuous operation at 1173 C, however, work by Skelly [25] showed that edge-insulated windows crack when temperature gradients of 90 C develop between the center and edge of the glass. Therefore, to prevent the glass from cracking it was secured in place from the inside of the compartment with washers approximately every 10 cm along the edge. This allowed the whole surface of the glass to be heated evenly. The window performed well through all fires and up to temperatures of 1400 K with no loss of integrity.

A 15 kg load cell (A&D Inc.), with 1 gram resolution, was used to measure the fuel volatilization rate. To isolate the load cell from the fire, it was placed in the center of the air distribution plenum below the fire compartment floor. A 2.54 cm aluminum rod with square pieces of aluminum plate perpendicularly attached to each end was used to extend the weighing platform through a 3.2 cm hole in the floor of the fire compartment. The fuel sample was placed on the top of the extension platform.

Temperature measurements were made with a vertical tree of eight aspirated thermocouples located in the front corner of the compartment. The thermocouple tree consisted of type K, 30-gage thermocouples uniformly spaced 10 cm apart starting 10 cm from the ceiling. The tree was positioned 10 cm away from the walls to avoid wall jet effects. An unshielded type K thermocouple was also positioned at the sampling probe location.

2.2.2 Hood and Exhaust System

A 1.5 x 1.5 m hood positioned over the exhaust vent collected all fire effluent. The hood was exhausted through a 45.7 cm diameter, instrumented duct fitted with a gas sampling probe, smoke measurement device and an orifice plate, see Figure 2.2. The flow was induced with a 142 m^3/min (5000 cfm) blower downstream of the hood. The volumetric flow through the exhaust duct was measured using an A.S.T.M. designed 30.48 cm (12 in) inside diameter, sharp edged orifice plate, D and D/2 pressure taps, and a Datametrics Model 590 Barocel pressure sensor with a Model 1450 Electronic manometer. The design of the orifice meter and flow calculations were based on the A.S.M.E Research Committee on Fluid Meters report Fluid Meters [26].

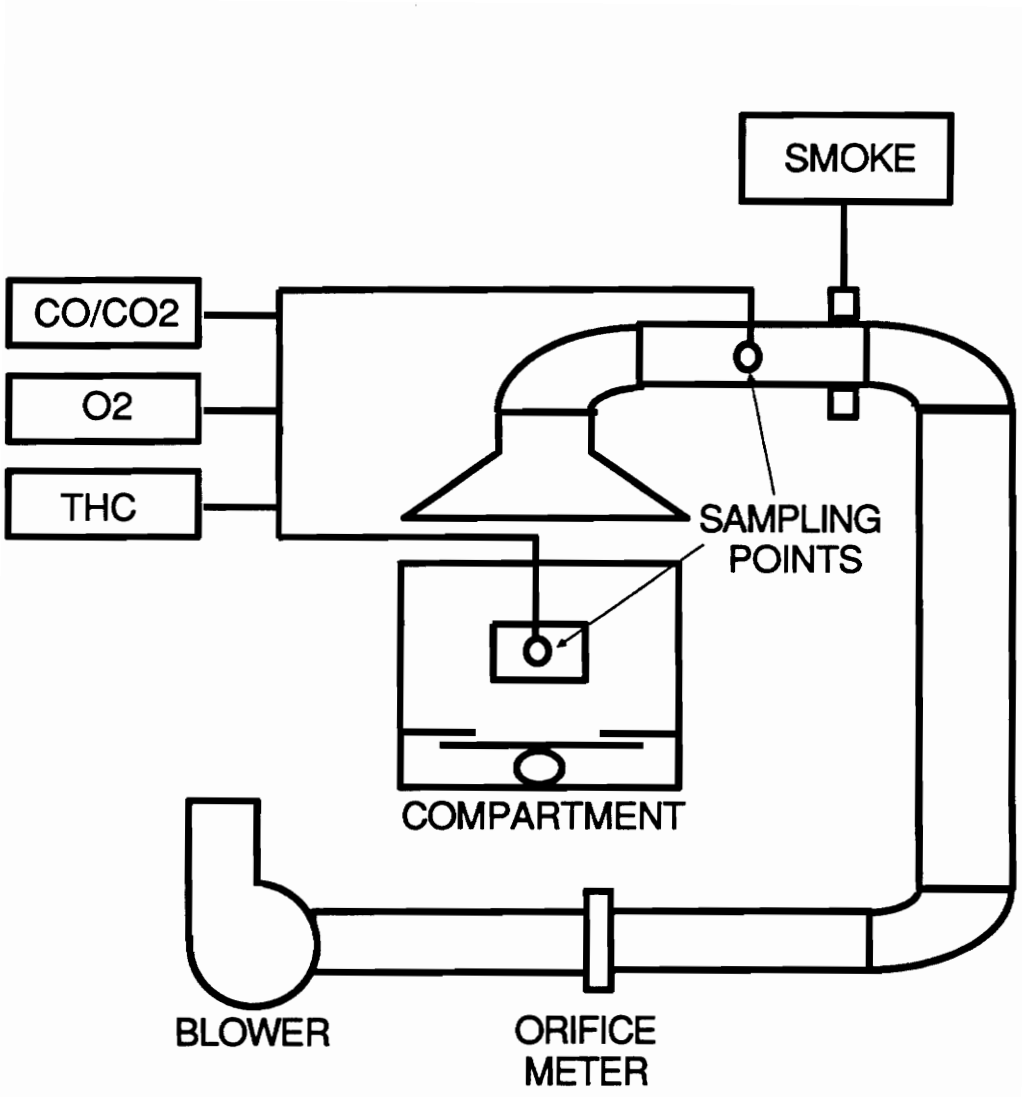

Figure 2.2 Schematic of hood and exhaust system.

Gas sampling was done by inserting a probe into the center of the exhaust duct. The probe was a 0.635 cm (.25 in) stainless steel tube with 0.3175 cm (0.125 in) holes drilled perpendicularly through the tube every 2.54 cm. The entire gas sampling system is discussed in section 2.2.3.

The smoke measurement device was situated 2.4 diameters downstream of the sampling probe and 3.7 diameters upstream of the orifice plate. The smoke measurement device, shown in Figure 2.3, provided extinction coefficients by measuring the attenuation of a 670 nm laser beam passed through the exhaust duct. The laser was a 5 mW LDA-1001 diode laser with mini module (D. O. Industries). Oriel neutral density filters and diffusers were placed in front of the photodiodes to balance the output from each device with atmospheric air in the duct. From the extinction coefficient the mass optical density and the smoke yield were formulated as detailed below.

According to Bouguer's Law, the extinction coefficient, K, can be expressed as follows:

$$K = - (1/L) * \ln (I/I_0) \qquad [2.1]$$

where L is the optical path length (m) through the attenuating medium, I is the light intensity after passing through the medium and I_0 is the initial light intensity.

The optical density per unit length, D' (m^{-1}), and subsequently, the mass optical density per unit length, D'_{mass} (m^2/g), are calculated as:

$$D' = K / 2.303 \qquad [2.2]$$

$$D'_{mass} = D' * Q / G_f \qquad [2.3]$$

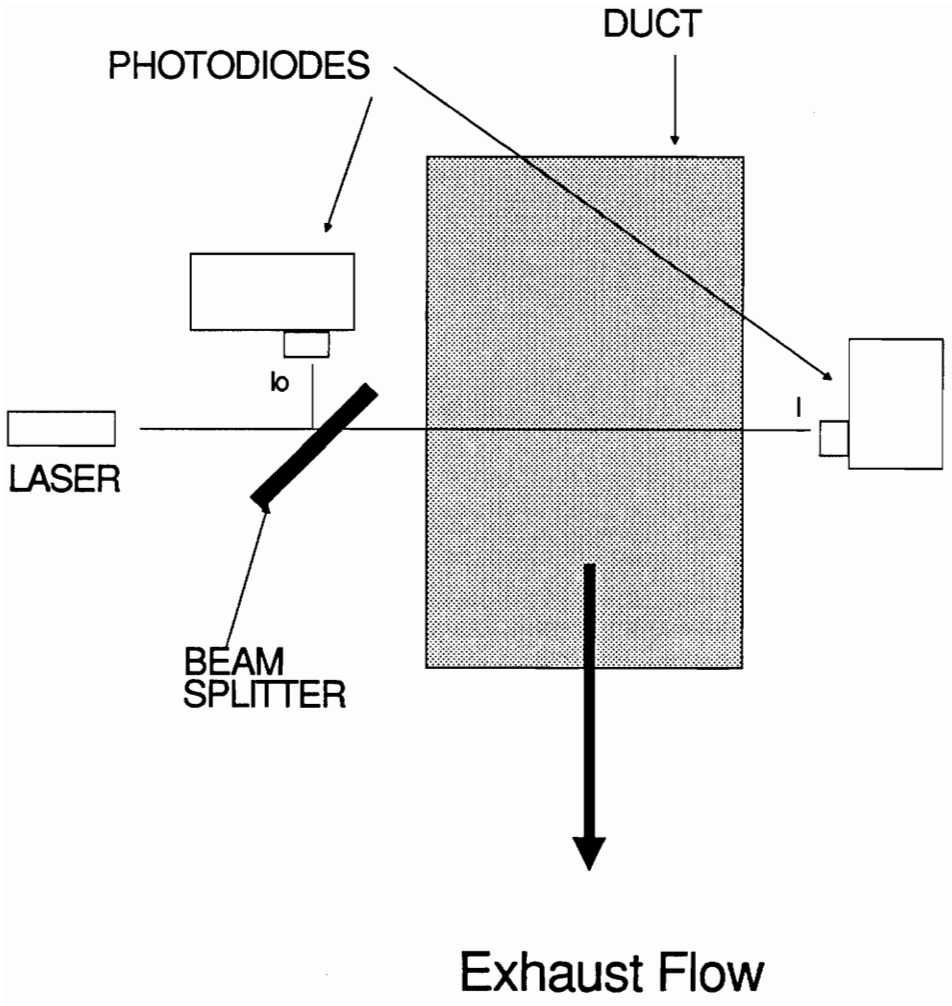

Figure 2.3 Schematic of smoke measurement device.

where Q is the volumetric flow rate through the exhaust duct and G_f is the fuel volatilization rate [27].

The yield of smoke, Y_s, is defined as the grams of smoke produced per gram of fuel burned and can be expressed as:

$$Y_s = D'_{mass} / \xi \qquad [2.4]$$

where ξ is the specific extinction coefficient of smoke [27]. The specific extinction coefficient is not a well characterized value especially for underventilated compartment fire conditions. As an approximation for well-ventilated flaming fires, Tewarson suggests the following relationship for ξ based on the incident wavelength of light, λ, and the density of smoke, ρ, (a density value of 1.1 g/cm^3 is also suggested) [27, 49]:

$$\xi = 3.213 / (\lambda * \rho) \qquad [2.5]$$

In the absence of a detailed characterization of the specific extinction coefficient and since a broad range of ventilation-controlled fires were investigated, the above relationship was used in this work to calculate the smoke yield. The smoke yield measurements were used as relative measurements to compare the burning behavior of various fuels and to determine the effect of external burning on downstream yield. Actual yields may be as much as 50 percent low due to the uncertainty associated with ξ.

2.2.3 Gas Sampling System

The upper layer gas mixture was sampled using an uncooled 0.635 cm stainless steel tube placed 13 cm into the compartment through the center of the exhaust vent. This location for the probe was chosen after species concentration and temperature

measurements, taken at several locations in the upper layer, showed a reasonably well mixed uniform layer (see section 3.2).

Figure 2.4 shows a schematic of the sampling system. The gas sample was drawn from the compartment or the exhaust duct by Thomas 2107 CA18 diaphragm pumps just upstream of the analyzers. The entire sampling line was approximately 9 m long from the compartment to the analyzers and consisted of 0.635 cm (.25 in), 0.0889 cm (0.035 in) wall stainless steel tubing. Polyethylene, 0.635 cm tubing was used from the main bypass flow meter to the CO, CO_2 and O_2 analyzers and from the exhaust duct probe to the sample selection valve. In order to prevent high molecular weight hydrocarbons from condensing out of the sample, the flow system from the compartment to the total hydrocarbon analyzer was maintained over 130 C with the use of Thermolyne heating tape.

From the compartment, the sample flow to all analyzers was passed through a Balston 915A borosilica glass filter with a 93% retention at the 0.1 micron level. The sample flow to the CO, CO_2 and O_2 analyzers was passed through a -10 C cold trap to condense out water vapor, as required by the instruments. A high bypass flow was used to reduce the sampling response time between the compartment and the analyzers to 15 seconds. This included the response time for the analyzers which was less than 2 seconds for all instruments. The flows to the analyzers were regulated with Matheson flow meters located upstream of the instruments. Atmospheric pressure was maintained in the analyzers by placing all flow controls upstream of the devices and exhausting the flows directly to atmosphere. The flow system to the total hydrocarbon analyzer is described in section 2.2.4.3.

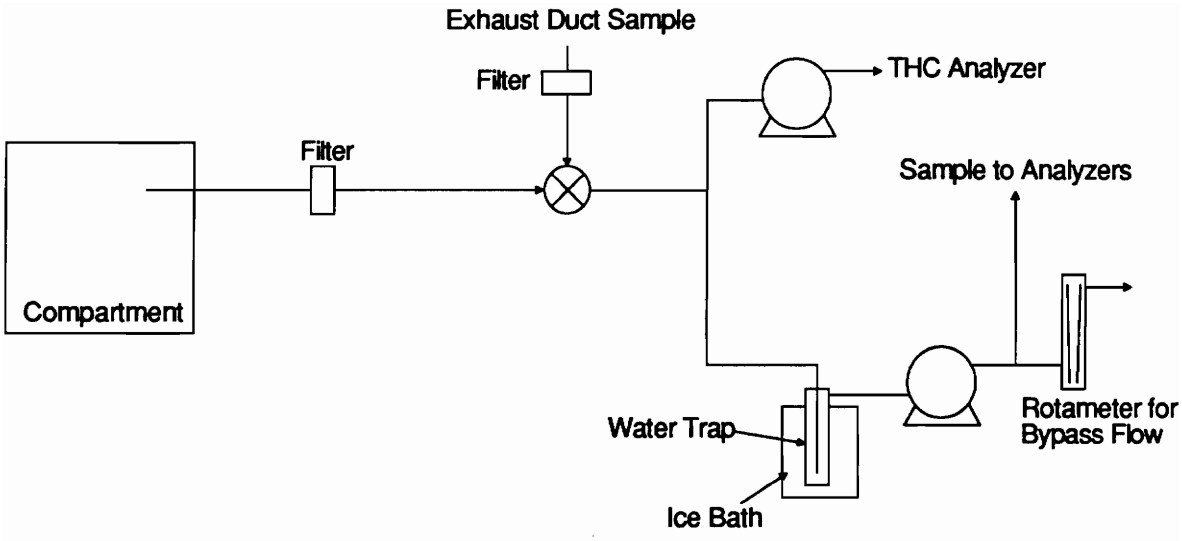

Figure 2.4 Schematic of gas sampling system.

2.2.4 Gas Analysis System

Gas analysis primarily consisted of CO, CO_2 and O_2 concentration measurements. Total hydrocarbon measurements were only performed for the last hexane-fueled experiments. Analyzers were calibrated before each experiment with zero N_2 gas and certified span gases.

2.2.4.1 CO and CO_2 Analyzers

Carbon monoxide and carbon dioxide concentrations were measured with individual Beckman NDIR model 880 analyzers with reported accuracies of one percent of full scale (CO: 0-1000ppm, 0-1%, 0-10%; CO_2: 0-15%, 0-20%). Compartment samples were typically analyzed with the 10% CO range and the 20% CO_2 range. Calibration gases were certified mixtures of CO, CO_2 and N_2 balance at 90% full scale values. The 1000 ppm CO range was used for fires expected to be overventilated and for exhaust duct samples. Measured concentrations were compensated for the water removed based on the assumption that the molar ratio of H_2O to CO_2 at any equivalence ratio is equal to the calculated molar ratio at stoichiometric conditions. This assumption leads to an estimated uncertainty in the calculated wet concentration of 1 to 6% of the value as the dry CO_2 mole fraction increases from 0.01 to 0.20. Since the H_2O assumption depends on the measured CO_2 mole fraction, the uncertainty in the wet species concentration increases slightly as the dry CO_2 mole fraction increases.

2.2.4.2 O_2 Analyzer

Oxygen concentrations were measured with a Siemens paramagnetic Oxymat 5E analyzer set to a 22% range with a reported accuracy of one percent of full scale. The

sample flow was 1 l/min to the analyzer. Measured concentrations were compensated for the water removed based on the assumption that the molar ratio of H_2O to CO_2 at any equivalence ratio is equal to the calculated molar ratio at stoichiometric conditions.

2.2.4.3 Total Hydrocarbon Analyzer

Total hydrocarbon measurements were only obtained for the last hexane-fueled experiments. The total hydrocarbon (THC) analyzer design is shown in Figure 2.5. A Gowmac model 12-800 flame ionization detector (FID) was used with a Gowmac model 40-900 electrometer to measure the total hydrocarbon concentration on a C_2 basis. The FID required a small sample flow in the range of 20 to 40 cc/min, therefore, a 3.5 l/min bypass flow was incorporated to minimize the response time of the sampling system to the analyzer. The constant sample flow to the analyzer was achieved by maintaining a 1.5 psig pressure at the entrance to a calibrated capillary tube connected to the FID inlet port. Sample flow not sent to the FID was bypassed to the atmosphere through a Matheson flowmeter. The set pressure was maintained with a 0-2 psig Fairchild model 10 pressure regulator placed downstream of the capillary tube. Changes in the capillary flow rate due to changes in gas viscosity were estimated to be within 7 percent based on typical gas compositions from the hexane fires.

The sample line was maintained at 130 C or higher using Thermolyne isolating heating tape and the FID was maintained at 105 C in an oven. Heating the sample line minimizes the effect of water condensation and wall adsorption of higher molecular weight hydrocarbons. Since the FID is insensitive to water, total hydrocarbon concentrations require no correction to obtain wet measurements as do the CO, CO_2 and O_2 measurements. Water was not removed from the sample.

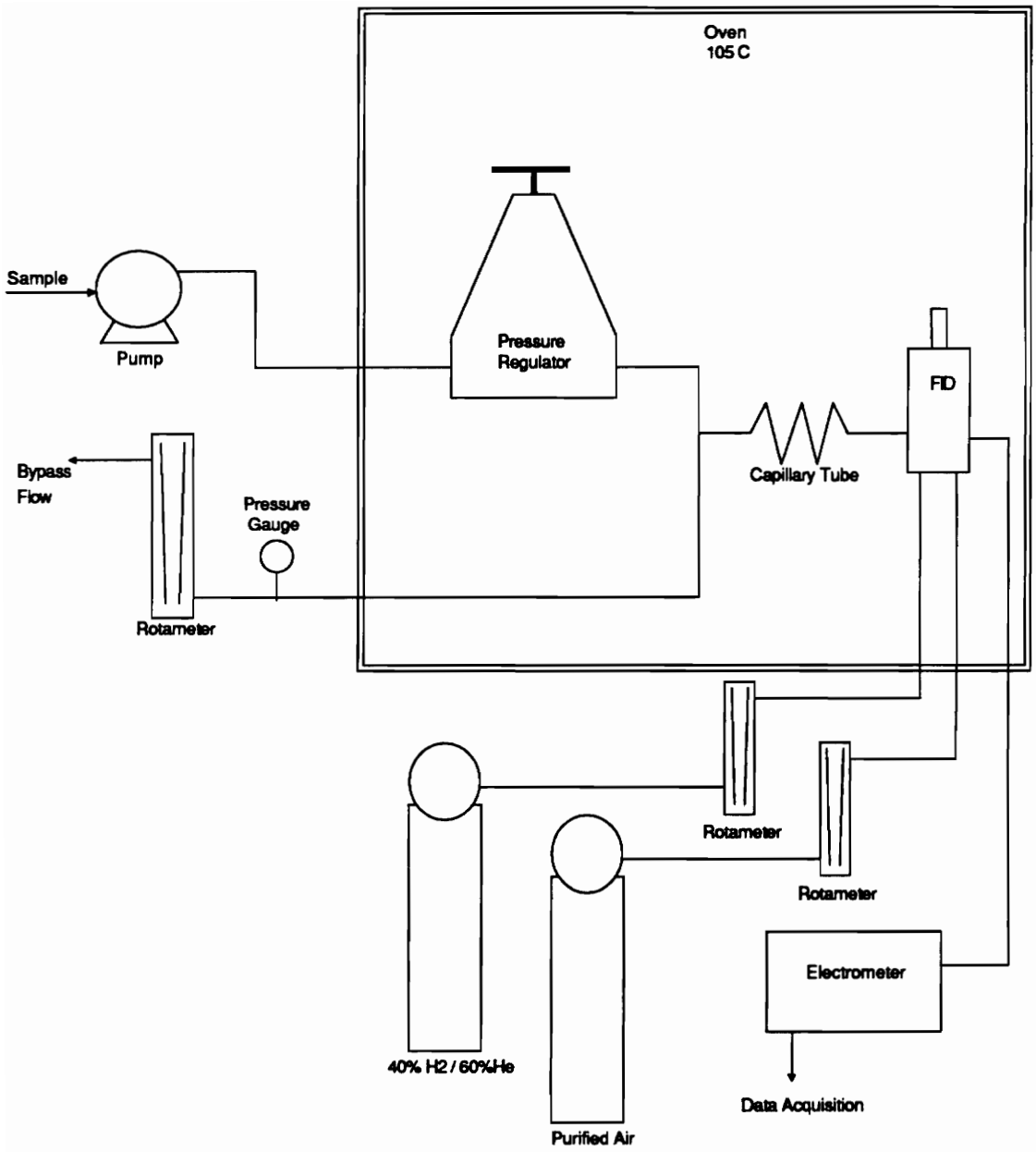

Figure 2.5 Schematic of total hydrocarbon analyzer.

A 40/60 mixture of H_2/He fuel was used for the FID to reduce oxygen synergism effects related to samples with varying oxygen concentrations. Ethylene (4.71%) was used as a calibration gas because it is believed to be more representative of the THC present in the sample than methane, which is typically used. Although the FID response is linearly proportional to carbon atoms for compounds in the same homologous series, methane is a more stable and anomalous compound.

2.2.5 Data Acquisition System

The data acquisition system consisted of a 286 Epson Equity II computer and two Data Translation 2801-A boards with a DT707 and a DT756-Y screw terminal panels. The DT 2801-A boards were used as analog to digital input boards with 12-bit resolution. The boards supported either 16 single ended or 8 differential input channels. Differential inputs were used for all the instruments connected to the DT707 to take advantage of common mode noise rejection.

The DT756-Y panel was used for up to 16 thermocouple signals. Since differential inputs are required for thermocouples, the 756-Y board was unique in that it converted 16 single ended input channels on the 2801-A board to 16 differential input channels. The 756-Y also provided the necessary cold-junction compensation for the type K thermocouples used in the experiments.

Data acquisition was performed with a compiled GWBASIC program using Data Translation's PCLAB subroutine library. Data reduction was then performed with a FORTRAN code written for these experiments (see Appendix B).

2.3 Test Samples

2.3.1 Selection

Four fuels were tested: 1) hexane, 2) cast polymethylmethacrylate (PMMA), 3) spruce and 4) flexible TDI-based polyurethane foam. The fuels investigated were chosen to provide a varied selection in order to determine if similar species yield-equivalence ratio correlations existed for different fuel types. Additionally, hexane, PMMA and spruce were chosen to establish comparisons between Beyler's yield-equivalence ratio correlations [14,15] and those expected in this work.

Beyler burned ponderosa pine as his wood selection. However, due to lack of availability of ponderosa pine, spruce was chosen as most similar in chemical and physical properties. Hexane was chosen as a well characterized liquid fuel. PMMA was selected as a simple thermoplastic fuel which breaks down almost entirely to its monomer as it volatilizes. TDI-based polyurethane, however, is a more complex polymer that does not decompose to simple monomers. Furthermore, spruce represents a complex cellulosic material that decomposes directly from a solid to volatiles and char. Also, polyurethane and wood are common items used in building construction and furnishings.

2.3.2 Chemical Characterization of Fuels

In order to plot the data against the plume equivalence ratio, the stoichiometric fuel-to-air ratio must be defined for each fuel. For hexane and PMMA, the stoichiometric fuel-to-air ratio is simply calculated since the elemental composition of the volatiles is readily known. Table 2.1 shows the physicochemical properties used for the four fuels. The elemental composition of 44.1 kg/m^3 flexible polyurethane foam was taken to be $CH_{1.74}O_{0.323}N_{0.07}$ [28]. This composition was also verified by an elemental analysis

TABLE 2.1. Physicochemical property data used for the fuels studied.

FUEL	Volatiles COMPOSITION	$(A/F)_{st}$	kco	kco_2	ko_2
Hexane	C_6H_{14}	15.2	1.95	3.06	3.53
PMMA	$C_5H_8O_2$	8.26	1.4	2.20	1.92
Spruce	$CH_{2.473}O_{1.07}$*	4.72	0.89	1.39	1.10
PU	$CH_{1.74}O_{0.323}N_{0.698}$**	8.83	1.41	2.21	2.05

$(A/F)_{st}$ = stoichiometric air-to-fuel ratio (mass units)

ki = maximum yield of species i

PU = 44 kg/m3 TDI-based flexible polyurethane foam

* - assumes 25% char

** - does not include nonvolatile filler

performed by Galbraith Labs. A filler accounted for 45 percent of the original weight of the polyurethane and remained as a powder and solid crust after the fire, but had no apparent effect on the composition of volatiles. An elemental analysis, also performed by Galbraith Labs, reported a composition of $CH_{1.689}O_{0.731}$ for the spruce burned. The composition of the volatiles was obtained by adjusting the wood composition for an observed average of 25 percent char; resulting in a volatiles composition of $CH_{2.473}O_{1.07}$. The char was assumed to be all carbon. To calculate the char fraction, the crib weight was first determined at the time in the fire, after steady-state burning, at which the upper layer O_2 concentration started to rise rapidly and the CO_2 concentration was also decreasing sharply. The char fraction was then calculated as the weight remaining at this time divided by the initial crib weight.

2.3.3 Characterization of Fuel Samples

Hexane was burned in 6.4 cm deep circular aluminum pans (0.32-cm-thick) ranging from 15 to 28 cm in diameter. The PMMA samples burned consisted of 0.95 cm and 1.9-cm-thick samples ranging in size from 20x20 cm to 46x46 cm squares (400 cm^2 to 2116 cm^2). These sheets were ignited by igniting hexane-soaked PMMA shavings that were evenly piled on top of the sheet to assure a rapid uniform ignition, thus, decreasing the time to steady-state burning. Spruce sticks, 3.81 cm square, were burned in fuel surface controlled cribs. Fuel surface controlled means stick spacing is large enough to allow sufficient air into the center of the crib. Therefore, the burning rate is dependant on the fuel surface [29]. Crib sizes ranged from 4 to 7 layers and consisted of 3 sticks per layer for 30.5 cm long sticks and 4 sticks per layer for 45.7 cm long sticks. The cribs were placed on aluminum foil pans and ignited with a thin film of hexane poured into the pan. The moisture content of the wood ranged from 11 to 18 percent with an approximate

average of 14 percent. The square polyurethane samples were 12.7-cm-thick and ranged in size from 30.5 to 45.7 cm on a side. The flexible foam had a density of 44.1 kg/m^3 and was not fire treated. Each polyurethane sample was burned horizontally on the square side and ignited with a propane torch on the top center of the sample. In all cases the fuel was supported by the load cell in the center of the compartment 5 cm above the floor.

2.4 Test Procedures and Data Reduction

Experiments were classified as either upper layer-sampled tests or downstream-sampled tests. Upper layer-sample tests were performed for all fuels. The downstream-sampled tests consisted of burning hexane fires under the same conditions as the upper layer-sampled hexane tests. Sampling downstream of the compartment in the exhaust duct provided measurements of the effect of external burning on the yields of CO and CO_2 exiting the compartment compared to the initial yields in the upper layer. For both types of tests data reduction was essentially the same. This section describes the basic calculations and test procedures.

2.4.1 Common Experimental Procedure and Treatment of Data

The general procedure was to set the fuel sample in the center of the fire compartment on the load cell extension platform and to set the exhaust vent size by changing the front fire board panel. The fuel was ignited and the data acquisition system started. Data was collected and stored with the time every 2 seconds. The data acquisition was run past the end of the fire to account for the sample delay between the compartment and the analyzers. Measured delay times were used in the data reduction code to adjust the gas concentration measurements with respect to the instantaneously measured fuel burning rate, entrained air rate and temperature measurements.

During the fire, a video was taken of the exhaust vent flow and any external burning that occurred. Another video was taken through the observation window to record the fire inside the compartment and the upper layer development.

2.4.1.1 Equivalence Ratio

The two ventilation path setup allowed direct measurement of the plume equivalence ratio. The plume equivalence ratio, ϕ_p, is the ratio of the fuel volatilization rate to the air entrainment rate normalized by the stoichiometric fuel to air ratio. Most compartment fire work performed to date consisted of compartments with one ventilation opening in which both inflow and outflow of gases occurred [30,31,32]. Consequently, the entrained air into the compartment could only be estimated from the ventilation parameter $Ah^{1/2}$ [17]. The apparatus used for this investigation allowed the entrained air to be measured directly with the use of the hot film velocity probe placed in the inlet duct and the fuel burning rate was measured directly with the load cell. Based on the air entrainment and fuel volatilization, measurements the calculated equivalence ratio measurements have an uncertainty of ± 10 percent.

A range of equivalence ratios was obtained by varying the exhaust vent size and fuel sample size. The air entrainment rate was primarily a function of the exhaust vent size and remained essentially steady throughout a fire. Therefore, to obtain higher equivalence ratio fires, a larger fuel sample was used or the vent size was decreased. In the case of polyurethane and spruce, the test apparatus proved to be a limitation on the range of equivalence ratios obtained. For the largest sample sizes, only slightly underventilated fires were obtained. The exhaust vent size could not be reduced further because the entrained air velocity would be too small to measure accurately.

2.4.1.2 Species Yields

Beyler [14,15] and Tewarson [17] reported the generation of major species, i, in the upper layer environments in terms of a mass yield, Y_i. Species yields are defined as the grams of species produced per gram of fuel burned. The yield (actually depletion) of O_2 is the grams of O_2 consumed per gram of fuel burned. Similar to Tewarson's development the yield was calculated as follows:

$$Y_i = \frac{X_{i,wet}\,(m_{air} + m_{fuel})\,M_i}{m_{fuel}\;M_{mix}} \qquad [2.6]$$

where $X_{i,wet}$ is the corrected wet mole fraction of species i, m_{air} is the mass air entrainment rate, m_{fuel} is the mass burning rate, M_i is the molecular weight of species i and M_{mix} is the molecular weight of the mixture assumed to be that of air.

The normalized yield, f_i, is the yield divided by the theoretical maximum yield of species i for the given fuel, k_i. By definition, the normalized yields range from 0 to 1 and are, thus, good indicators of the completeness of combustion. The conservation of carbon requires that

$$f_{CO} + f_{CO2} + f_{THC} + f_{res.C} = 1 \qquad [2.7]$$

where $f_{res.C}$ is the yield of residual carbon, such as carbon in smoke or high molecular weight hydrocarbons that condense out of the sample. Normalized yields are particularly useful in comparing results between fuel types. This is discussed in section 4.4. Normalized yields, f_i, are reported and discussed as yields. True yields, Y_i, are discussed as unnormalized yields.

A simple model for the most complete combustion of a fuel can be represented by the following expressions [14]:

$$f_{CO2} = f_{O2} = 1 \qquad \text{for } \phi < 1 \qquad [2.8a]$$

$$f_{CO2} = f_{O2} = 1/\phi \qquad \text{for } \phi > 1 \qquad [2.8b]$$

$$f_{CO} = f_{H2} = 0 \qquad \text{for all } \phi \qquad [2.8c]$$

$$f_{THC} = 0 \qquad \text{for } \phi < 1 \qquad [2.8d]$$

$$f_{THC} = 1 - 1/\phi \qquad \text{for } \phi > 1 \qquad [2.8e]$$

These yield expressions are plotted with the results for comparison. The ratio of the normalized yield of CO_2 or O_2 to the predicted values of the expressions above is defined here as the yield coefficient, B_{CO2} and B_{O2}, respectively. These terms are useful in discussing characteristics of the combustion efficiency; for example, an O_2 yield coefficient of 1 indicates complete utilization of available O_2. In the case of CO_2, deviation from the model (as indicated by smaller B_{CO2}) is a measure of the degree of incomplete combustion.

2.4.1.3 Heat of Combustion

The combustion efficiency, X_c, is the ratio of the actual heat release rate to the maximum theoretical heat release rate for complete combustion of all fuel (water as vapor). The maximum theoretical heat release rate is simply calculated by multiplying the heat of combustion by the fuel burning rate. The actual heat release rate can be calculated from either the generation rate of CO and CO_2 or the depletion rate of O_2 [33]. Due to incomplete combustion and the incomplete utilization of O_2, the O_2 depletion

method is not as accurate at underventilated conditions and, therefore, the combustion efficiency data presented here is calculated from CO and CO_2 generation.

Ideal maximum combustion efficiency is unity. However, the maximum possible combustion efficiency is considerably lower for underventilated conditions. For equivalence ratios greater than one, available oxygen becomes the limiting factor of how much fuel can be burned. The maximum possible combustion efficiency, Xc_{max}, can be expressed as:

$$Xc_{max} = 1 \qquad \text{for } \phi<1 \qquad [2.9a]$$

$$Xc_{max} = 1/\phi \qquad \text{for } \phi>1 \qquad [2.9b]$$

2.4.1.4 Quasi-Steady State Period

A quasi-steady-state period was identified for each fire during the time at which the equivalence ratio leveled out and, in some cases, about the time at which the equivalence ratio peaked. All quantities were averaged over 20 second periods for most fires of hexane and polyurethane and for 60 seconds for most PMMA and underventilated spruce fires depending on the length of the steady-state period. Typically, the experiments ran for 250 to 1000 seconds (i.e., time from ignition to burn out). The quasi-steady-state nature of the fires is discussed in detail in section 3.3.1. The results presented are quasi-steady-state averages except where otherwise noted.

2.4.2 Upper Layer-Sampled Experiments

Upper layer-sampled experiments were conducted to study the generation of CO in the upper layer of two layer compartment fires. Except for several tests discussed below,

all of the tests were conducted with the gas sampling probe placed 13 cm into the compartment through the center of the exhaust vent.

A set of tests were conducted to characterize and to determine the uniformity of the upper layer in the compartment. Due to the quasi-steady-state nature and relatively short burning time of the fires, it was not possible to sample in various locations in the upper layer during a single test. Therefore, a series of hexane fires with the same initial conditions were burned and the upper layer was sampled in a different location for each test.

The initial conditions were chosen to result in a fire with a high equivalence ratio, thereby, encompassing both over and underventilated conditions in one experiment. Each test consisted of 1.19 kg of hexane burning in a 23 cm diameter pan with a 25-cm-wide by 16-cm-high exhaust vent. The initial compartment temperature was approximately 30 C for each test. The upper layer was sampled at 4 locations: A) 13 cm in through the center of the exhaust vent, B) in the front right corner, 30 cm in from each wall and 28 cm down from the ceiling, C) in the back right corner, 30 cm in from each wall and 28 cm down from the ceiling and D) in the back right corner, 30 cm in from each wall and 14 cm down from the ceiling. Locations A and B were sampled with probes that extended through the exhaust vent. Since locations C and D were in the back of the compartment, the gas sampling probe was inserted through the ceiling instead of through the exhaust duct to avoid passing the probe through the fire plume. An unshielded thermocouple was positioned in each corner of the compartment 30 cm from the walls and at the same depth as the probe. The aspirated thermocouple tree placed in the front right corner provided vertical temperature distributions. The results of this set of experiments is presented in section 3.2.2.

The videos obtained of the upper layer-sampled tests were used to correlate instantaneous equivalence ratios with the time that various modes of external burning occurred. The videos of the interior of the compartment provided times at which layer ignition occurred and measurements of layer depths.

2.4.3 Downstream-Sampled Experiments

Downstream-sampled experiments were conducted to study the effect of external burning on the levels of CO leaving the compartment. The downstream-sampled tests consisted of burning hexane-fueled fires under the same conditions as the hexane-fueled upper layer-sampled tests. Sampling downstream of the compartment in the exhaust duct provided measurements of the effect of external burning on the yields of CO and CO_2 exiting the compartment compared to the initial yields in the upper layer. Smoke measurements during the periods of external burning were compared to smoke levels just prior to the phenomenon.

CHAPTER 3

RESULTS: CHEMICAL SPECIES PRODUCTION IN THE UPPER LAYER

3.1. Introduction

This chapter presents the results of the upper layer-sampled tests for all fuels burned. General observations of layer development are presented and discussed along with the results for the tests designed to examine upper layer uniformity. Results presented for each fuel include a description of the general burning dynamics of the fuel and the correlations between layer composition and the plume equivalence ratio.

3.2 Upper Layer Development and Uniformity

The window in the side of the compartment allowed visual observation of the layer interface. For all fuels, the upper layer quickly formed to a depth below the exhaust vent. The upper layer depth varied depending on the fuel and the time into the fire. The layer formed to a depth corresponding to the top of the fuel source in the case of spruce and polyurethane (70 to 100 cm). For PMMA and hexane, typical overventilated layer depths were approximately 54 cm. For underventilated conditions the layer interface descended to a depth that was about 23 cm above the PMMA and hexane fuel surface (i.e., a depth of 86 cm). The fire plume extended into the upper layer for all fires.

The layer interface was characterized by horizontal flow of upper layer gases toward the plume and, although wavy in nature, there appeared to be no mixing between layers except at the plume. This implies that all air in the upper layer entered through the plume. The layer interface was generally 2 to 5 cm-thick. Visual observation confirmed that a distinct recirculating flow pattern developed in the upper layer due to the buoyant

force of the plume and the establishment of the thermal layer interface. For overventilated fires, the fire plumes were smaller and ceiling flame jets were small or nonexistent. Ceiling and wall flame jets were observed for underventilated fires for all fuels, however, layer burning only occurred for the hexane fires and possibly for several PMMA fires. The occurrence of layer burning was hard to detect for PMMA fires due to excessive smoke build up on the window. For very underventilated hexane fires, layer burning occurred and the upper layer appeared to be engulfed in flame as viewed through the observation window. Upon layer burning, the layer interface became thicker and more turbulent as cellular flame zones appeared along the interface.

A set of tests were conducted to characterize the upper layer in the compartment. Due to the quasi-steady-state nature and relatively short burning time of the fires, it was not possible to sample in various locations in the upper layer during a single test. Therefore, a series of hexane fires with the same initial conditions were burned and the upper layer was sampled in a different location for each test as described in section 2.4.2.

Figure 3.1 shows the layer temperature profiles from the vertical aspirated rake during the quasi-steady-state period for each fire, A, B, C and D. It can be seen that the upper layer is quite uniform during the quasi-steady-state period. The data also shows that the fires were quite reproducible; thus, justifying that data comparison between probe sampling locations can be accomplished with different fires.

It should be noted that in some instances, temperatures deviated up to 20 percent from top to bottom in the layer. This appeared to occur more so during the transition to underventilated conditions and for the overventilated polyurethane and spruce fires. Typically the more underventilated fires for all fuels had uniform temperature distributions. This is attributed to the larger ceiling and wall jets which enhanced mixing

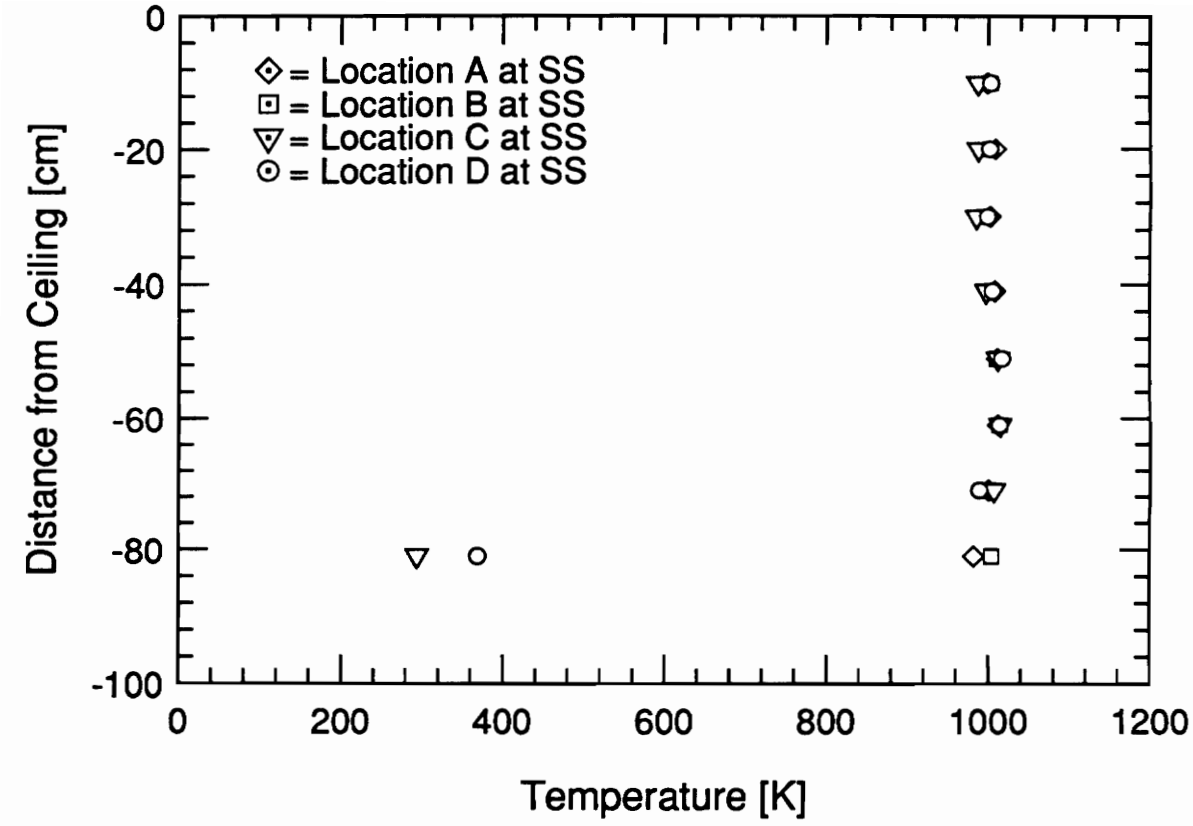

Figure 3.1 Instantaneous upper layer vertical temperature profiles for four hexane fires used to study upper layer uniformity. Profiles correspond to a time midway through the steady-state period.

in the upper layer. Figure 3.2 shows the time history of the equivalence ratio for each of the four fires. The similarity between curves is a second check that the tests are essentially the same considering the turbulent nature of these fires.

The lateral thermal uniformity of the upper layer can be seen in Figure 3.3 which shows the temperature time histories at each corner of the upper layer for fire C. This plot is typical for all the fires studied. The upper layer temperature varied within 40 K from corner to corner except at the beginning of the quasi-steady-state period. At this time all fires were observed to have a peak elevated temperature of approximately 40 to 100 K higher in the back right corner than in the other corners. Although this peak is not fully explained, this time was observed to correspond to the time just after layer burning started. Typically, the upper layer was characterized by about a 20 K temperature rise from front to back in the compartment. This was due to the fact that the inlet duct was attached to the front of the compartment which created a flow pattern leading to more air entrainment into the front of the fire plume. The plume was observed to be slightly deflected towards the rear of the compartment for all fires.

The comparison of upper layer composition measurements obtained for different sampling locations is presented in Figures 3.4 to 3.6. Figure 3.4 shows the CO concentration for the four fires. Considering that the sampling locations were obtained for different fires which vary to some degree, the CO concentration is quite similar between sampling locations; the CO concentration deviates within ± 9 percent from the steady-state average of 3.2 for all four fires.

Figure 3.5 shows the CO_2 concentration time profiles for the four sampling locations. Similar to the CO, there is no appreciable difference between sampling

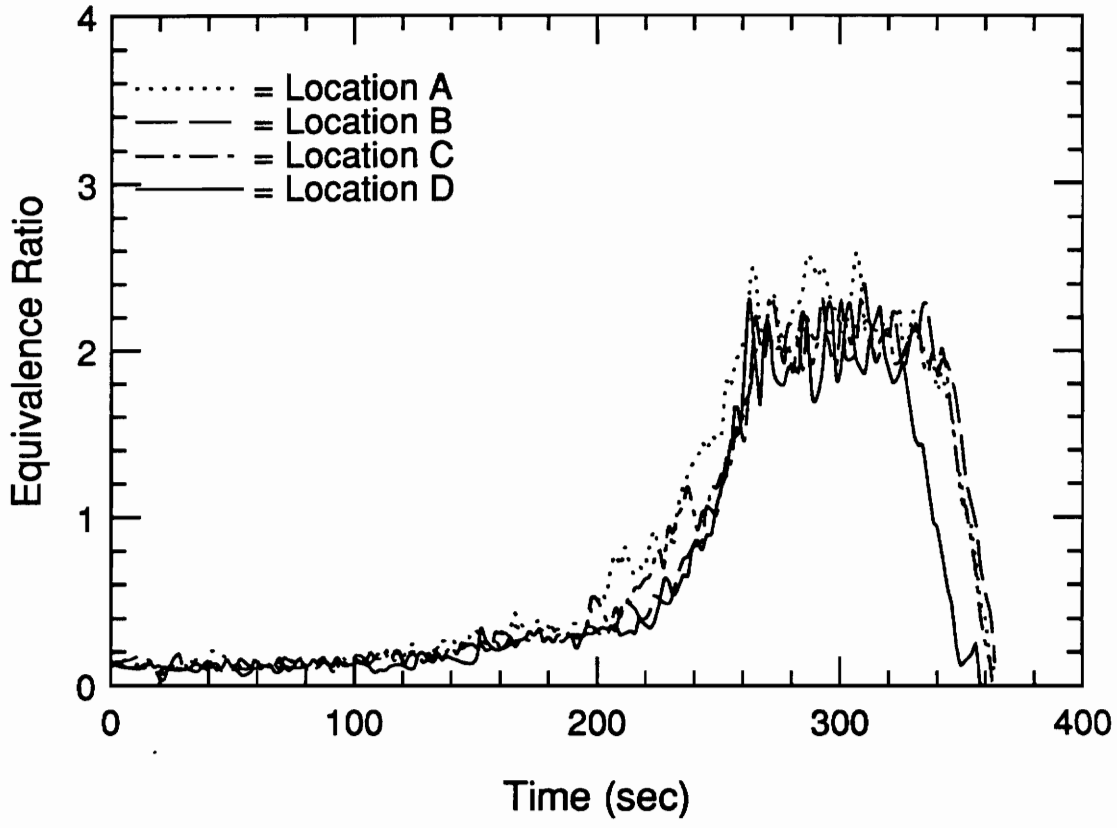

Figure 3.2 Time history of equivalence ratio for each of four fires used in the upper layer uniformity study.

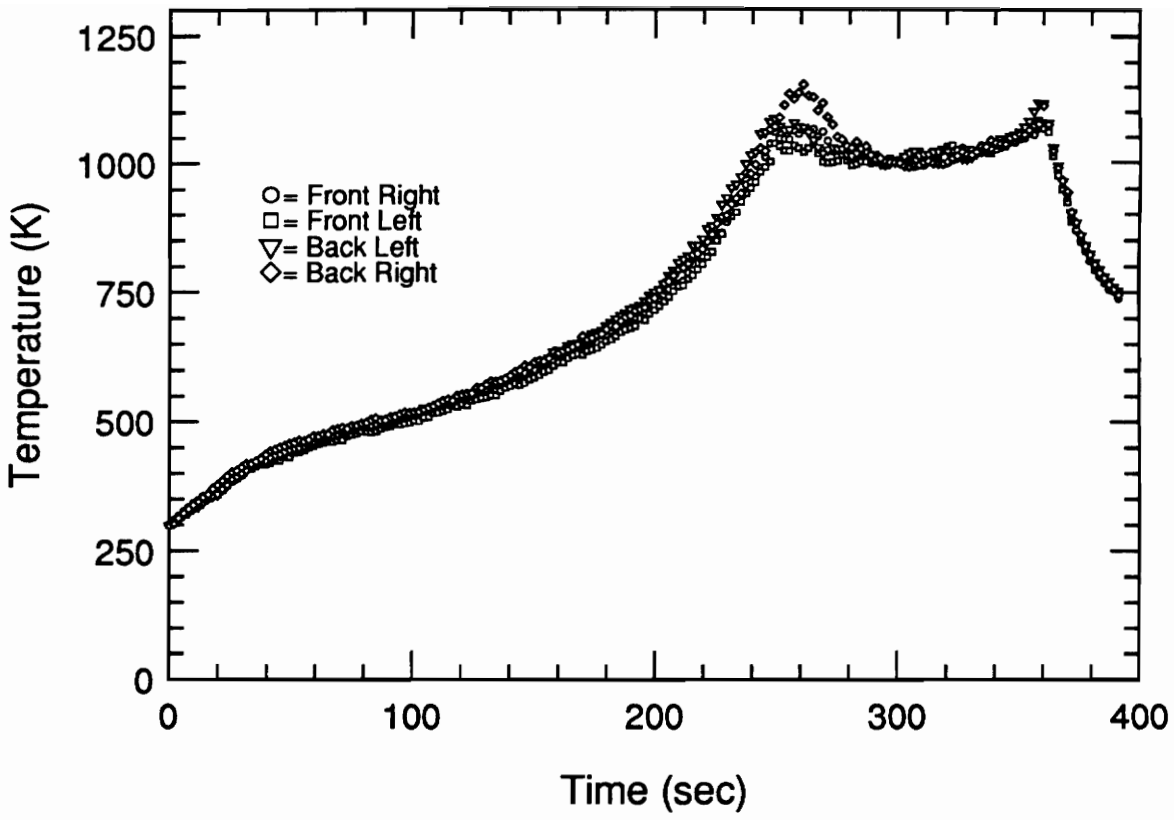

Figure 3.3 Temperature time histories at each corner of the upper layer for fire C of the upper layer uniformity study.

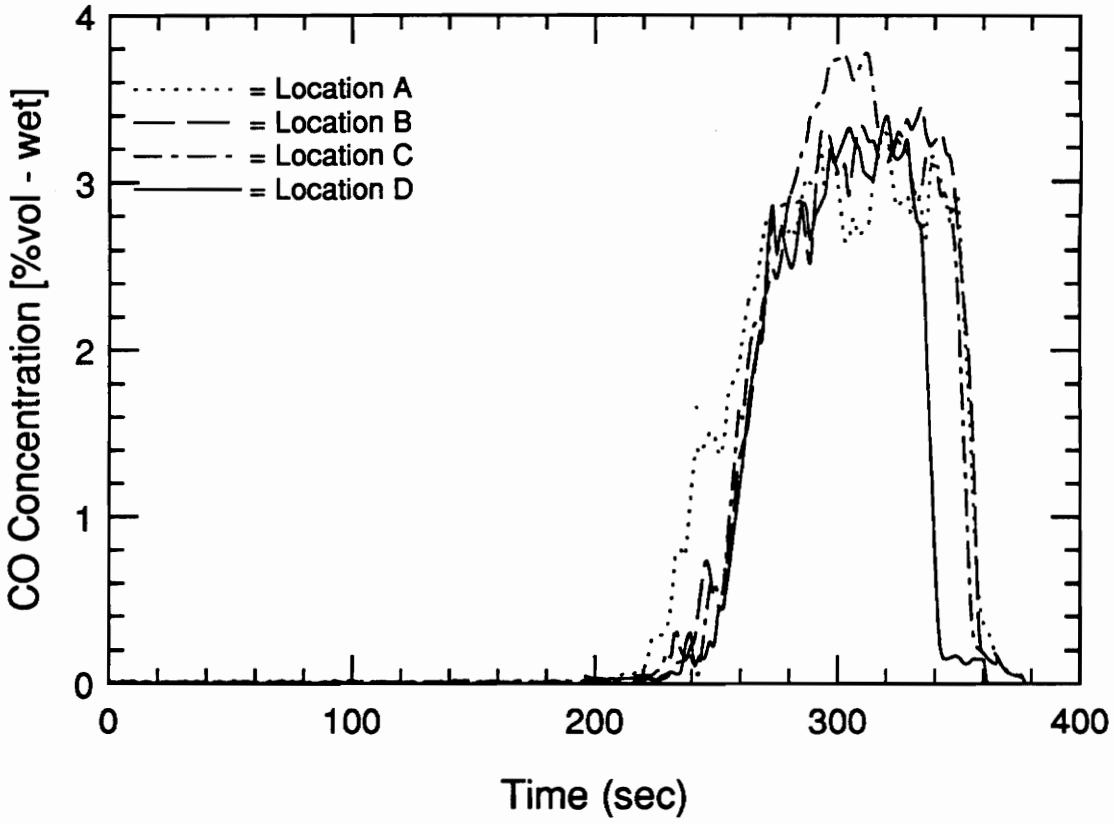

Figure 3.4 Comparison of transient CO concentrations sampled at four locations in the upper layer (fires A through D of upper layer uniformity study).

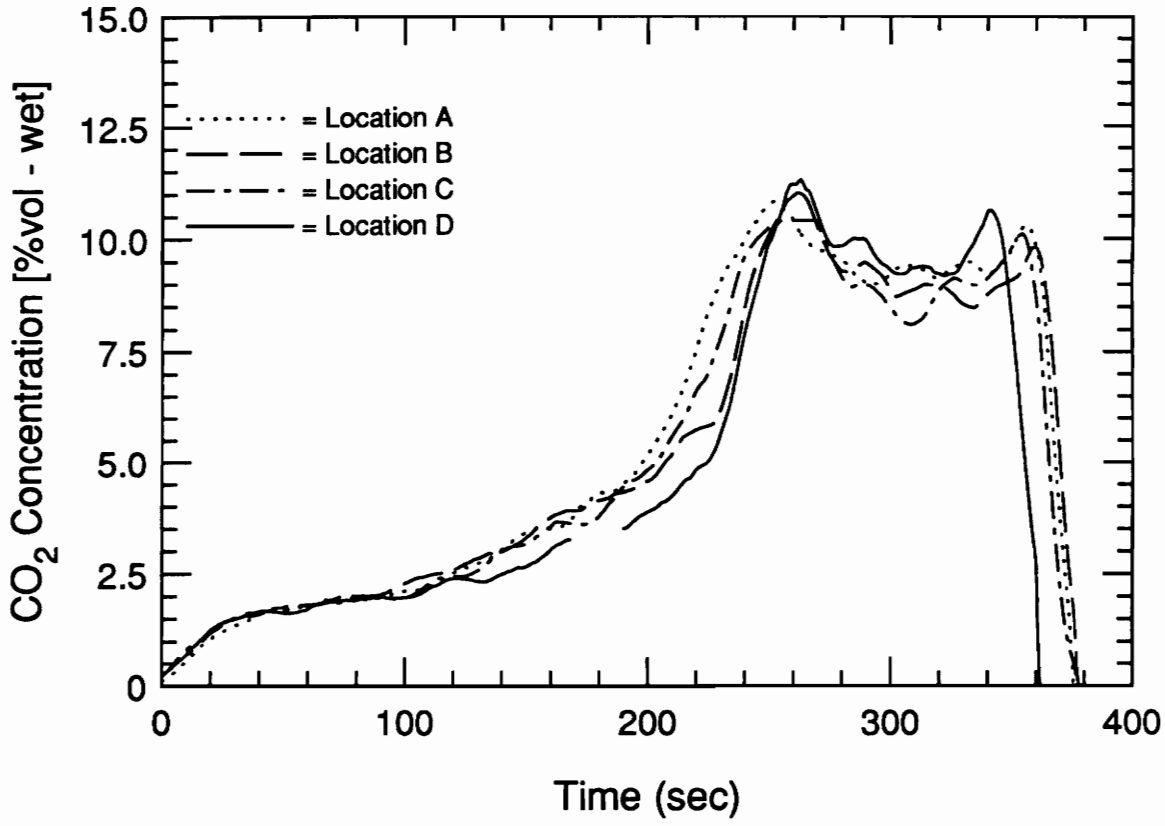

Figure 3.5 Comparison of transient CO_2 concentrations sampled at four locations in the upper layer (fires A through D of upper layer uniformity study).

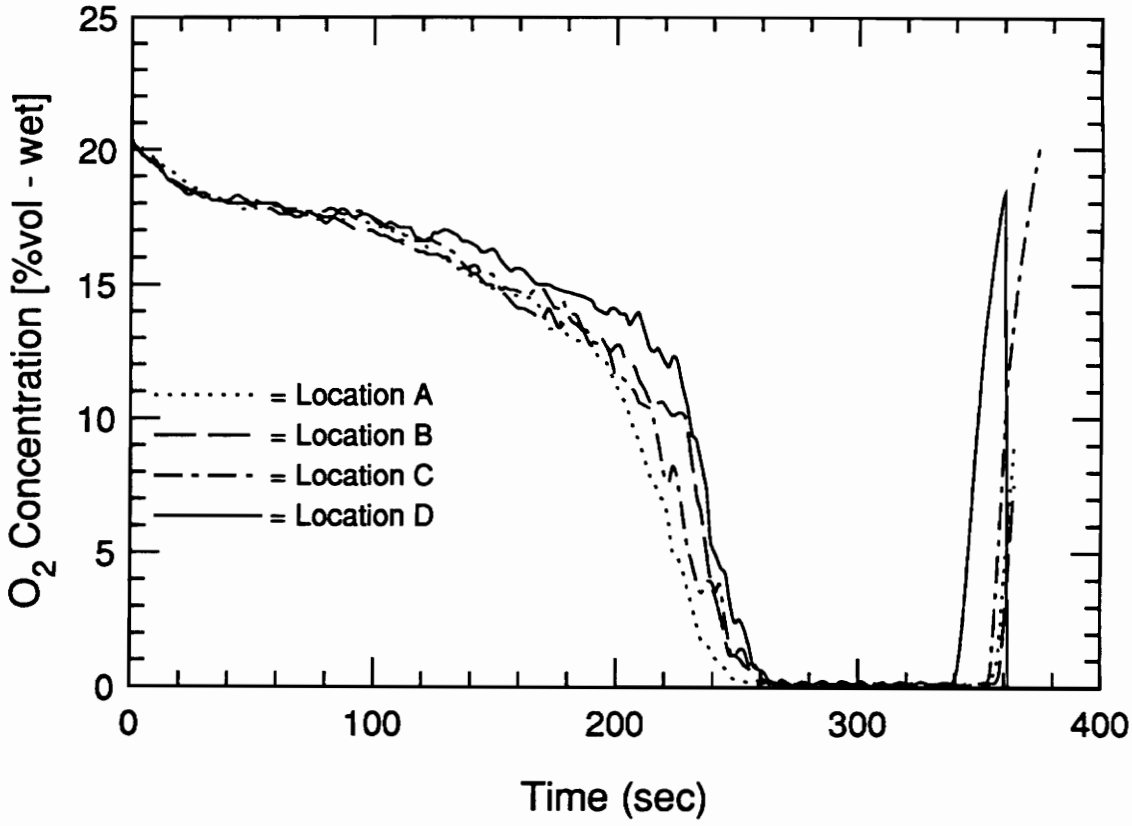

Figure 3.6 Comparison of transient O_2 concentrations sampled at four locations in the upper layer (fires A through D of upper layer uniformity study).

locations. Figure 3.6 also shows that during the quasi-steady-state period the O_2 concentration is independent of sampling location. Therefore, both the temperature and gas concentration measurements show that the upper layer can be considered uniform. Visual observation of the smoke patterns and flow dynamics also suggested a well-mixed layer.

3.3 Hexane

A large range of hexane fires was burned with theoretical heat release rates ranging from 75 to 665 kW. A typical time history of equivalence ratio, and CO and O_2 concentrations for a hexane fire is presented in Figure 3.7. As can be seen by the equivalence ratio, the fire burned slowly at first and accelerated as the temperature of the upper layer increased. A steady-state burning period developed toward the end of the fire and then rapid burnout occurred as denoted by the sudden rise in O_2 and sudden decrease in CO, CO_2 and the plume equivalence ratio. The rapid burnout of fuel is typical of pan fires as the decreasing volume allows the fuel to heat and volatilize more quickly. Shorter steady-state periods were observed for overventilated fires.

The CO concentration is typically near zero (less than 1000 ppm) for overventilated conditions and increases quickly as the fire becomes underventilated. In this case a hazardous level of 3.5 percent CO was maintained during the steady-state period. During the transition to underventilated conditions the O_2 concentration decreases quickly to less than 0.02 percent.

Figure 3.8 shows the average upper layer temperature plotted against the equivalence ratio for each hexane fire. The average upper layer temperature is the average of the top four aspirated thermocouple measurements in the compartment, i.e.,

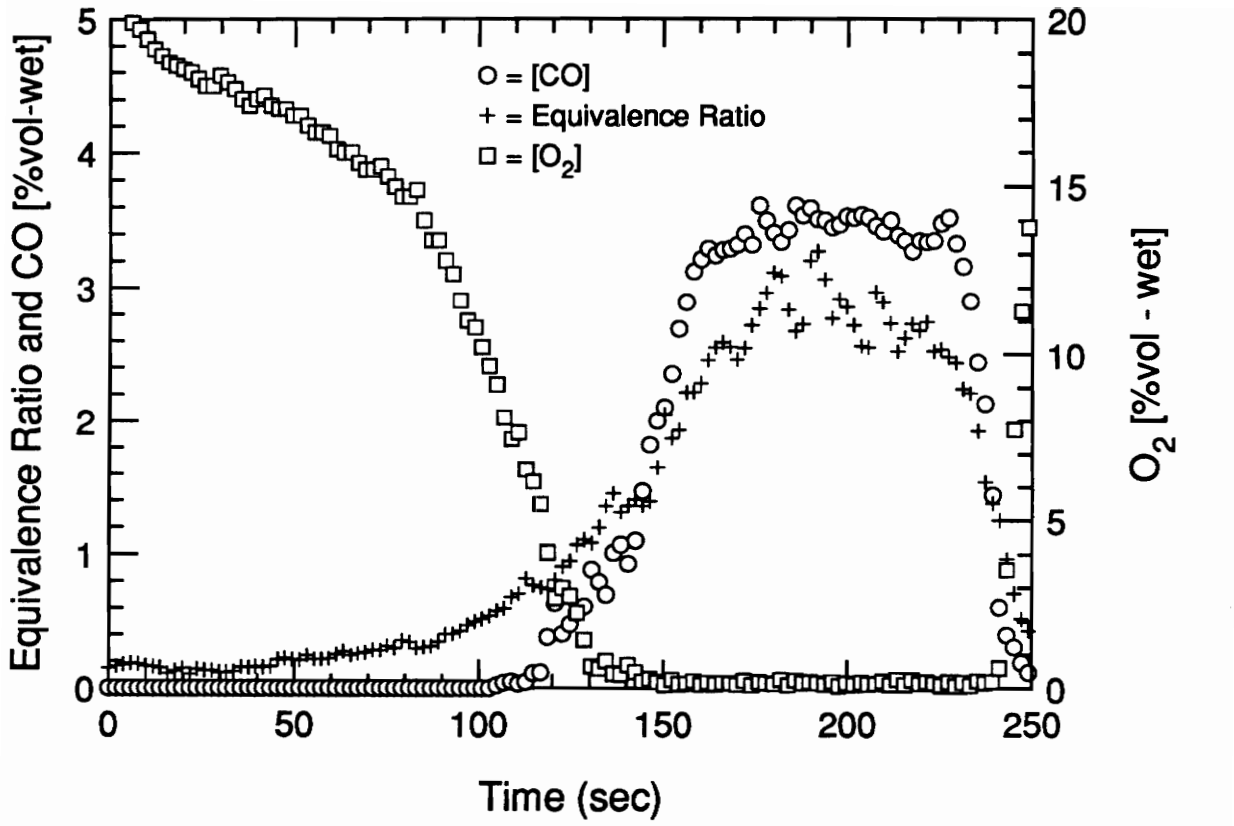

Figure 3.7 Typical time history of species concentrations and plume equivalence ratio for a hexane compartment fire.

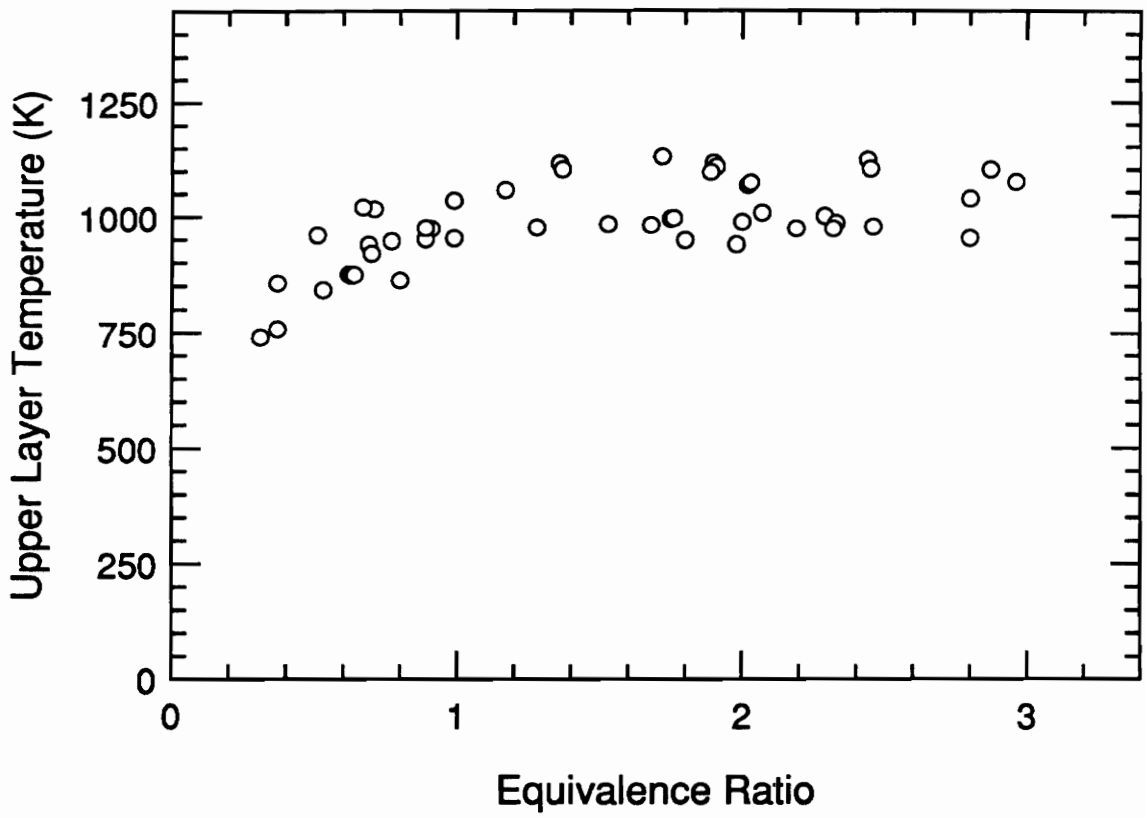

Figure 3.8 Average upper layer temperature versus plume equivalence ratio for hexane compartment fires.

about the top half of the enclosure. The temperature rises with increasing equivalence ratio for overventilated fires and levels out to a fairly constant value for underventilated fires. For underventilated fires it was observed that the temperature was dictated by the size of the fire. Primarily all upper layer temperatures less than or equal to 1000 K were for fire with 400 kW theoretical heat release rates or less. Larger fires (> 400 kW) had upper layer temperatures of approximately 1100 K.

The upper layer CO concentrations are plotted against the equivalence ratio in Figure 3.9 for the compartment fires and Beyler's hood fires. Beyler's data is included in all plots of species concentrations for the purpose of future comparison and is not discussed in this chapter. Comparison of correlations between experiments is discussed in section 4.2.3. As can be seen, a clearly defined correlation exits for the compartment fires. For overventilated fires, CO concentrations are below 0.2 percent. With increasing underventilated conditions, fires produced more CO. The peak concentrations observed were over 3.5 percent for fires with equivalence ratios about 3.

Figure 3.10 shows the upper layer CO_2 concentration plotted against the equivalence ratio for all hexane fires. The concentrations are correlated quite well by the equivalence ratio. The CO_2 concentration increases with equivalence ratio for overventilated conditions and peaks at about 11 percent for near stoichiometric conditions. Underventilated fires with higher equivalence ratios produced less CO_2 as more CO was formed.

Figure 3.11 shows the upper layer O_2 concentration plotted against the equivalence ratio for all hexane fires. The upper layer oxygen concentration decrease with increasing equivalence ratio. Low O_2 concentrations (less than 5 percent) were observed for even

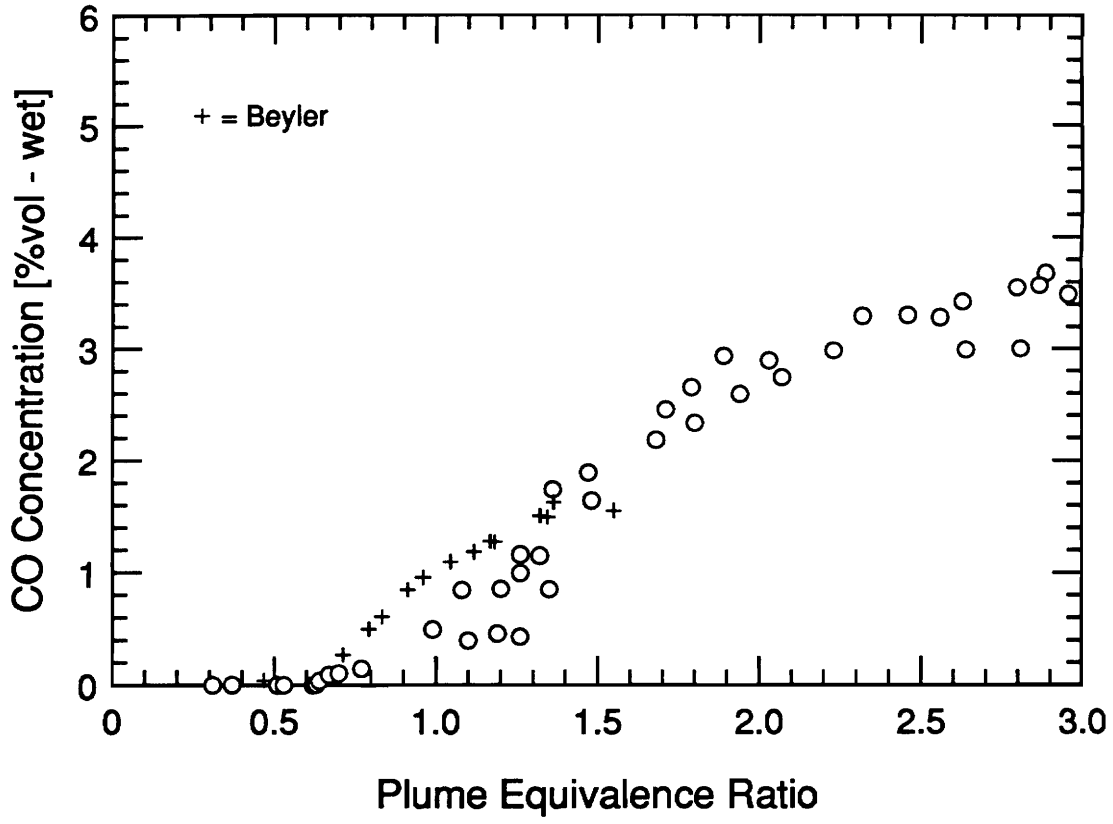

Figure 3.9 Upper layer CO concentration versus plume equivalence ratio for hexane compartment fires and Beyler's hood fires.

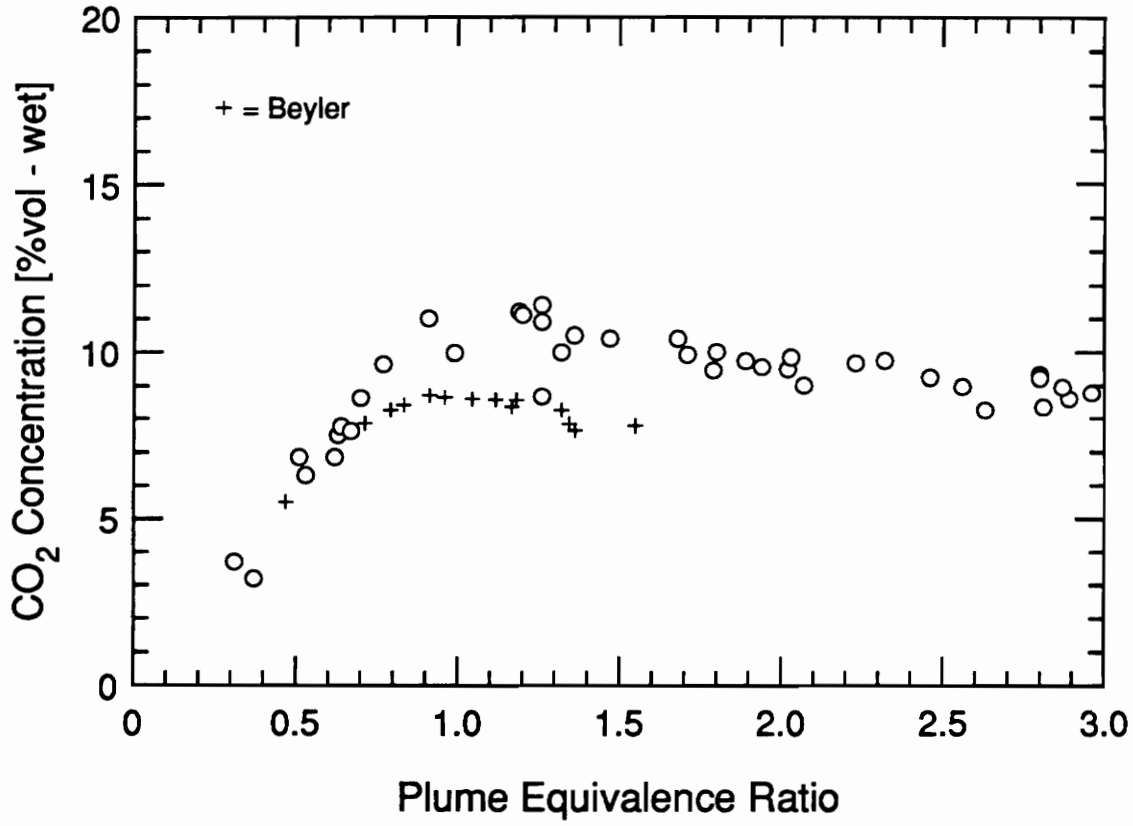

Figure 3.10 Upper layer CO_2 concentration versus plume equivalence ratio for hexane compartment fires and Beyler's hood fires.

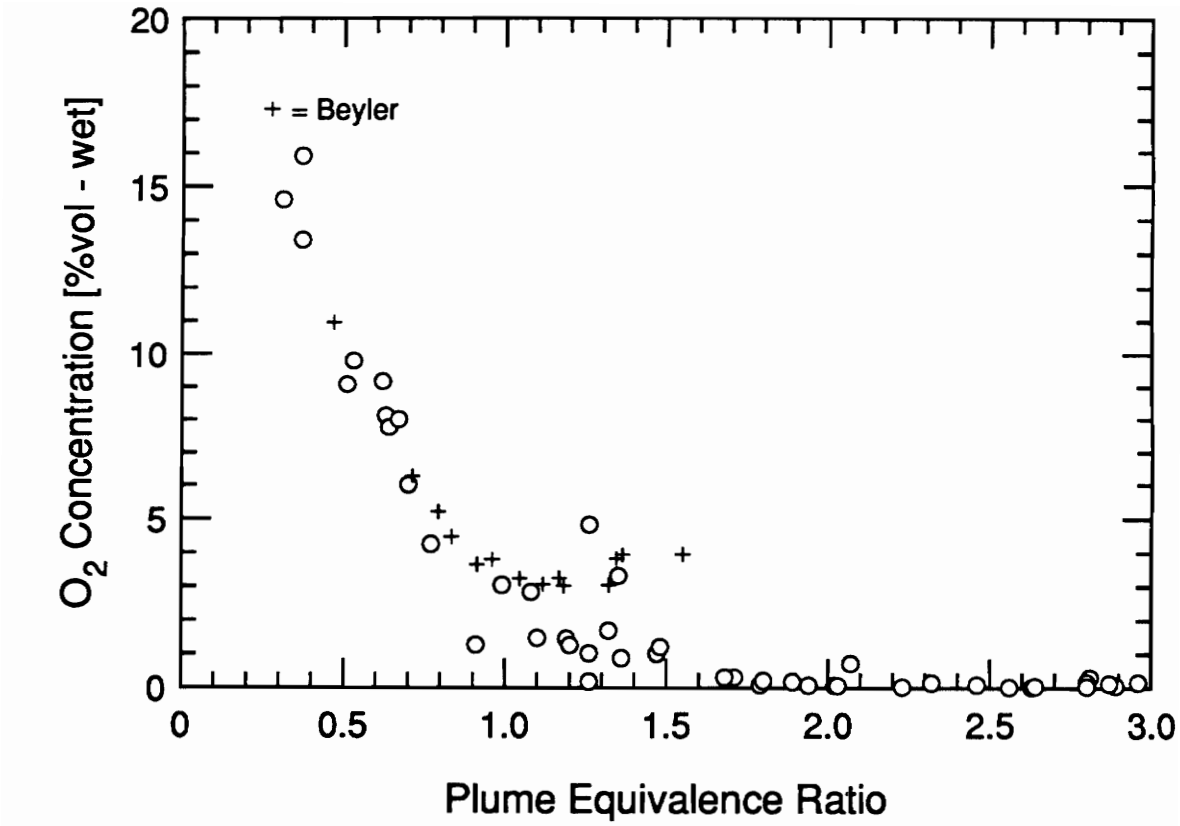

Figure 3.11 Upper layer O_2 concentration versus plume equivalence ratio for hexane compartment fires and Beyler's hood fires.

slightly overventilated fires. For very underventilated fires ($\phi_p > 1.5$) all available oxygen is completely consumed by the fire.

The hexane fire normalized CO yields are plotted versus the plume equivalence ratio in Figure 3.12. The figure shows that the upper layer CO yield is well correlated with the plume equivalence ratio. Carbon monoxide yields are near zero for fires with equivalence ratios less than 0.6. Above ϕ_p of 0.6, CO yields start to rise; however, significant levels (> 0.05) are obtained only for underventilated fires. Carbon monoxide yields increase dramatically with equivalence ratio for the range of ϕ_p between 1 and 1.5. For equivalence ratios greater than 1.5 the CO yield appears to level out to an average, constant value of 0.11. The data may also be interpreted as decreasing slightly with equivalence ratio the for these highly underventilated fires.

As can be seen in Figure 3.13, the CO_2 yield correlates well with the plume equivalence ratio. The simple model discussed in section 2.4.1.2 is included on all CO_2 and O_2 yield plots for comparison. The CO_2 yield is approximately one for overventilated conditions and decreases proportionately as $1/\phi_p$ with increasing underventilated conditions. A similar correlation is observed for the normalized O_2 yield, Figure 3.14. However, the O_2 yield agrees quite well with the simple model.

Figure 3.15 shows the transient CO yield versus equivalence ratio data for a hexane fire that obtained a steady-state average ϕ_p of 3. The transient data is for the same fire shown in Figure 3.7 and includes data for each sampling time up to the mid point of the steady-state period. The correlation between the transient CO yield and the equivalence ratio is quite good. As can be seen in Figures 3.16 and 3.17, similarly well defined correlations are observed for the transient CO_2 and O_2 yields for the same fire as in

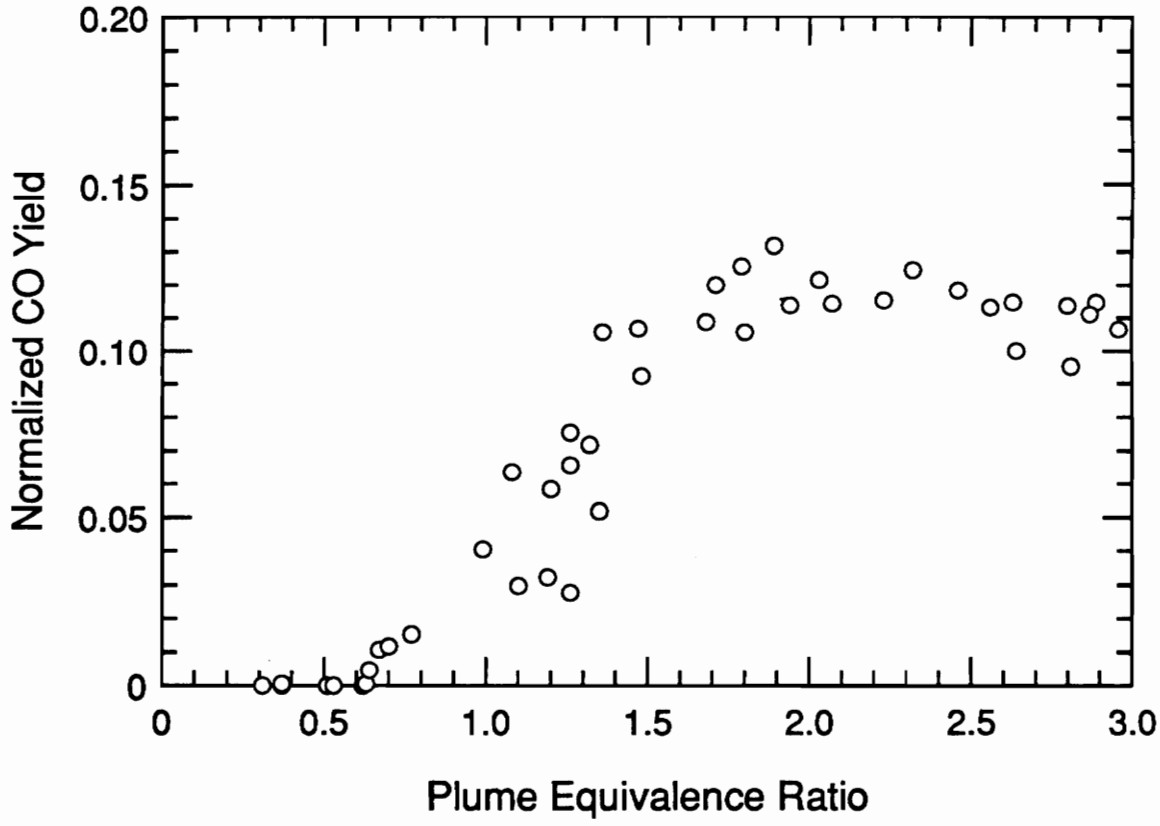

Figure 3.12 Upper layer normalized CO yield versus plume equivalence ratio for hexane compartment fires.

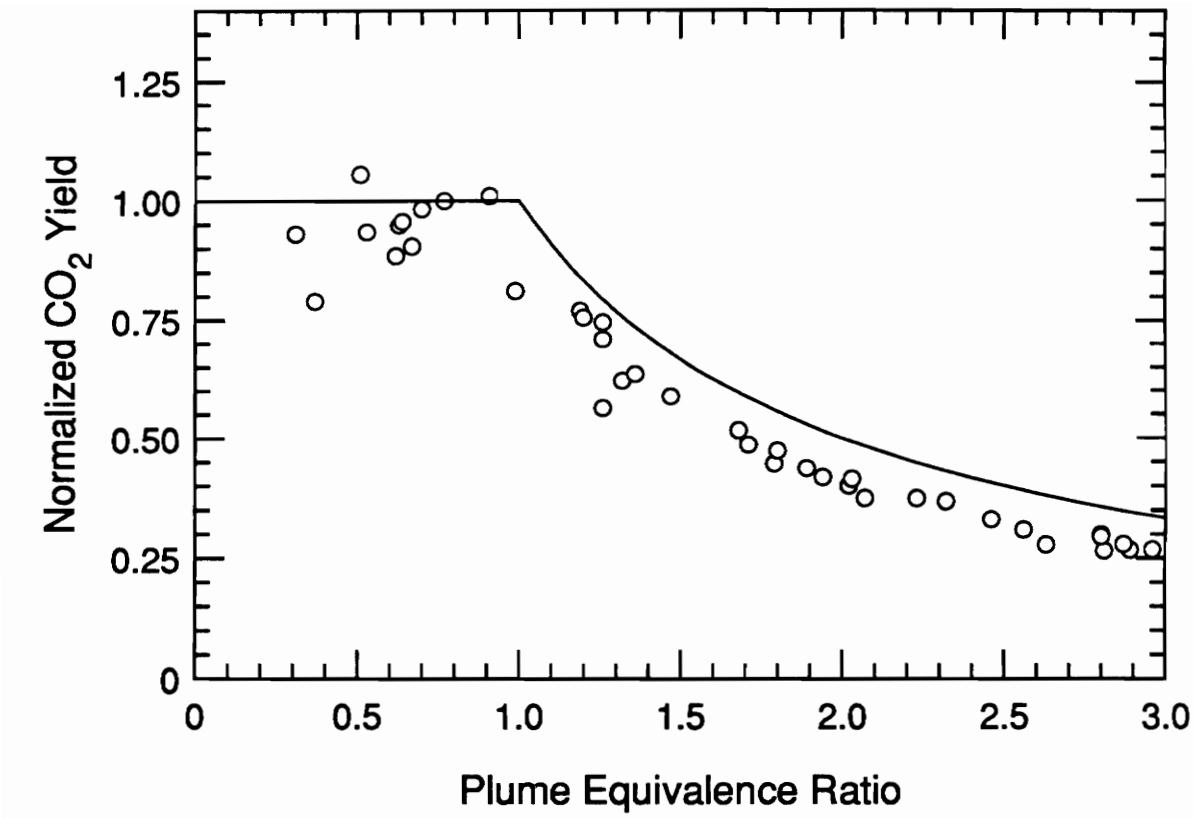

Figure 3.13 Upper layer normalized CO_2 yield versus plume equivalence ratio for hexane compartment fires.

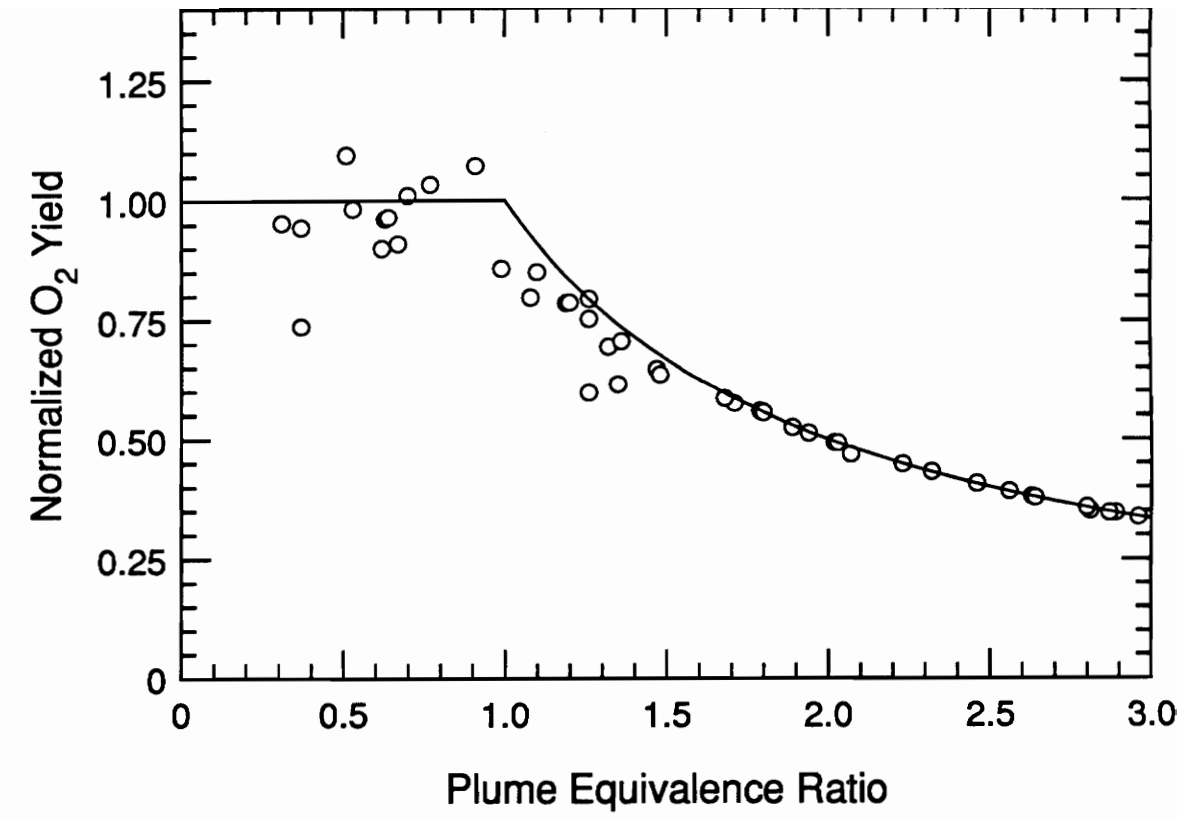

Figure 3.14 Upper layer normalized O_2 yield versus plume equivalence ratio for hexane compartment fires.

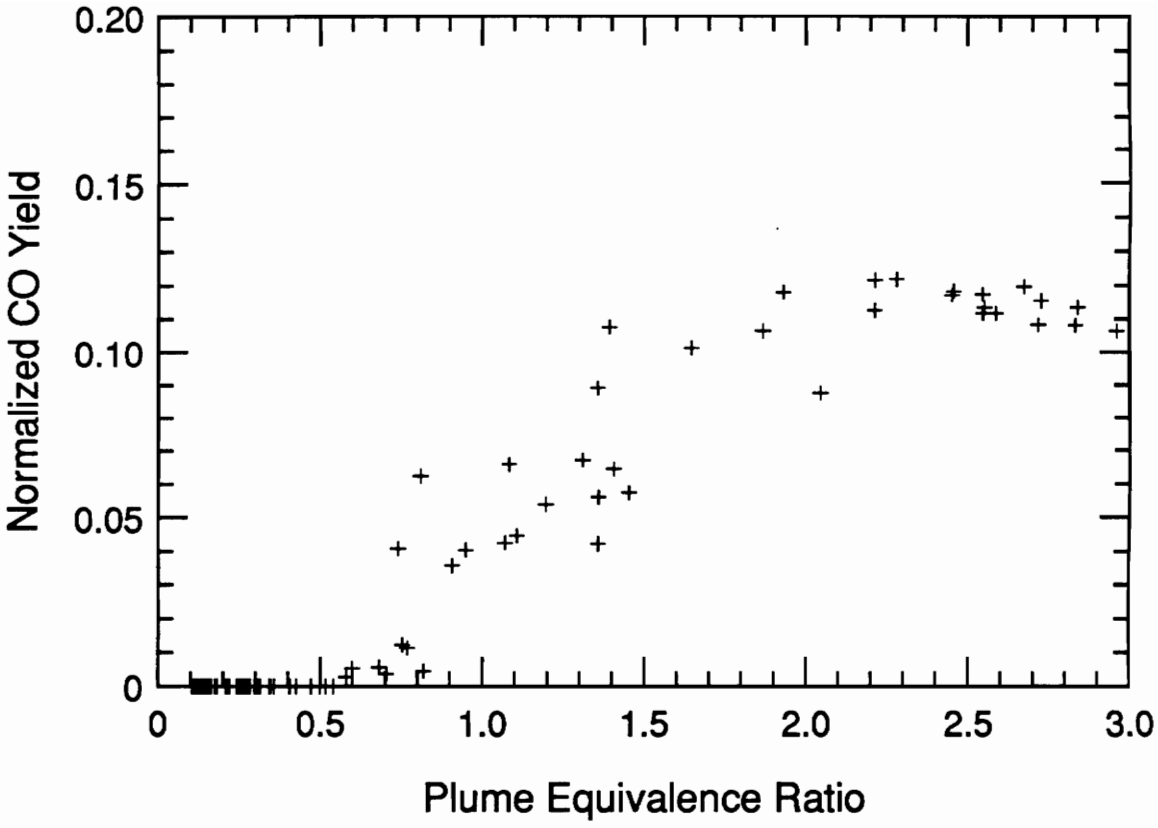

Figure 3.15 Transient, upper layer normalized CO yield versus plume equivalence ratio for a hexane compartment fire with an average steady-state ϕ_p of 3.

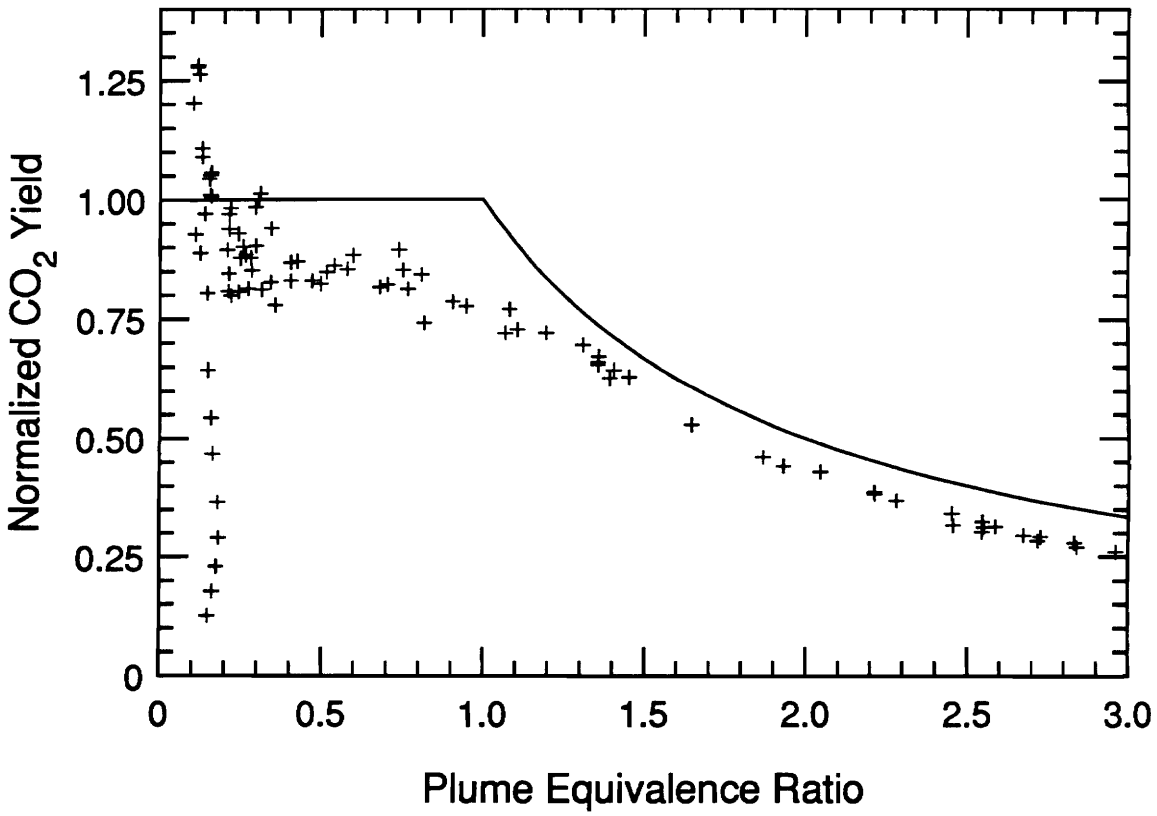

Figure 3.16 Transient, upper layer normalized CO_2 yield versus plume equivalence ratio for a hexane compartment fire with an average steady-state ϕ_p of 3.

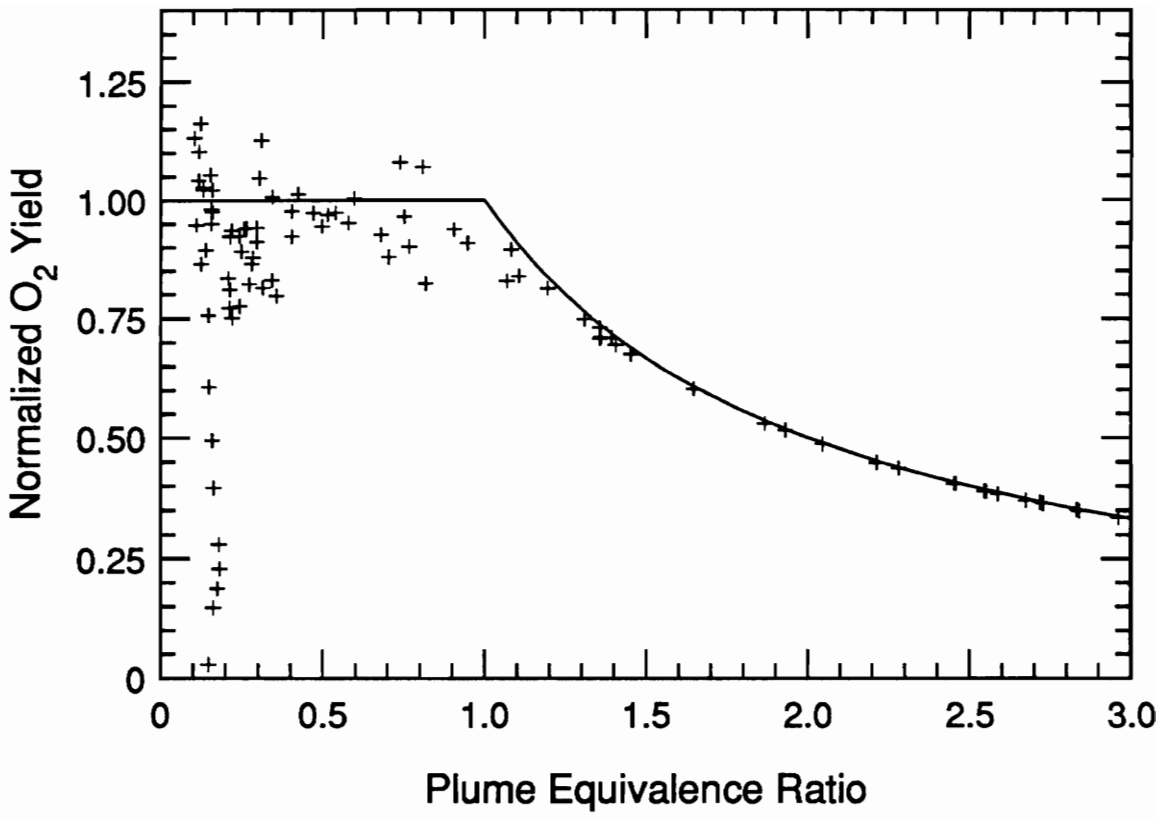

Figure 3.17 Transient, upper layer normalized O_2 yield versus plume equivalence ratio for a hexane compartment fire with an average steady-state ϕ_p of 3.

Figure 3.15. The very low CO_2 and O_2 yields at equivalence ratios below 0.2 are not physically representative and are a result of not accounting for the initial air in the compartment before the layer is established. Generally close agreement is seen between the transient data and the model, more so for the O_2 yields. The largest deviation from the model occurs for CO_2 in the range of ϕ_p from 0.5 to about 1.

The transient total hydrocarbon yield data is plotted with the steady-state data in Figure 3.18. The yield of unburned hydrocarbons is near zero for $\phi_p < 1$ and rises with equivalence ratio for underventilated conditions. For the experiments with THC measurements, the yield of residual carbon ranged from 0.04 to 0.3 for equivalence ratios from 0.64 to 3.0, respectively. However, typical values ranged from 0.1 to 0.2. The increase in residual carbon with the equivalence ratio can be partially attributed to the increase in soot formation and possibly loss of higher molecular weight hydrocarbons in the sampling system for the very underventilated fires. Beyler typically observed residual carbon yields of 0.1. Considering the maximum ϕ observed by Beyler was 1.55 these results are consistent when compared for similar equivalence ratios.

The unnormalized smoke yield data is presented in Figure 3.19. Due to the location of the smoke measurement device in the exhaust duct, the measurements reflect downstream smoke yields. In the case of fires with external burning ($\phi_p > 1.7$, see chapter 5) downstream smoke yields are lower than the yield of smoke exiting the compartment. Despite the large scatter in the data, the smoke yield is observed to be constant for overventilated fires at an average of 0.016, and a decrease in smoke yields is observed for fires with $\phi_p > 1.7$.

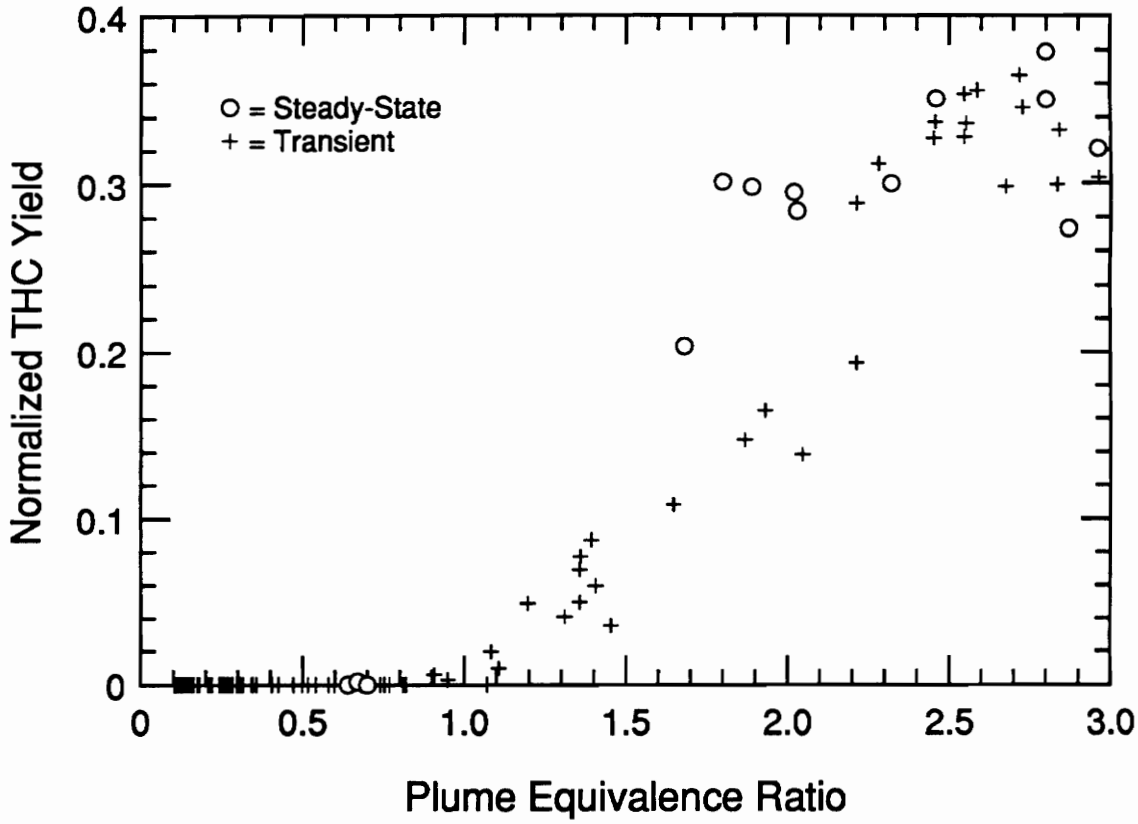

Figure 3.18 Transient, upper layer normalized total hydrocarbon yield versus plume equivalence ratio for a hexane compartment fire with an average steady-state ϕ_p of 3. Steady-state data for all hexane compartment fires is also plotted.

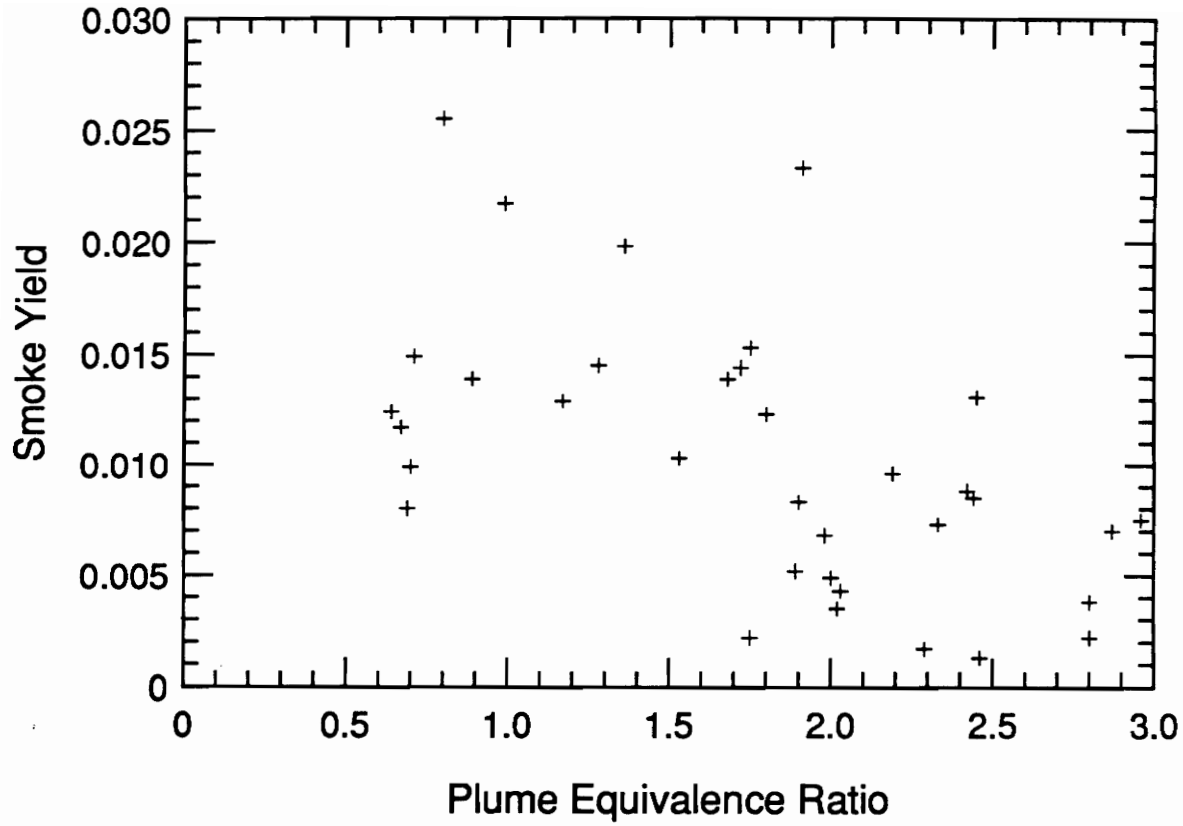

Figure 3.19 Unnormalized smoke yield versus plume equivalence ratio for hexane compartment fires.

3.4 PMMA

Theoretical heat release rates ranged from 30 to 400 kW for the PMMA fires studied. A typical time history of equivalence ratio, and CO and O_2 concentrations is presented in Figure 3.20. As can be seen by the equivalence ratio, the fire burned slowly at first and then accelerated to a steady burning condition. Similar to the hexane fires a steady-state burning period developed toward the end of the fire with rapid burnout of the fuel as denoted by the sudden rise in O_2 and the sudden decrease in CO, CO_2 and the plume equivalence ratio. Overventilated fires were characterized with slower transitions to the peak burning rate.

Similar to the hexane results, the CO concentrations are near zero for overventilated conditions and increase quickly as fires become underventilated. A concentration of 5.6 percent is observed just prior to the fuel burning out. The oxygen concentration approaches zero as CO formation starts to occur. There is no measurable O_2 in the upper layer during the quasi-steady burning period. The increase in O_2 concentration at a time of about 200 seconds is due to the burn out of the PMMA shavings used to ignite the slab.

Figure 3.21 shows the average upper layer temperature plotted against the equivalence ratio for each PMMA fire. Temperatures ranged from 536 to 1412 K for the fires examined. The layer temperature rises with increasing equivalence ratio for overventilated fires and levels out to a fairly constant value for underventilated fires. The scatter in the underventilated temperatures is fairly reflective of the theoretical heat release rates for each fire.

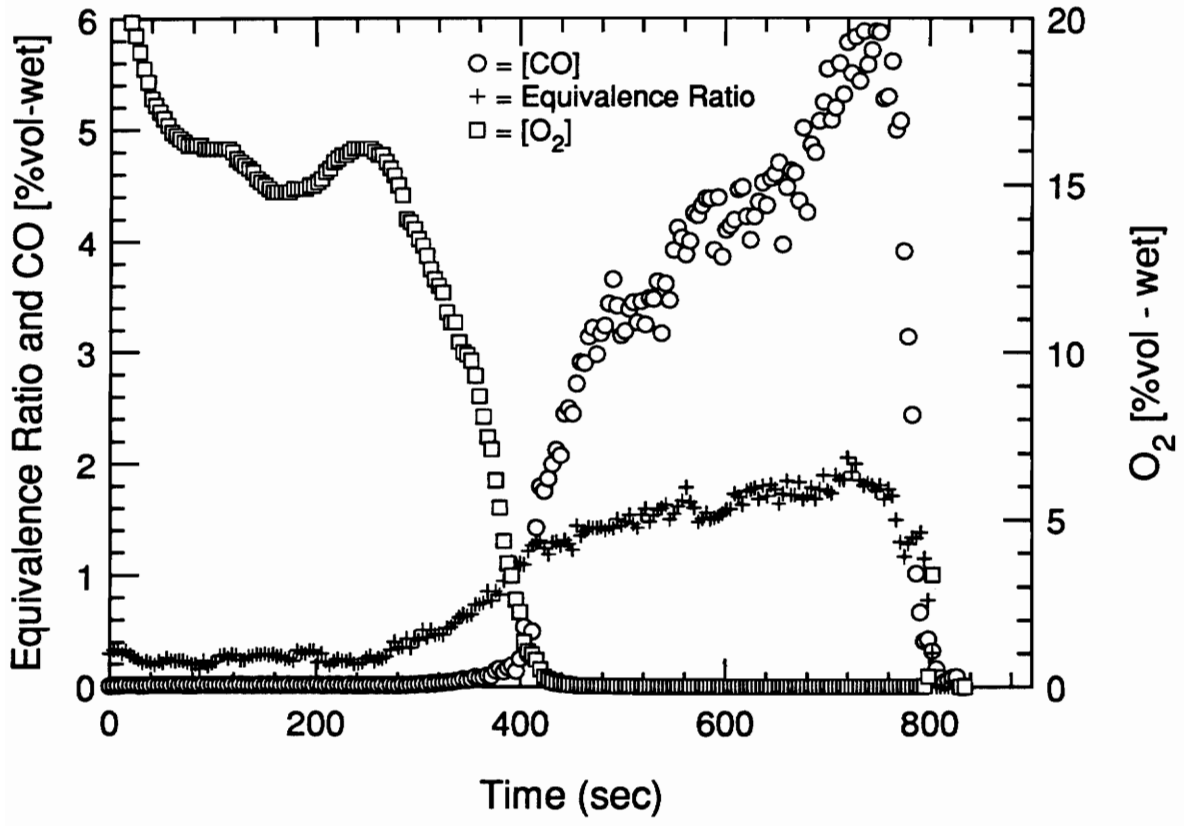

Figure 3.20 Typical time history of species concentrations and plume equivalence ratio for a PMMA compartment fire.

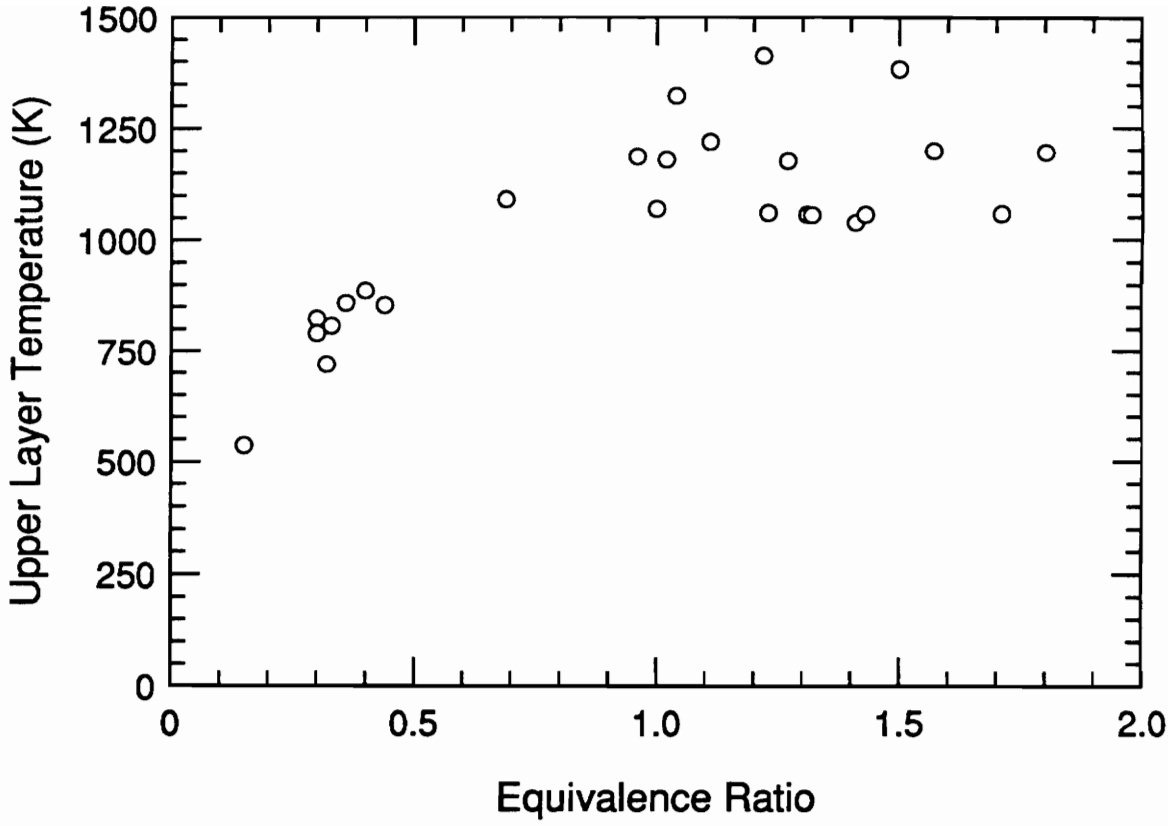

Figure 3.21 Average upper layer temperature versus plume equivalence ratio for PMMA compartment fires.

The upper layer CO concentrations are plotted against equivalence ratio in Figure 3.22. For overventilated fires, CO concentrations are essentially zero. The data shows the general trend of higher CO production for fires with higher equivalence ratios. However the highest CO concentrations (5.6 and 6.3 percent) were observed for fires with equivalence ratios of about 1.4. These two fires were for the largest sized samples burned, however, the burning rates were approximately half that of other samples of the same size. As a result, the upper layer temperatures were among the lowest observed. The high concentrations are not fully explained.

Figure 3.23 shows the upper layer CO_2 concentration plotted against the equivalence ratio for all PMMA fires. The concentrations are correlated reasonably well by using the equivalence ratio. The CO_2 concentration increases with equivalence ratio for overventilated conditions and appears to peak at 15 percent, slightly rich of stoichiometric conditions.

Figure 3.24 shows the upper layer O_2 concentration plotted against the equivalence ratio for all PMMA fires. The same general behavior is observed as noted for hexane. For overventilated fires, the upper layer oxygen concentration decreases with increasing equivalence ratios and is nearly zero for all underventilated fires.

The normalized PMMA CO yields are plotted versus the plume equivalence ratio in Figure 3.25. The figure shows that the upper layer CO yield is reasonably correlated with the plume equivalence ratio. The correlation is qualitatively similar to the CO concentration in Figure 3.22. For overventilated fires, the yields are negligible (below 0.005). Above ϕ_p of 1.0, CO yields increase with equivalence ratio. The maximum yield observed was 0.3. The higher CO yields for fires with ϕ_p of approximately 1.2 to 1.4 are

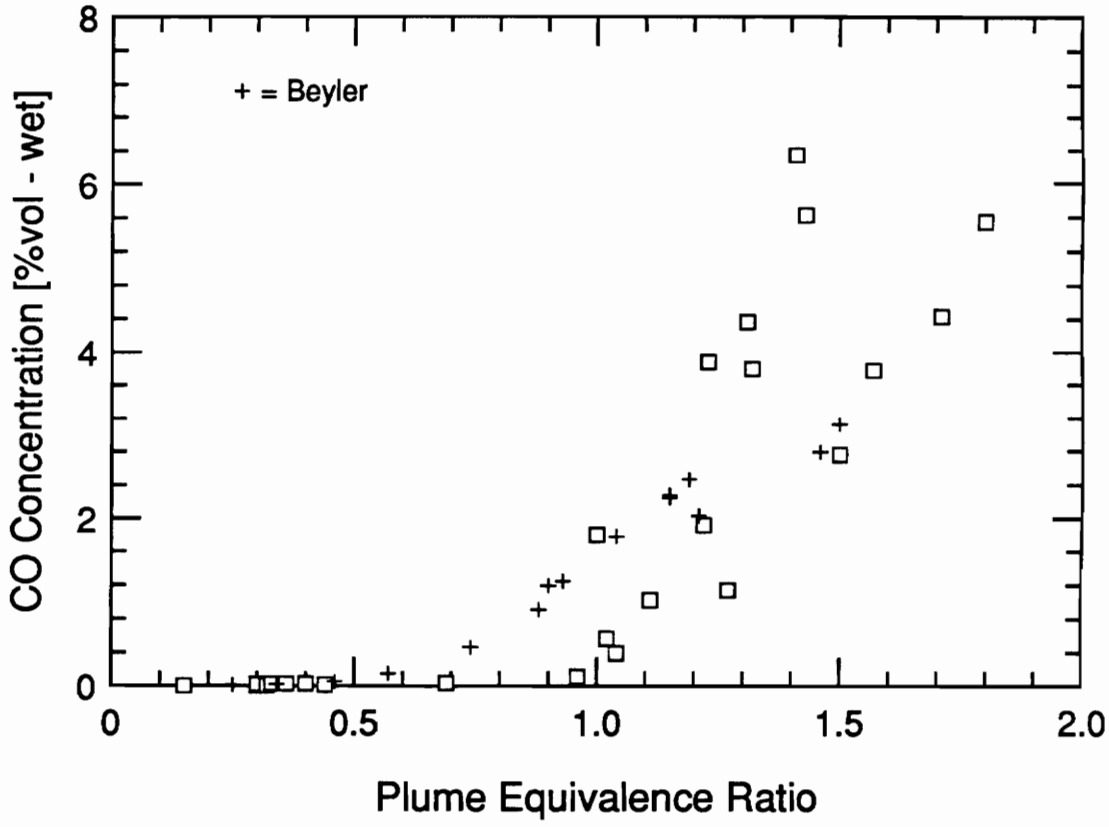

Figure 3.22 Upper layer CO concentration versus plume equivalence ratio for PMMA compartment fires and Beyler's hood fires.

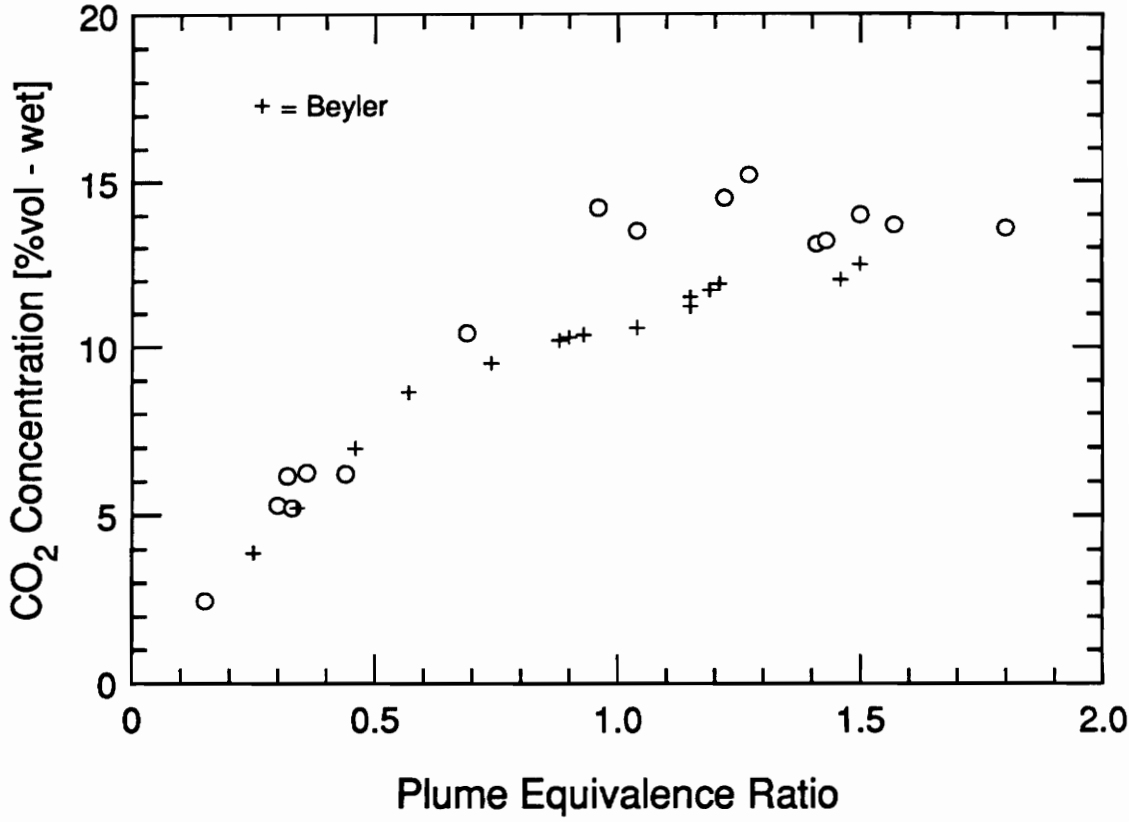

Figure 3.23 Upper layer CO_2 concentration versus plume equivalence ratio for PMMA compartment fires and Beyler's hood fires.

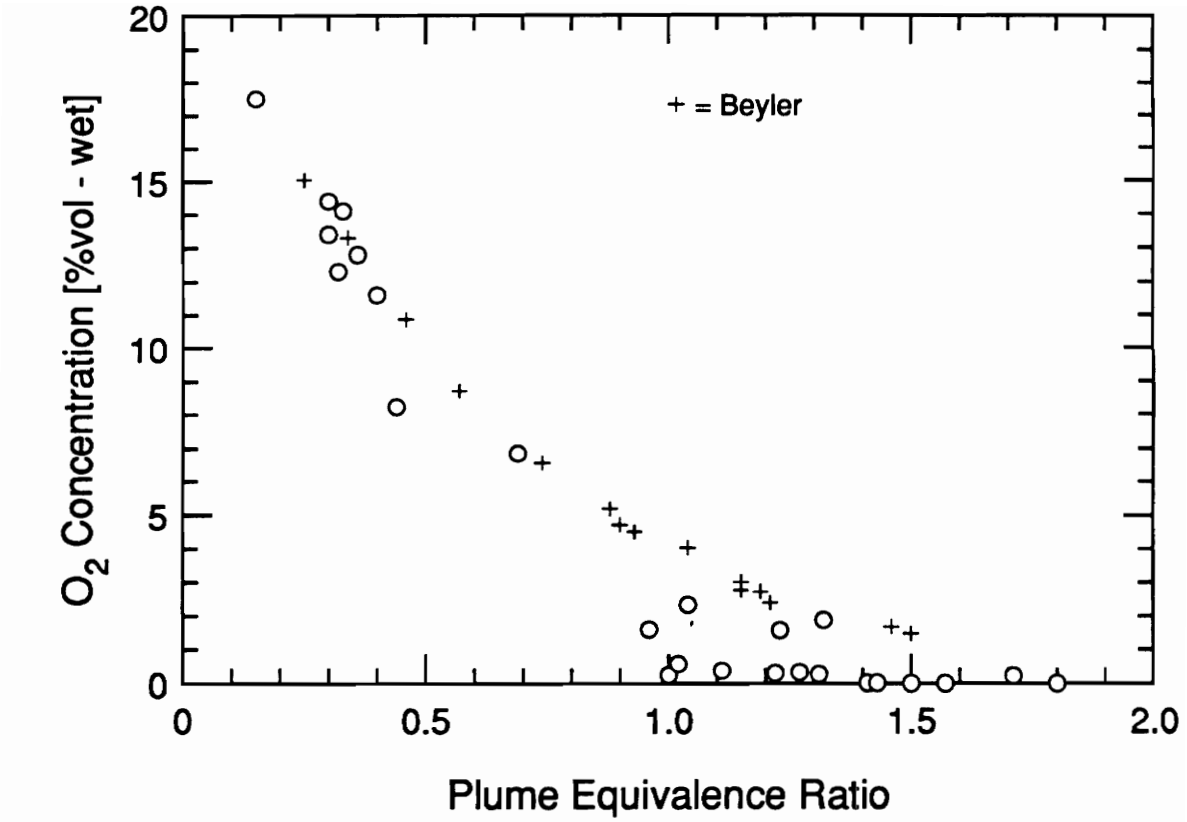

Figure 3.24 Upper layer O_2 concentration versus plume equivalence ratio for PMMA compartment fires and Beyler's hood fires.

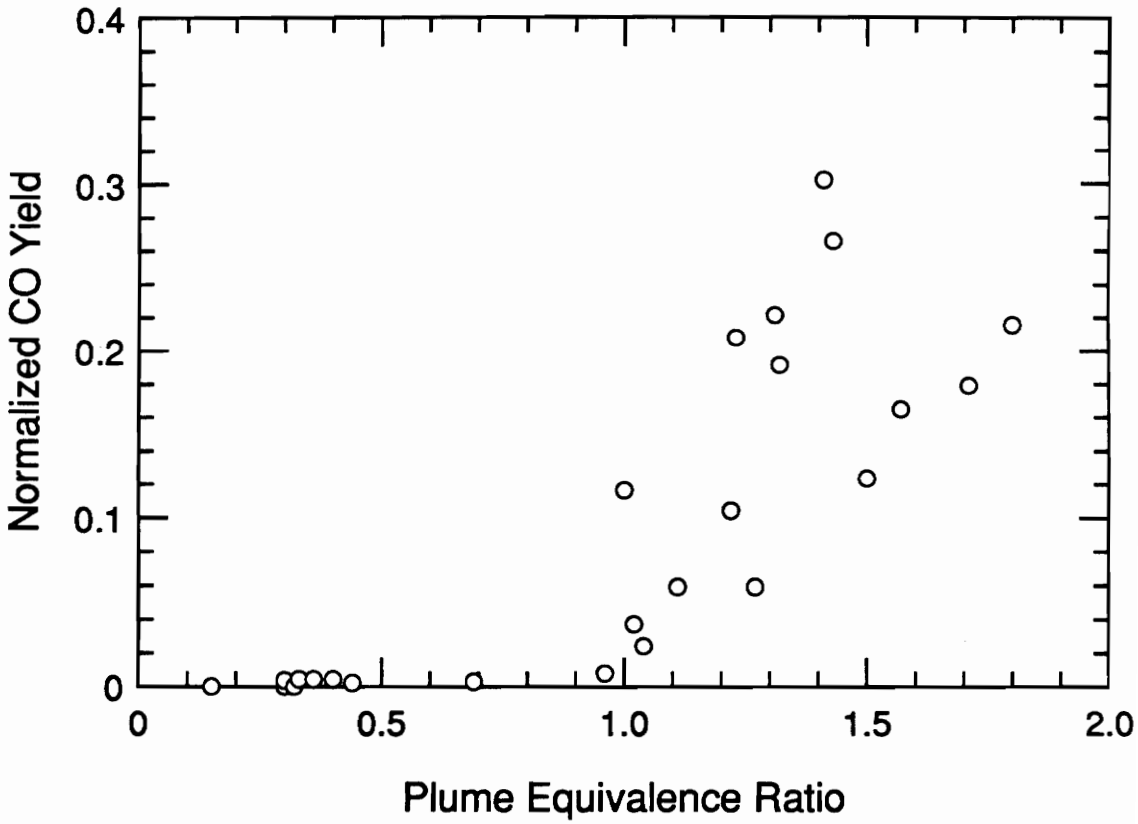

Figure 3.25 Upper layer normalized CO yield versus plume equivalence ratio for PMMA compartment fires.

partially attributed to temperature as is discussed in section 4.3. These fires had upper layer temperatures (~1050 K) that were 150 to 350 K below the fires with yields of about 0.1 and similar equivalence ratios.

As can be seen in Figure 3.26 and 3.27, the CO_2 and O_2 yields correlate well with the plume equivalence ratio for the PMMA fires studied. In both cases, the average overventilated yields are about 1, in agreement with the model. The scatter at low equivalence ratios is due to the low burning rates being of the order of the load cell resolution. The yields decrease proportionately as $1/\phi_p$ with increasing underventilated conditions. The O_2 yield agrees quite well with the simple model, while CO_2 is consistently lower.

Figure 3.28 shows the transient CO yield versus equivalence ratio data for a PMMA fire that obtained a steady-state average ϕ of 1.8. The transient data is for the same fire shown in Figure 3.20 and includes data for each sampling time up to the midpoint of the quasi-steady-state period. Figures 3.29 and 3.30, present the similar transient correlations obtained for the CO_2 and O_2 yields for the same fire as in Figure 3.28. As discussed for hexane the very low CO_2 and O_2 yields are not physically representative and should be ignored. For both species, the transient yield is approximately 0.2 to 0.25 below the expected value of one for overventilated conditions, but agree quite well with the model for underventilated conditions.

3.5 Spruce

Theoretical heat release rates for spruce fires ranged from 71 to 171 kW. A typical time history of equivalence ratio, and CO and O_2 concentrations is presented in Figure 3.31. Spruce-fueled fires burned rapidly after ignition and reached quasi-steady-state

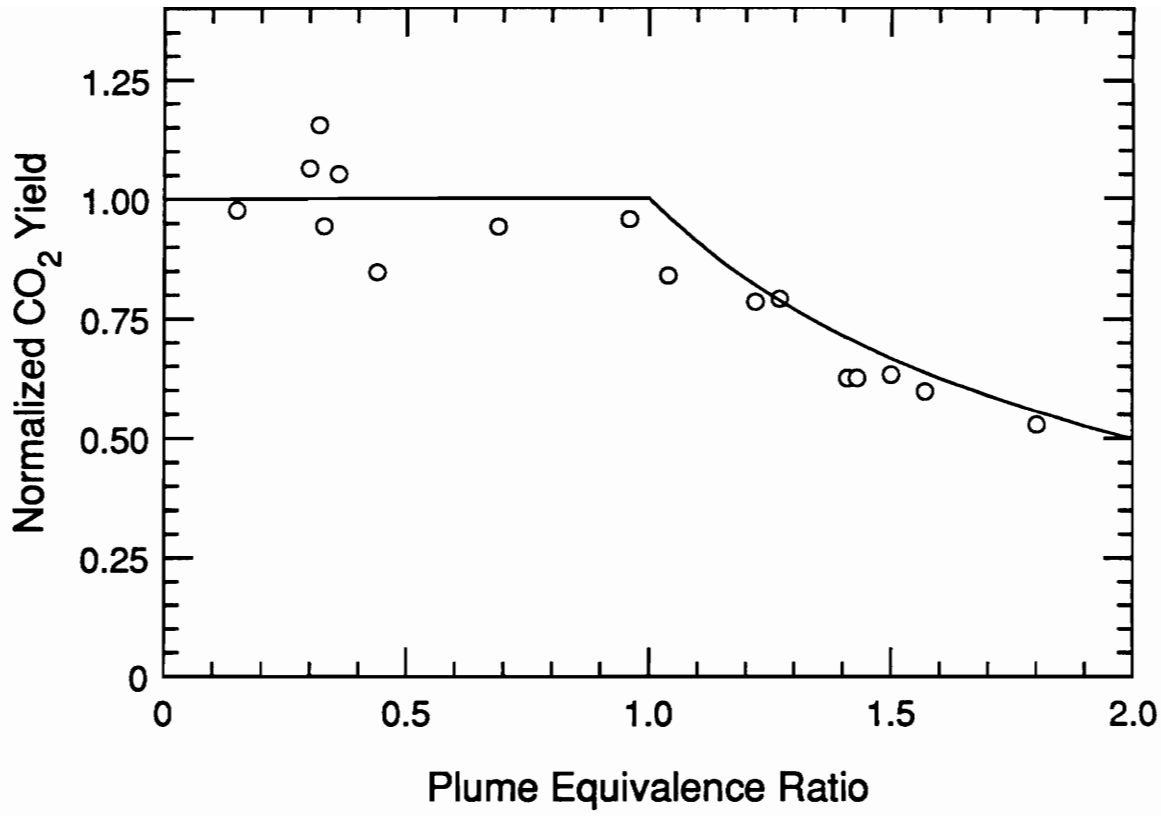

Figure 3.26 Upper layer normalized CO_2 yield versus plume equivalence ratio for PMMA compartment fires.

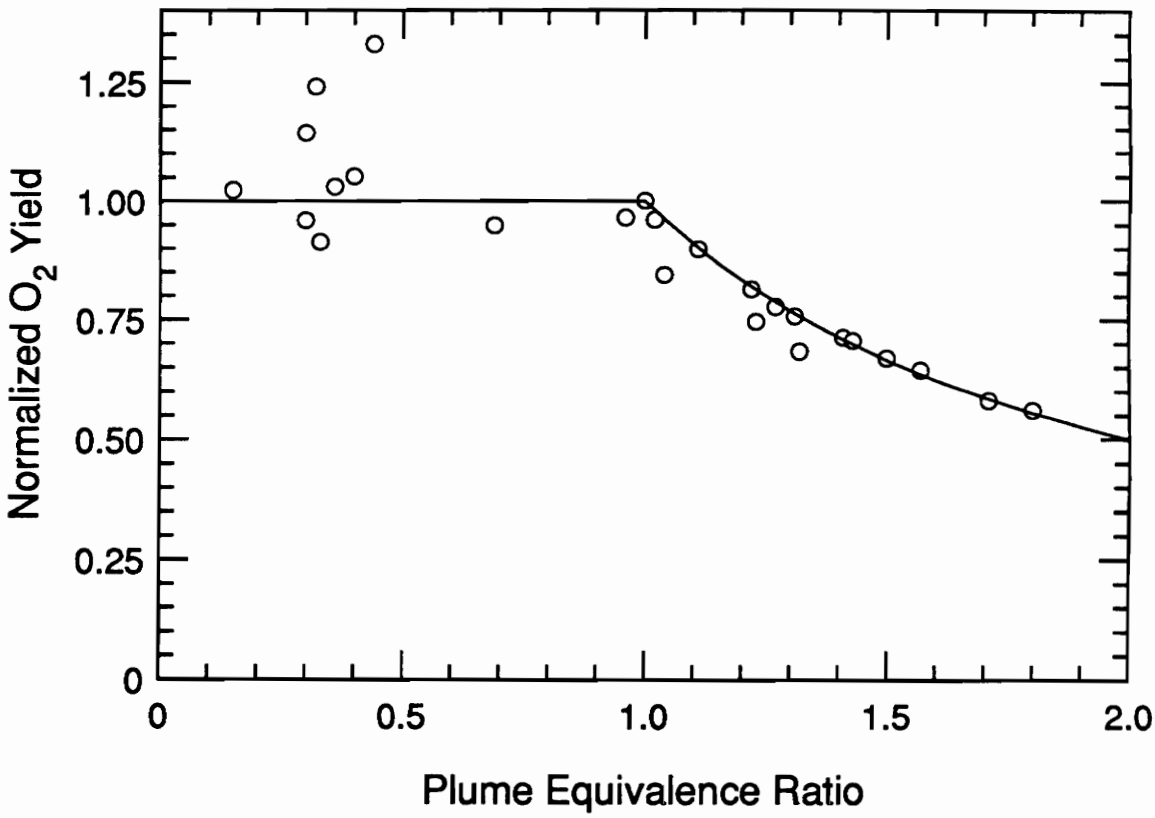

Figure 3.27 Upper layer normalized O_2 yield versus plume equivalence ratio for PMMA compartment fires.

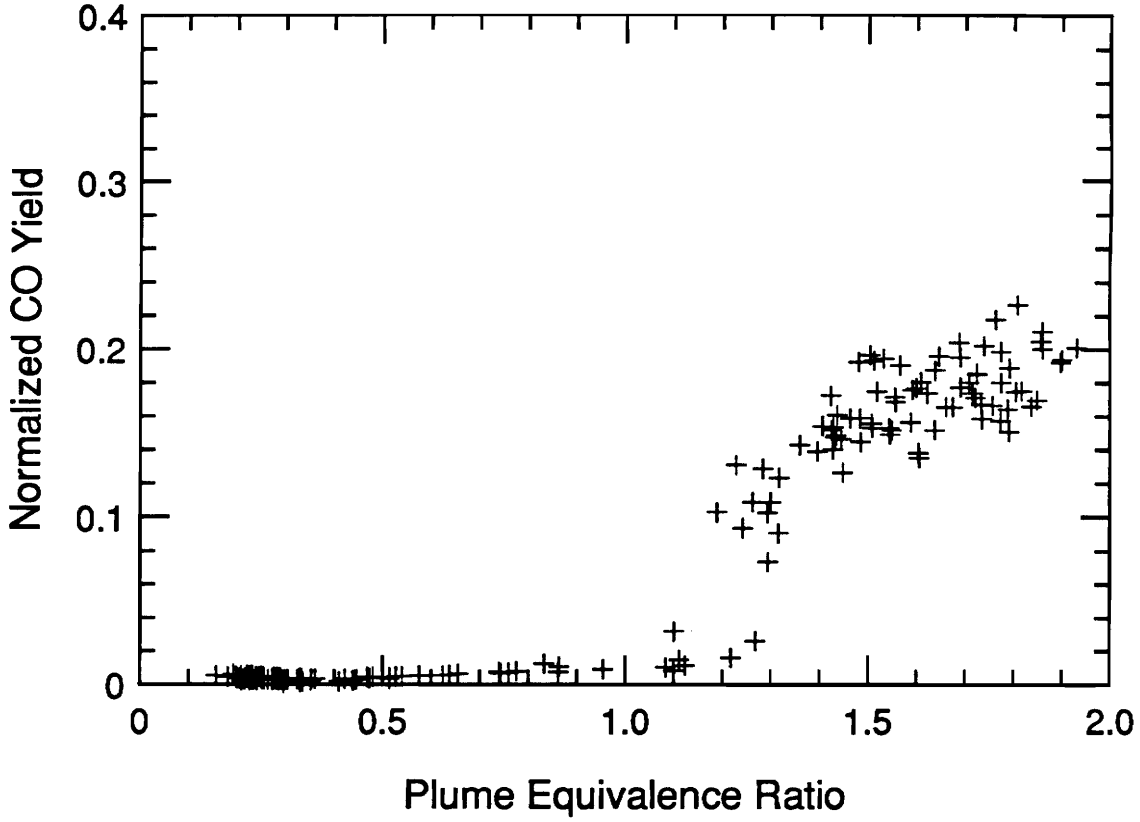

Figure 3.28 Transient, upper layer normalized CO yield versus plume equivalence ratio for a PMMA compartment fire with an average steady-state ϕ_p of 1.8.

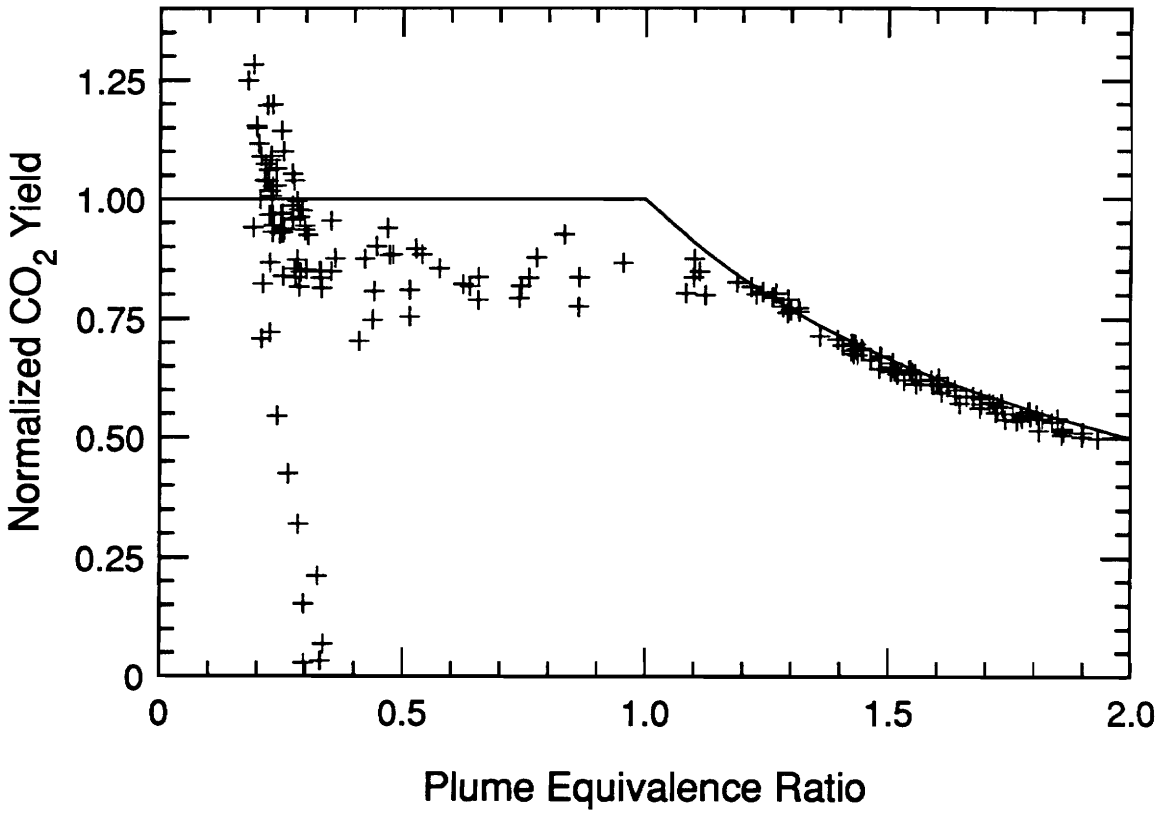

Figure 3.29 Transient, upper layer normalized CO_2 yield versus plume equivalence ratio for a PMMA compartment fire with an average steady-state ϕ_p of 1.8.

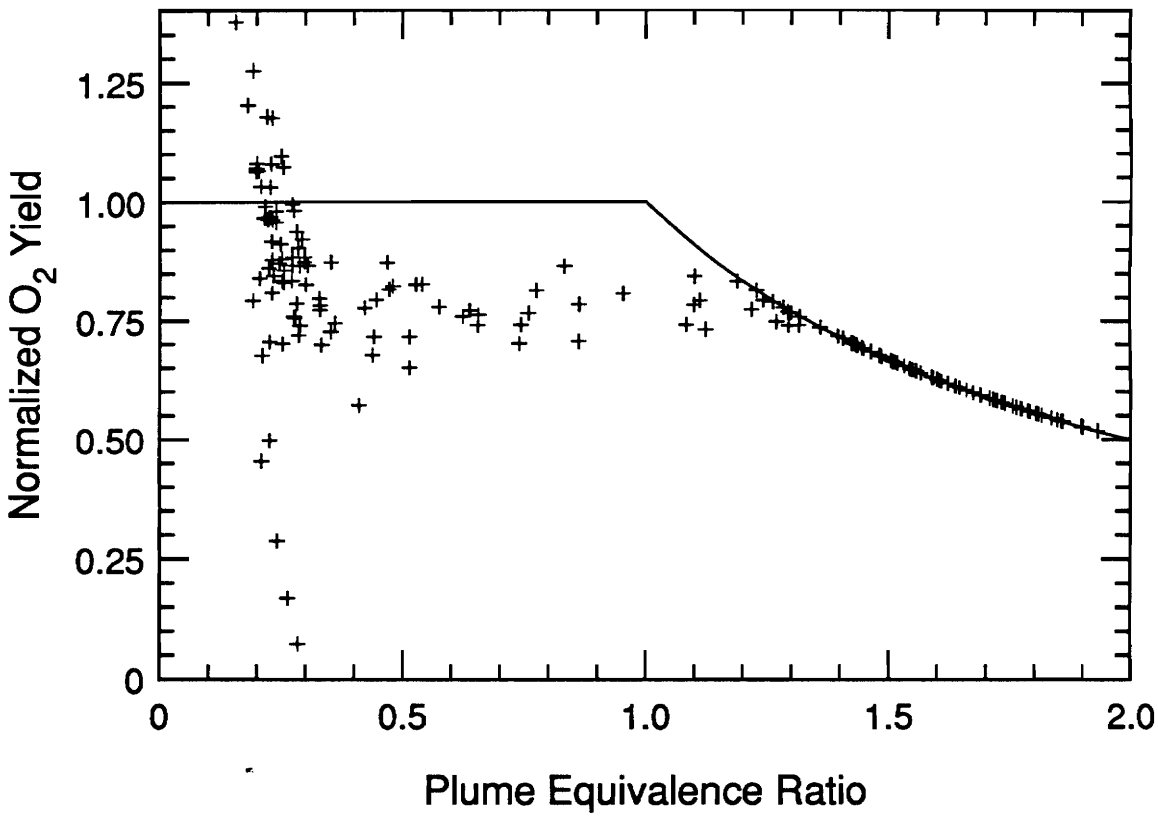

Figure 3.30 Transient, upper layer normalized O_2 yield versus plume equivalence ratio for a PMMA compartment fire with an average steady-state ϕ_p of 1.8.

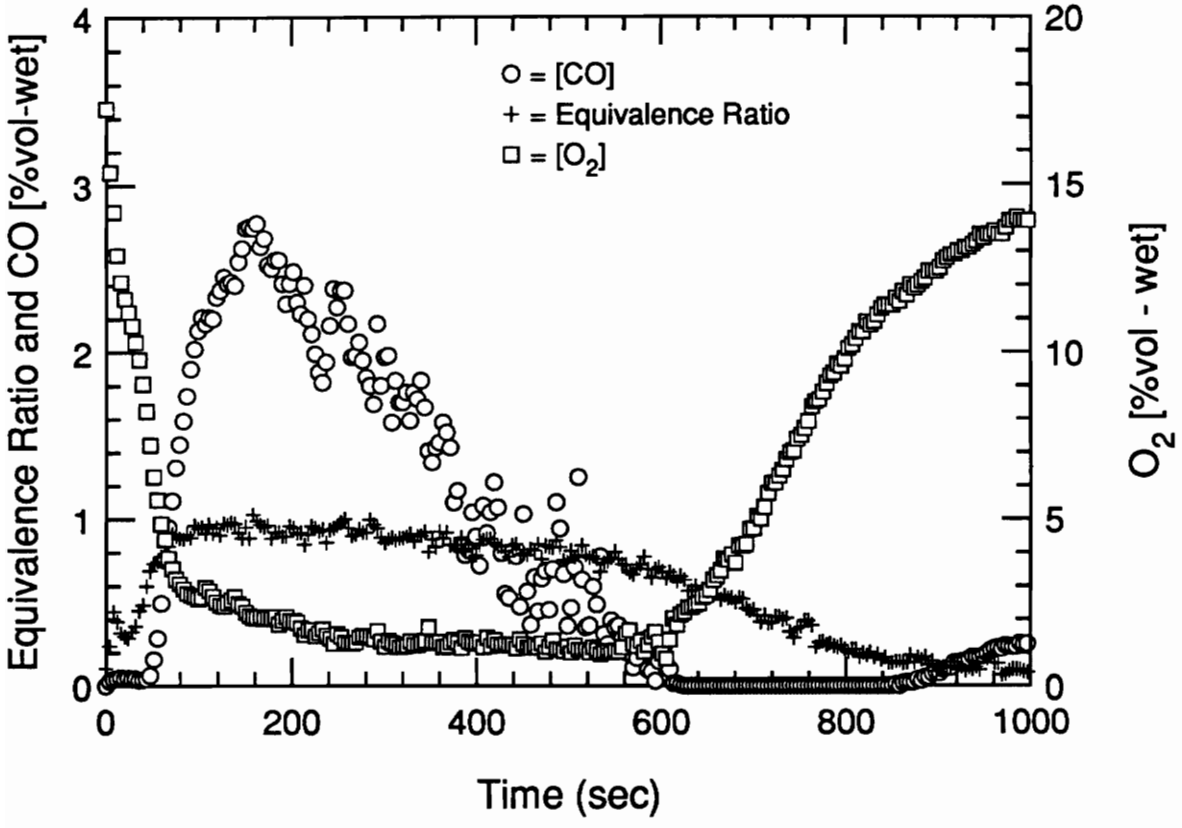

Figure 3.31 Typical time history of species concentrations and plume equivalence ratio for a spruce compartment fire.

burning periods which were sustained for some time as the fuel was consumed. As can be seen in Figure 3.31, CO concentrations increase quickly as the fresh surfaces of the crib start to burn and then decrease with the equivalence ratio. For the fire shown, CO concentrations are quite high (> 2 %) considering the fire barely became underventilated. Consistent with the rapid fire growth, the upper layer O_2 concentration decreased quickly early in the fire. As shown in the figure, late in the spruce crib fires the CO concentration decreased to near zero and the O_2 concentration rose sharply. At the same time the equivalence ratio started to decrease more quickly. These changes were assumed to mark the transition from fuel volatile combustion to char burning. Allowing the fire to continue, lead to incomplete char oxidation and a second increase in CO concentration, in some cases to appreciable levels (> 2000 ppm).

Figure 3.32 shows the average upper layer temperature plotted against the equivalence ratio for each spruce fire. Temperatures ranged from 630 to 890 K and increased with increasing equivalence ratio for overventilated fires.

The upper layer CO concentrations are plotted against the equivalence ratios in Figure 3.33. Carbon monoxide begins to be formed at equivalence ratios of 0.5 and significant levels are obtained for overventilated fires. The maximum CO concentration observed was 3.7 percent. Figure 3.34 shows the upper layer CO_2 concentration plotted against the equivalence ratio for all fires. As can be seen, a distinct correlation exists as the CO_2 concentration increases for fires with increasing equivalence ratio. Figure 3.35 shows that the O_2 concentrations are correlated well and appear to be approaching near zero values for underventilated conditions.

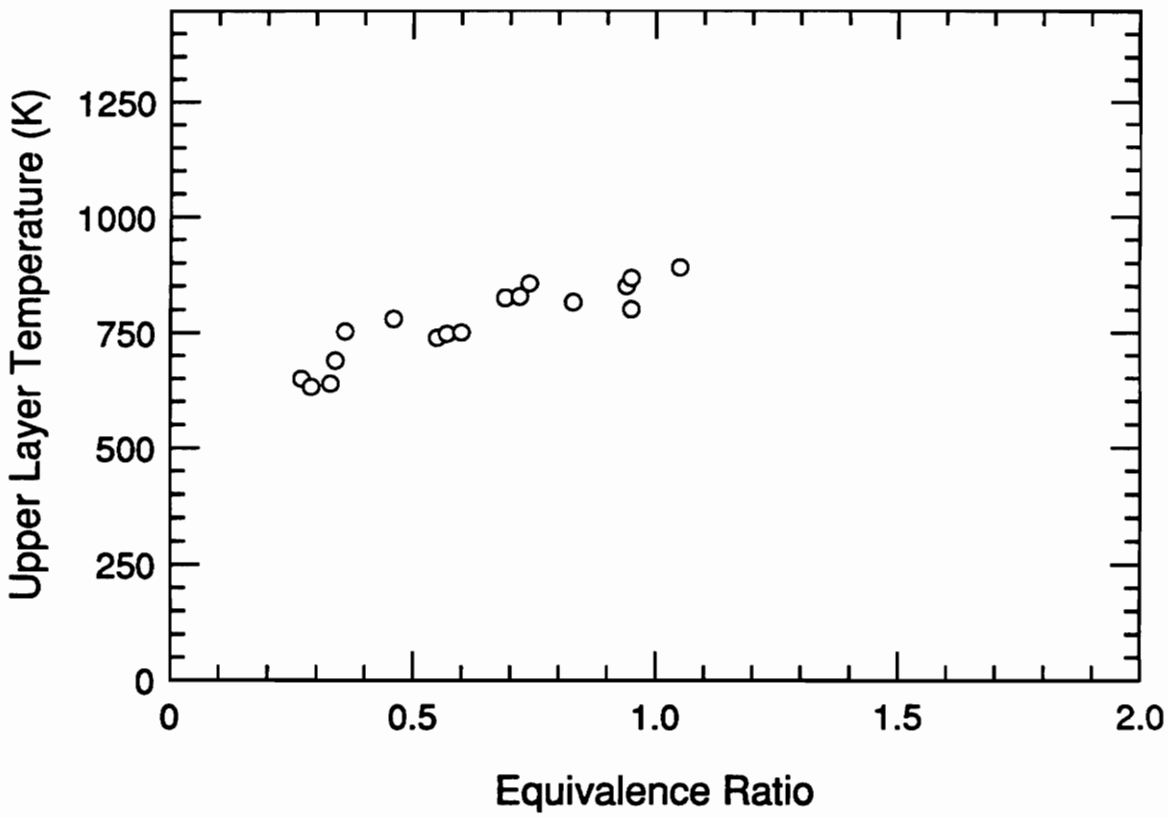

Figure 3.32 Average upper layer temperature versus plume equivalence ratio for spruce compartment fires.

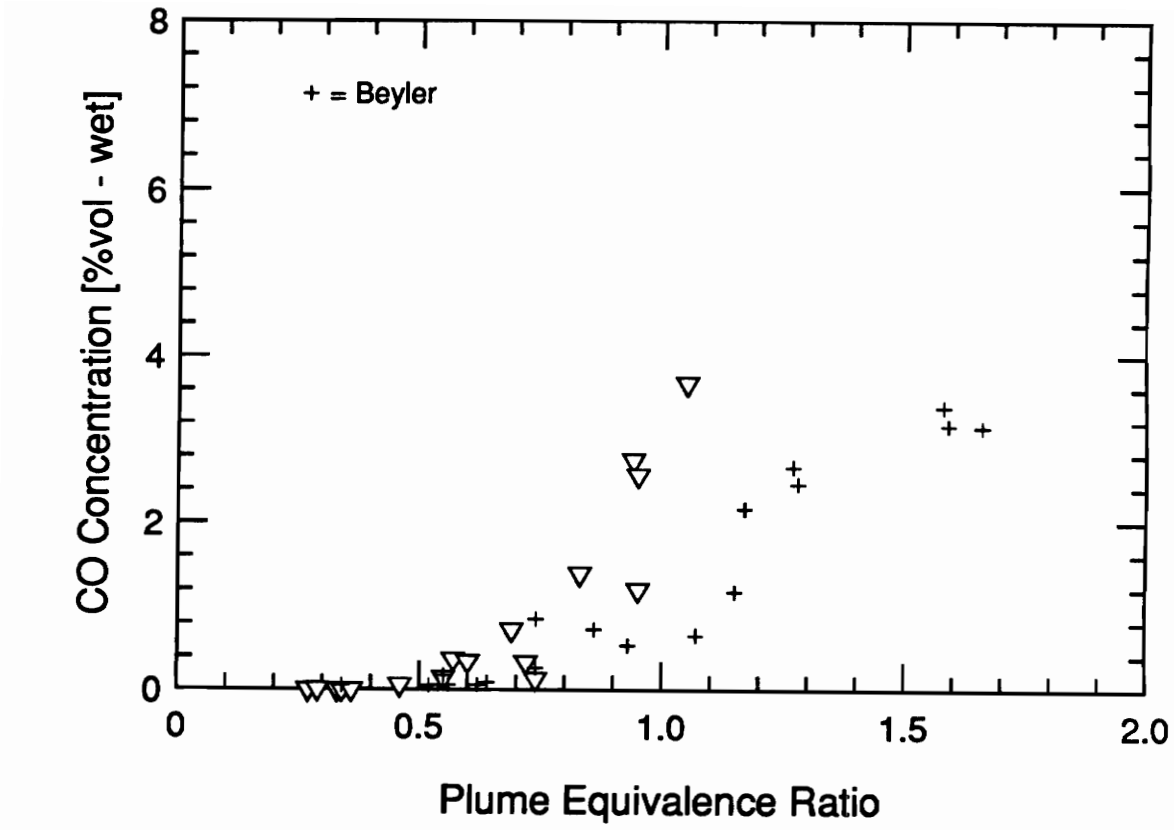

Figure 3.33 Upper layer CO concentration versus plume equivalence ratio for spruce compartment fires and Beyler's ponderosa pine hood fires.

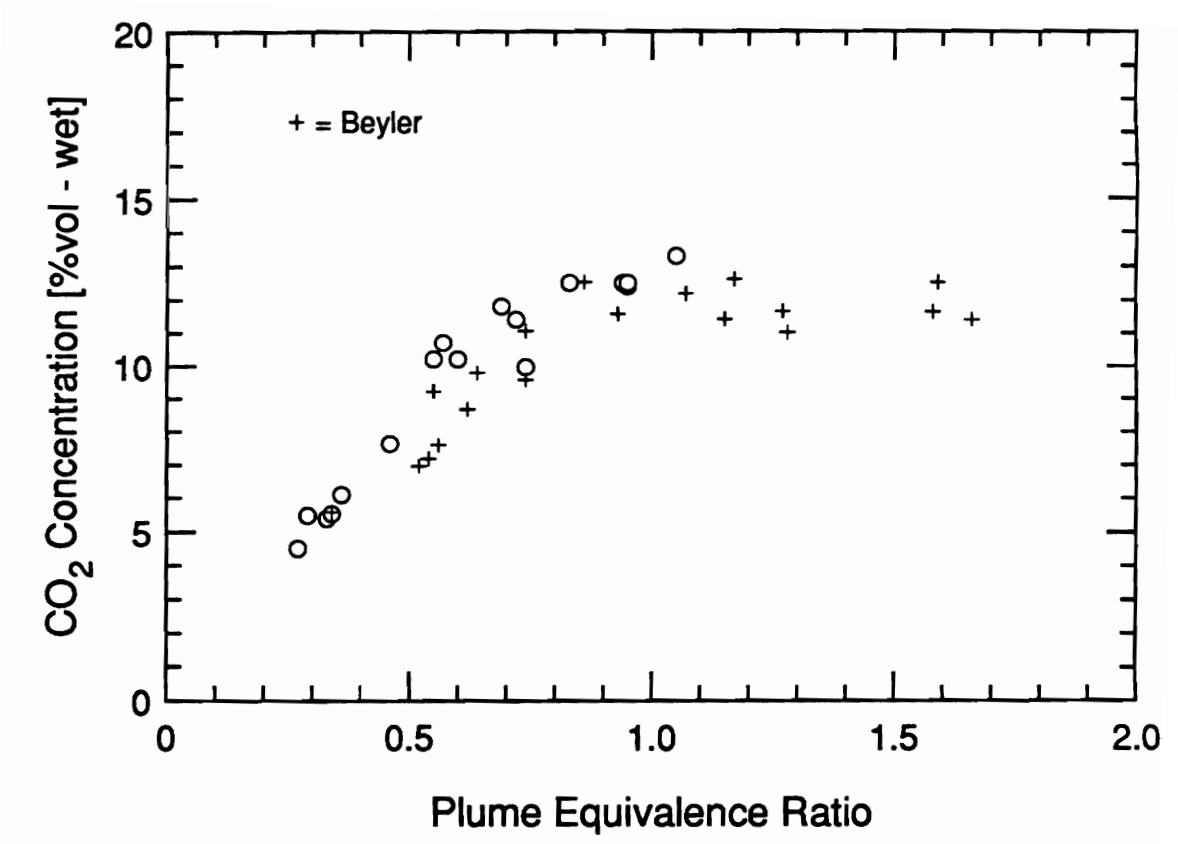

Figure 3.34 Upper layer CO_2 concentration versus plume equivalence ratio for spruce compartment fires and Beyler's ponderosa pine hood fires.

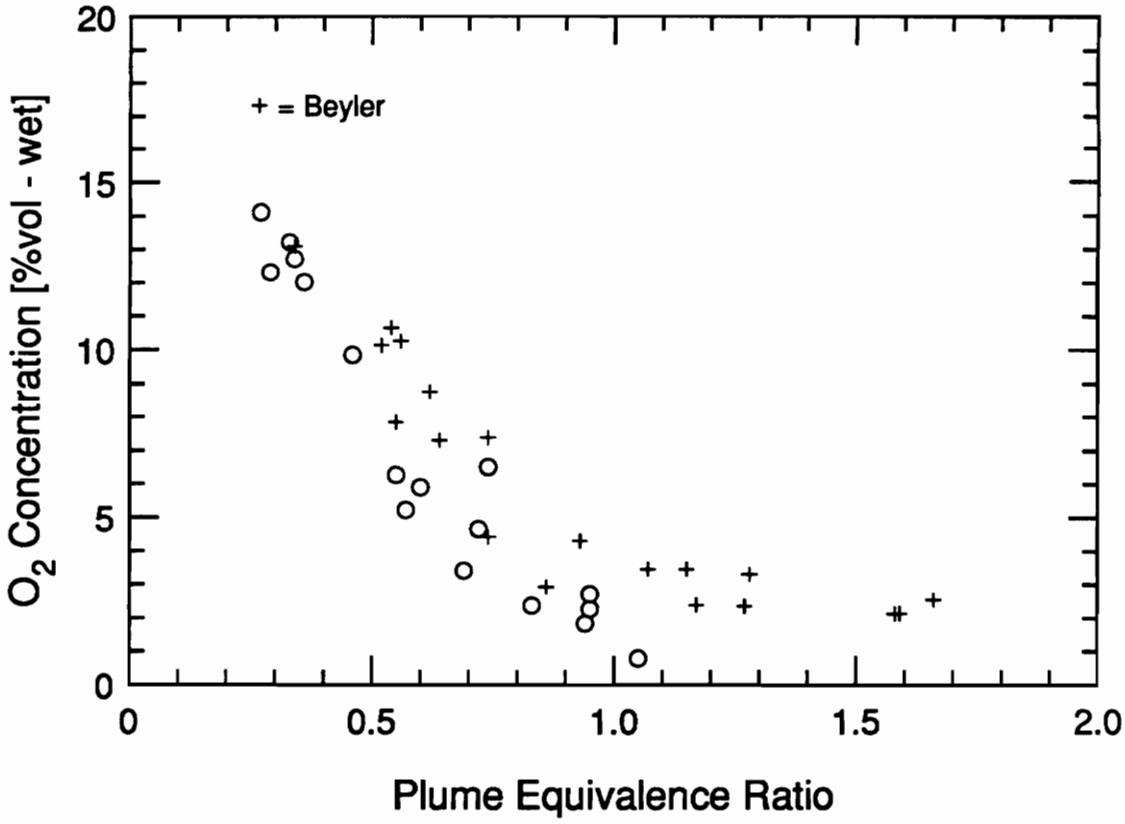

Figure 3.35 Upper layer O_2 concentration versus plume equivalence ratio for spruce compartment fires and Beyler's ponderosa pine hood fires.

The normalized CO yields are plotted versus the plume equivalence ratio in Figure 3.36 for all the spruce fires examined. The figure shows that the upper layer CO yield is reasonably correlated with the plume equivalence ratio. Carbon monoxide production starts at an equivalence ratio of about 0.5 and the yield increases to substantial levels for overventilated fires. The maximum yield observed was 0.24 which occurred at near stoichiometric conditions.

Figures 3.37 and 3.38 present the normalized CO_2 and O_2 yield data plotted versus the plume equivalence ratio. The CO_2 yields agree with the model reasonably well with an average value of 1 for overventilated conditions. Although there is a reasonable amount of scatter in the data, the O_2 yields correlate fairly well with the equivalence ratio with an average value of 1.1 for overventilated fires.

The transient CO yield versus equivalence ratio data for a spruce fire that obtained a steady-state average ϕ_p of 0.95 is presented in Figure 3.39. The transient data is for the same fire shown in Figure 3.31 and includes data for each sampling time up to the midpoint of the quasi-steady-state period. The transient data shows a clearly defined correlation between the yield and equivalence ratio. Significant production of CO starts to occur at a ϕ_p of 0.7 and continues to increase sharply to a peak value of 0.2.

Figures 3.40 and 3.41, present similar transient correlations obtained for the CO_2 and O_2 yields for the same fire as in Figure 3.39. As discussed for hexane the very low CO_2 and O_2 yields are not physically representative and should be ignored. However, the yields of both species are lower than the expected value of one for overventilated conditions.

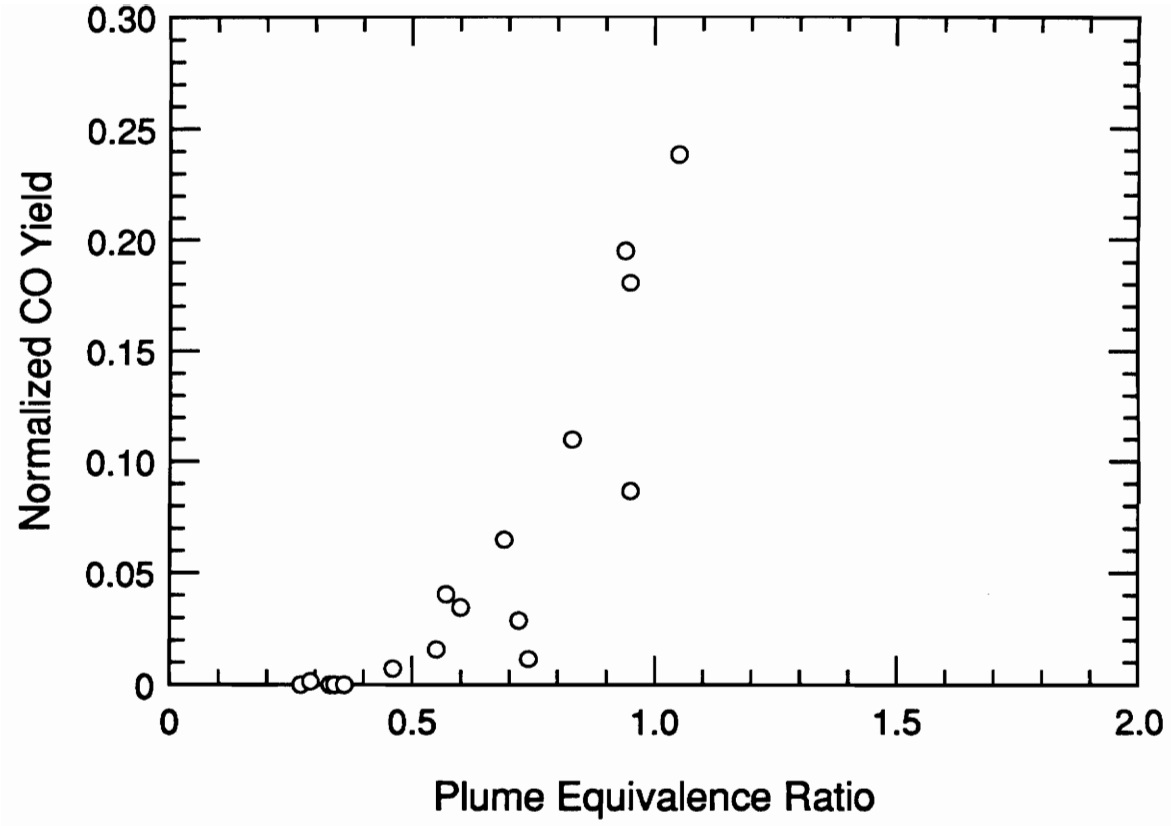

Figure 3.36 Upper layer normalized CO yield versus plume equivalence ratio for spruce compartment fires.

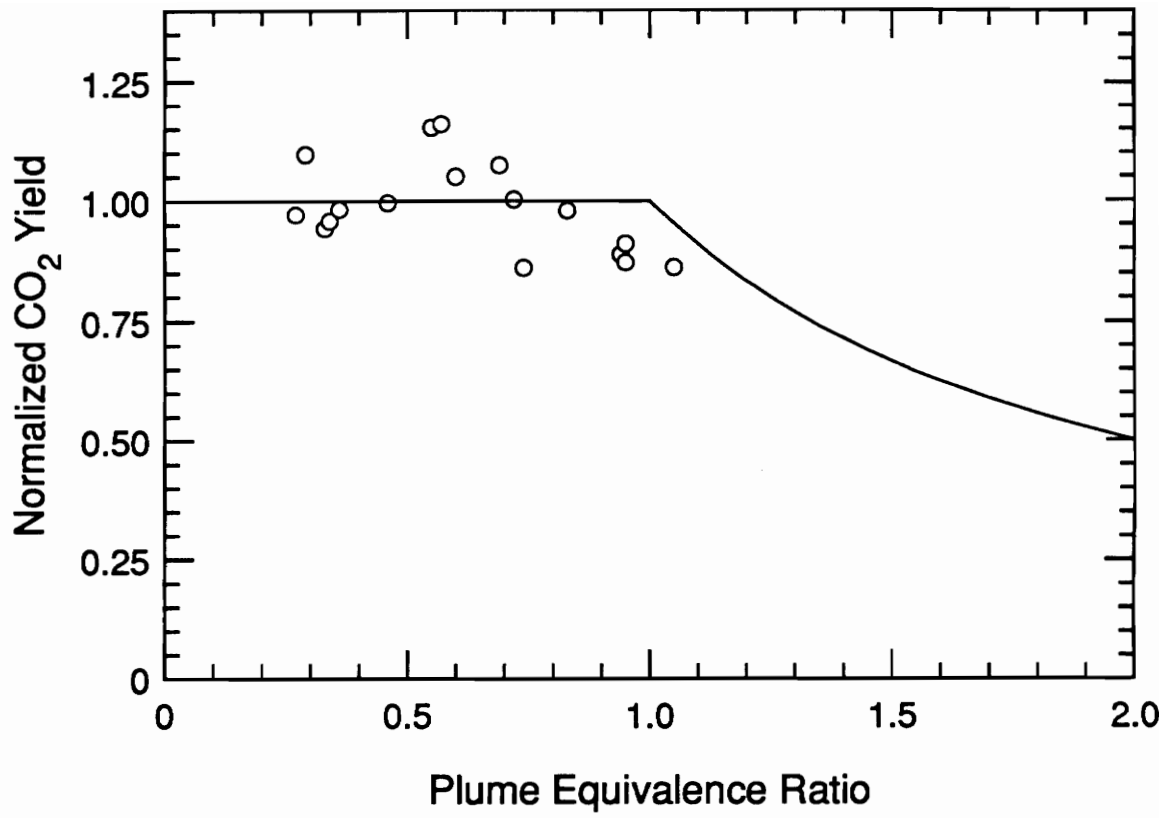

Figure 3.37 Upper layer normalized CO_2 yield versus plume equivalence ratio for spruce compartment fires.

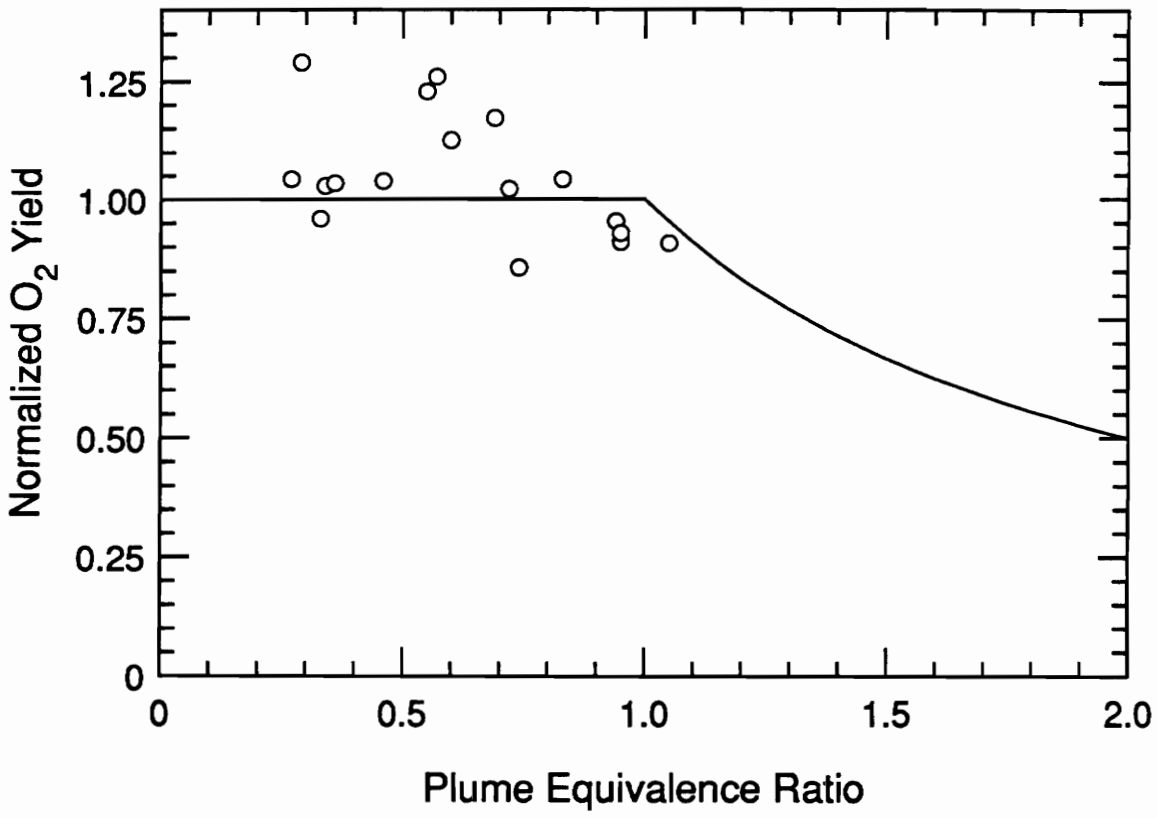

Figure 3.38 Upper layer normalized O_2 yield versus plume equivalence ratio for spruce compartment fires.

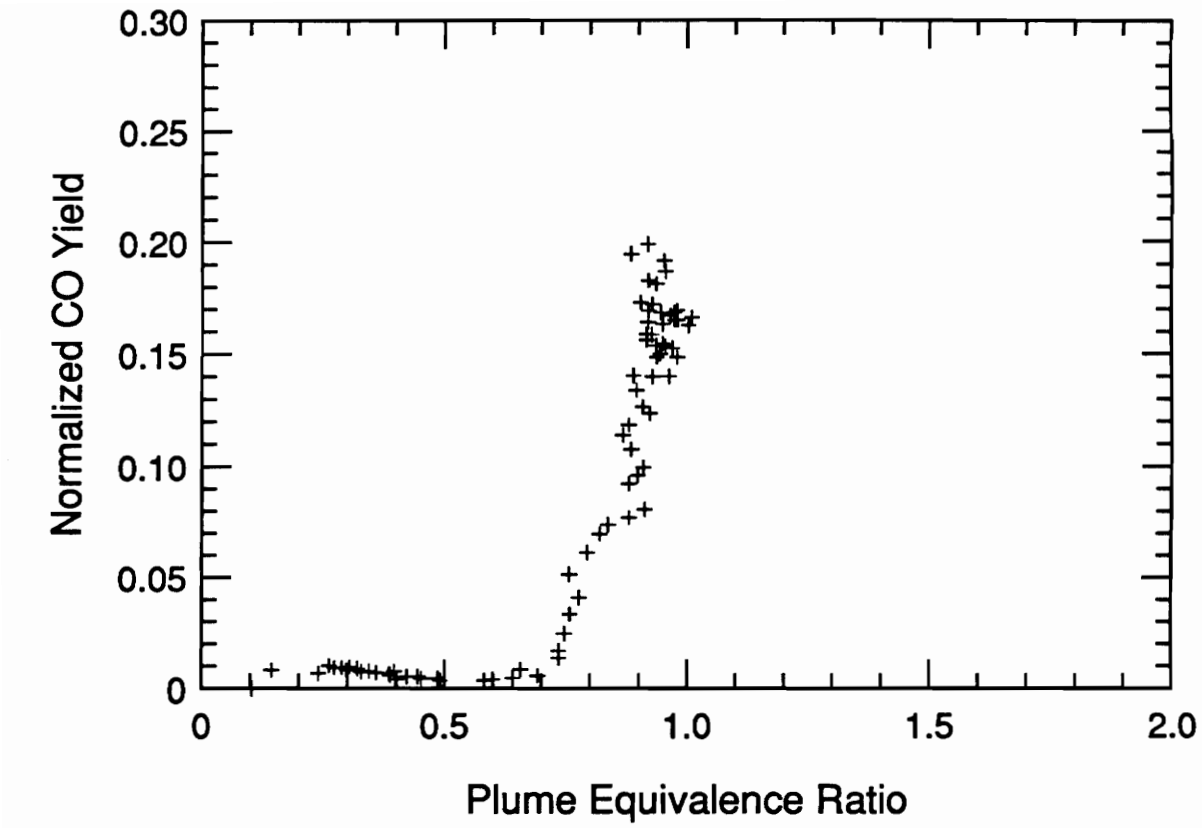

Figure 3.39 Transient, upper layer normalized CO yield versus plume equivalence ratio for a spruce compartment fire with an average steady-state ϕ_p of 0.95.

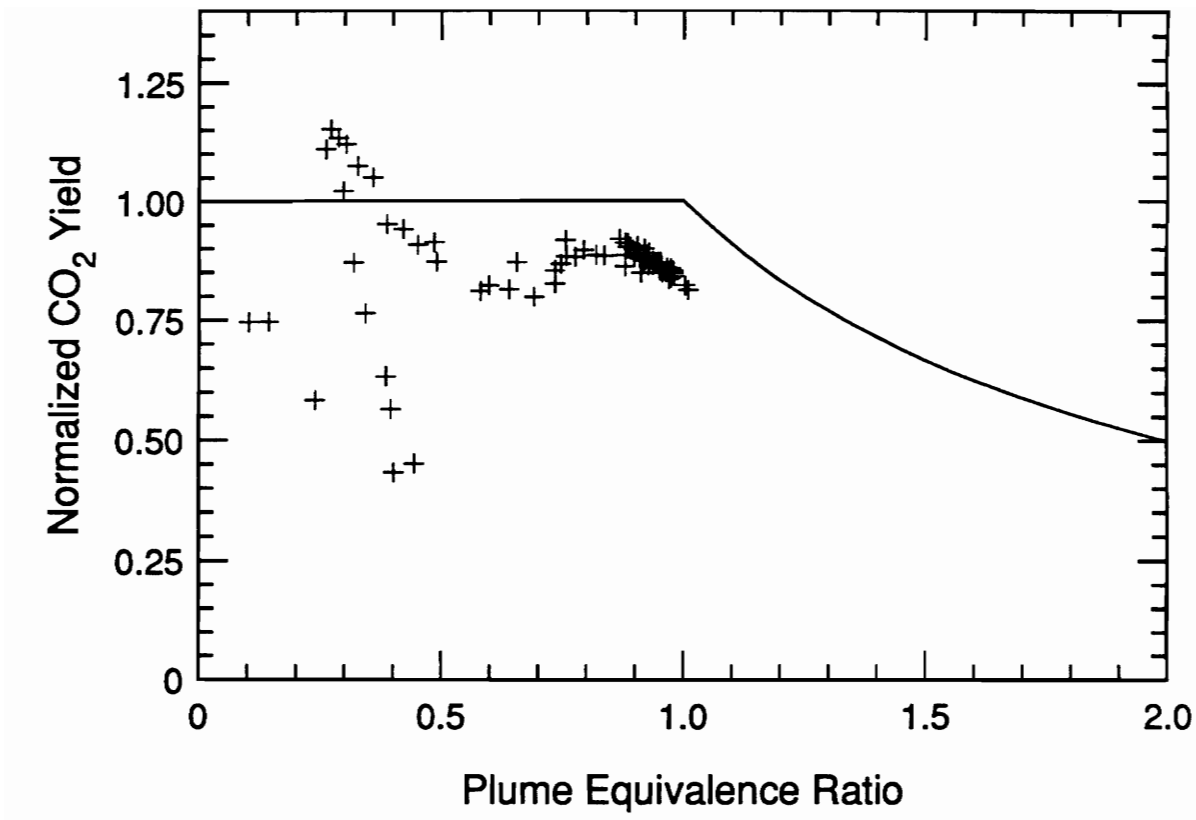

Figure 3.40 Transient, upper layer normalized CO_2 yield versus plume equivalence ratio for a spruce compartment fire with an average steady-state ϕ_p of 0.95.

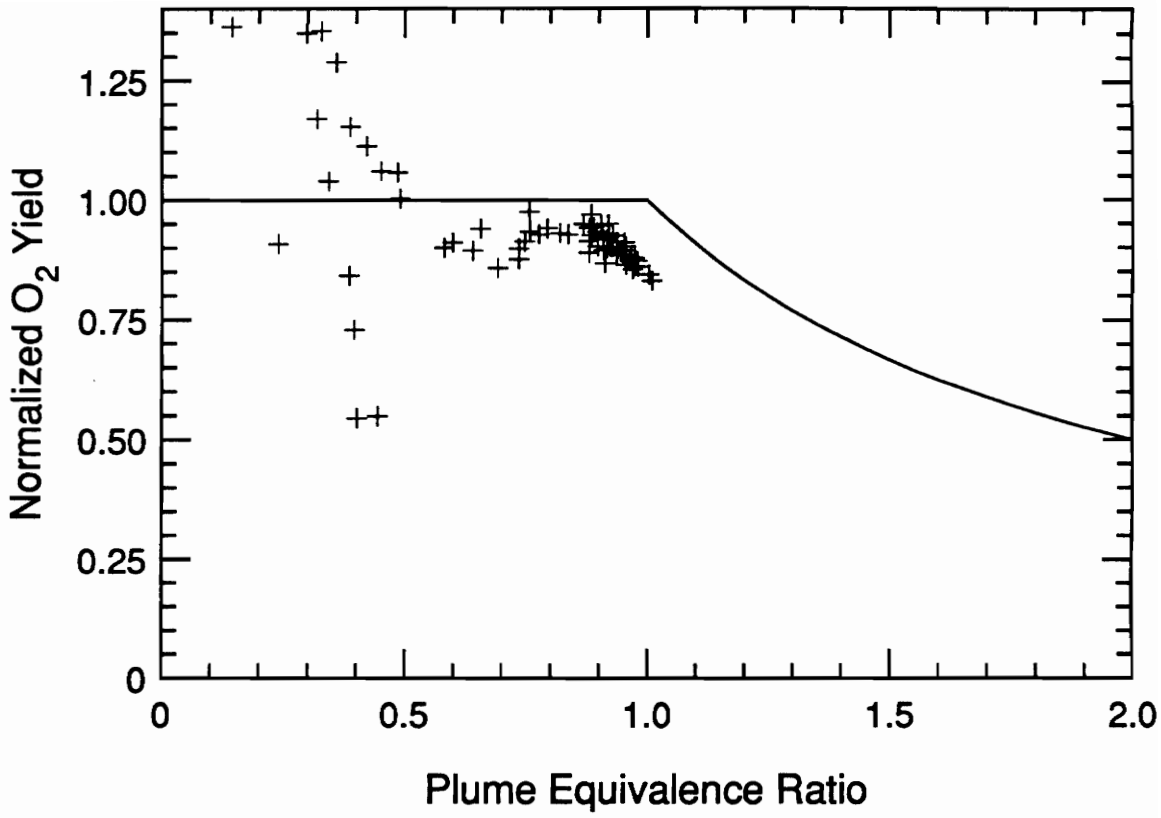

Figure 3.41 Transient, upper layer normalized O_2 yield versus plume equivalence ratio for a spruce compartment fire with an average steady-state ϕ_p of 0.95.

The average smoke yield data for each spruce fire is presented in Figure 3.42 versus the equivalence ratio. There is a rise in the yield at very low equivalence ratios, but above a ϕ_p of 0.5, the yield is relatively constant at an average value of 0.0046.

3.6 Polyurethane

Theoretical heat release rates for polyurethane fires ranged from 36 to 241 kW. A typical time history of equivalence ratio, and CO and O_2 concentrations for an underventilated fire is presented in Figure 3.43. Each sample burned slowly at first as the fire grew radially outward from the top center of the sample. As the fire progressed down the sides of the block, the burning rate increased and reached a peak or quasi-steady-state and then decreased relatively slowly. The decrease in the plume equivalence was due to the burning rate decreasing as the surface area of the polyurethane block diminished during burning. As the fire engulfed the whole sample, CO concentrations in the upper layer increased quickly and remained high while the fuel burned in the quasi-steady period. The overventilated fires obtained much shorter steady-state periods, and in some cases, the concentrations merely peaked during a 10 second period.

Figure 3.44 shows the average upper layer temperature plotted against the equivalence ratio for each polyurethane fire. Temperatures ranged from 628 to 996 K and increased with increasing equivalence ratio for overventilated fires.

The upper layer CO concentrations are plotted against the equivalence ratios in Figure 3.45. Carbon monoxide concentrations were below 0.2 percent for fires with equivalence ratios less than 0.8. Above ϕ_p of 0.8, CO concentrations were on the order of 2 percent or higher. A maximum vale of 3.8 percent was observed. Figure 3.46 shows the upper layer CO_2 concentration plotted against the equivalence ratio for all polyurethane

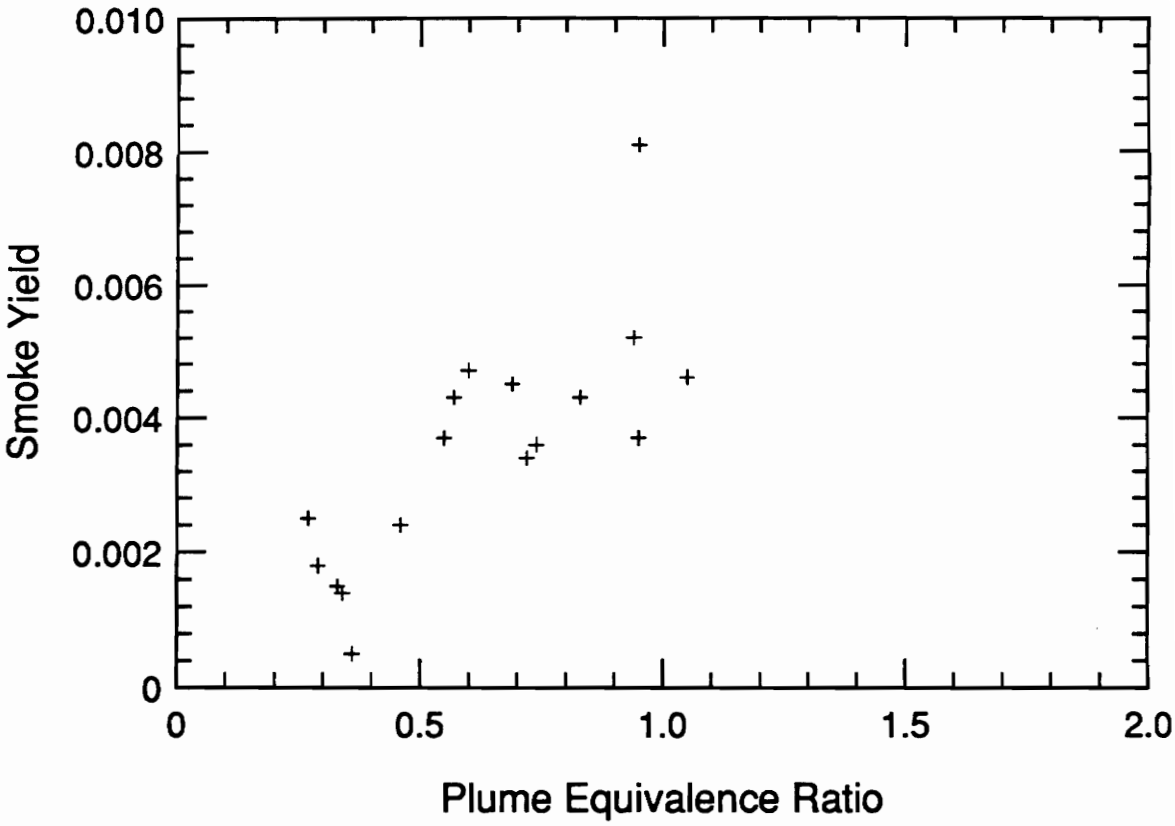

Figure 3.42 Unnormalized smoke yield versus plume equivalence ratio for spruce compartment fires.

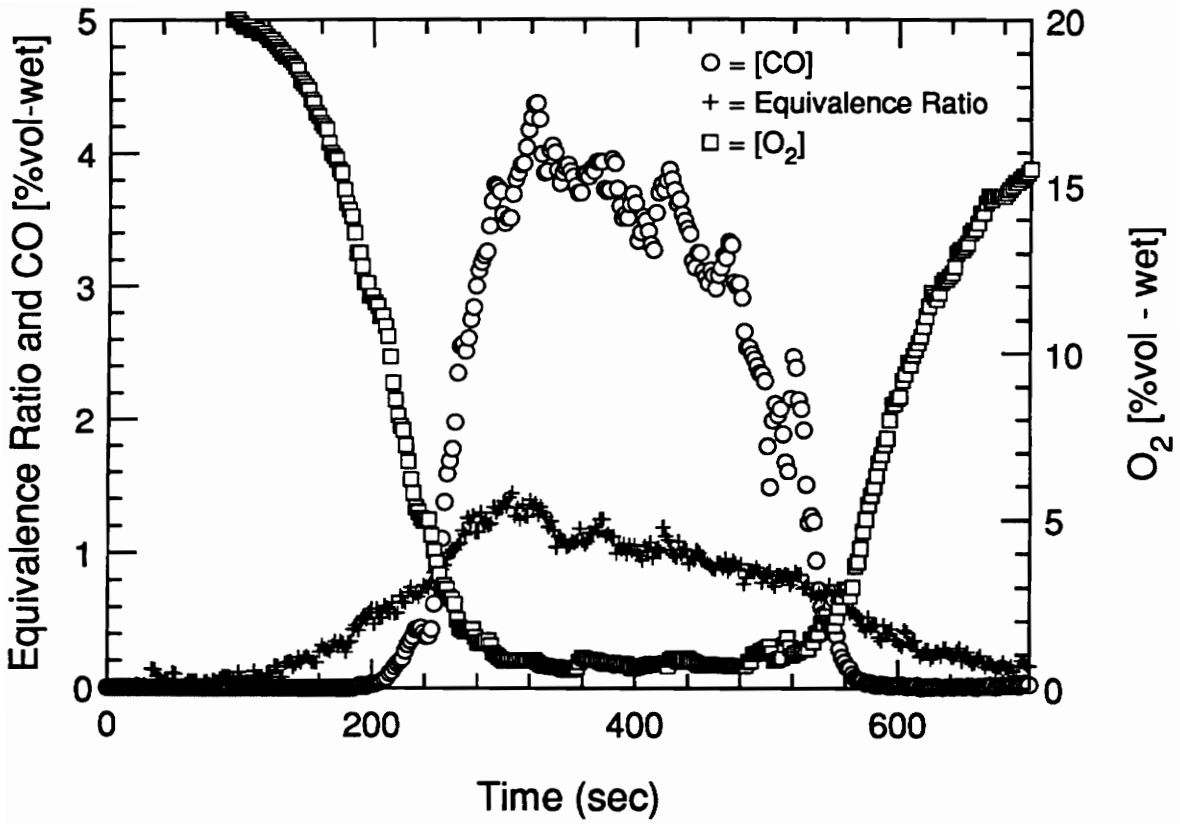

Figure 3.43 Typical time history of species concentrations and plume equivalence ratio for a polyurethane compartment fire.

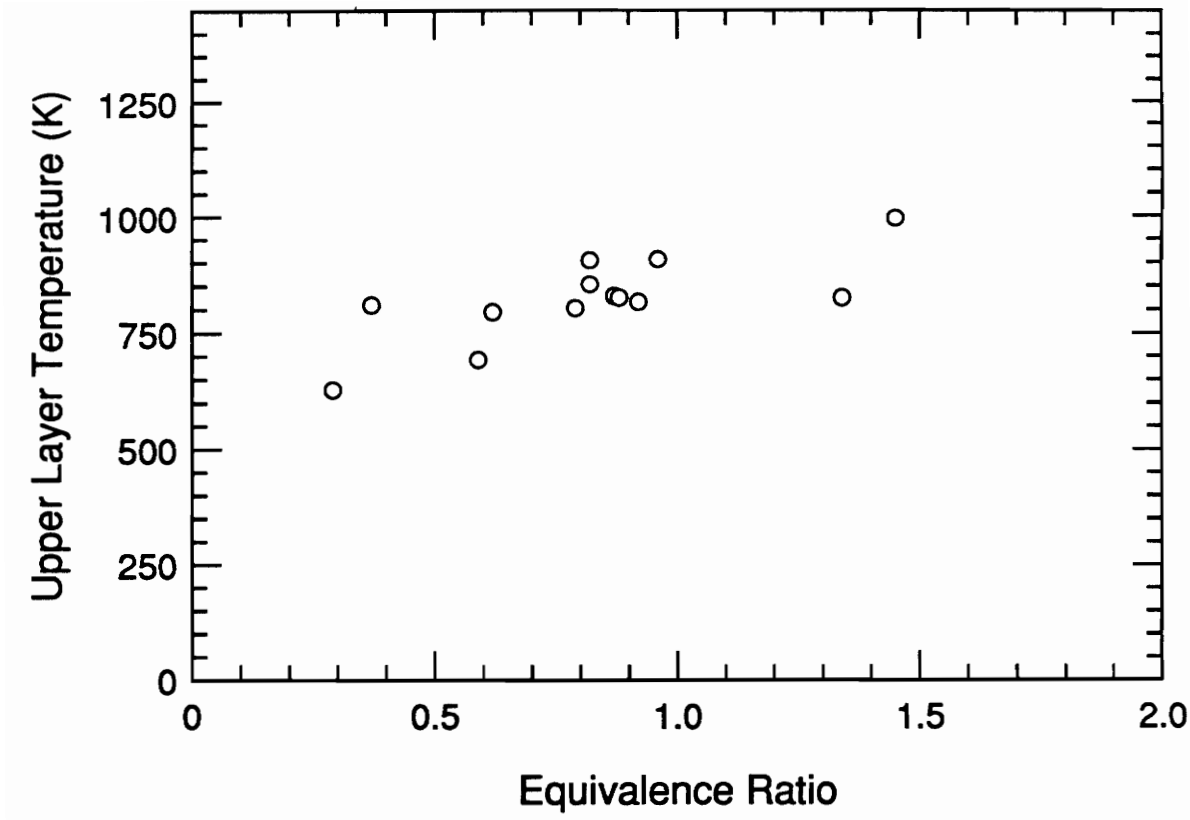

Figure 3.44 Average upper layer temperature versus plume equivalence ratio for polyurethane compartment fires.

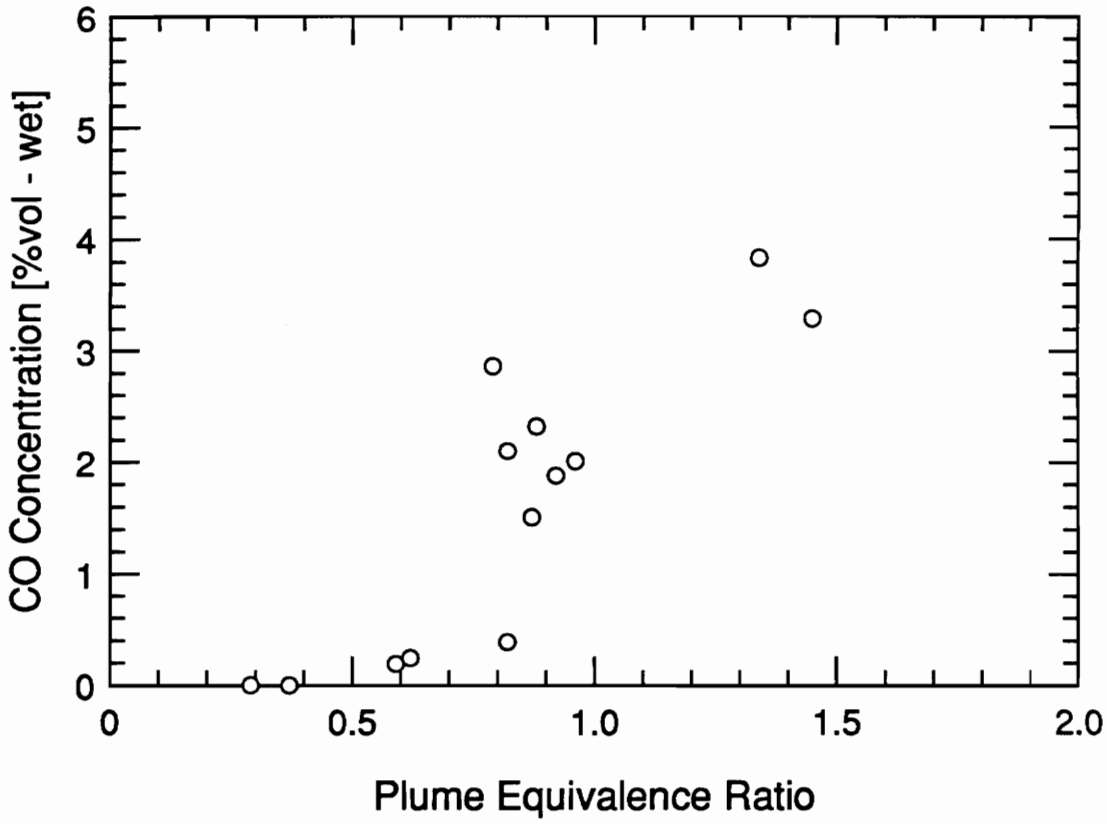

Figure 3.45 Upper layer CO concentration versus plume equivalence ratio for polyurethane compartment fires.

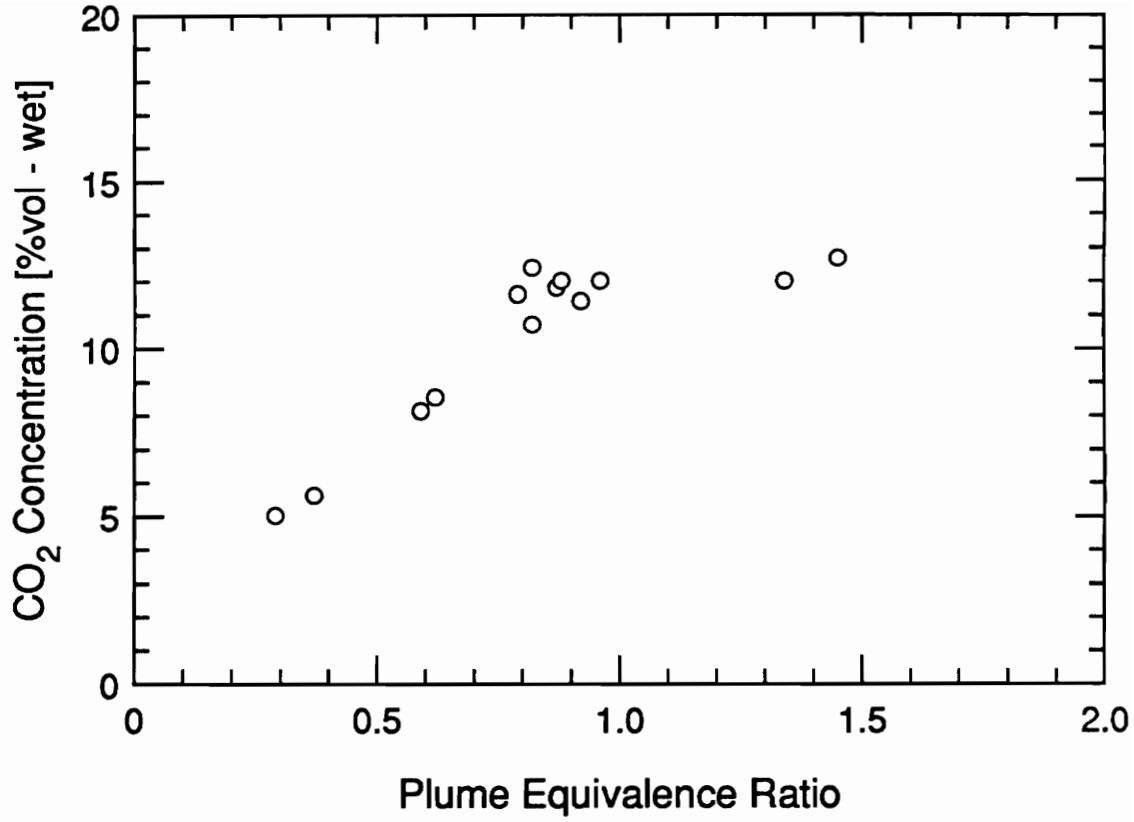

Figure 3.46 Upper layer CO_2 concentration versus plume equivalence ratio for polyurethane compartment fires.

fires. As can be seen, a distinct correlation exists as the CO_2 concentration increases for fires with increasing equivalence ratio. Figure 3.47 shows that the O_2 concentrations are correlated well with the equivalence ration and are below one percent for underventilated conditions.

The normalized CO yields are plotted versus the plume equivalence ratio in Figure 3.48 for all the polyurethane fires. The figure shows that the upper layer CO yield is reasonably correlated with the plume equivalence ratio. Carbon monoxide production starts at an equivalence ratio of about 0.6 but significant levels are not observed until a ϕ_p of 0.8 and higher. The maximum yield observed was 0.24. The data suggests that the yield may level out to a constant value of about 0.18 for underventilated conditions. Figures 3.49 and 3.50 present the normalized CO_2 and O_2 yield data plotted versus the plume equivalence ratio. The yield data correlate reasonably well with the equivalence ratio showing good agreement with the model.

The transient CO yield versus equivalence ratio data for a polyurethane fire that obtained a steady-state average ϕ_p of 1.3 is presented in Figure 3.51. The transient data is for the same fire shown in Figure 3.43 and includes data for each sampling time up to the midpoint of the quasi-steady-state period. The transient data shows a clearly defined correlation between the yield and equivalence ratio as CO production starts at a ϕ_p of 0.6 and increase with increasing equivalence ratio.

Figures 3.52 and 3.53, present the transient CO_2 and O_2 yields versus equivalence ratio for the same fire as in Figure 3.51. As discussed for hexane, the very low CO_2 and O_2 yields are not physically representative and should be ignored. However, the yields of both species are lower than the expected value of one for overventilated conditions. For

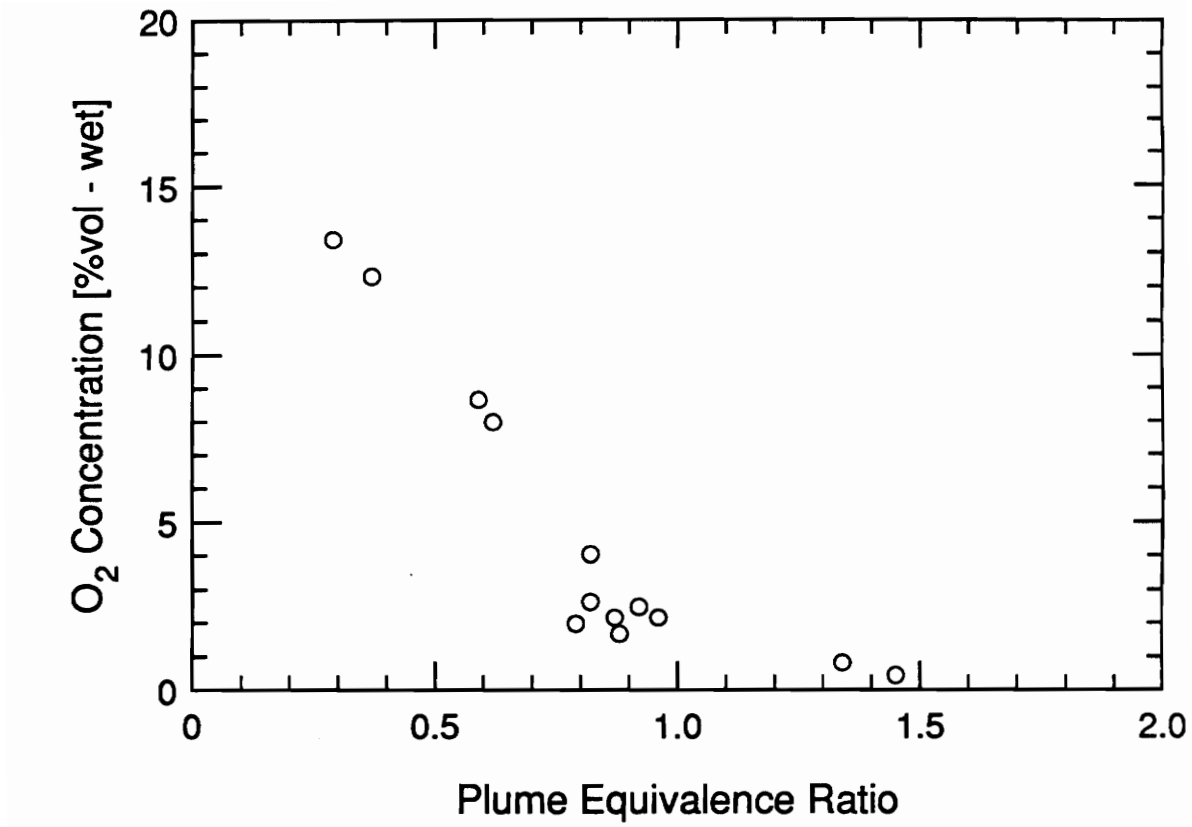

Figure 3.47 Upper layer O_2 concentration versus plume equivalence ratio for polyurethane compartment fires.

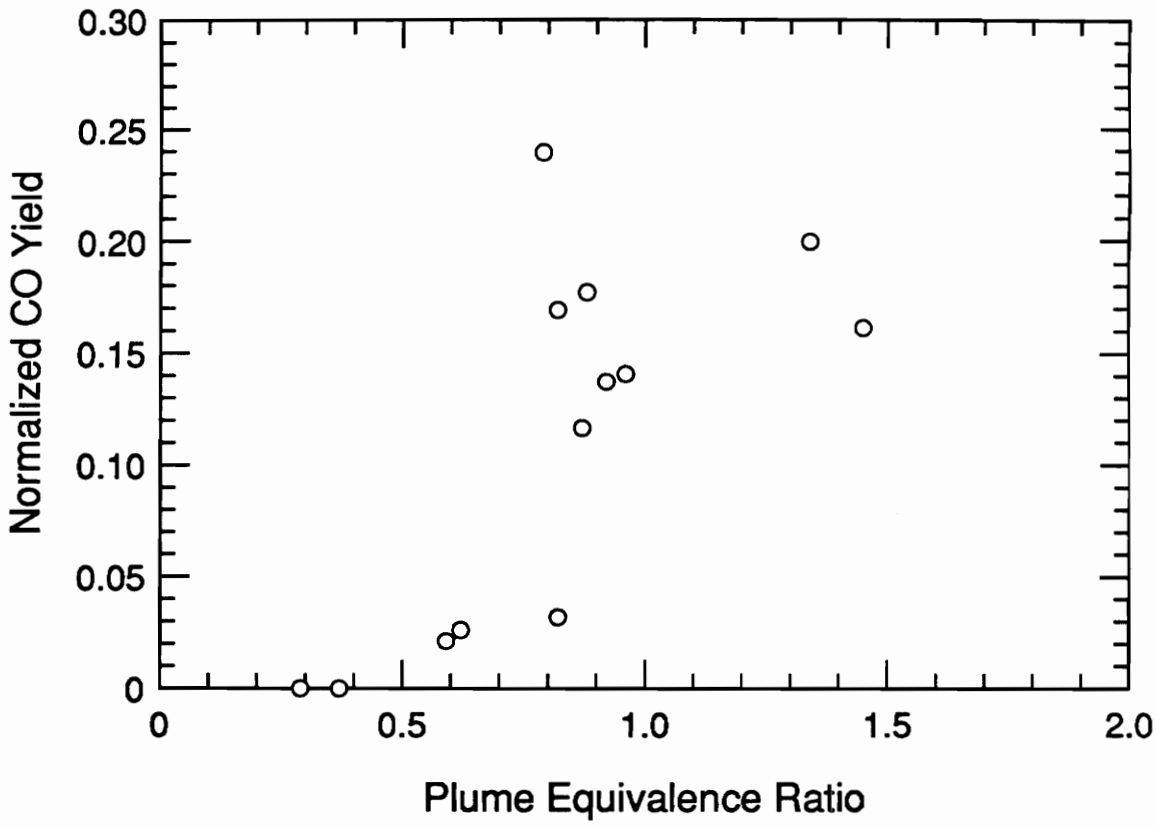

Figure 3.48 Upper layer normalized CO yield versus plume equivalence ratio for polyurethane compartment fires.

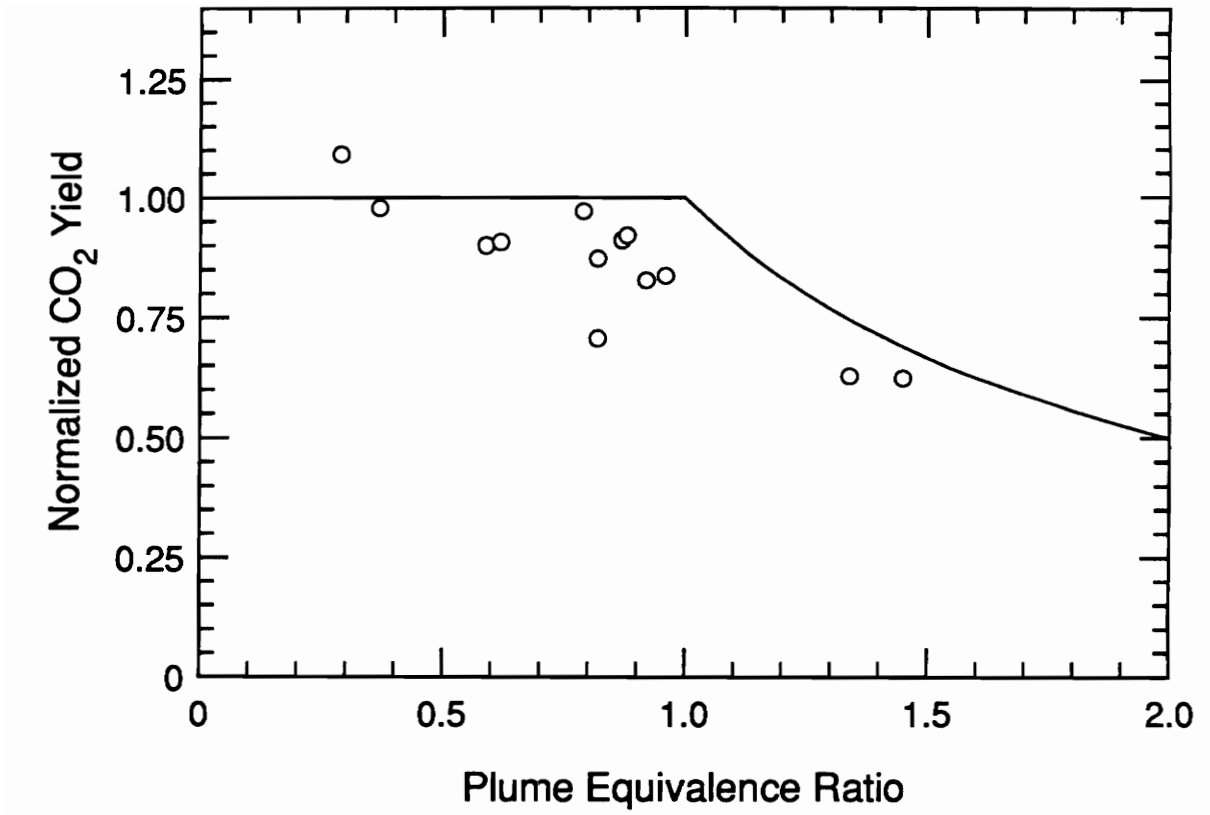

Figure 3.49 Upper layer normalized CO_2 yield versus plume equivalence ratio for polyurethane compartment fires.

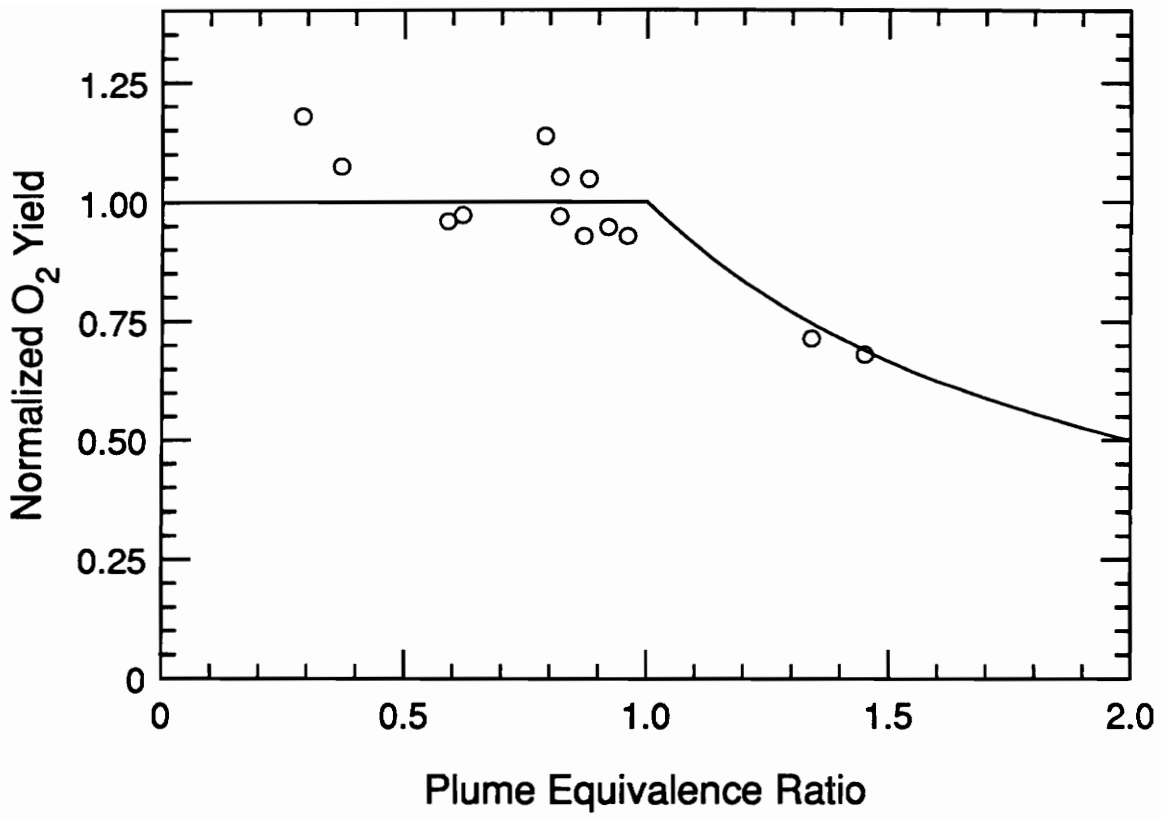

Figure 3.50 Upper layer normalized O_2 yield versus plume equivalence ratio for polyurethane compartment fires.

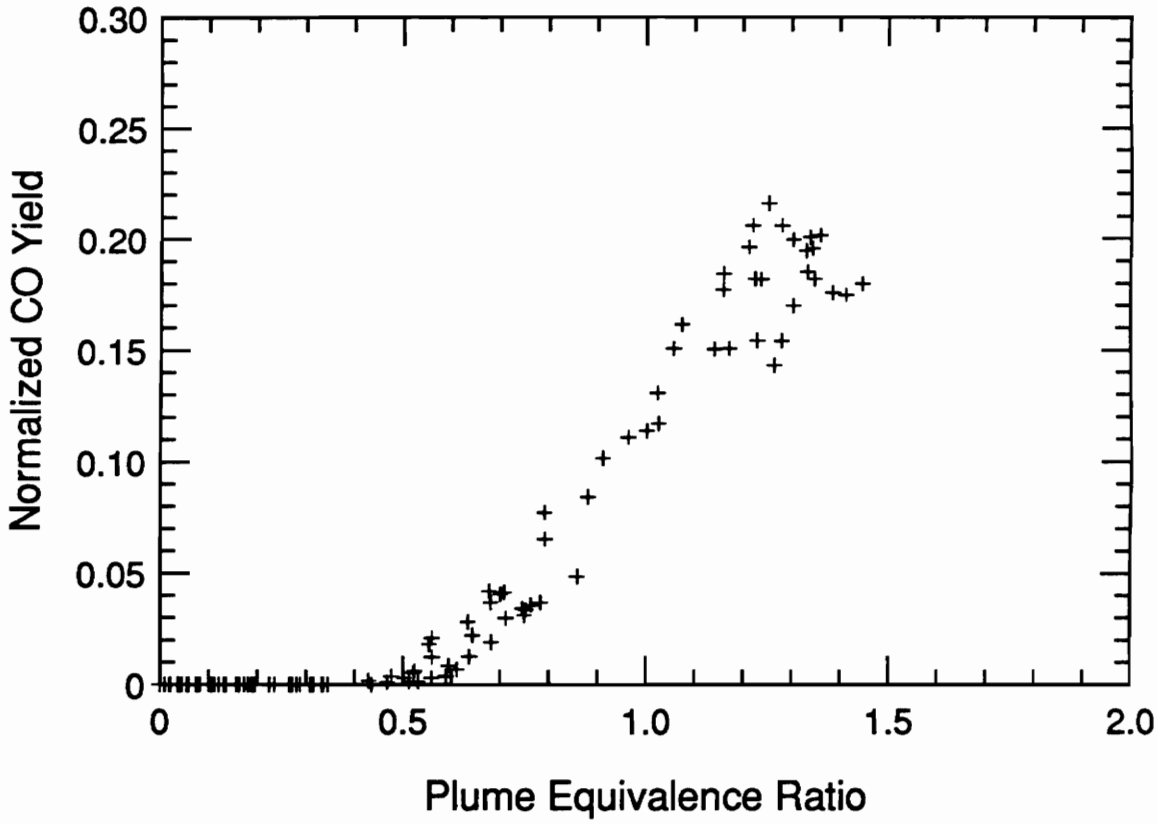

Figure 3.51 Transient, upper layer normalized CO yield versus plume equivalence ratio for a polyurethane compartment fire with an average steady-state ϕ_p of 1.3.

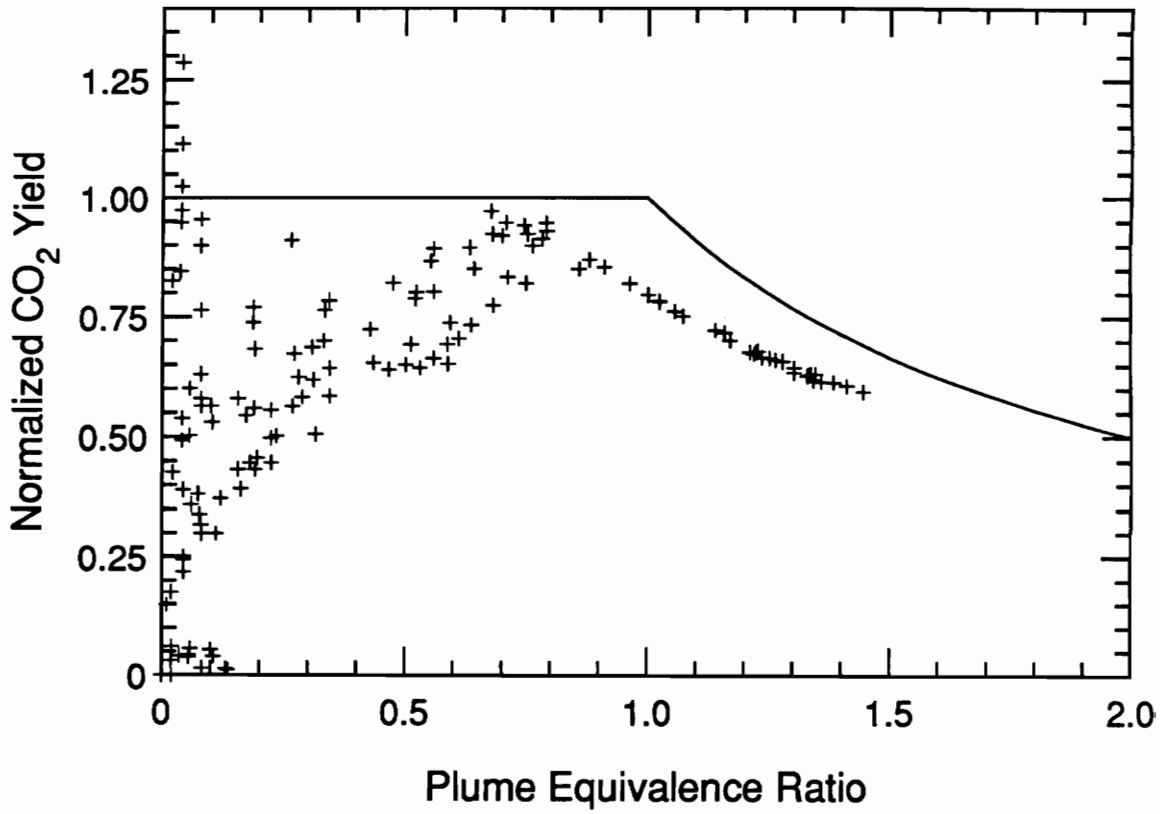

Figure 3.52 Transient, upper layer normalized CO_2 yield versus plume equivalence ratio for a polyurethane compartment fire with an average steady-state ϕ_p of 1.3.

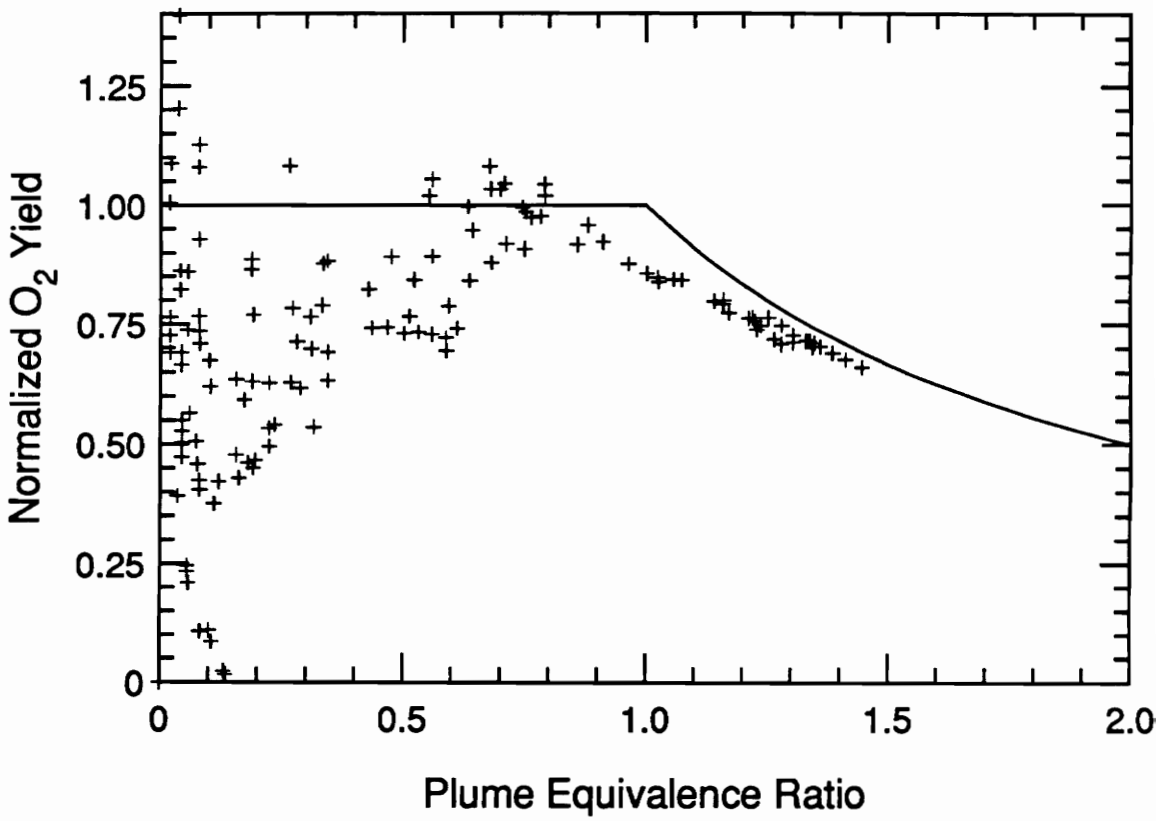

Figure 3.53 Transient, upper layer normalized O_2 yield versus plume equivalence ratio for a polyurethane compartment fire with an average steady-state ϕ_p of 1.3.

underventilated conditions both the CO_2 and O_2 yields decrease proportionately with $1/\phi_p$, but O_2 agrees more closely with the model.

The polyurethane smoke yield data is presented in Figure 3.54. The yield is relatively constant for overventilated conditions at an average value of 0.0126. The two underventilated fires had average smoke yields of 0.23 which is approximately twice as high as for the overventilated fires.

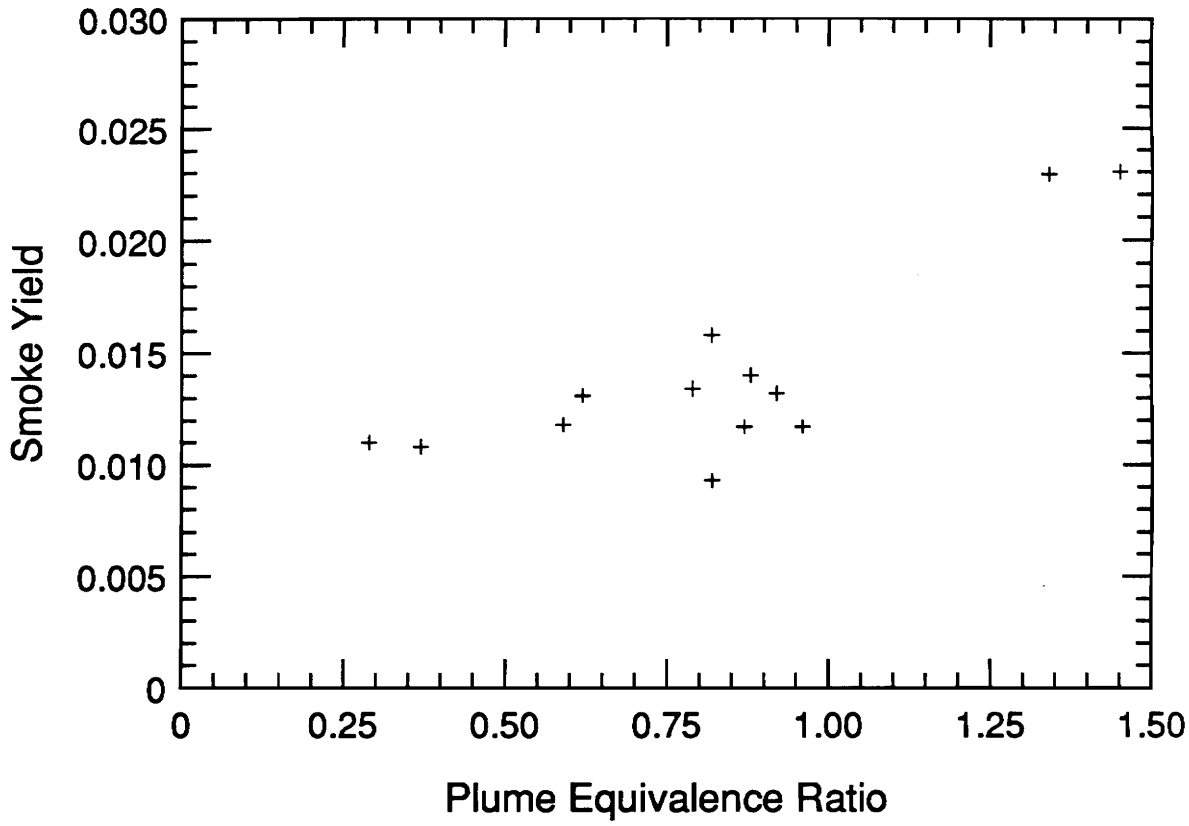

Figure 3.54 Unnormalized smoke yield versus plume equivalence ratio for polyurethane compartment fires.

CHAPTER 4

DISCUSSION OF CHEMICAL SPECIES PRODUCTION IN THE UPPER LAYER

4.1 Introduction

This chapter discusses the results of the upper layer-sampled experiments that were presented in chapter 3. Discussion of species production in the upper layer consists of comparing the current results to previous work in section 4.2 and then a comparison of the compartment fire correlations obtained for different fuels presented in section 4.3.

4.2 Comparison to Previous Work

Very few systematic studies of species production in compartment fire environments have been performed. Previous work by Beyler [14,15], Toner [13] and Morehart [16] studied the production of species in simplified layer environments created in a hood (see section 1.3). However, Toner and Morehart only investigated gaseous fuels which were not investigated in this study and, therefore, direct comparisons are only made with Beyler's results for similarly tested fuels: hexane, PMMA and wood.

4.2.1 Upper Layer Environment and Fire Dynamics

A main objective of this work was to determine the effect of actual compartment fire dynamics on the species yield correlations observed by Beyler for a simplified layer environment. Although a uniform two-layer system was developed in both the hood and compartment fire investigations, the fire dynamics were significantly different. Larger fires were burned in the compartment experiments with theoretical heat release rates ranging from 27 to 660 kW compared to 11 to 19 kW for the hood experiments. Although

the larger fires are primarily a result of using fuel samples that were twice as large in surface area as those used by Beyler there is also a temperature dependence on the fuel burning rate.

Table 4.1 presents the upper layer temperature data for this study along with the data from Beyler's hood experiments. The data is presented for two ranges of equivalence ratios for the purpose of comparing the fuels and for comparing the hood and compartment experiments. For each fuel, an average for all underventilated fires is presented and shows that the temperature ranks each fuel in the following order: PMMA > hexane > polyurethane > spruce. The average underventilated upper layer temperatures vary from 13 to 24 percent for the compartment fires contrary to Beyler's hood experiments in which the temperatures agreed within 5 percent of each another for all fuels. The range between an equivalence ratio of 0.5 and 1.5 is of importance in comparing the yield correlations obtained from Beyler's experiments and this study (see section 4.3). Beyler observed average temperatures from about 240 to 620 K below those observed for the compartment fires. This difference can be seen in Figures 4.1 to 4.3 which present the average hexane, PMMA and wood upper layer temperature versus equivalence ratio data for the compartment and hood experiments. Due to the elevated temperatures in the compartment fires radiant heat transfer to the fuel surface is increased resulting in higher burning rates on the order of 5 to 10 g/s as compared to 0.5 to 1.5 g/s for Beyler's hood experiments.

A premixed flame exhibits a temperature that increases with increasing equivalence ratio, peaks near stoichiometric conditions and decreases under fuel-rich conditions. For equivalence ratios less than one, the addition of fuel provides more energy release and an increase in temperature. However, for $\phi > 1$, additional fuel acts as

Table 4.1 Average upper layer temperatures (K) for selected ranges of equivalence ratios for both the compartment and Beyler's hood fires. The standard deviation is shown in parentheses.

FUEL	TEMPERATURE (K)	
	$0.5<\phi<1.5$	$\phi>1$
Hexane	970 (83)	1038 (62)
PMMA	1164 (129)	1165 (126)
Spruce*	815 (51)	890 (0)
Polyurethane#	840 (77)	910 (122)
BEYLER:		
Hexane	556 (34)	529 (25)
PMMA	547 (145)	525 (37)
Pine	574 (36)	537 (37)

* $\phi_p > 1$ represents only one fire

$\phi_p > 1$ represents only two fires

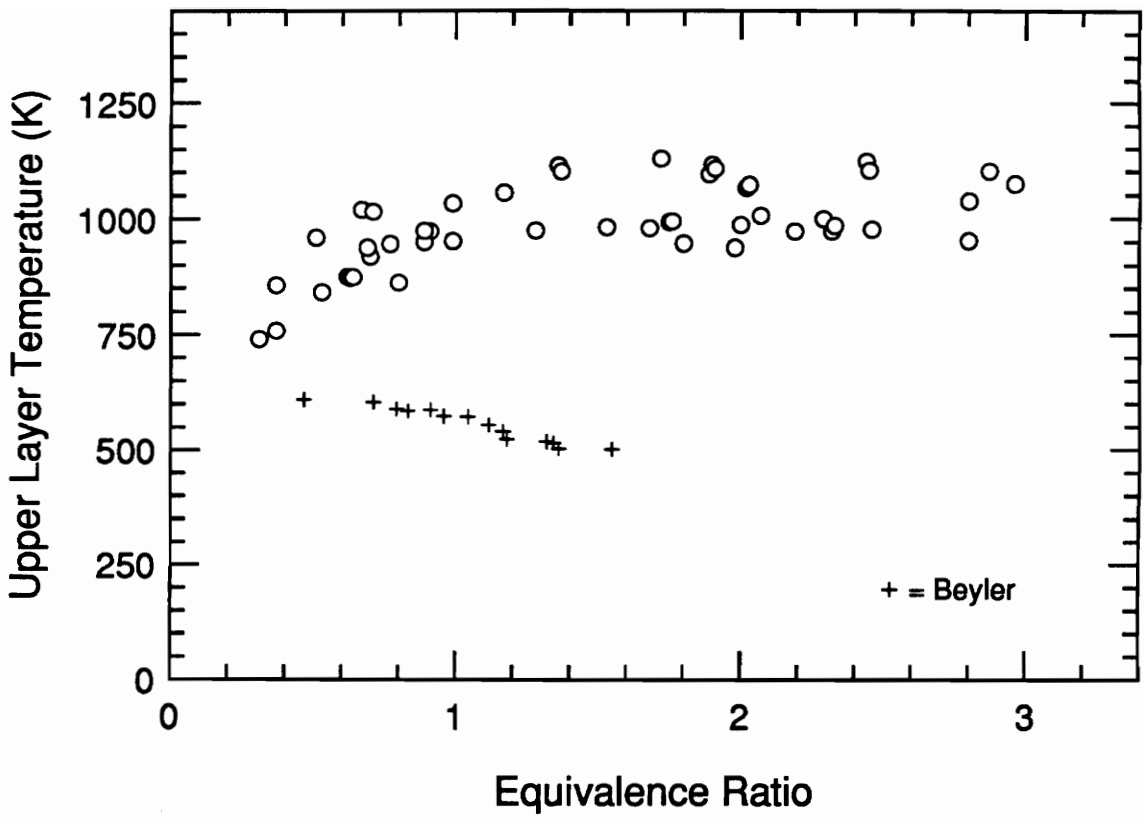

Figure 4.1 Comparison of average upper layer temperatures for hexane fires in the compartment and in Beyler's hood.

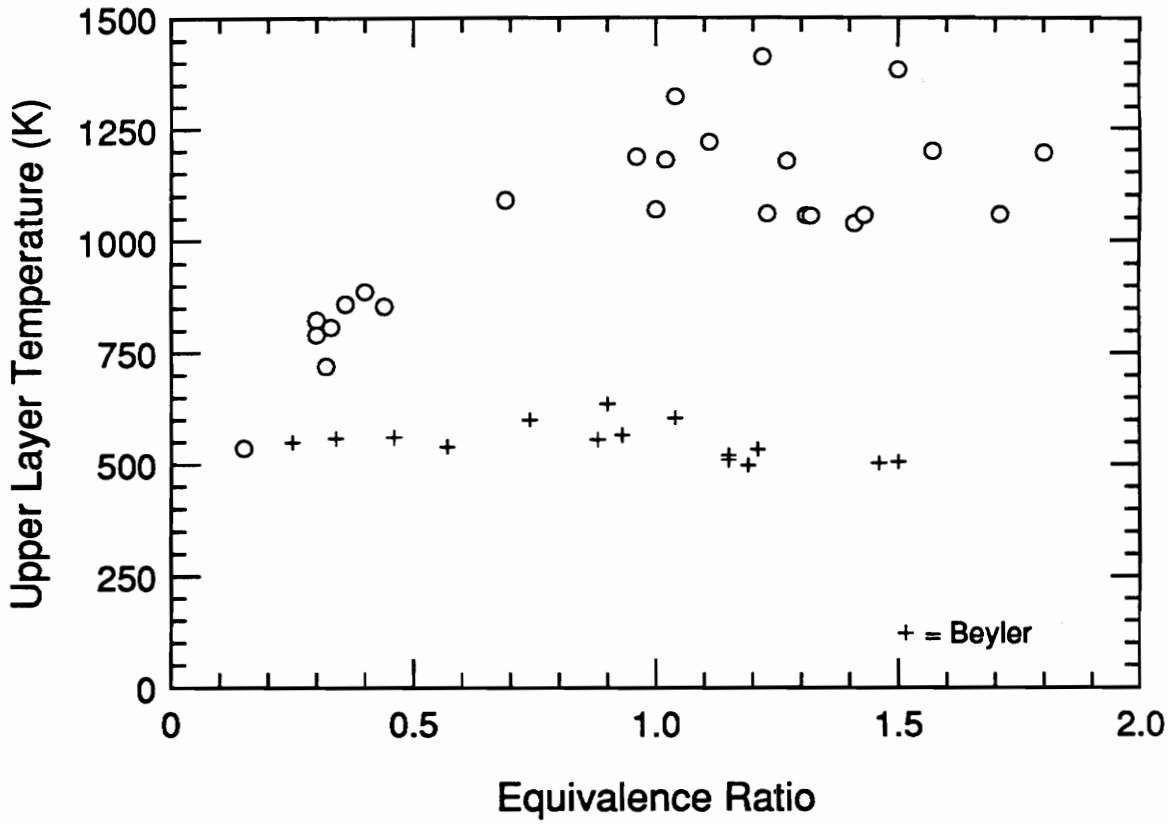

Figure 4.2 Comparison of average upper layer temperatures for PMMA fires in the compartment and in Beyler's hood.

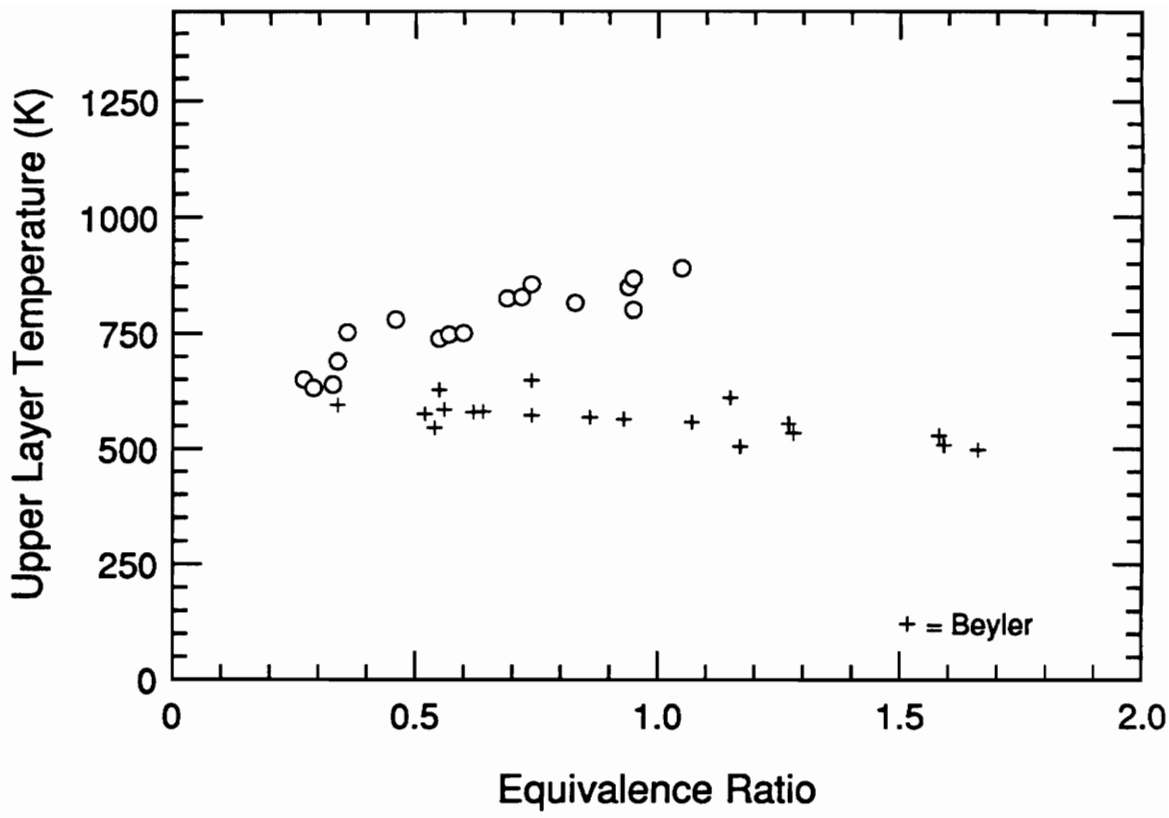

Figure 4.3 Comparison of average upper layer temperatures for wood fires in the compartment and in Beyler's hood.

a diluent and a heat sink which lowers the flame temperature. A diffusion flame burning in the open will burn at near stoichiometric conditions with a nearly constant temperature independent of the fuel supply rate. The temperature of the upper layer in a compartment fire will reflect the temperature of the fire plume. Since the fire plume is a diffusion flame, it in itself is not expected to significantly increase the temperature observed in a compartment fire as fuel burning rates increase. This assumes the plume burns independently from the layer and the entrained gas temperature is a constant, which are reasonable assumptions for the purpose of this discussion. Although the plume is a diffusion flame, a relationship between upper layer temperature and the plume equivalence ratio, similar to that of a premixed flame, can exist due to the layer being a large thermal reservoir which stores heat as the heat release of the fire increases with equivalence ratio.

The temperature correlations shown in Figures 4.1 to 4.3 show that temperatures in Beyler's hood layers were fairly constant for overventilated conditions for all fuels. This is an indication that large radiation losses from the upper layer and plume controlled the layer temperature even though higher equivalence ratios equate to more energy being supplied by the plume to the layer. For underventilated conditions, Beyler observed that increasing the equivalence ratio decreased the upper layer temperature similar to the described relationship. The compartment fires studied, exhibited quite different temperature-equivalence ratio relationships than observed in the hood experiments. The upper layer temperature increased with increasing equivalence ratio for overventilated conditions and remained fairly constant for underventilated conditions. The full enclosure apparatus resulted in reduced heat losses from the layer, and thus higher temperatures which reflect the increased energy release with increasing ϕ for overventilated

conditions. The large thermal mass of the compartment walls and upper layer was not affected by increased fuel addition during underventilated conditions as indicated by relatively constant temperatures. This is attributed to the fact that the additional fuel mass is negligible compared to the thermal mass of the upper layer environment.

In addition to a significant temperature difference between the hood and compartment fires, the larger compartment fires were observed to have larger ceiling and wall flame jets. More so for the underventilated fires, the plume would impinge on the compartment ceiling and spread radially outward. Wall flame jets, extending nearly to the layer, were observed for some compartment fires. This is contrasted by the hood experiments for which no significant flame jets existed. Layer burning was observed for hexane fires both in the hood and these compartment fires. However, when layer burning occurred in the hood experiments the layer could not be contained, thus, resulting in the inability to measure the air entrainment rate. Therefore, Beyler's yield-equivalence ratio correlations only include data for fires with no layer burning. The correlations identified for the compartment fires, however, do include cases in which layer burning was occurring. Lastly, the compartment fires were much more transient than the fires studied by Beyler. The typical concentration and equivalence ratio time histories presented in chapter 3 (Figures 3.7, 3.20 and 3.31) showed the transient nature of the fires, which is also discussed in the next section.

4.2.2 Transient Nature

Particularly for hexane, since finite fuel sources were used in the compartment study, the fires were expected to be more transient in nature than the hood experiment fires. In order to determine whether the species yield correlations developed were

applicable to transient or steady-state fire environments, the steady-state nature of the fires was investigated by studying the residence time and a steady-state time ratio.

The residence time was defined as the time required for a unit volume of air to move through the upper layer volume and was calculated by dividing a representative upper layer volume by the inlet air volumetric flow rate. Residence times ranged from 3 to 80 seconds. Typically, residence times were 4-10 seconds for hexane and PMMA fires and 15-20 seconds for spruce and polyurethane fires. Beyler's upper layer residence times were on the order of 40 seconds.

A steady-state time ratio was defined as the ratio of the residence time to a characteristic growth time of the fire. Fire growth is directly related to the fuel volatilization rate. Therefore, the ratio of the fuel rate to the derivative of the fuel rate was deemed a representative growth time of the fire. The steady-state time ratios were well below 1.0 for all fires, thereby, signifying quasi-steady-state fire situations. Investigation of individual fires showed that the steady-state ratio decreased below 1.0 at very early times in the fire, thus, suggesting that the fires were of a quasi-steady-state nature almost from the start. Typically, the ratio was well below 0.1 for the steady-state periods over which data was averaged. The steady-state ratio increased over 0.1 and in some cases approached a value of one during the transition from over- to underventilated conditions. However, the ratio quickly decreased as a steady underventilated condition was reached. The assumption is therefore made that the plume and upper layer equivalence ratios are equal during the "steady-state" period and comparison between the hood experiments and these compartment fires are on an equivalent basis. So comparison between the hood and compartment fires provides little information on the effect of transient conditions on the species yield correlations.

To investigate the effect of transient conditions on the species yield correlations, the yield to equivalence ratio relationship was examined for individual fires from the time of ignition to the steady state period. Examples of these transient correlations were included in the results for each fuel in chapter 3. Figures 4.4 shows the steady-state hexane CO yield correlation along with the transient yield versus equivalence ratio data for a hexane fire that obtained a steady-state average ϕ of 3. The agreement between the transient and steady-state correlations is quite good. For the same hexane fire, the CO_2 and O_2 transient yields are compared to the steady-state correlations in Figures 4.5 and 4.6. The correlations agree well. Figures 4.7 to 4.15 present the comparison of the transient species yield correlations to the steady-state correlations for the other three fuels.

For all fuels tested, the transient yield data agrees well with the quasi-steady-state yield-equivalence ratio correlations. However, it can be seen that the transient CO_2 and O_2 yields were lower than the steady-state correlations for some overventilated conditions, typically for $0.5 < \phi_p < 1$. This departure is the result of the transient nature of the fire. As discussed previously, the quasi-steady state periods were characterized as such by the steady-state time ratios less than 0.1 and the observation of species concentrations and the equivalence ratio leveling out. However, during the transition to underventilated conditions in which the equivalence ratio changes quickly, the steady-state time ratio increase over 0.1. Although values of 1 are not obtained, the increase in the steady-state time ratio is indicative of more transient conditions. As a result, the upper layer acts as a collection reservoir in which the species concentrations become time averaged. Therefore, the CO_2 and O_2 concentrations are effectively diluted and, thus, the yields decrease, as the fires grow during the transitory periods.

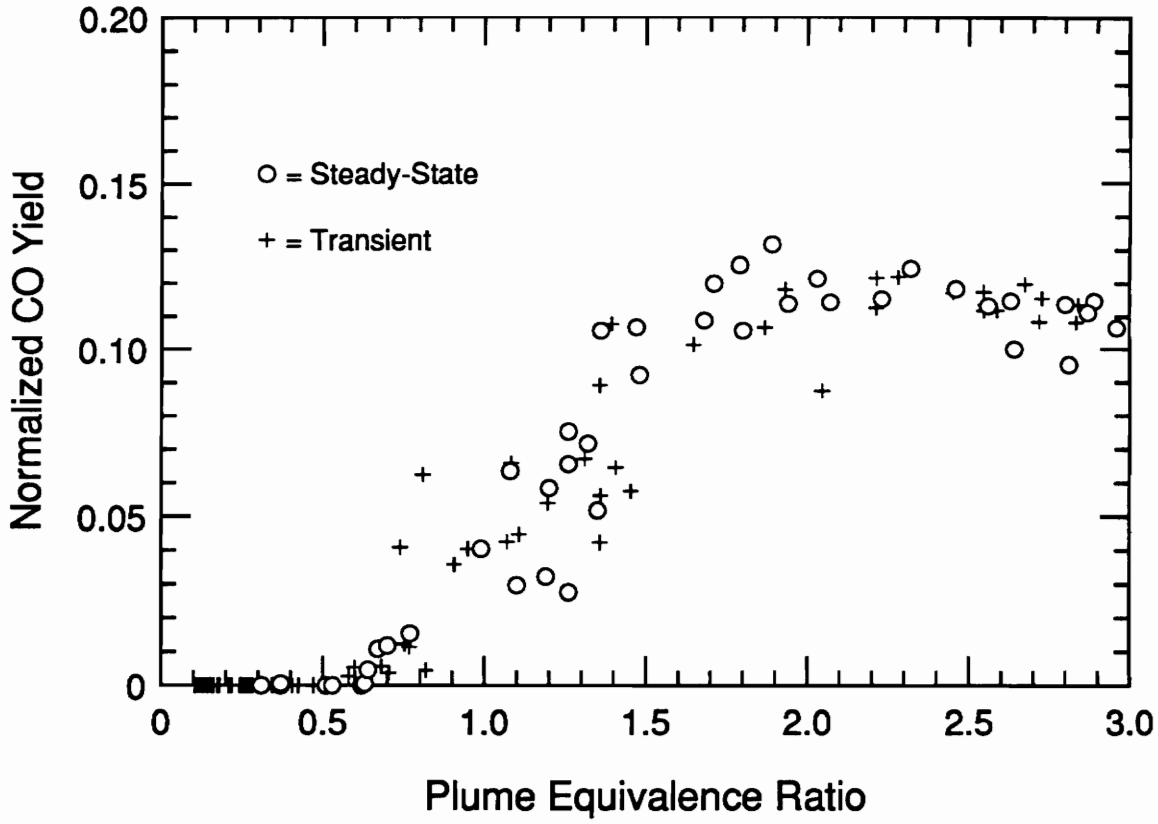

Figure 4.4 Comparison between a transient, normalized CO yield correlation for a hexane fire with an average steady-state ϕ_p of 3 and the steady-state correlation for all hexane fires.

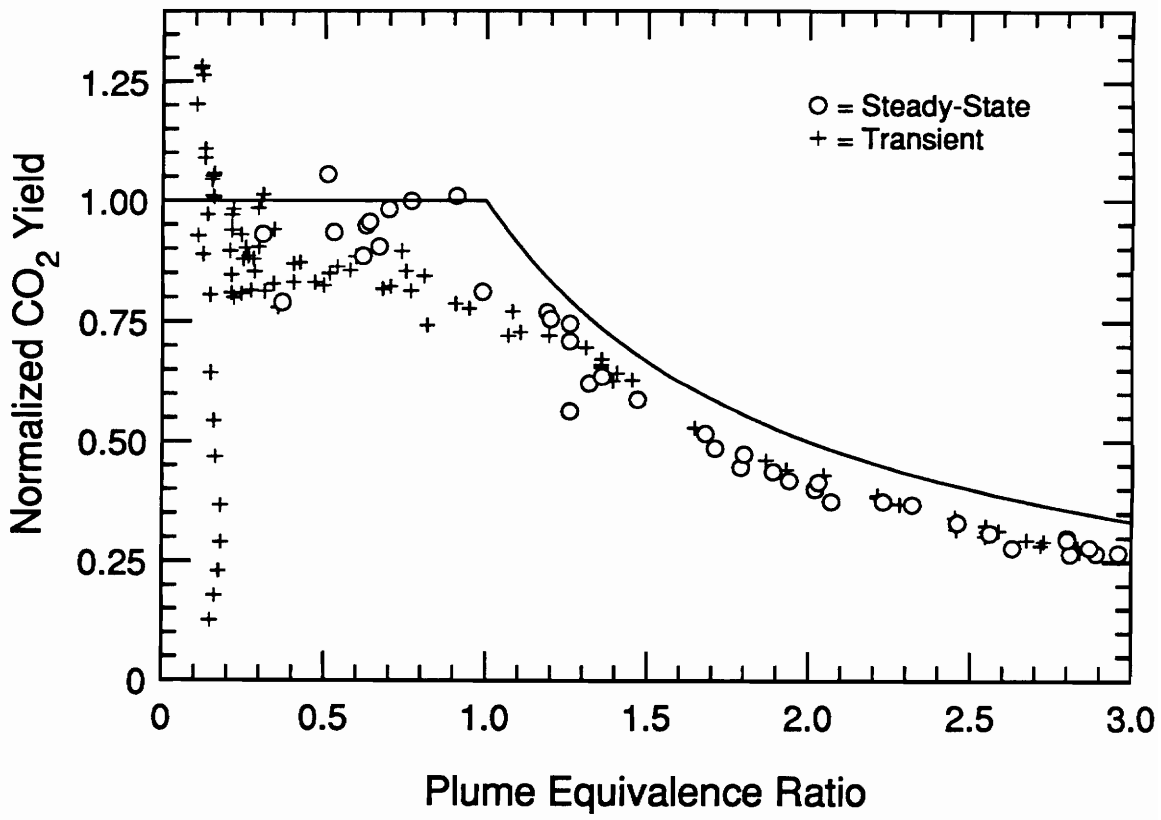

Figure 4.5 Comparison between a transient, normalized CO_2 yield correlation for a hexane fire with an average steady-state ϕ_p of 3 and the steady-state correlation for all hexane fires.

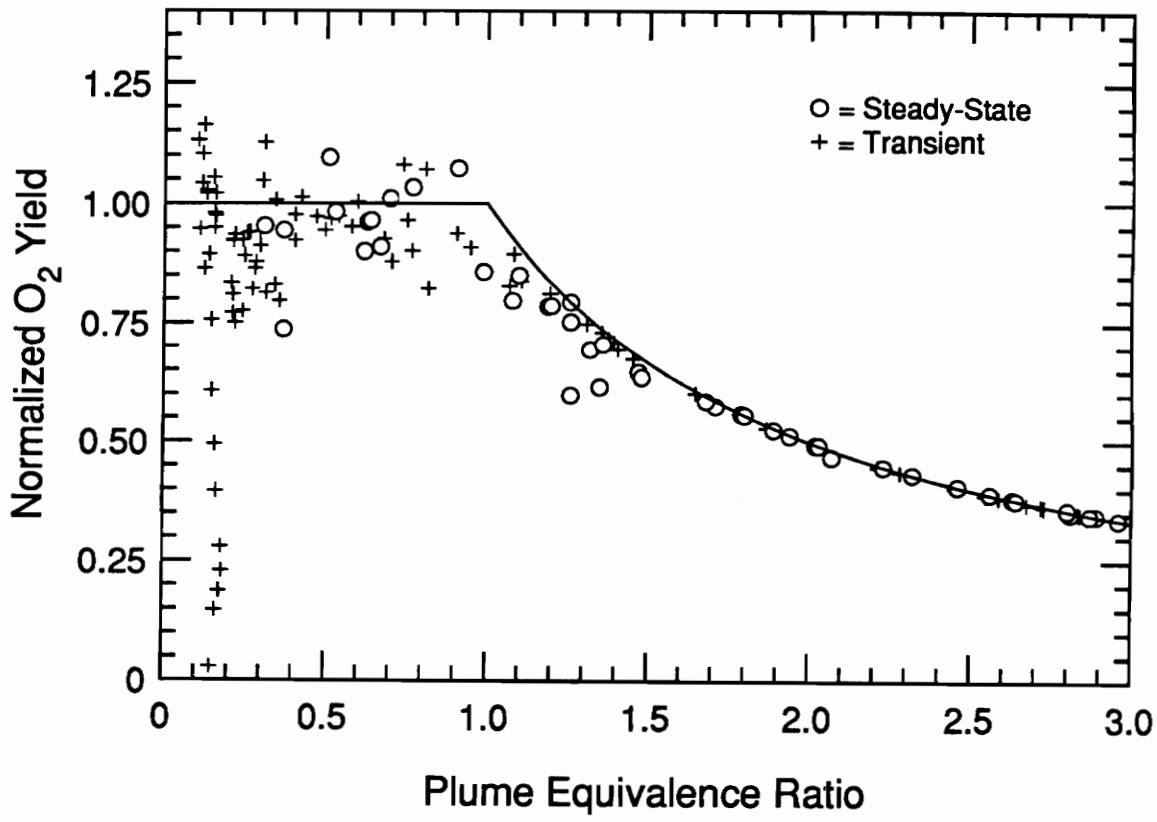

Figure 4.6 Comparison between a transient, normalized O_2 yield correlation for a hexane fire with an average steady-state ϕ_p of 3 and the steady-state correlation for all PMMA fires.

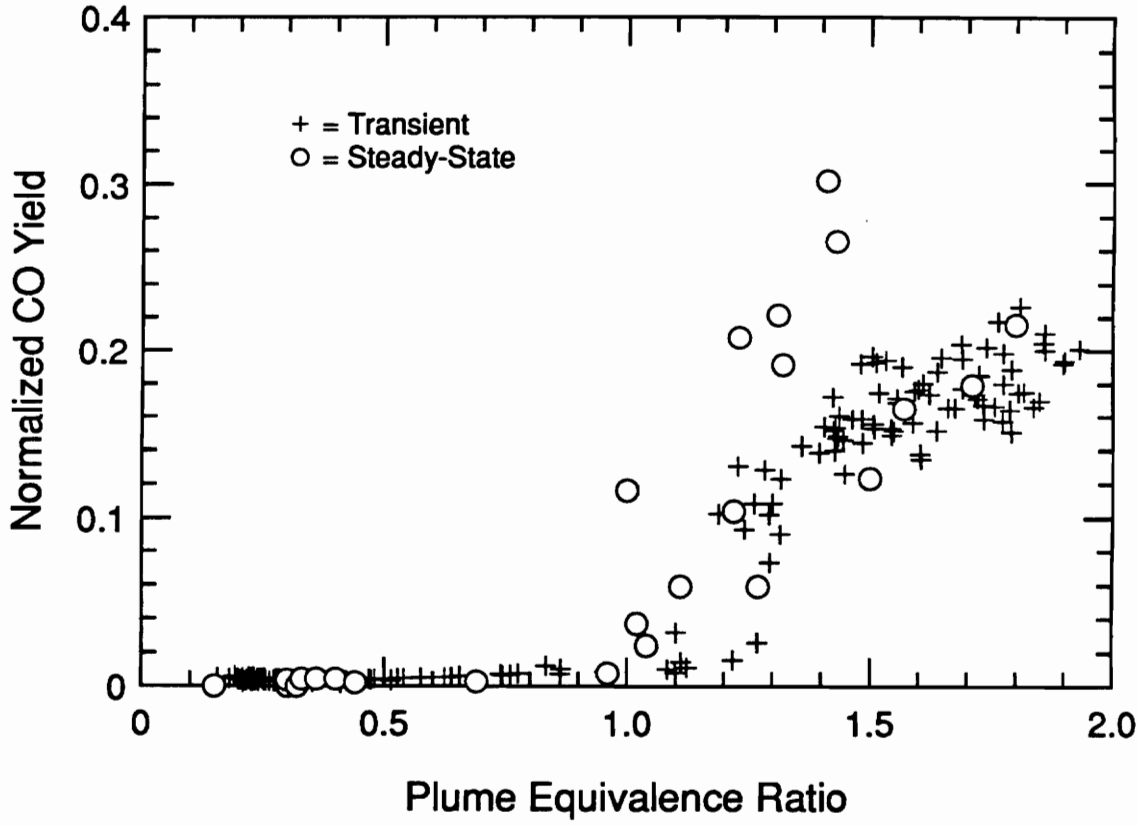

Figure 4.7 Comparison between a transient, normalized CO yield correlation for a PMMA fire with an average steady-state ϕ_p of 1.8 and the steady-state correlation for all PMMA fires.

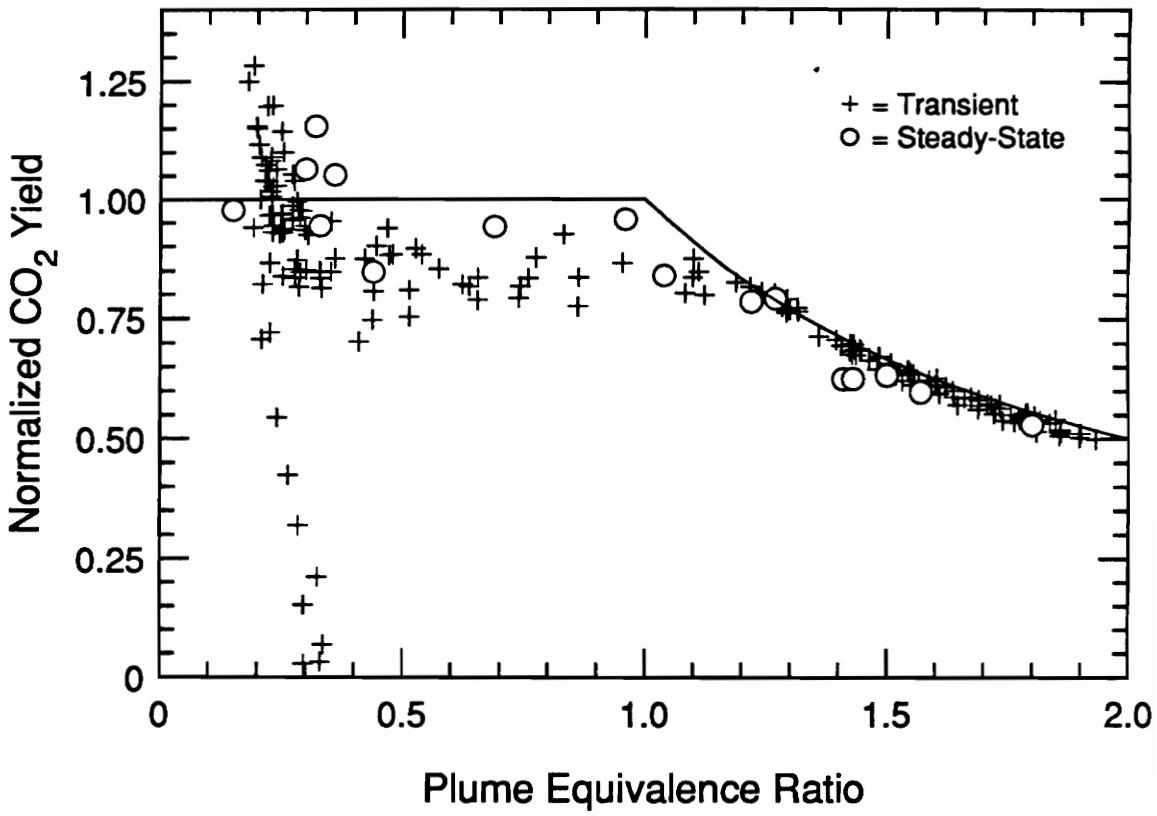

Figure 4.8 Comparison between a transient, normalized CO_2 yield correlation for a PMMA fire with an average steady-state ϕ_p of 1.8 and the steady-state correlation for all PMMA fires.

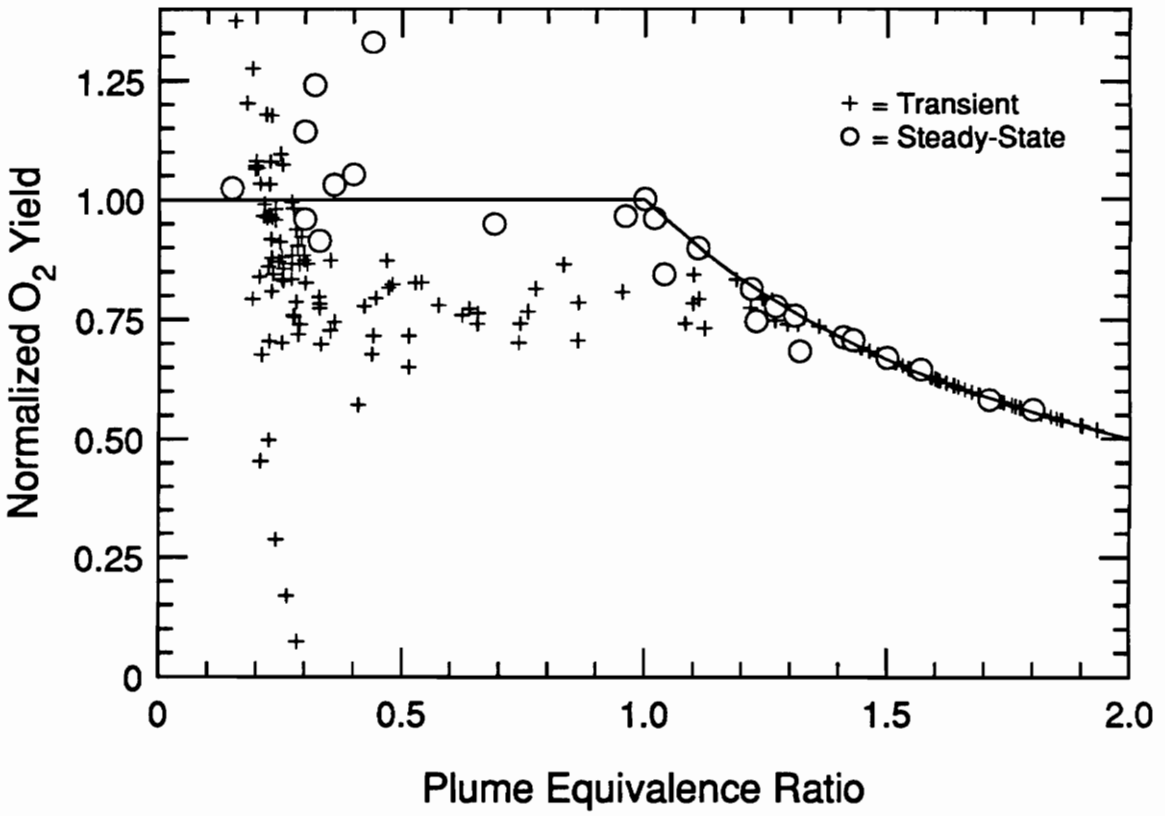

Figure 4.9 Comparison between a transient, normalized O_2 yield correlation for a PMMA fire with an average steady-state ϕ_p of 1.8 and the steady-state correlation for all PMMA fires.

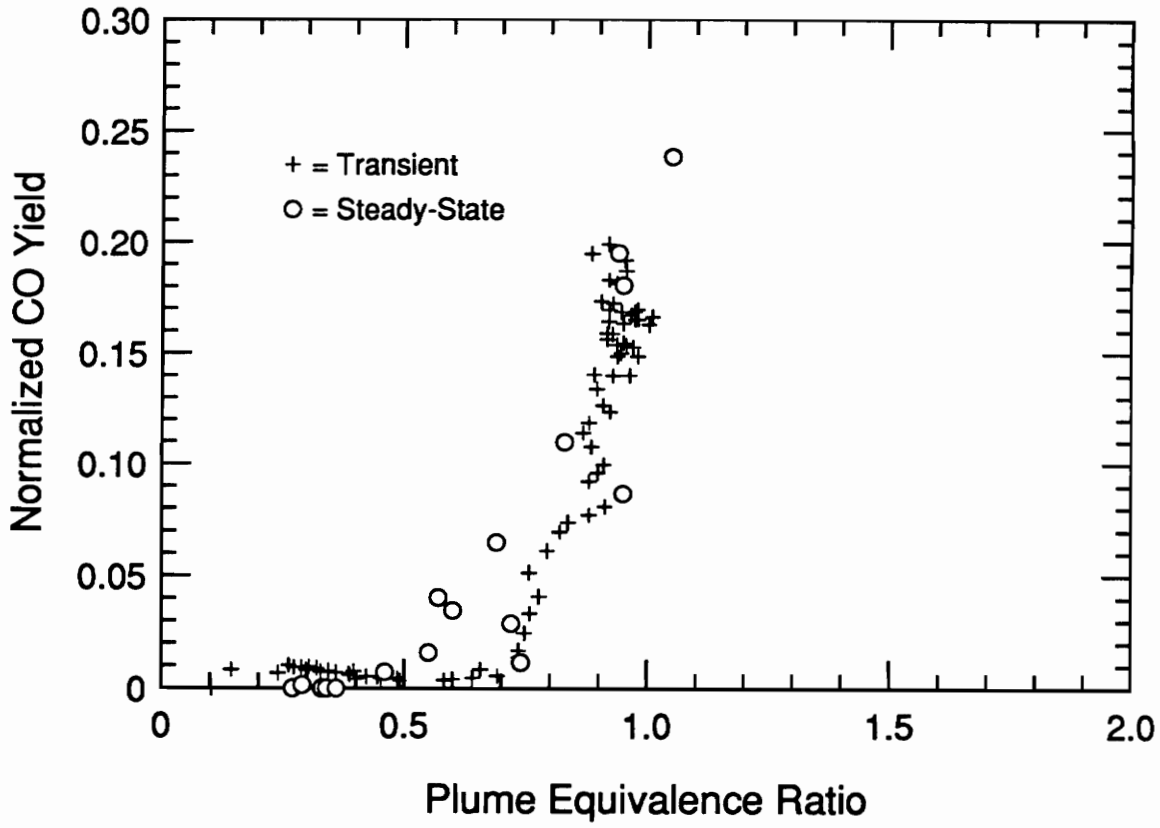

Figure 4.10 Comparison between a transient, normalized CO yield correlation for a spruce fire with an average steady-state ϕ_p of 0.95 and the steady-state correlation for all spruce fires.

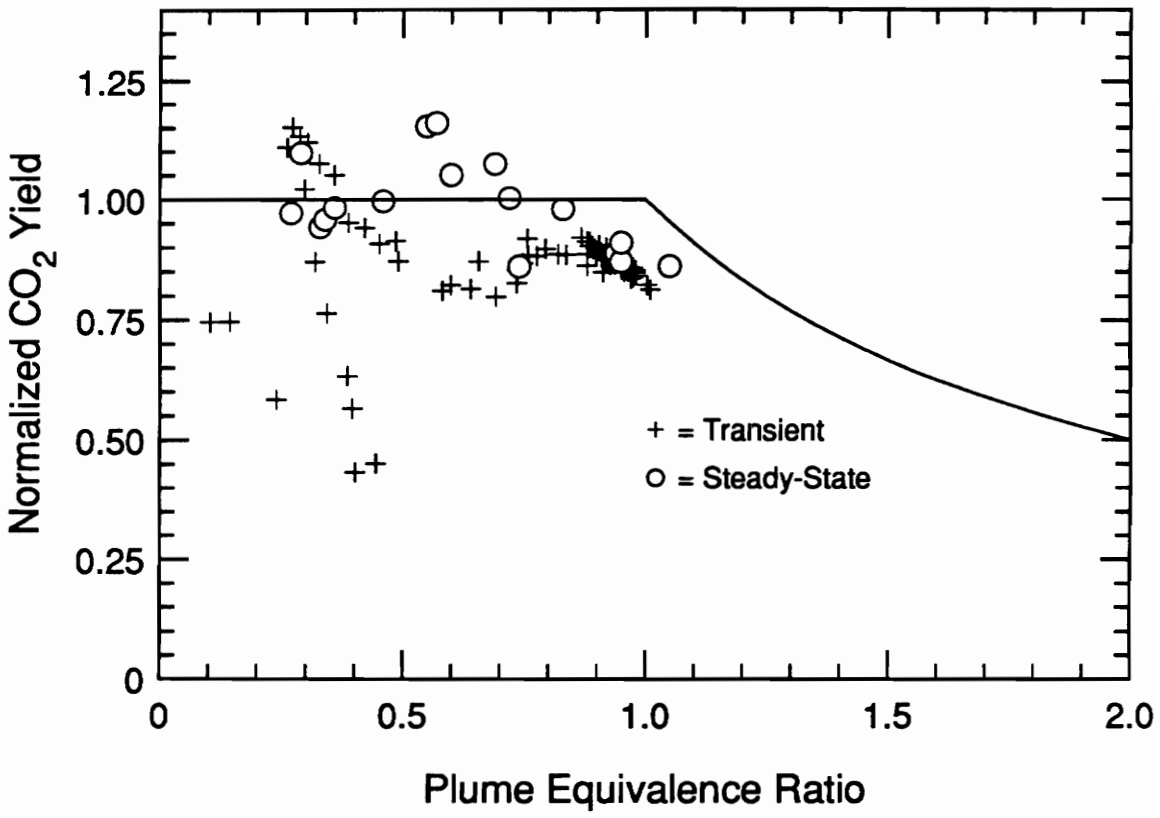

Figure 4.11 Comparison between a transient, normalized CO_2 yield correlation for a spruce fire with an average steady-state ϕ_p of 0.95 and the steady-state correlation for all spruce fires.

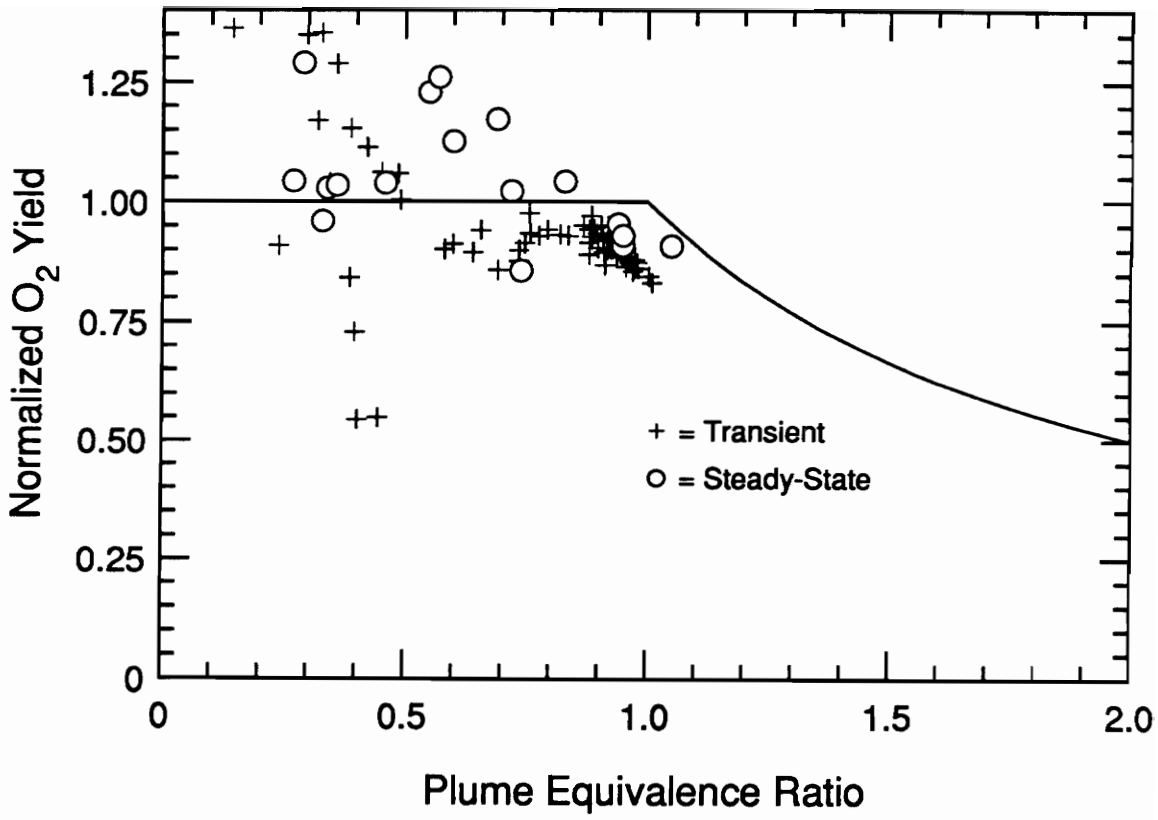

Figure 4.12 Comparison between a transient, normalized O_2 yield correlation for a spruce fire with an average steady-state ϕ_p of 0.95 and the steady-state correlation for all spruce fires.

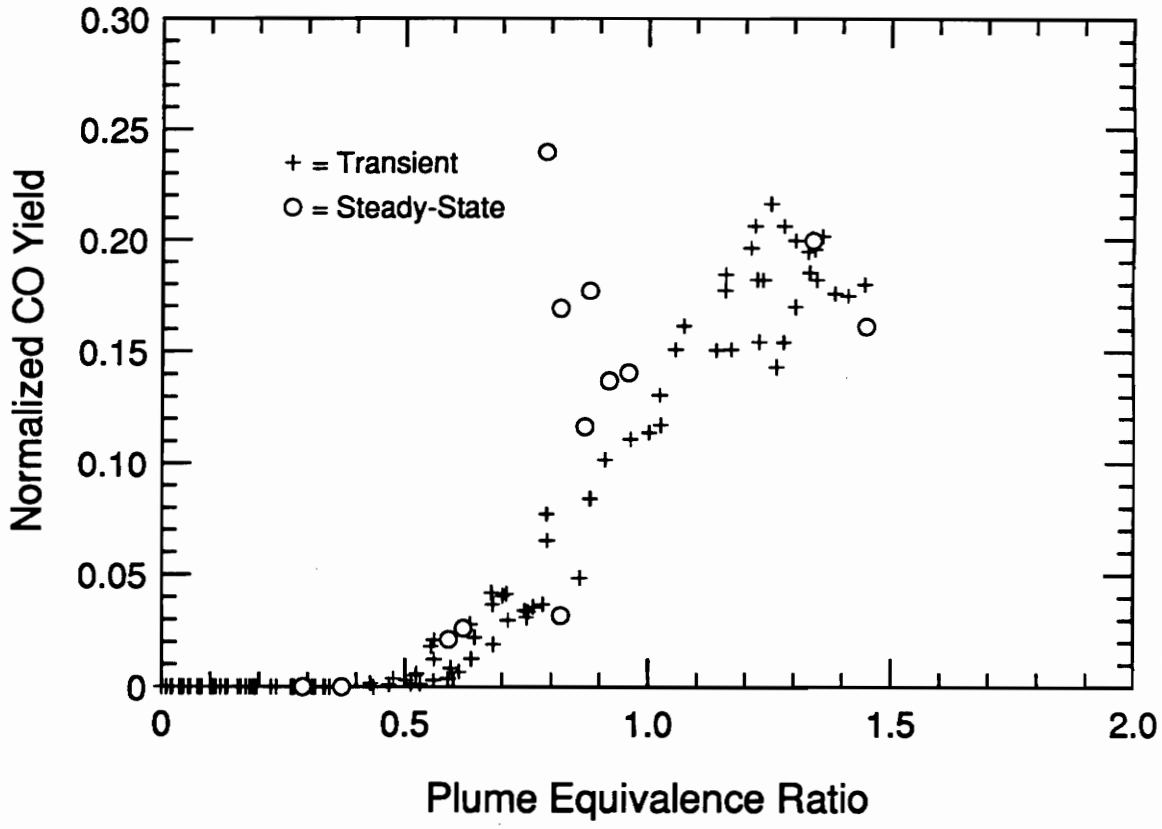

Figure 4.13 Comparison between a transient, normalized CO yield correlation for a polyurethane fire with an average steady-state ϕ_p of 1.3 and the steady-state correlation for all polyurethane fires.

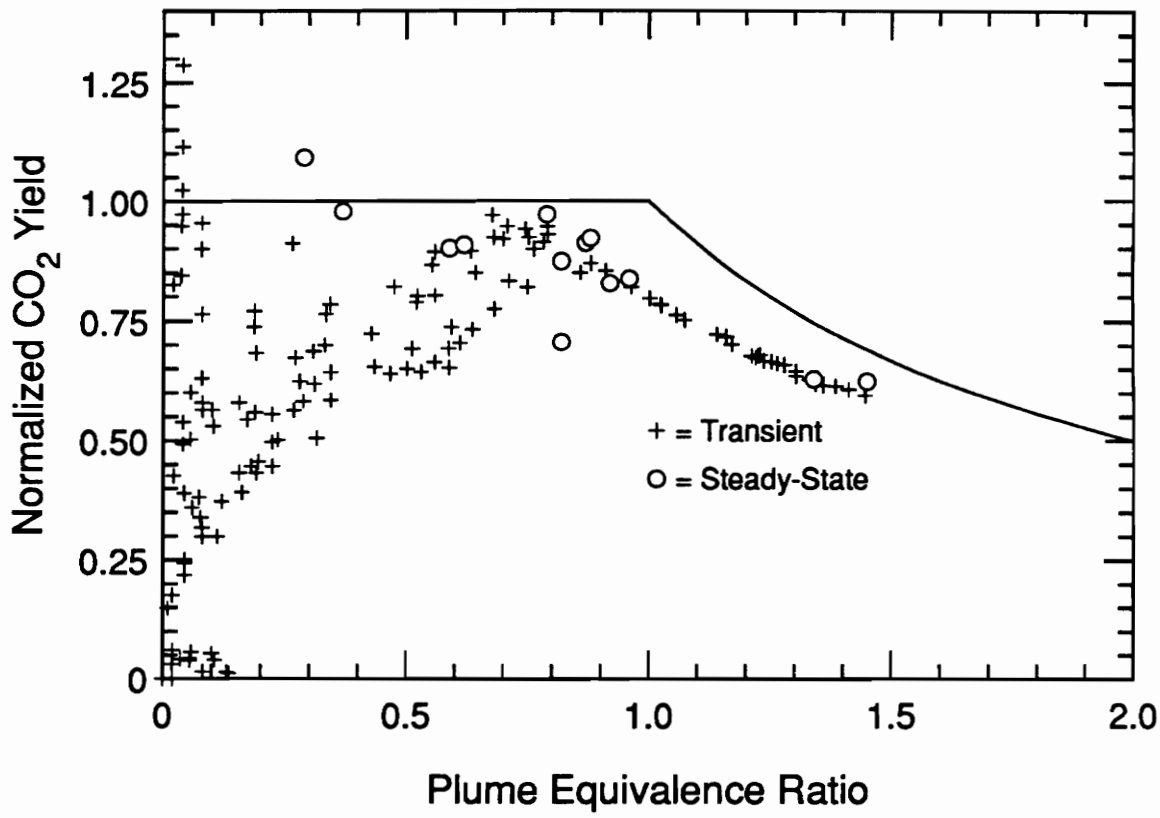

Figure 4.14 Comparison between a transient, normalized CO_2 yield correlation for a polyurethane fire with an average steady-state ϕ_p of 1.3 and the steady-state correlation for all polyurethane fires.

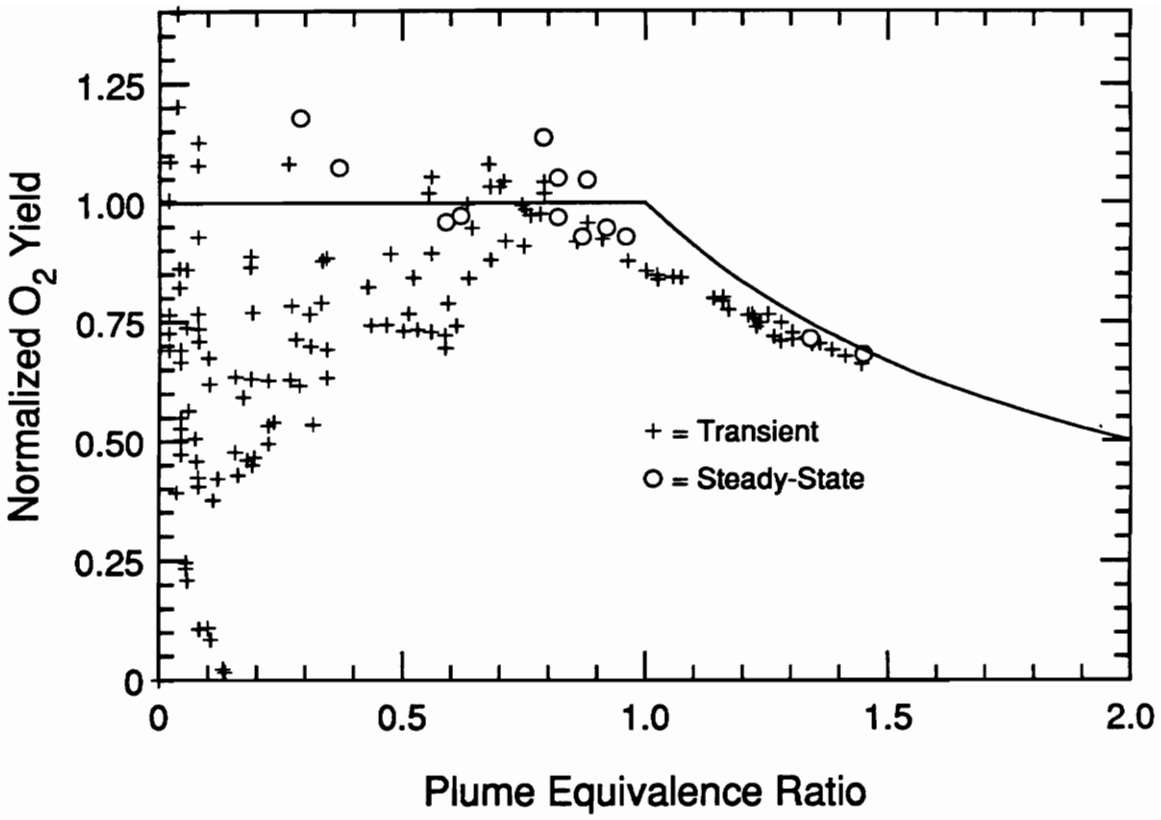

Figure 4.15 Comparison between a transient, normalized O_2 yield correlation for a polyurethane fire with an average steady-state ϕ_p of 1.3 and the steady-state correlation for all polyurethane fires.

An example of this is seen in Figure 4.16 which presents the CO yield, equivalence ratio and steady-state time ratio for the spruce fire shown in Figures 4.10 to 4.12 as transient data. The fire grew rapidly at first as indicated by the high steady-state time ratios. At 77 seconds the steady-state time ratio fell below 0.1 and the equivalence ratio began to level out at about 0.9 indicating a steady-state burning condition was achieved. Therefore, the transient overventilated CO_2 and O_2 yields are expected to be less than unity due to ϕ_{ul} lagging behind ϕ_p during the rapid growth period from very overventilated ($\phi_p < 0.4$) to underventilated conditions. The transient CO yield is also affected in the same manner as seen in Figure 4.12.

Although more transient in nature, the compartment fires are characterized as primarily quasi-steady in nature and therefore, do not differ significantly from Beyler's hood experiments in this respect. This analysis also shows that the species yield correlations developed for steady-state conditions are representative of the quasi-steady growth periods of these fires except when very transient conditions occur, such as the transition from over- to underventilated conditions.

4.2.3 Layer Composition

4.2.3.1 Hexane

In general the species yields in the compartment fires correlate very well with the plume equivalence ratio as was seen in the results of Chapter 3. Comparison of these compartment fire yield correlations to those obtained from the hood fires of Beyler are discussed below for each fuel.

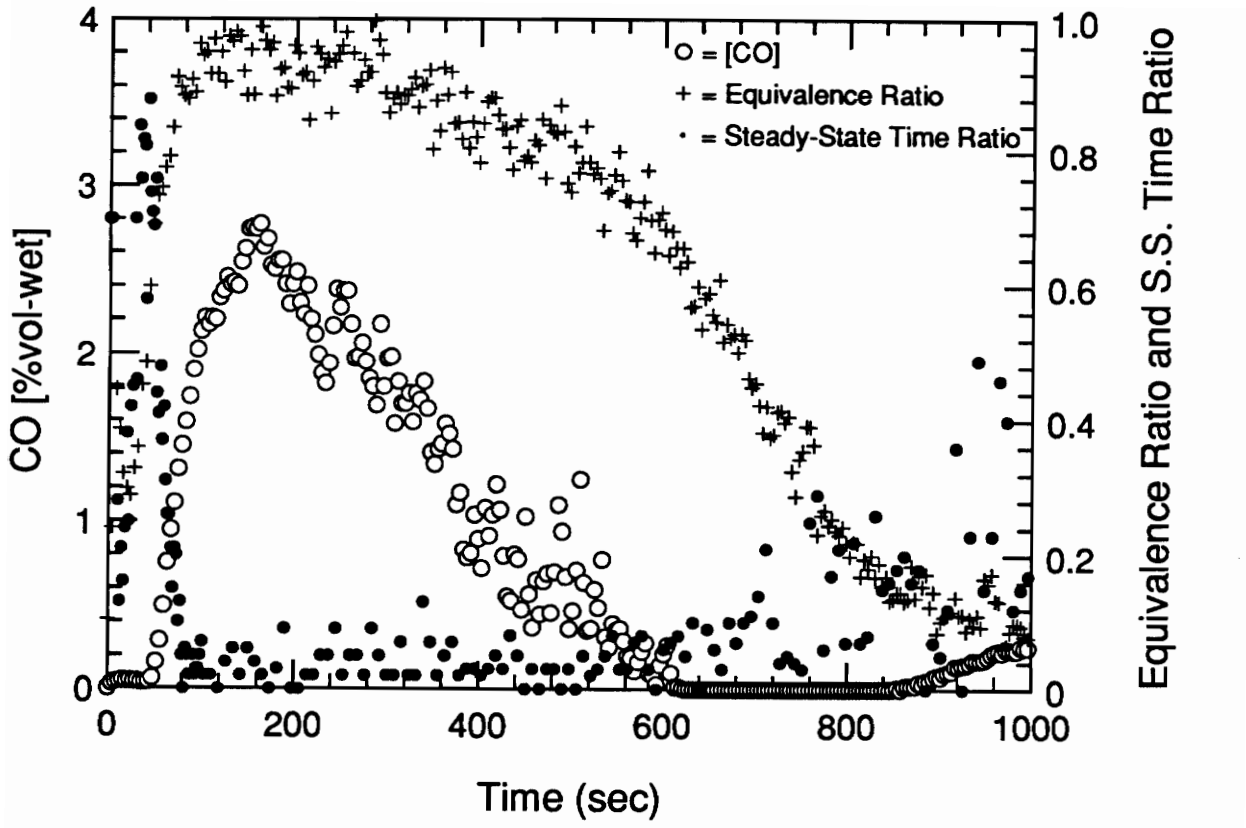

Figure 4.16 Time history of CO yield, equivalence ratio and steady-state time ratio for the spruce fire shown in Figures 4.10 to 4.12 as transient data.

Figure 4.17 shows the CO yield correlations obtained from both the compartment fires and Beyler's hood fires. As can be seen for the compartment fires, CO yields are near zero for fires with equivalence ratios less than 0.6. Above ϕ_p of 0.6, CO production starts to occur; however, significant levels are obtained only for underventilated fires. This is illustrated in Figure 3.9 which shows CO concentrations under 2000 ppm for overventilated fires. Beyler's CO yields begin to rise at about the same equivalence ratio, but are considerably higher for fires with ϕ_p up to about 1.3. Although qualitatively similar, the differences between correlations leads to a significant different hazard assessment for overventilated and slightly underventilated fires. Similarly for both types of experiments, CO yields appear to level out for very underventilated fires. The CO yield approaches a value of 0.9 for the hood fires, and clearly levels out to an average of 0.11 for the compartment fires.

The normalized CO_2 and O_2 yield correlations are presented in Figures 4.18 and 4.19 for the compartment and hood hexane fires. The compartment CO_2 and O_2 normalized yields agree more closely with the model than the hood data. Departure from the model is represented by the yield coefficient, which is the yield divided by the predicted value. As can be seen in Figure 4.18, the CO_2 yield coefficient, B_{CO2}, increases only slightly with equivalence ratio and can be represented as an average of 0.83 for $\phi >$ 1. The hood fires are characterized with an average B_{CO2} of 0.61 which also is quite independent of ϕ_p, for $\phi_p > 1$. Table 4.2 presents the average yield coefficients for all the fuels tested, including Beyler's data.

The compartment fires exhibited nearly complete utilization of O_2 (B_{O2} of 0.96), whereas, the hood fires were less efficient with an average yield coefficient, B_{O2}, of 0.82 for $\phi > 1$. This is also illustrated in Figure 3.11 which shows typically 1 percent to no

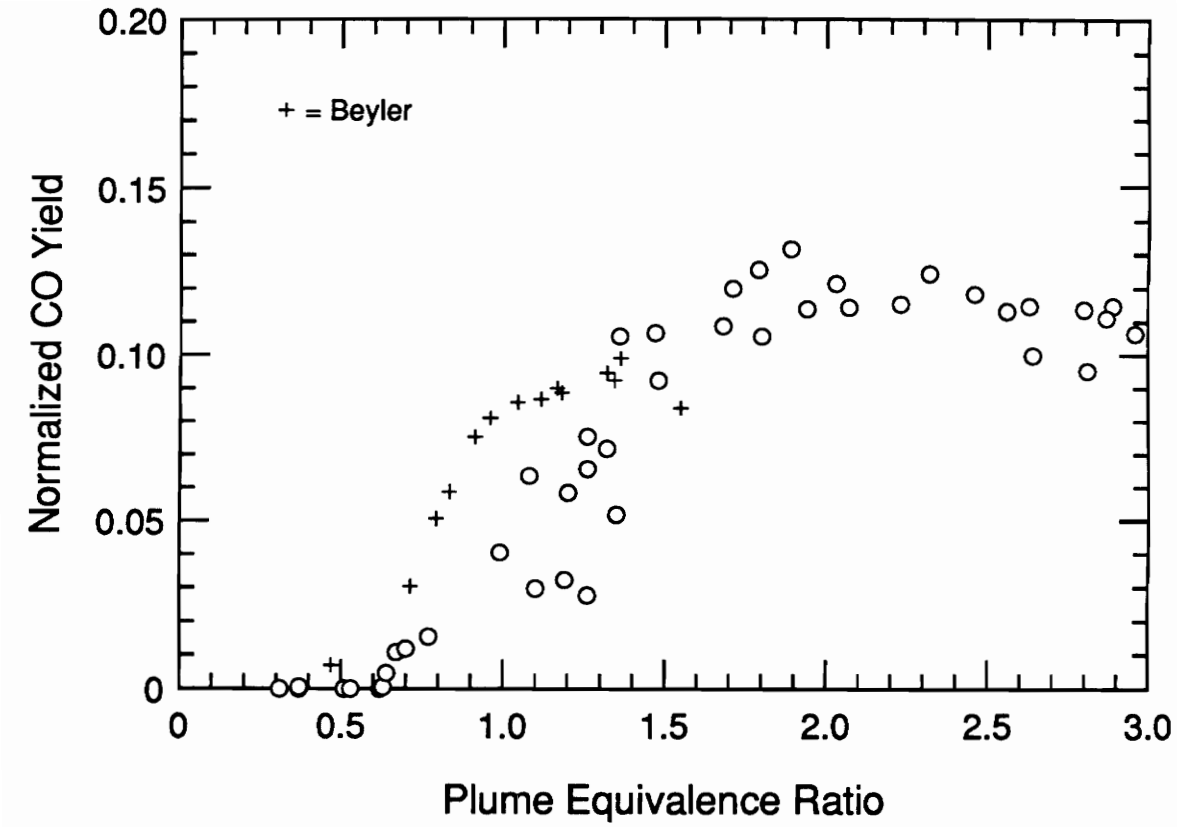

Figure 4.17 Comparison of normalized CO yield correlations obtained for hexane fires in the compartment and in Beyler's hood.

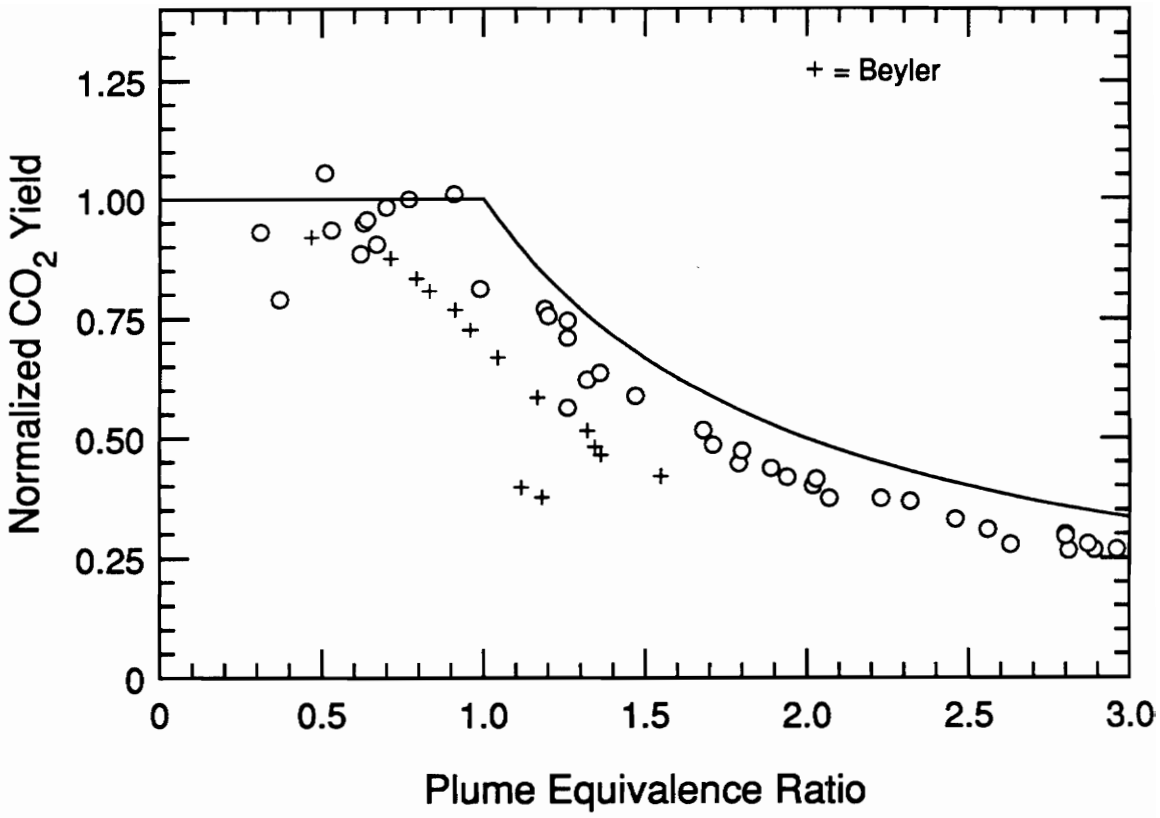

Figure 4.18 Comparison of normalized CO_2 yield correlations obtained for hexane fires in the compartment and in Beyler's hood.

Table 4.2 Average CO_2 and O_2 yield coefficients for all the fuels tested in the compartment fires and for the similar fuels tested by Beyler in hood experiments. The standard deviation is shown in parentheses.

FUEL	B_{CO2}		B_{O2}	
	$\phi<1$	$\phi>1$	$\phi<1$	$\phi>1$
Hexane	0.93 (0.08)	0.83 (0.05)	0.95 (0.09)	0.96 (0.06)
PMMA	0.99 (0.09)	0.93 (0.04)	1.06 (0.14)	0.98 (0.04)
Spruce*	0.99 (0.09)	0.90 (0)	1.05 (0.13)	0.95 (0)
Polyurethane#	0.90 (0.10)	0.87 (0.04)	1.02 (0.09)	0.97 (0.02)
BEYLER:				
Hexane	0.82 (0.07)	0.61 (0.10)	0.92 (0.04)	0.82 (0.02)
PMMA	0.83 (0.10)	0.77 (0.06)	0.90 (0.07)	0.92 (0.19)
Ponderosa Pine	0.92 (0.08)	0.85 (0.05)	0.93 (0.10)	0.89 (0.03)

* $\phi_p > 1$ represents only one fire

$\phi_p > 1$ represents only two fires

measurable O_2 in the compartment upper layers for underventilated fires and about 3 percent O_2 for the hood fires. For fires with available O_2 in the upper layer (i.e. $\phi_p \leq 1.5$) combustion is more complete in the compartment apparatus as indicated by the lower CO and higher CO_2 yields than in the hood experiments. As can be seen in Figure 4.19, full utilization of O_2 in the compartment fires occurs for $\phi_p > 1.5$. It is for these same fires that the CO yield plateaus. With the fact that B_{CO2} does not decrease, this indicates that the additional fuel does not contribute to the chemistry of the fire but only increases the yield of unburned hydrocarbons. The data bears this out, as measured total hydrocarbon production increases with increasing equivalence ratio.

4.2.3.2 PMMA

The comparison between PMMA yield correlations obtained from the compartment and the hood experiments is quite similar to that of hexane. Figure 4.20 presents the normalized CO yield correlations for both the compartment and hood experiments. In the compartment fires, CO yields are near zero for overventilated fires and increase with increasing underventilated conditions. Typically, Beyler observed higher CO yields than in this study for fires with $\phi \leq 1.3$. Similar to the hood hexane correlation, Beyler observed quite high yields for overventilated fires, in contrast to virtually no CO production in the compartment. Beyler's results also show the yield leveling off to a value of about 0.14, which is 30 to 50 percent lower than the yields observed for the underventilated compartment fires. Carbon monoxide levels as high as 6.3 percent by volume were observed for the compartment fires, approximately twice that observed by Beyler.

As can be seen in Figures 4.21 and 4.22, the compartment CO_2 and O_2 normalized yields for PMMA agree better with the model than does the hood data. The compartment

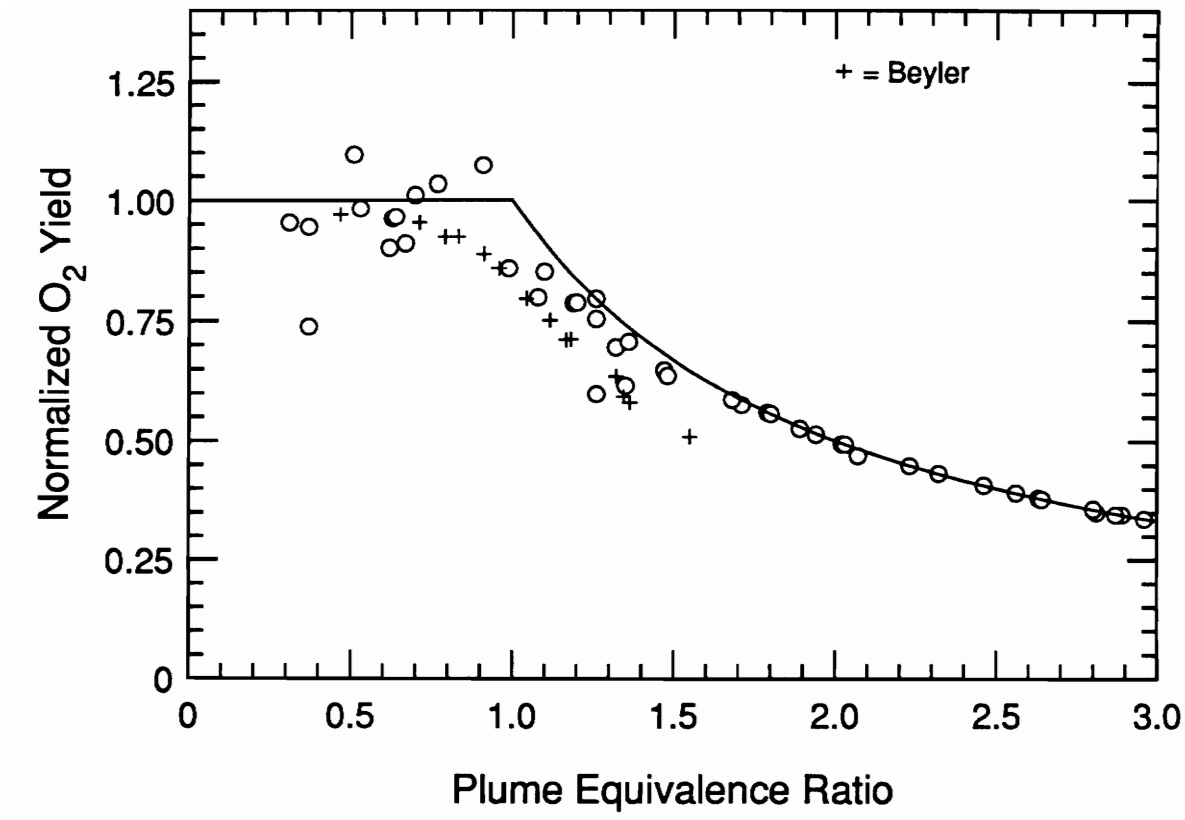

Figure 4.19 Comparison of normalized O_2 yield correlations obtained for hexane fires in the compartment and in Beyler's hood.

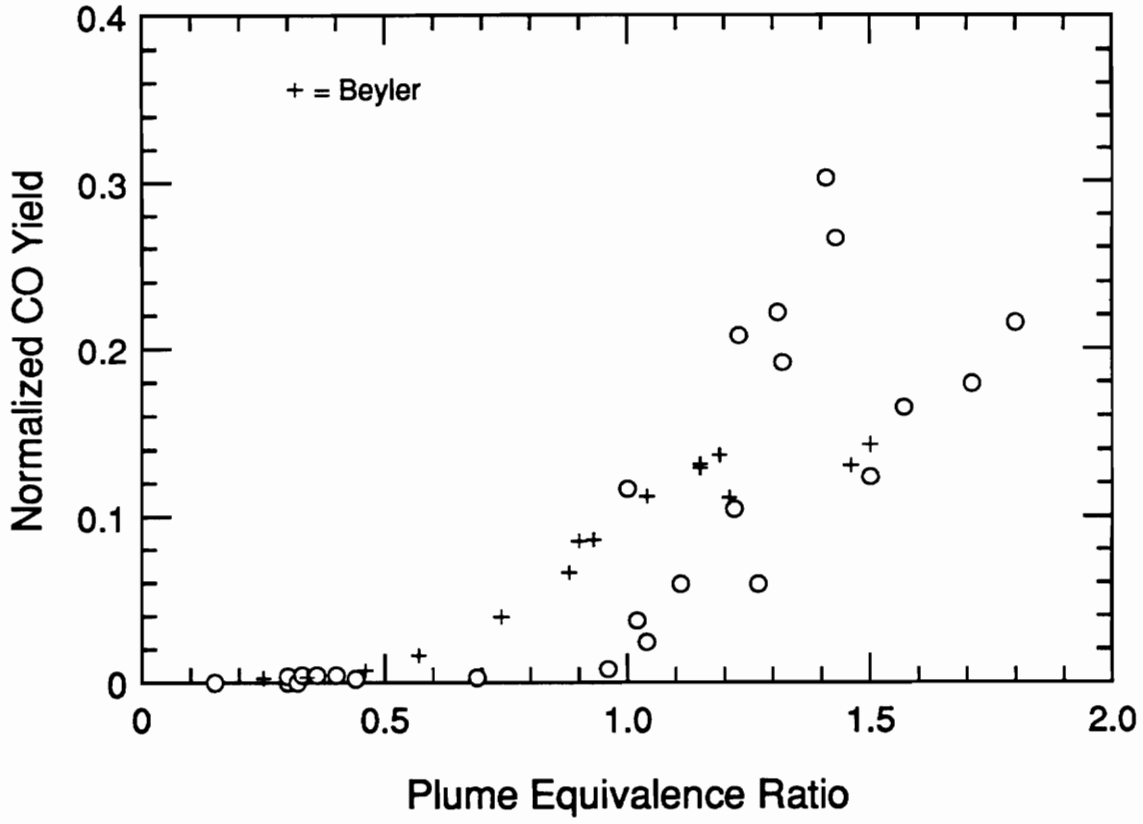

Figure 4.20 Comparison of normalized CO yield correlations obtained for PMMA fires in the compartment and in Beyler's hood.

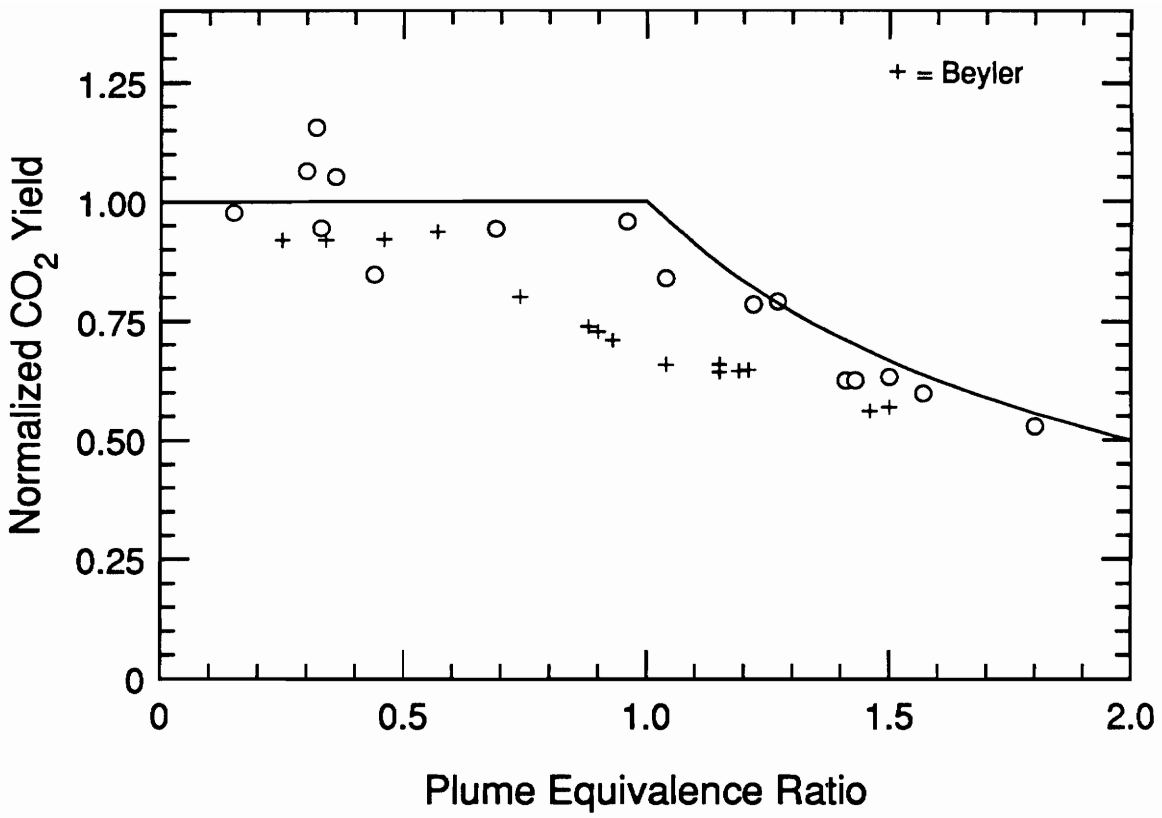

Figure 4.21 Comparison of normalized CO_2 yield correlations obtained for PMMA fires in the compartment and in Beyler's hood.

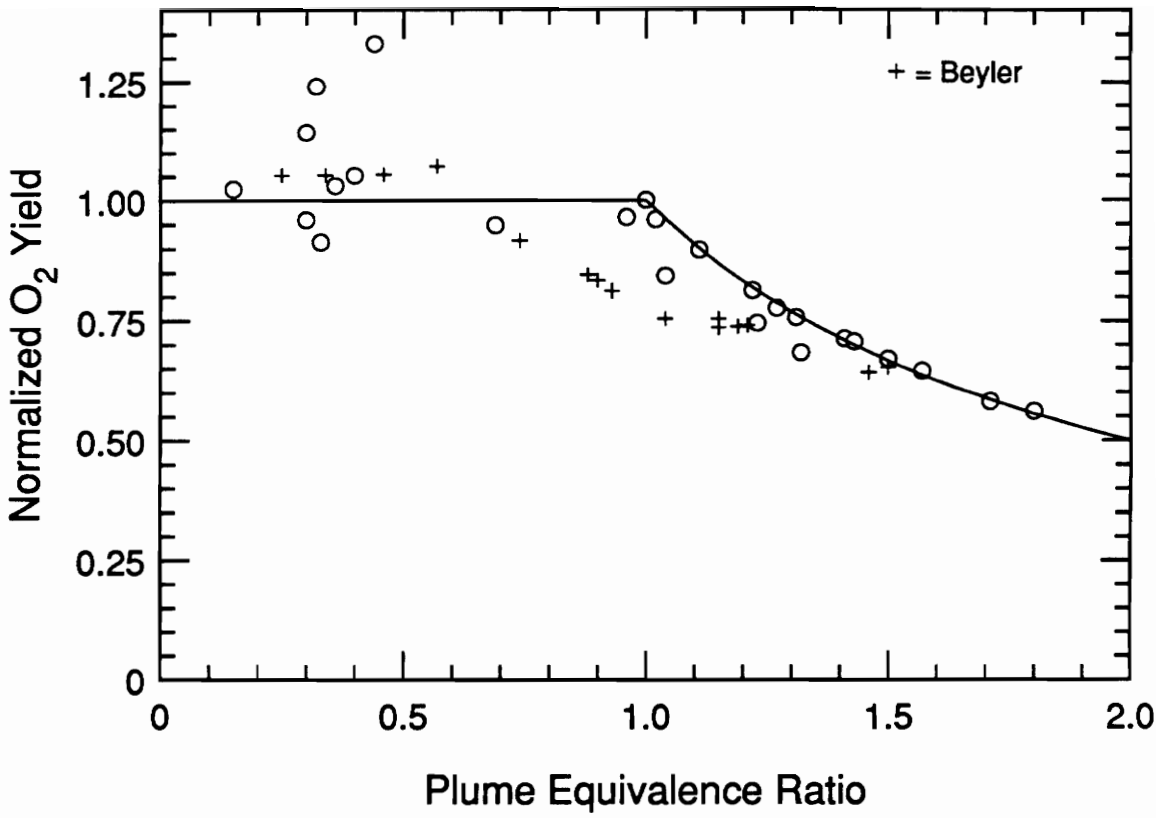

Figure 4.22 Comparison of normalized O_2 yield correlations obtained for PMMA fires in the compartment and in Beyler's hood.

fires exhibited nearly complete utilization of O_2, whereas, the hood fires were less efficient with an average O_2 yield coefficient of 0.92 for $\phi > 1$ compared to 0.98 for the compartment tests.

4.2.3.3 Wood

Unlike the hexane and PMMA comparisons, the wood yield correlations are relatively the same between the hood and compartment fires. As can be seen in Figure 4.23, CO yields begin to rise about an equivalence ratio of 0.6 for both the compartment and hood environments. However, higher CO yields were observed in the compartment than in the hood upper layers. Beyler observed CO yields leveling out at an average of 0.155 which is about two-thirds of the maximum yield observed in the compartment.

Figures 4.24 and 4.25 show the normalized CO_2 and O_2 yield correlations for the compartment and hood wood crib fires. The agreement between data is quite good with similar yield coefficients for both experiments.

It is important to note, though, that Beyler's wood data is based on an assumed composition. Beyler burned ponderosa pine and determined the theoretical maximum yields (k_{CO2}, k_{O2} and k_{H2O}) from the low fuel-to-air ratio yield data. He then estimated the empirical chemical formula by choosing a composition that reasonably represented all three yields [15]. In contrast, the spruce burned in the compartment fires was analyzed to determine the elemental composition. Although a direct comparison between normalized yield-equivalence ratio correlations may be questioned, the agreement in concentration data (which is unaffected by the choice of chemical formula), shown in Figures 4.26 to 4.28, suggest that the comparison of normalized yield data is reasonable. However, Beyler's correlations may be shifted with respect to the equivalence ratio.

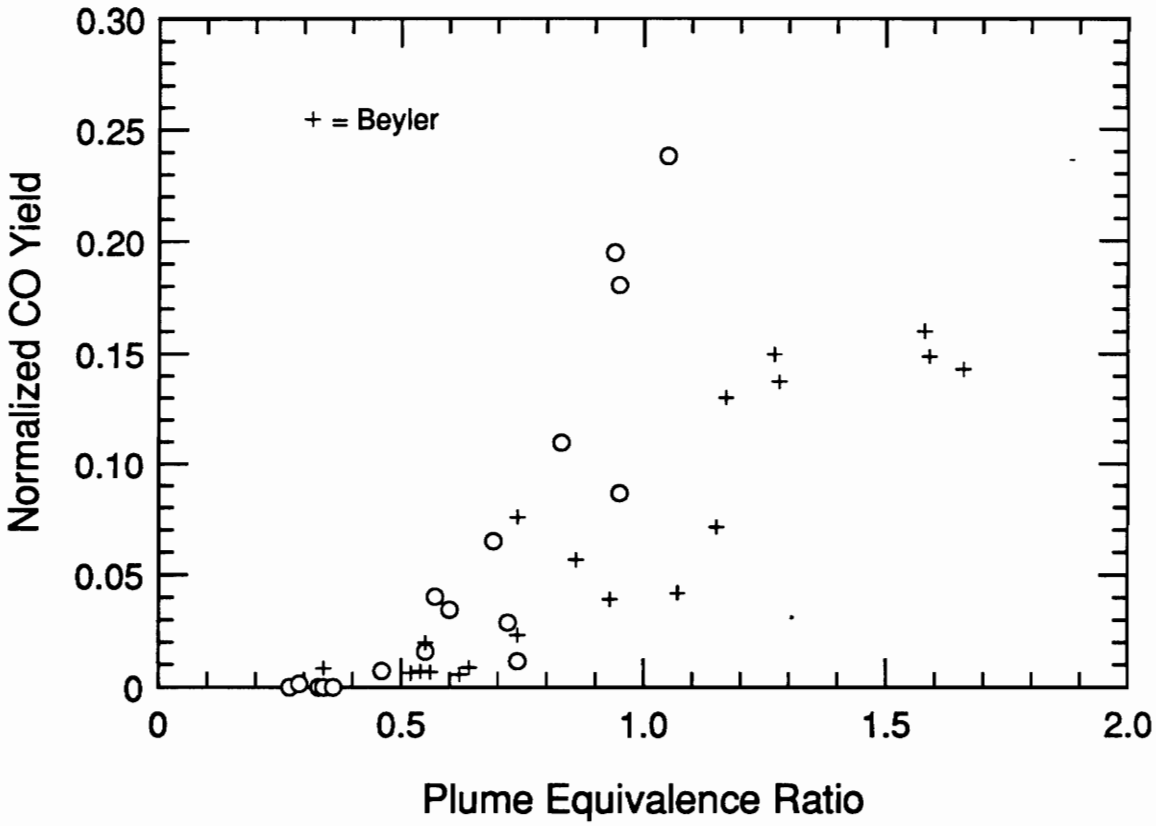

Figure 4.23 Comparison of normalized CO yield correlations obtained for wood fires in the compartment and in Beyler's hood.

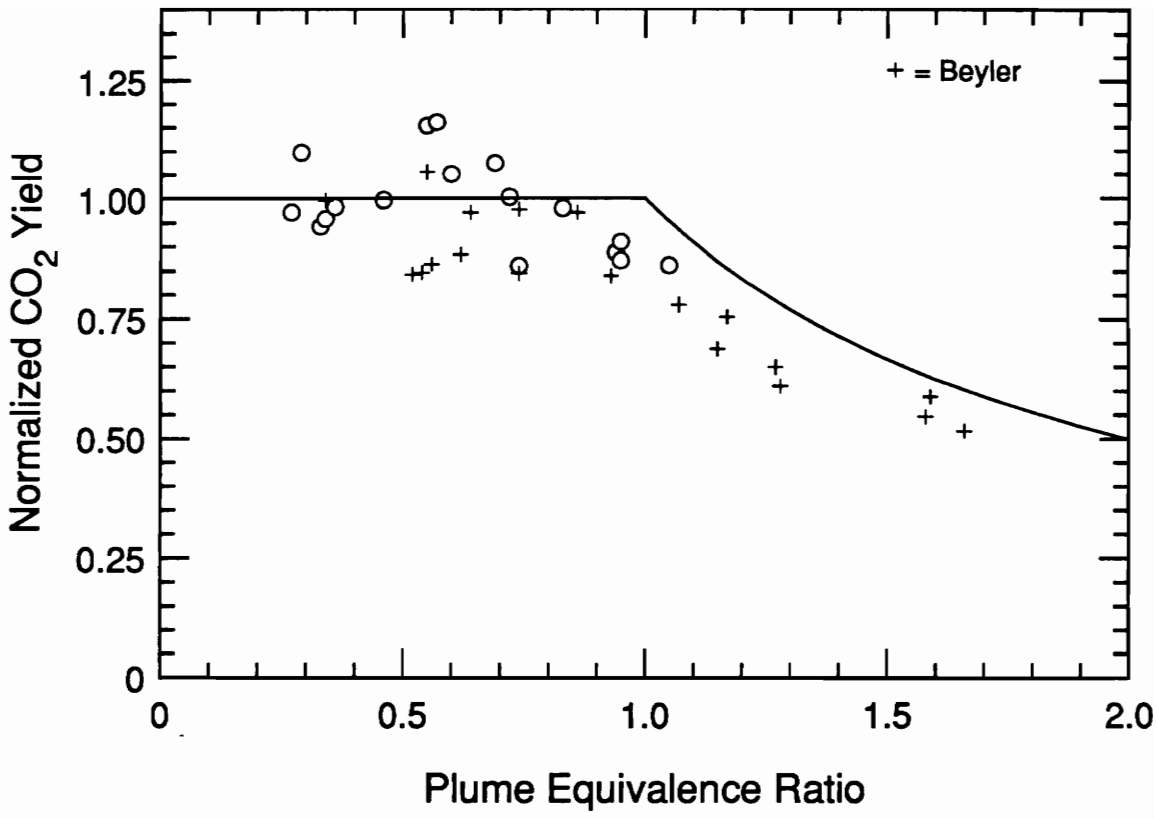

Figure 4.24 Comparison of normalized CO_2 yield correlations obtained for wood fires in the compartment and in Beyler's hood.

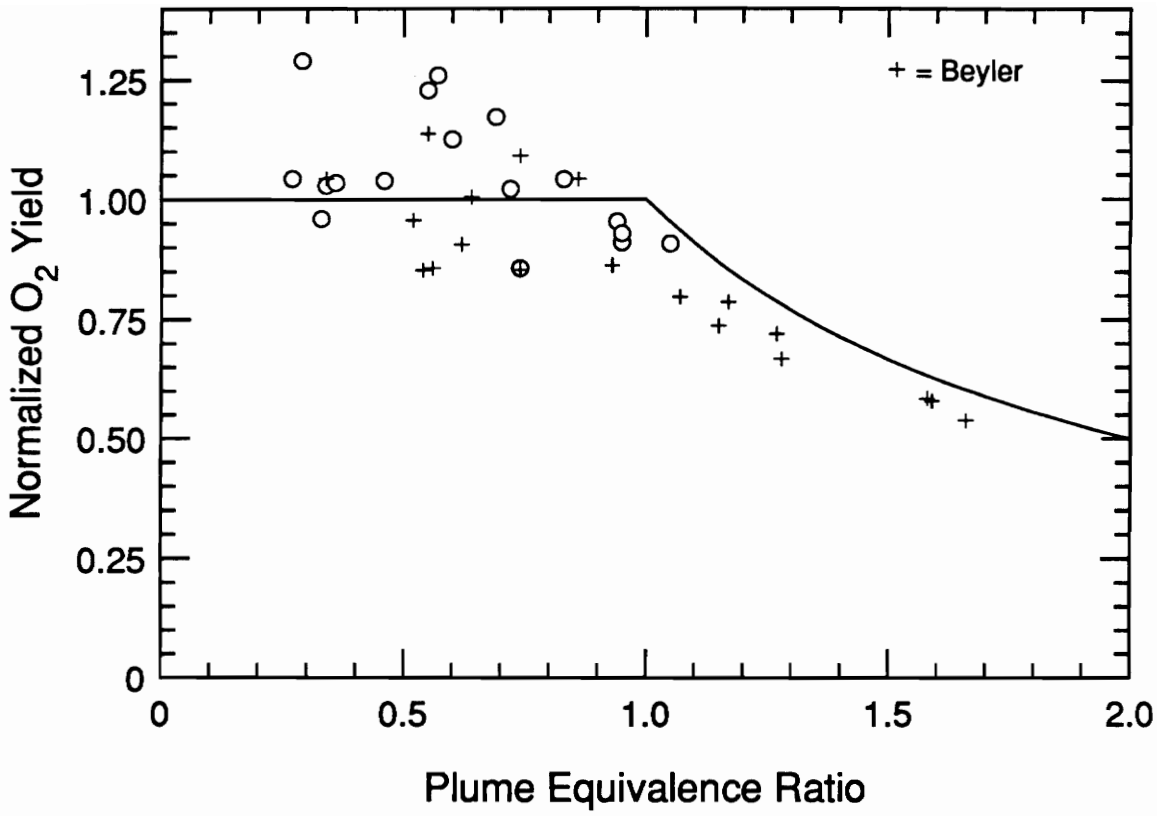

Figure 4.25 Comparison of normalized O_2 yield correlations obtained for wood fires in the compartment and in Beyler's hood.

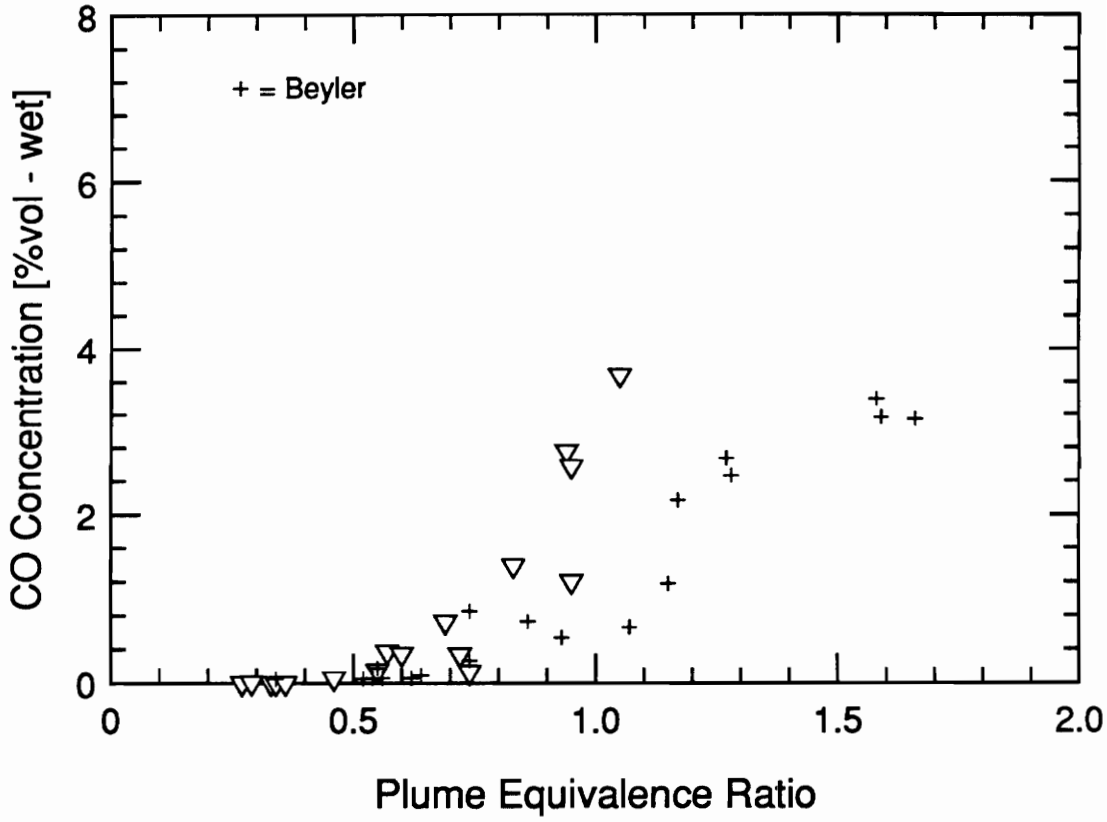

Figure 4.26 Comparison of upper layer CO concentration versus plume equivalence ratio for wood compartment and hood fires.

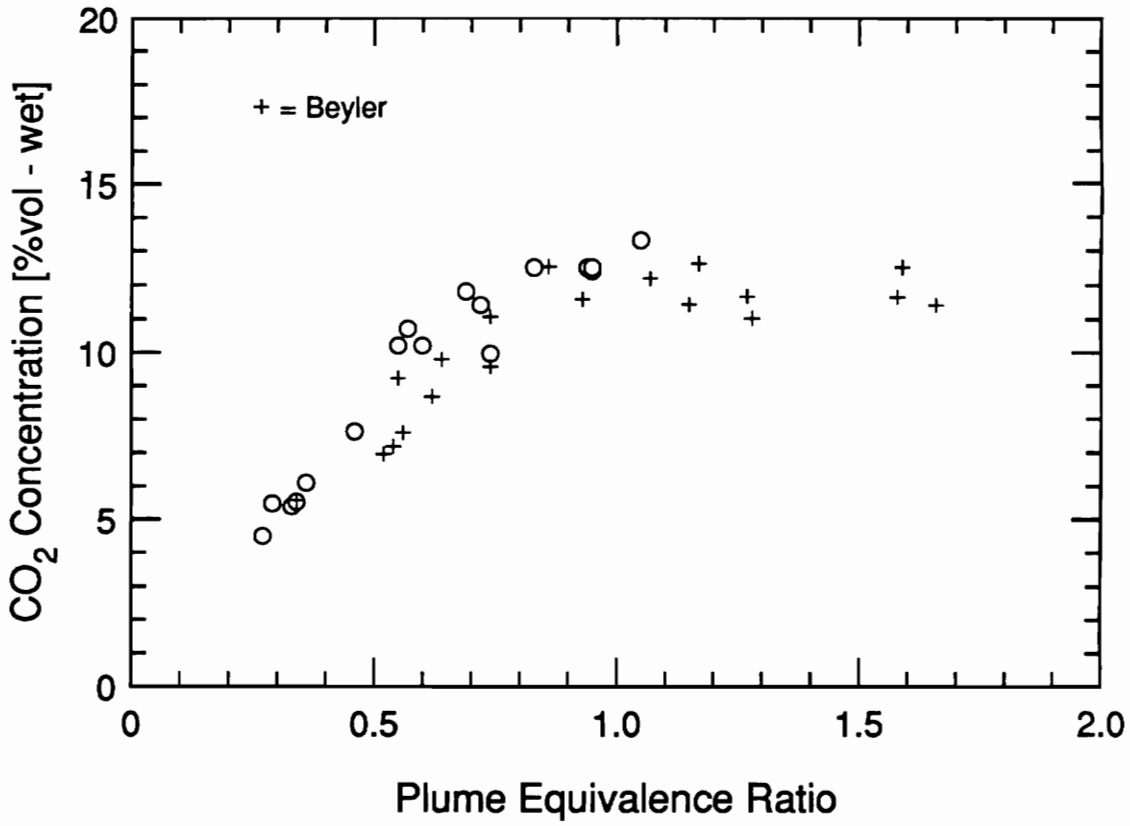

Figure 4.27 Comparison of upper layer CO_2 concentration versus plume equivalence ratio for wood compartment and hood fires.

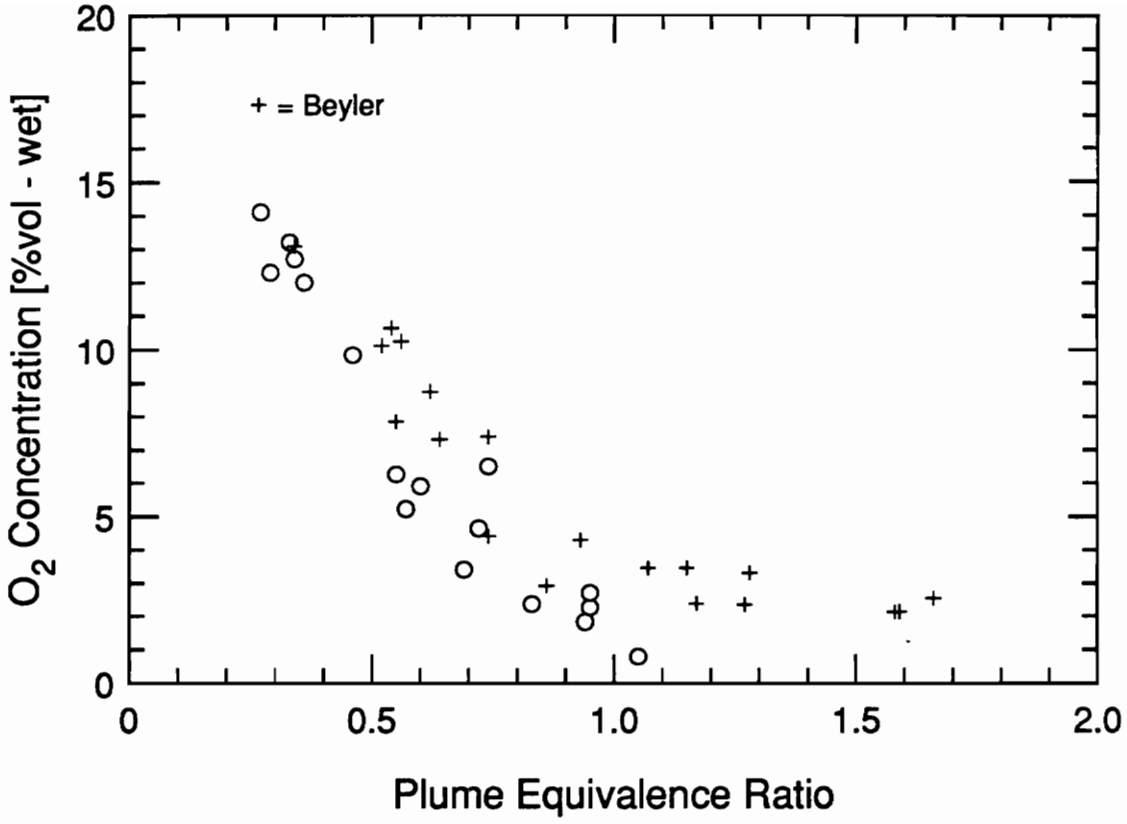

Figure 4.28 Comparison of upper layer O_2 concentration versus plume equivalence ratio for wood compartment and hood fires.

4.2.4 Temperature Dependence

The species yield correlations obtained in these compartment fires are qualitatively similar to those from Beyler's hood experiments, however significant differences exist. The differences between hood and compartment fire correlations are basically the same for both hexane and PMMA fires. For the range of equivalence ratios from about 0.5 to 1.3, higher CO production is measured in the hood experiments than in the compartment. Consistent with the production of CO, the normalized CO_2 and O_2 yields are lower for the hood fires. Thus, the compartment fires exhibit better utilization of oxygen and more complete combustion as indicated by the higher CO_2 yields. For equivalence ratios above 1.3, compartment fire CO yields increased to higher values than the hood yields.

The main difference in the fire environments between the two types of experiments is the upper layer temperature difference. For the primary region of discrepancy between equivalence ratios of 0.5 and 1.5, Beyler observed average temperatures from about 240 to 620 K below those observed for the compartment fires which were higher than 900 K (see Table 4.1).

Work by Morehart showed that the upper layer composition was effected by temperature [16]. A simple chemical kinetic investigation of the upper layer at one equivalence ratio indicated that temperatures over 800 K may lead to further reaction in the compartment upper layer with an increase in CO. Although this trend is contrary to the discrepancies for overventilated fires, it suggests a temperature dependence exists. Morehart also studied the effect of increasing temperature on layer composition by adding different levels of insulation to his hood. He concluded for the range of temperatures studied (500 to 675) that substantial increases in products of complete

combustion and decreases in fuel and oxygen occurred with increasing layer temperature. This work suggests that the increased temperatures in the compartment fires resulted in more complete combustion, as is indicated by the data.

The conversion of CO to CO_2 occurs via a reaction with a large temperature dependence. Therefore, it is expected that cooler layers freeze out the conversion of CO to CO_2, thus, resulting in higher CO concentrations. A kinetic study of the upper layer was performed to investigate the above theory and determine the effect of temperature on upper reactivity.

4.3 Chemical Kinetics Study of Upper Layer Gases

The goal of the study was to assess the reactivity of the upper layer gases in Beyler's experiments for a range of isothermal conditions characteristic of both the hood and compartment environments. It was expected that at temperatures characteristic of the compartment fire upper layers, the upper layer composition of Beyler's hood experiments would react and result in a composition similar to that in the compartment.

Due to the complexity and uncharacterized mixing and temperature gradients in a compartment fire plume, current kinetic schemes are unable to model the complete behavior of the reacting flows and, therefore, are unable to predict final layer compositions. However, modeling of upper layer gas phase chemistry is within the scope of current technology. Therefore, the study was conducted under the assumption that the generation of upper layer gases from a plume is independent of upper layer properties and surrounding compartment effects, such as radiation. That is to say at a given equivalence ratio, the plume generates the same products whether in the hood apparatus or in the compartment. The underlying assumption is that the upper layer and fire plume

can be separated as two distinct control volumes. For this study, the plume represents a source of generation of the initial upper layer composition.

Currently, kinetics modeling is a very active area of combustion research. Homogeneous gas phase reactions are reasonably well understood. However, heterogeneous chemistry, such as soot formation, is ill defined and, therefore, could not be incorporated into a kinetic model for this study.

4.3.1 Procedure

Kee, et al. at Sandia National Laboratories have developed a framework of computer codes and libraries known as CHEMKIN [34]. CHEMKIN provides the user with a framework to solve a set of differential equations describing gas phase elementary reactions. The libraries perform various chemical and thermodynamic operations and provide thermodynamic data. The user is required to formulate a kinetics model and driver code to run the CHEMKIN package.

Sandia provided a code SENKIN [35] which was modified to run on a VAX 11/780. This code was used to model the upper layer as a plug flow reactor. The code also performed sensitivity analysis to identify the key reactions for selected species.

The upper layer could have been modeled as either a perfectly-stirred reactor (PSR) or as a plug flow process. The PSR is characterized by fast mixing and approaches the plug flow process (slow mixing) as the upper layer residence time approaches zero. A similar study performed by Pitts has shown no significant differences in results for each method [36]. Due to familiarity with the code, the plug flow condition was used.

The kinetics model used was a subset of the Miller and Bowman mechanism [37], primarily a C_1-C_2 hydrocarbon oxidation model. All initial hydrocarbons were represented as ethylene (C_2H_4), consistent with Beyler's measurements which were used as initial inputs. Chakir, et al. made measurements of major species in a premixed, jet-stirred reactor for the oxidation of N-Heptane [38]. The results showed for a range of equivalence ratios from 0.5 to 2.0 and temperatures from 900 to 1170 K that ethylene was the major constituent of unburned hydrocarbons. Methane was the second highest constituent and typically accounted for only 6 to 12 percent of the total carbon in unburned hydrocarbons. A case in this study where 10 percent of the carbon in total hydrocarbons was represented as CH_4 showed no notable difference compared to assuming 100 percent C_2H_4. Therefore, the use of a C_1-C_2 mechanism is reasonable under the assumption that all hydrocarbons are represented as ethylene. Moreover, Dagaut, et al., reported that the inclusion of a C_3-C_4 submechanism was of minor importance in modeling the oxidation of ethylene with a C_1-C_4 mechanism [39].

The kinetic rates are represented using the modified Arrhenius equation:

$$k = A\, T^{\beta} \exp(-E/R\, T) \qquad [4.1]$$

where A is the pre-exponential term, T is the gas temperature, E is the activation energy and R is the universal gas constant. Appendix B includes the reaction mechanism and rate constant data used.

The general procedure was to use Beyler's hexane upper layer composition measurements as the initial mixtures. This provided a range of cases from ϕ_p of 0.47 to 1.55. Each case was then run at the corresponding hood upper layer temperature and at a temperature representative of the compartment upper layer for fires with the same

equivalence ratio. The model calculated species concentrations with respect to time for a period of 40 seconds, which was a typical residence time for the hood experiments.

4.3.2 Results

Figures 4.29 to 4.31 show the calculated CO, CO_2 and O_2 concentrations at both the hood and compartment layer temperatures for hexane fires plotted versus the equivalence ratio. For both sets of temperatures, the calculated concentrations are reported for a time of 40 seconds. The initial species concentration at each equivalence ratio is also plotted. The results show that the upper layer was unreactive at the hood temperatures as indicated by no change in the species concentrations from initial conditions. At the compartment temperatures, the composition is significantly changed. As can be seen in Figure 4.29 and 4.30 for overventilated fires, CO is almost entirely oxidized to CO_2. Figure 4.31 shows that the O_2 concentrations decrease with equivalence ratio to values below the initial conditions, consistent with the oxidation of CO and hydrocarbons.

The underventilated results show a dramatic increase in the CO levels at the elevated compartment fire temperatures. This is subsequently accompanied by a decrease in CO_2 with increasing equivalence ratio. However, in comparison to the initial composition, the higher underventilated CO_2 concentrations are relatively unchanged, indicating that the O_2 is utilized entirely for hydrocarbon oxidation and CO oxidation is frozen.

Figure 4.32 and 4.33 present the calculated major species concentrations plotted in time for an over- and underventilated case (ϕ_p = 0.91 and 1.36) at compartment fire temperatures. As can be seen in Figure 4.32 for an overventilated fire, the CO

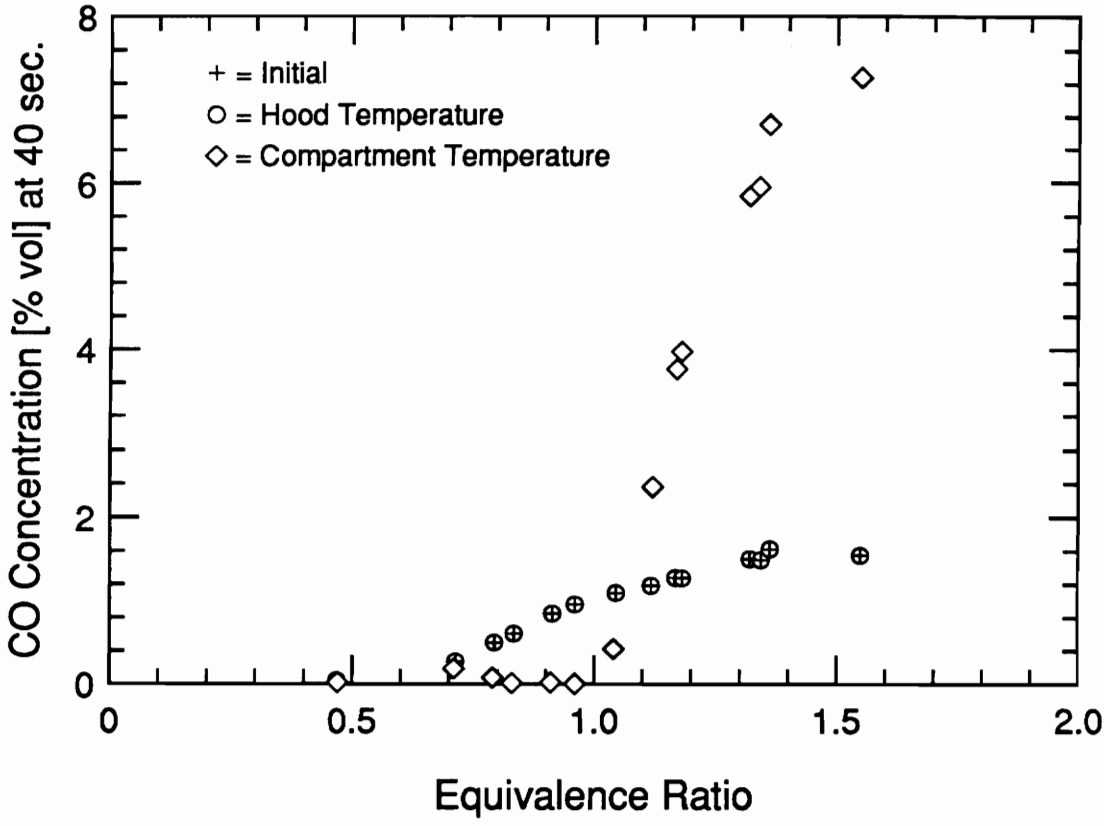

Figure 4.29 Chemical kinetics model calculated CO concentrations versus plume equivalence ratio for cases run at hood layer temperatures and cases run at compartment layer temperatures.

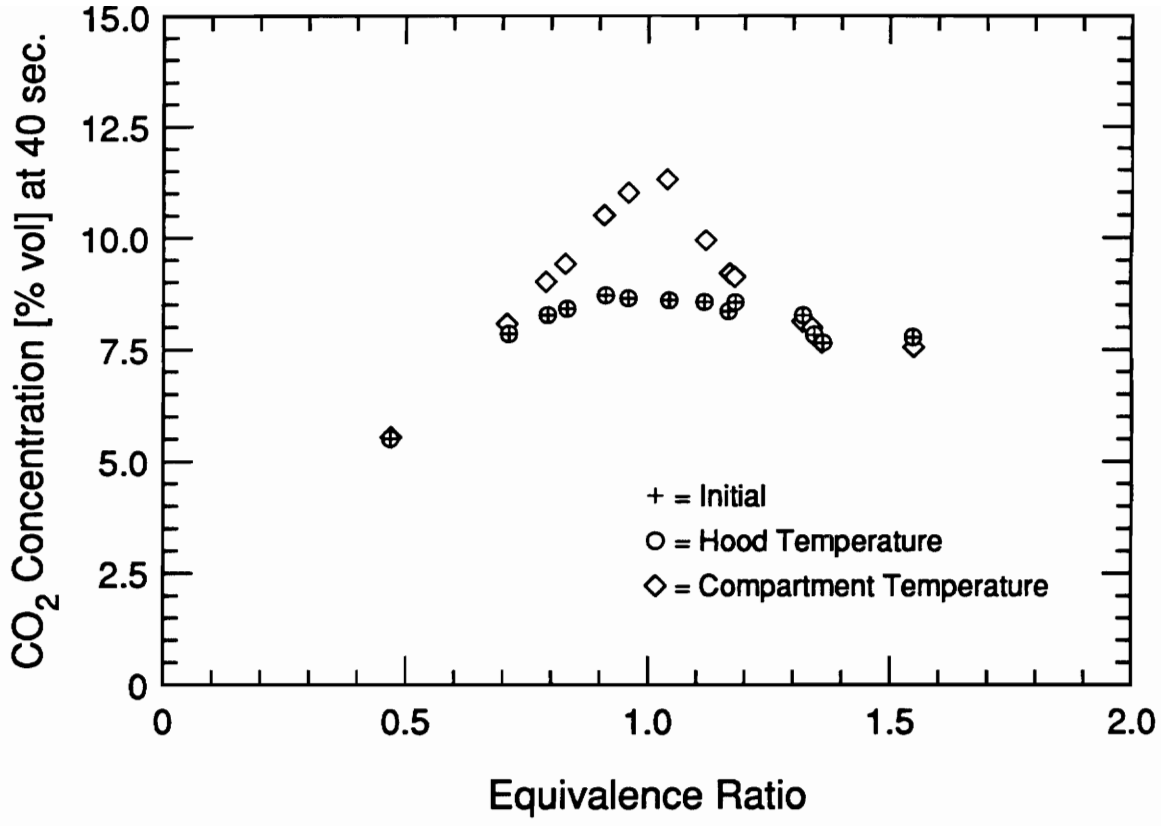

Figure 4.30 Chemical kinetics model calculated CO_2 concentrations versus plume equivalence ratio for cases run at hood layer temperatures and cases run at compartment layer temperatures.

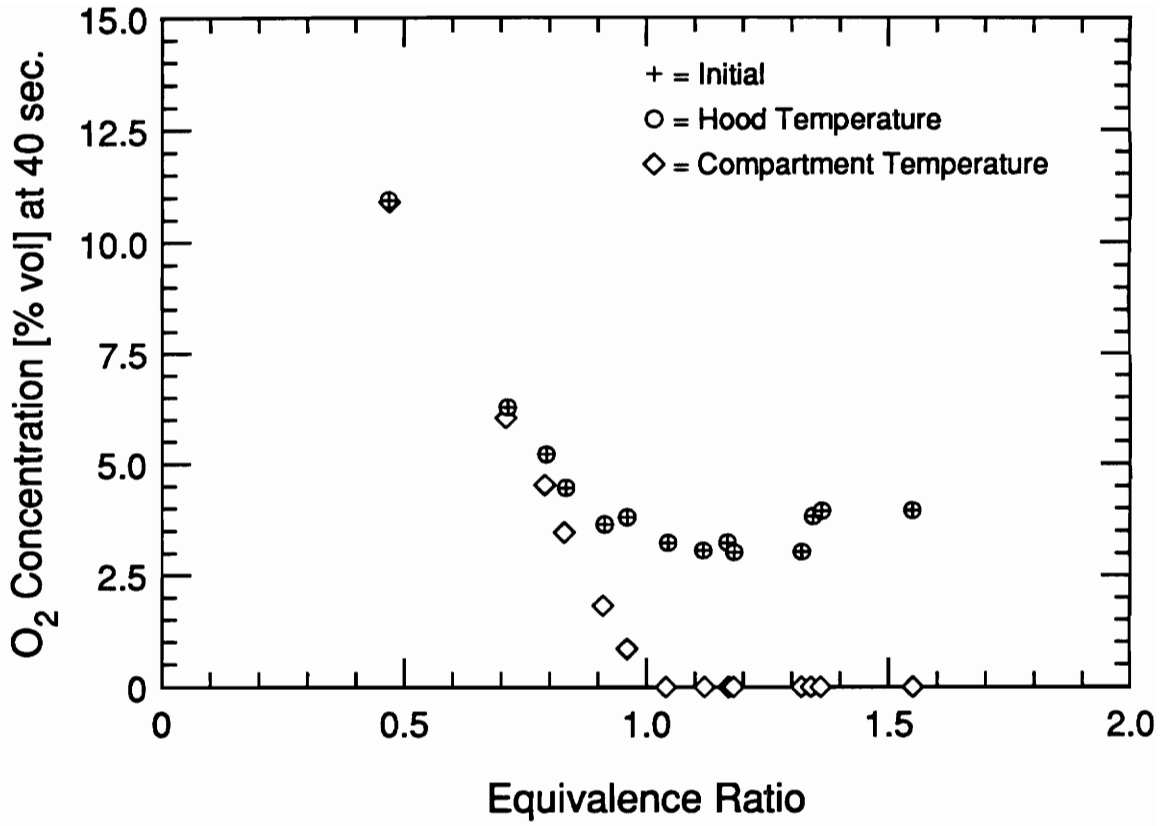

Figure 4.31 Chemical kinetics model calculated O_2 concentrations versus plume equivalence ratio for cases run at hood layer temperatures and cases run at compartment layer temperatures.

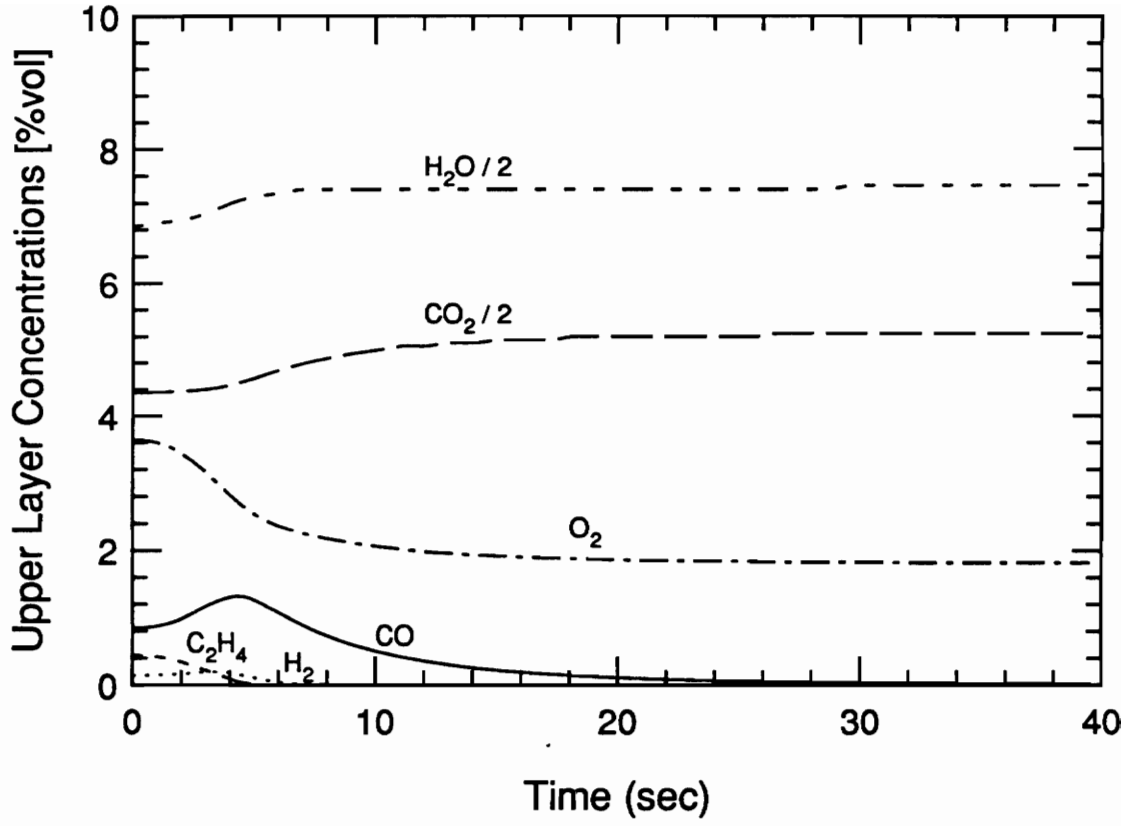

Figure 4.32 Model calculated major species concentrations versus time for of $\phi_p = 0.91$ and T = 900 K.

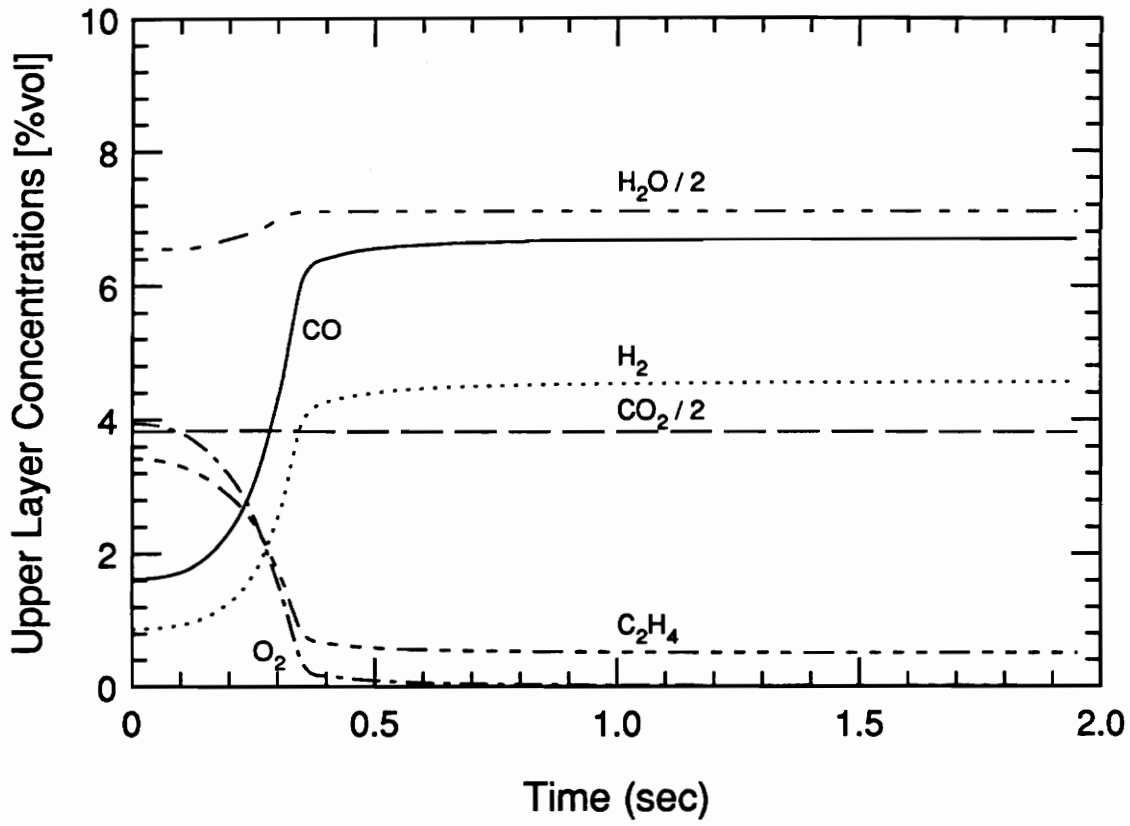

Figure 4.33 Model calculated major species concentrations versus time for ϕ_p = 1.36 and T = 1000 K.

concentration initially rises as C_2H_4 is oxidized and the CO_2 remains fairly constant. When the C_2H_4 is consumed, CO begins to oxidize to CO_2 resulting in a net depletion of CO for times greater than 8 seconds.

For the underventilated fire shown in Figure 4.33, CO rises quickly as C_2H_4 is oxidized. Oxygen is depleted before all C_2H_4 is oxidized resulting in a CO concentration over three times the initial value. Carbon dioxide remains unchanged.

The effect of temperature is presented in Figures 4.34 and 4.35 which show the CO concentration as a function of time and upper layer temperature for both an over- and underventilated case (fp = 0.91 and 1.36), respectively. As is clearly seen, the net CO concentration in the upper layer is strongly dependent on both the temperature and the residence time. Overventilated cases such as Figure 4.34, indicate that the net depletion of CO will not occur (within realistic residence times) unless the temperature is about 875 K or higher. The rise in CO concentrations in Figures 4.34 and 4.35 is due to the oxidation of C_2H_4 as was shown in Figures 4.32 and 4.33. The results presented in Figure 4.35 for an underventilated fire suggest that a temperature between 800 to 850 K is needed to promote the reactions governing hydrocarbon oxidation.

To determine the effective freeze out temperature for CO oxidation, the model was run at different temperatures for a case of ϕ_p equal to 0.71 in which the small initial concentration of C_2H_4 was omitted. The results showed that significant CO oxidation did not occur for temperatures below 800 K.

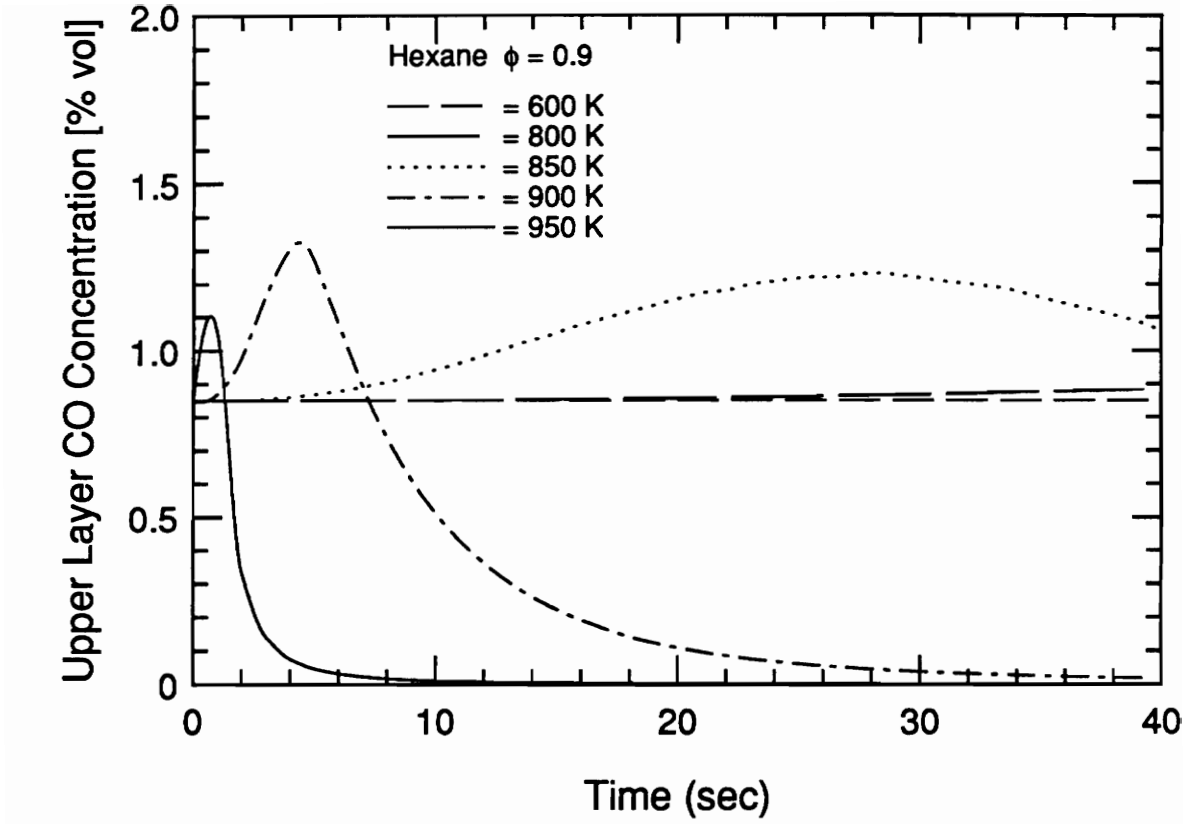

Figure 4.34 Model calculated CO concentration versus time at different isothermal conditions for $\phi_p = 0.91$.

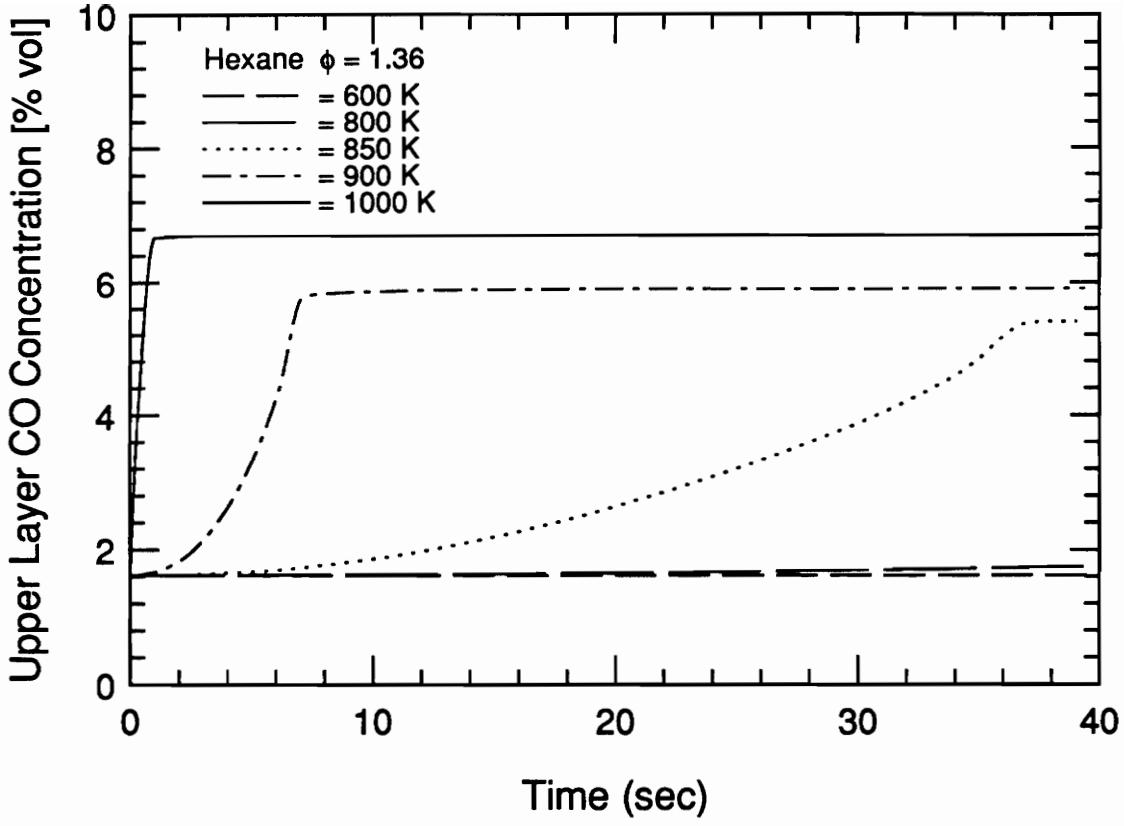

Figure 4.35 Model calculated CO concentration versus time at different isothermal conditions for $\phi_p = 1.36$.

4.3.3 Discussion

For overventilated conditions, the model-predicted upper layer composition agrees well with the compartment fire measurements, however the model considerably overpredicts CO concentrations for underventilated fires. This can be seen in Figures 4.36 to 4.38 which show the comparison between model calculated CO, CO_2 and O_2 concentrations at the hexane compartment fire temperatures and the hexane compartment fire measurements of this study plotted against the equivalence ratio. At compartment temperatures, the modeling shows the initial hood CO and O_2 concentrations decreasing and CO_2 increasing consistent with the measurements for overventilated fires.

For underventilated conditions the model-predicted upper layer composition does not agree with the compartment fire measurements. The calculated CO concentrations are 2 to 4 times higher than the concentrations measured in the compartment. The highest CO concentration observed in a compartment fire was 3.7% at ϕ_p of 2.9; the modeling results show concentrations as high as 7.3% at a ϕ_p of only 1.6. Model predicted CO_2 concentrations are as much as 26 percent lower than measured values and the calculated O_2 concentrations of zero are slightly lower than the compartment measurements of about one percent. It is interesting to note that for overventilated conditions, the kinetic model calculated results can also be obtained by using thermodynamic equilibrium; however, this is not true for underventilated conditions.

The modeling indicates that the oxidation of C_2H_4 is faster than CO oxidation. As can be seen in Figure 4.32, significant CO oxidation does not occur until nearly all available C_2H_4 is consumed. The CO concentration rises due to the initial hydrocarbon

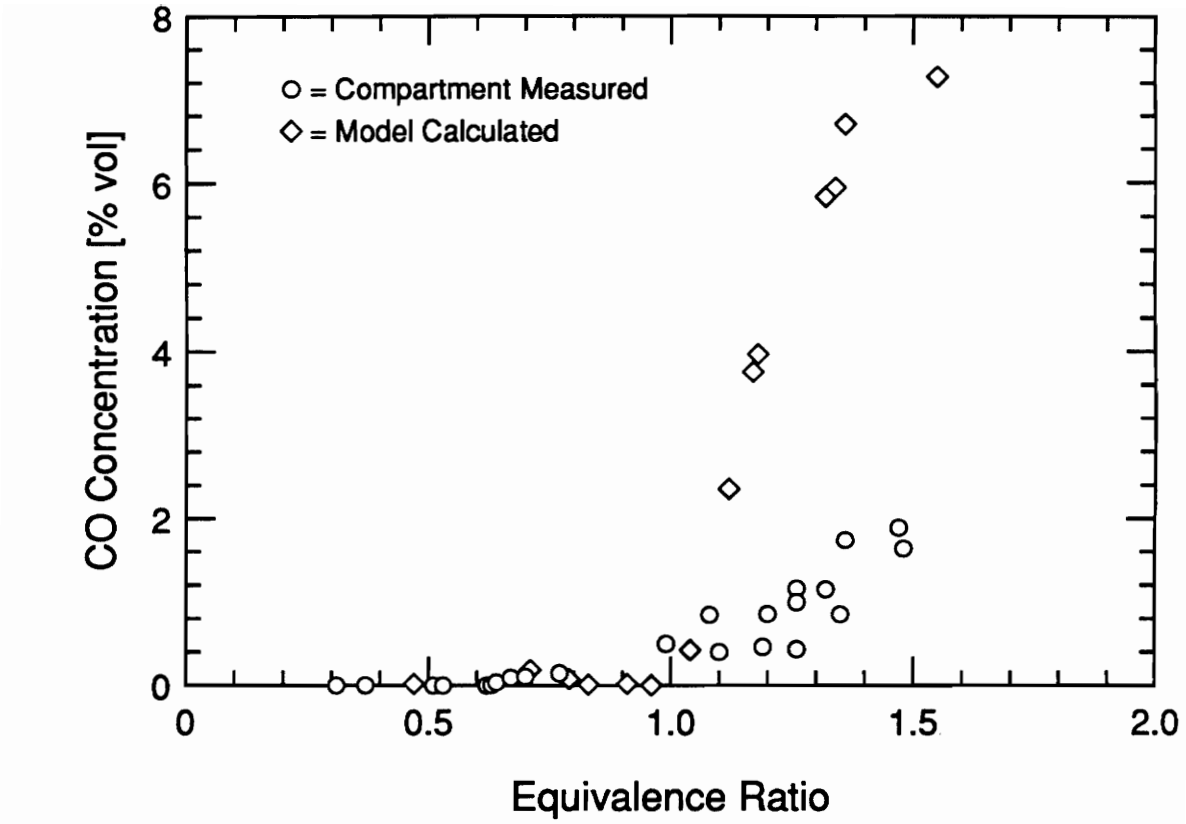

Figure 4.36 Comparison of calculated CO concentrations at compartment fire temperatures and compartment fire measurements plotted against plume equivalence ratio.

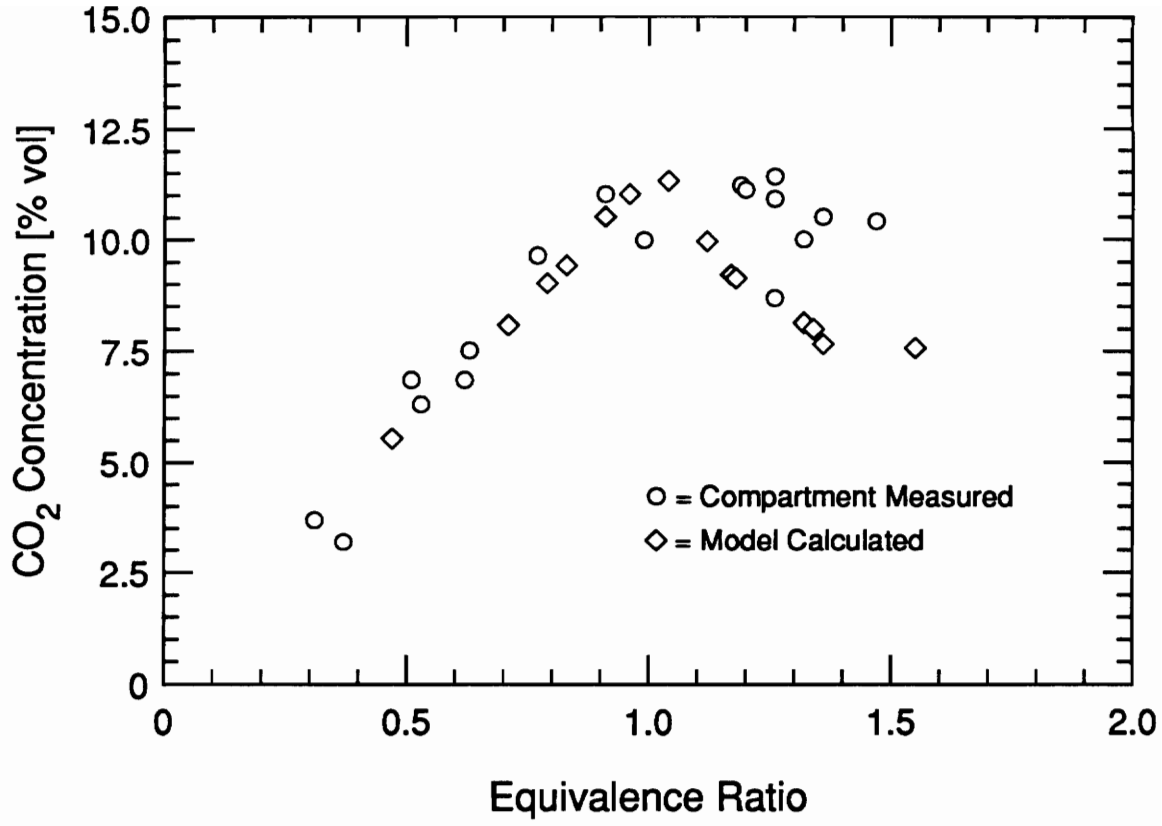

Figure 4.37 Comparison of calculated CO_2 concentrations at compartment fire temperatures and compartment fire measurements plotted against plume equivalence ratio.

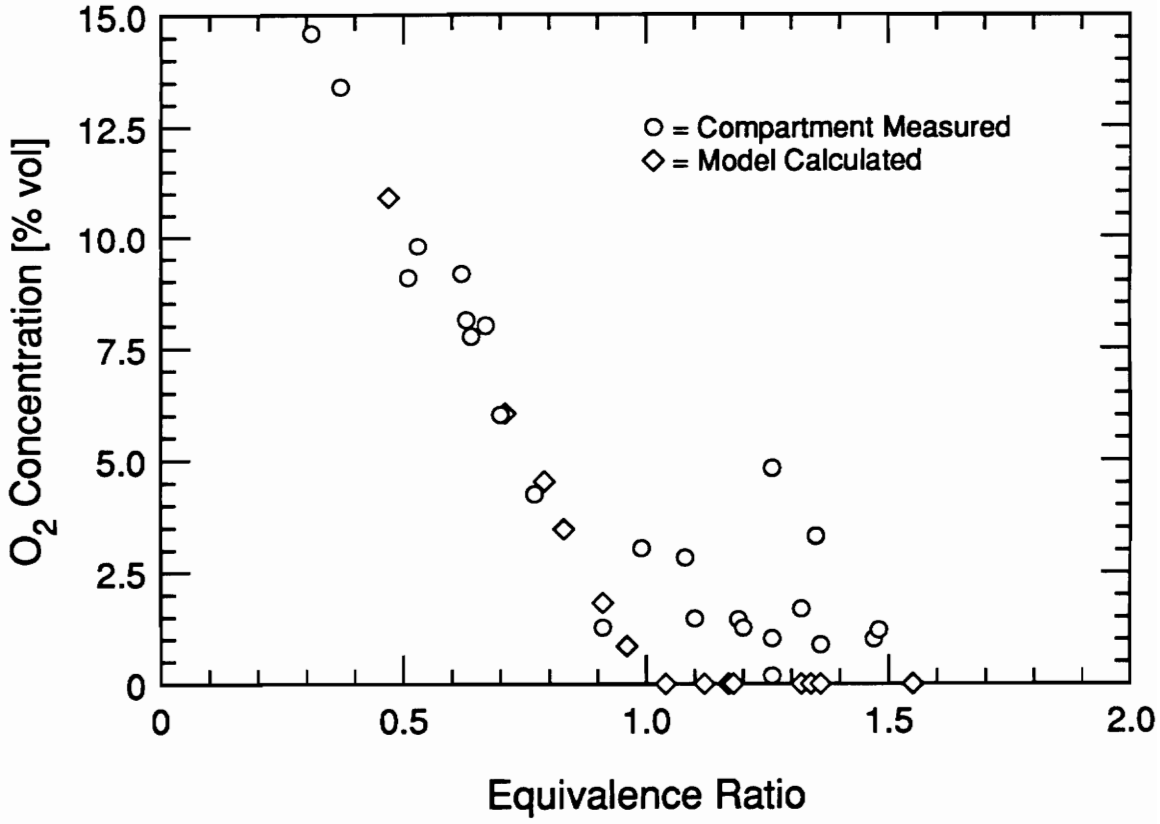

Figure 4.38 Comparison of calculated O_2 concentrations at compartment fire temperatures and compartment fire measurements plotted against plume equivalence ratio.

oxidation. As the C_2H_4 concentration decreases the remaining available O_2 is then used for the conversion of CO to CO_2.

As can be seen in Figure 4.20, ϕ_p of 1.3 marks a crossover point at which compartment CO measurements transition from lower to higher values than observed in the hood experiments. The modeling work shows the same transition, but at a slightly lower ϕ_p of 1.1 (Figure 4.29). Thus, the results indicate, for ϕ_p less than 1.1, that the elevated temperatures observed in the compartment fires (T > 900 K) allow nearly complete oxidation of CO to CO_2 in the upper layer for overventilated and slightly underventilated conditions and that at the hood temperatures the CO to CO_2 reaction is frozen resulting in elevated CO concentrations.

Although the discrepancy between the model results and the measurements exists, the kinetics still suggest that the elevated temperature difference is the reason for the lower CO measurements in the compartment fires than in the hood fires. As mentioned above, the crossover point at which compartment CO measurements transition from lower to higher values (than those observed in the hood experiments) occurs at an equivalence ratio of 1.3, only slightly higher than the same transition shown in the modeling results at a ϕ_p of 1.1.

It is of interest to understand why the model overpredicts the CO concentrations measured in the compartment upper layer. In analyzing this problem, significant insight is gained on the underlying physics and chemistry controlling CO formation in compartment fires. According to the model during underventilated conditions, O_2 is depleted during hydrocarbon oxidation due to the high initial C_2H_4 levels. This results in high levels of CO and H_2 and remaining C_2H_4. There is negligible CO_2 production

indicating that no CO oxidation occurs. Pitts, in a similar study using Morehart's methane data, observed similar results [36]. He states that the free radicals (H, OH and HO_2) needed for CO and H_2 oxidation remain at low levels since they are considerably more reactive with hydrocarbon fuels, such as ethylene. In the absence of hydrocarbons, the radical pool grows and CO is oxidized as in the overventilated cases.

4.3.3.1 Suitability of Chemical Kinetics

The discrepancy between underventilated model results and experimental measurements of CO can be the result of two primary problems: 1) the gas-phase kinetics are incorrect and 2) the modeling approach and assumptions are incorrect. The state of gas-phase kinetics is currently quite good although much work continues in refining kinetic rates and mechanisms. Models have successfully reproduced experimental results for a range of combustion conditions and fuels. For example, oxidation of simple fuels, such as $CO/H_2/O_2$ kinetics, in shock tubes and various reactor experiments has been modeled successfully by Yetter and Dryer [40,41]. The modeling of even more complex fuel oxidation such as CH_4 [42], C_2H_4 [43], C_2H_6 [44], nC_7H_{16} [38] and C_2H_5OH [45] has shown good agreement with experimental results and, thus, confirms the general validity of current gas phase kinetic modeling.

Although the kinetic modeling is reasonably accurate, the kinetics of CO oxidation in the range of temperature from 800 to 1100 K proves to be complex and not fully understood [36]. Pitts investigated the use of various mechanisms on the formation of CO using Morehart's methane results for initial conditions [36]. From his results, shown here as Figure 4.39, and an analysis of the mechanisms, he concludes that variations in CO concentration are due primarily to differences in the rates of reactions involving HO_2.

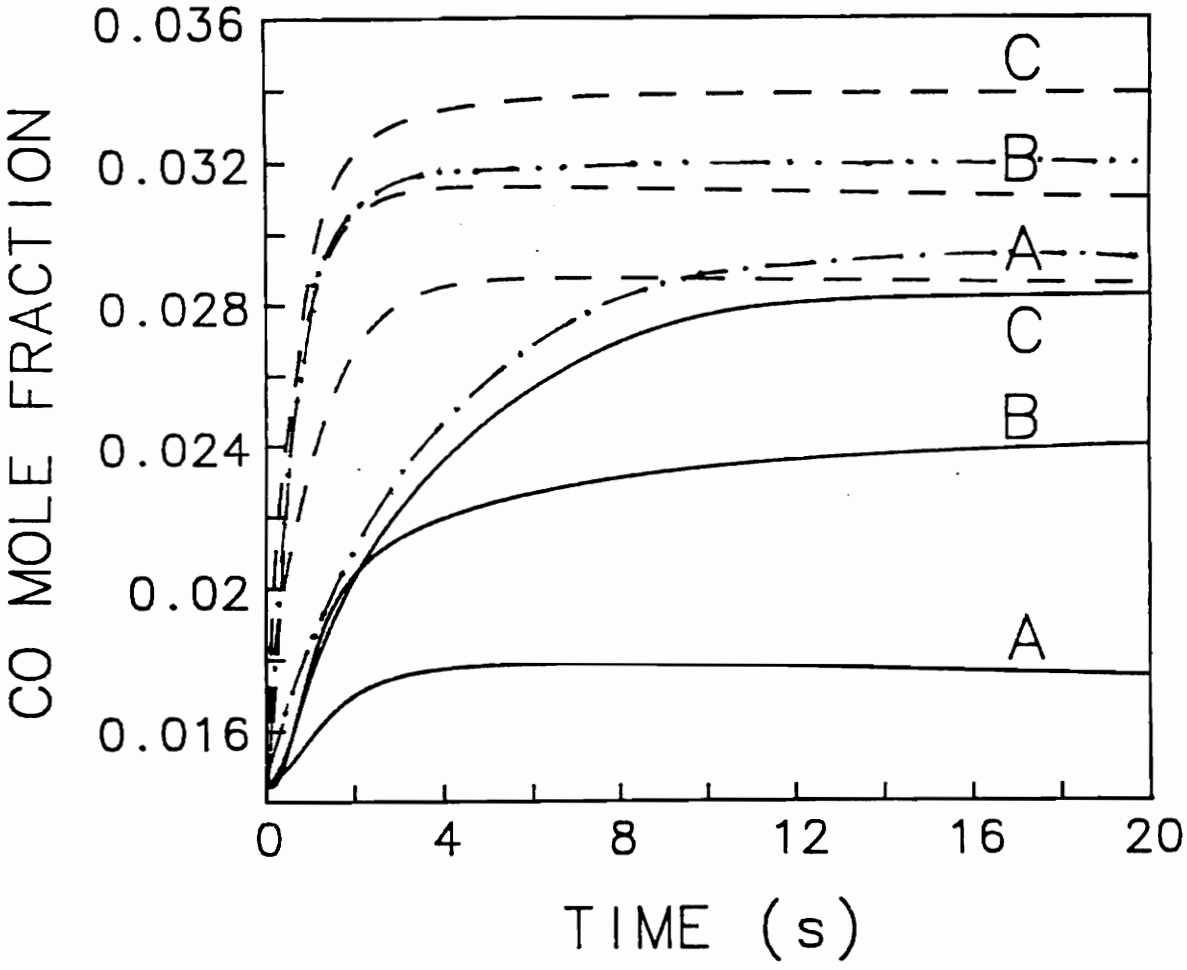

Figure 4.39 Carbon monoxide mole fractions plotted as a function of time for an isothermal plug flow reactor using three reaction mechanisms taken from the literature: A) Dagaut et al.'s methane oxidation mechanism [42], B) Dagaut et al.'s ethylene oxidation mechanism [39], and C) Morehart's mechanism [16]. Solid lines represent reactor temperatures of 900 K and dotted lines reactor temperatures of 1200 K. (Figure taken from Pitts [36]). Dot-dash and dot-dot-dash lines represent results of this study using a subset of Miller and Bowman's mechanism at 900 and 1200 K, respectively.

The Miller and Bowman (MB) mechanism was used to model the same case studied by Pitts in Figure 4.39. The results of these tests have been sketched on to Figure 4.39. As can be seen at 1200 K, the MB mechanism predicts similar CO concentrations as the other mechanisms. However, at 900 K, the MB mechanism predicts a CO level approximately 70 percent higher than that using Dagaut, et al.'s methane oxidation mechanism [42]. This comparison suggests that the predicted CO concentrations using Miller and Bowman may be as much as 70 percent high. This, however, is not sufficient to account for the factor of 2 to 4 difference between experimental CO measurements and model predicted values.

Before Pitts' work was reviewed, a study was performed in this investigation to determine the effect on CO production from updating the Miller and Bowman mechanism. The most current, applicable mechanism, considering only C_1-C_2 species, is that proposed by Dagaut, et al. for ethane oxidation [44]. Key reactions (identified with a sensitivity analysis) of the Miller and Bowman mechanism were updated with the rate data used in Dagaut's mechanism.

A sensitivity analysis was performed for the case of ϕ_p equal to 1.36 and a temperature of 1000 K and the results of for CO, C_2H_4 and CO_2 are presented in Figures 4.40 to 4.42. As can be seen in Figures 4.40 and 4.41, the top twelve key reactions for CO and C_2H_4 are the same. The rate constant data for all twelve reactions was updated and the model run for each case ($\phi_p = 1.36$ and $\phi_p = 0.91$).

The results of the sensitivity analysis indicate that both C_2H_4 and CO are most sensitive to the following five reactions (listed in decreasing order):

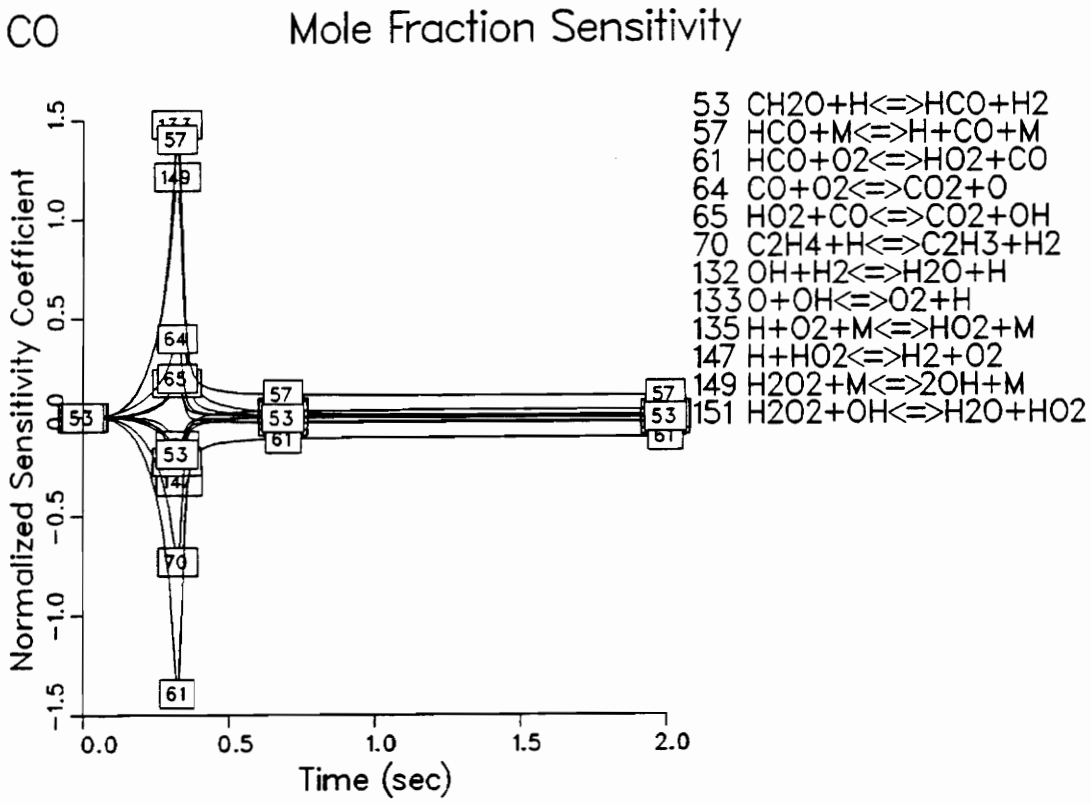

Figure 4.40 Normalized sensitivity coefficients for key reactions in Miller and Bowman mechanism of CO for a case of ϕ_p = 1.36 and T = 1000 K.

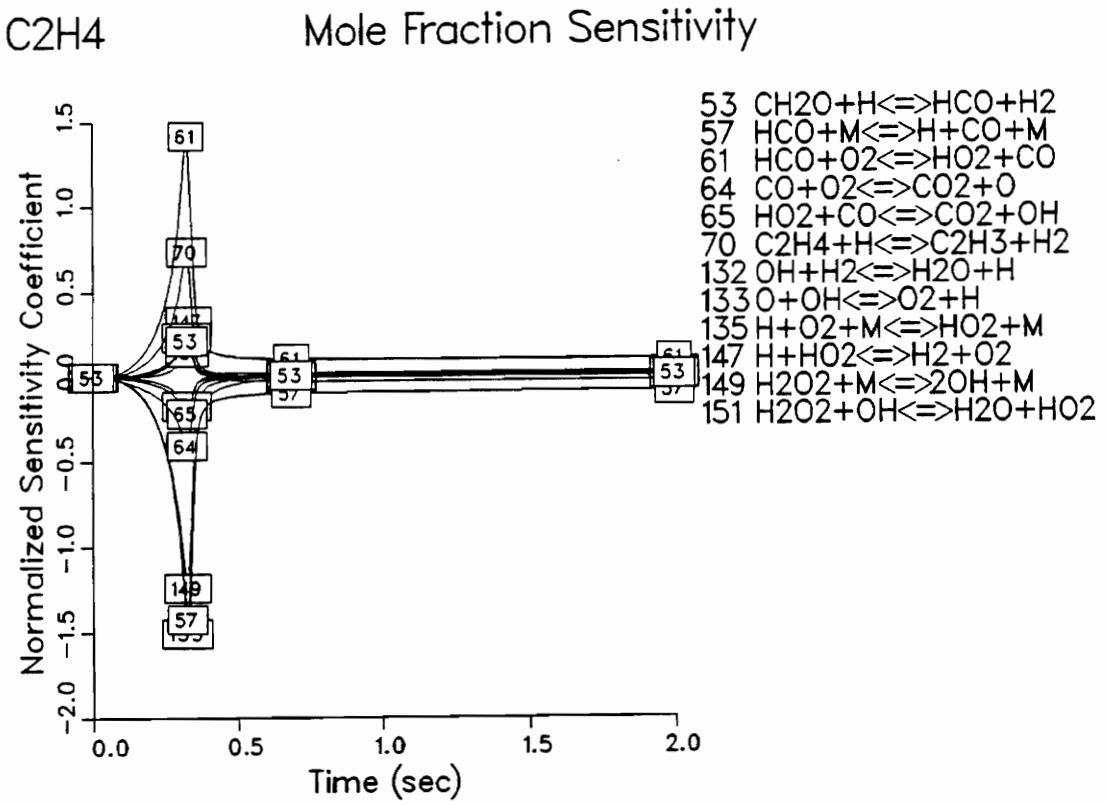

Figure 4.41 Normalized sensitivity coefficients for key reactions in Miller and Bowman mechanism of C_2H_4 for a case of ϕ_p = 1.36 and T = 1000 K.

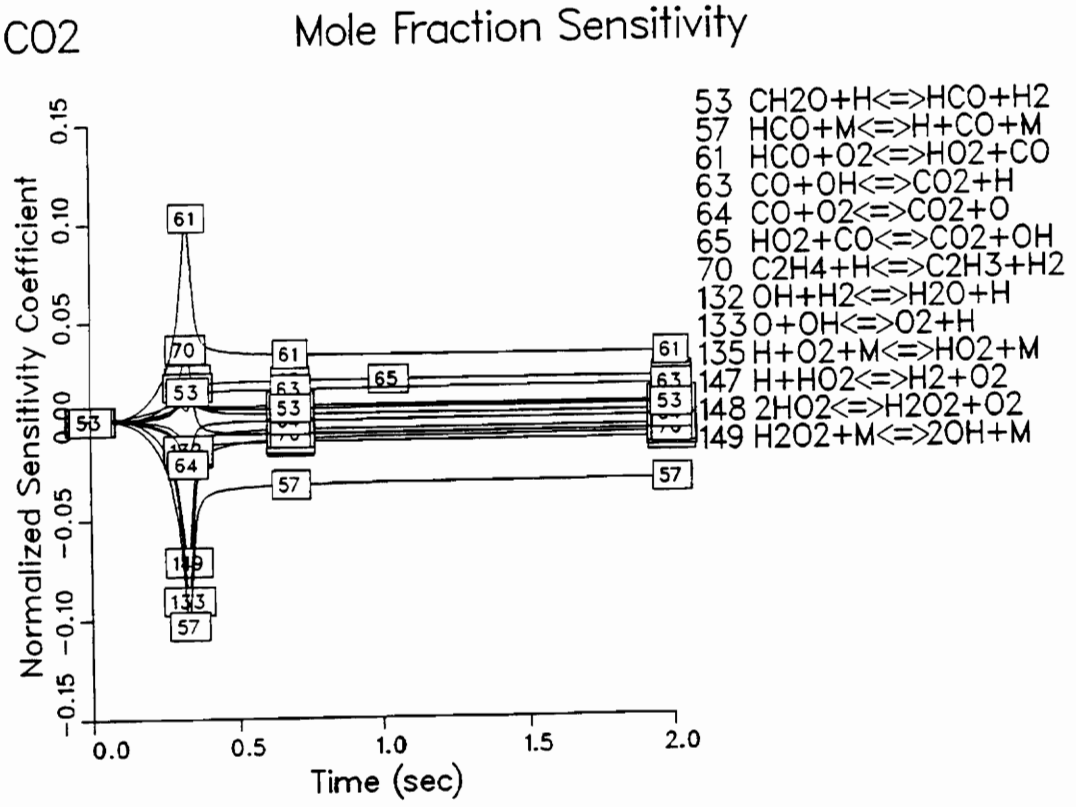

Figure 4.42 Normalized sensitivity coefficients for key reactions in Miller and Bowman mechanism of CO_2 for a case of ϕ_p = 1.36 and T = 1000 K.

(a) $O + OH <=> O_2 + H$ (1.5)

(b) $HCO + M <=> H + CO + M$ (1.4)

(c) $HCO + O_2 <=> HO_2 + CO$ (-1.4)

(d) $H_2O_2 + M <=> 2OH + M$ (1.2)

(e) $C_2H_3 + H_2 <=> C_2H_4 + H$ (-0.75)

The values in parenthesis are normalized sensitivity coefficients, which represent the percent change in CO with respect to a one percent change in the given reaction rate. For example, doubling the rate of reaction (a) would increase the production of CO by a factor of 3. The sensitivity coefficients for C_2H_4 are the same in magnitude but reverse in sign of those for CO.

Figure 4.42 shows that the key reactions for CO_2 formation are reactions (a) to (e) listed above. However, the low sensitivity coefficients of 0.1 and less indicate that the CO_2 concentration is minorly effected by the mechanism. The main reaction for the oxidation of carbon monoxide ($CO + OH <=> CO_2 + H$) does not even appear as one of the top twelve key reactions in the CO sensitivity analysis for underventilated conditions. This and the direct coupling between C_2H_4 and CO oxidation indicate that CO levels cannot be reduced without resulting in higher hydrocarbon concentrations. Experimental results agree with such an outcome, as do the results of using the updated mechanisms studied here and by Pitts [36].

The results for the case of ϕ_p equal to 1.36 using the updated mechanism are shown in Figure 4.43. Differences between mechanisms can be made by comparing the results

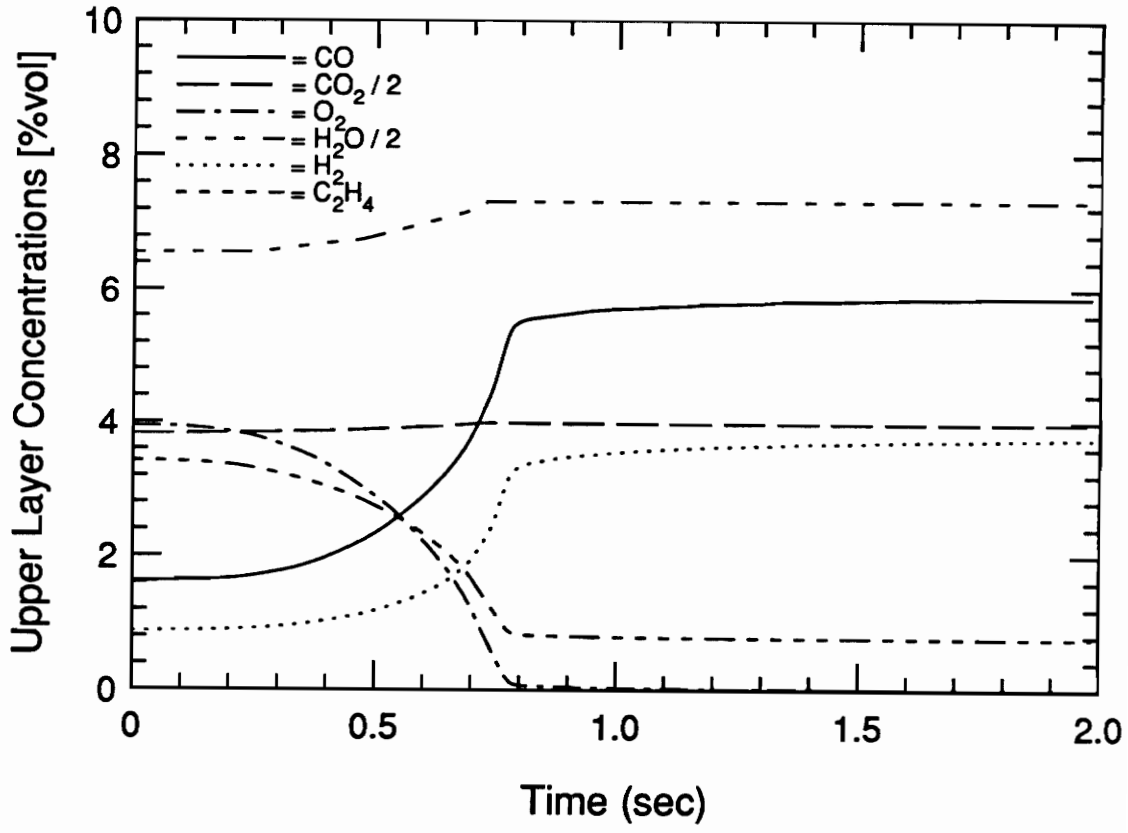

Figure 4.43 Calculated major species concentrations for ϕ_p = 1.36 and T = 1000 K using Miller and Bowman mechanism with 12 key reactions (identified in CO sensitivity analysis) updated with rate constant data from Dagaut, et al.'s ethane oxidation mechanism [44].

presented in Figure 4.43 and 4.33. The updated Miller and Bowman mechanism results in a doubling of the time needed for reaction and a net decrease of 12 percent in CO formation. The decrease in the net CO production is due primarily to reduced C_2H_4 oxidation and not to CO oxidation. These results are consistent with those of Pitts, presented in Figure 4.39, and confirm that although the gas phase kinetic mechanisms of CO oxidation continue to be refined, they do not appear to be the cause of the large discrepancy between predicted and experimental CO concentrations.

4.3.3.2 Analysis of Modeling Approach

Accepting the suitability of the kinetic mechanisms indicates that there must be a problem with the assumptions of the modeling approach. Two assumptions that were necessary to perform the study are identified as possible sources of error. One is the assumption that the generation of upper layer gases from a plume is independent of upper layer properties and surrounding compartment effects, such as radiation. That is to say at a given equivalence ratio, the plume generates the same products whether in the hood apparatus or in the compartment. The second suspect assumption is that the exclusion of soot formation in the model has no effect on CO formation.

The formation of soot occurs primarily in the fuel side of a flame under low O_2 and high temperature conditions. Temperatures of 1300 K and higher are needed to promote soot formation. The carbonaceous particles that are initially formed either oxidize in the flame or react further to form smoke [46]. Due to the existence of O_2 and the relatively low temperatures ($T < 1200$ K) in the modeled upper layer compositions, the formation of soot is unlikely. However, the interaction of existing soot in the initial composition with the gas phase species is uncertain. Hydrocarbons are expected to be adsorbed by the

soot particles, but due to the excess of hydrocarbons, it is doubtful that significant quantities would be consumed in this way to affect the net CO concentration. A second possibility is that soot may compete favorably for OH, thus, decreasing hydrocarbon oxidation. However, unless soot oxidizes completely, net CO levels would not be expected to decrease. The affect of soot on the hydrocarbon and CO chemistry cannot be fully determined, so excluding soot chemistry from the modeling remains as a possible source of error.

The fire plume is a complex diffusion flame created from the buoyancy dominated flow of vaporizing fuel particles and the subsequent entrained air flow. Due to the variable, localized temperature and species gradients, and turbulent mixing, the plume is difficult to characterize. However, study of the plume, in a global sense, provides useful insights into understanding the generation of upper layer species.

Beyler's propane results suggest that the production of upper layer gases is independent of the structure and fluid dynamics of the flame. Beyler modified a 19 cm burner by including a 2.8 cm lip to enhance turbulence and the large-scale structure of the flame [14]. Compared to the no lip burner, he reported that the flame was markedly changed and that air entrainment was increased by 30%. Yet, the species correlations were the same for both burners.

The insensitivity of species yields to the details of the flame structure is also suggested by the compartment fire hexane results. The correlations obtained included data from fires with a range of air entrainment rates from 50 to 128 g/s utilizing various size burn pans. In several cases, nearly equal steady-state equivalence ratio fires were obtained with different size pans and, consequently, quite varied burning rates and air entrainment rates (up to 50% different). The varied conditions and, yet, the good

correlation between yields and equivalence ratio suggest that the yields are not sensitive to the details of the flame structure.

Based on the observed temperature effect on the upper layer reactivity, it is reasonable to assume that the temperature difference between experiments results in different temperature plumes and, thus, varying species generation rates from the plume itself. Support for this can be found in the work of Morehart [16], which is described in detail in section 1.3.1. Morehart studied the effect of increasing temperature on layer composition by adding different levels of insulation to his hood. He concluded for the range of temperatures studied (500 to 675) that substantial increases in products of complete combustion and decreases in fuel and oxygen occurred with increasing layer temperature. Upper layer oxygen mass fraction was reduce by approximately 70 percent over the 175 K temperature increase. The temperatures of Morehart's upper layer were well below 800 K. Considering that the layer was unreactive at these temperatures, the change in layer composition must have been due to changes in the plume chemistry.

As illustrated by Morehart [16], the more complete combustion can be attributed to an extension of the flammability limits (or reaction zone) in the plume due to raising the flame temperature. The temperature of the plume can increase by two mechanisms when comparing varying experimental apparatus. One, the plume radiates less heat away when in a more enclosed or insulated space, and two, a hotter layer means entrainment of hotter gases into the upper part of the plume which is immersed in the layer.

The above discussion clearly demonstrates that changing the plume temperature can substantially increases the O_2 and fuel consumption and, primarily, increase the levels of products of complete combustion, with a small increase in CO. The conclusions of the above discussion are directly applicable in explaining the differences between the

modeling results and the hexane compartment fire measurements. To have correctly modeled the effect of temperature on layer reactivity, Beyler's layer composition should have been modified to account for the temperature effect on the plume generation of initial layer gases. Based on the this effect, the initial composition used in the modeling should have contained higher CO_2 and H_2O concentrations and lower O_2 and C_2H_4 concentrations. The net effect on the modeling results would be increased CO_2 levels and reduced CO levels from less incomplete hydrocarbon oxidation due to the lower availability of O_2 and C_2H_4 in the initial layer composition. These changes would be consistent with the experimental measurements and significantly reduce the disparity between model and experimental results for underventilated conditions.

4.3.4 Conclusion

To summarize, the effect of temperatures on compartment fire upper layer composition appears to be two fold; 1) the generation of species in the plume is changed and 2) oxidation of post flame gases in the layer is effected. Elevated compartment temperatures correlate with increased plume temperatures and more, primarily complete, oxidation of the fuel to CO_2 and H_2O. The layer temperature dictates post flame oxidation in the layer. Temperatures above 875 K allow nearly complete oxidation of CO to CO_2 for overventilated and slightly underventilated conditions. Layer temperatures below 875 K will result in freezing out the CO to CO_2 reaction, leaving high CO concentrations. During underventilated conditions, two mechanisms effecting net CO formation compete (CO and hydrocarbon oxidation). Increasing temperature over 875 K depletes CO by accelerating the CO to CO_2 conversion. However, with increasing equivalence ratios, incomplete oxidation of unburned hydrocarbons increases the CO

level. Since hydrocarbon oxidation is much faster than CO oxidation, net CO levels increase with equivalence ratio as unburned hydrocarbon concentrations increase.

4.4 Comparison of Correlations Between Fuels

In terms of fire safety engineering, ideal compartment fire behavior would be characterized with robust yield-equivalence ratio correlations that are independent of fuel type, temperature, compartment size and other fire parameters. This section discusses the effect of fuel composition on the correlations obtained for the compartment fires using hexane, PMMA, spruce and polyurethane as fuels.

4.4.1 Carbon Monoxide

The unnormalized and normalized CO yield correlations are presented for all fuels in Figures 4.44 and 4.45. The primary difference between correlations is that significant CO levels existed for overventilated spruce and polyurethane fires but not for the hexane or PMMA fires. The difference is believed to be a result of the upper layer temperature effect discussed in the previous sections. For the region of interest between ϕ_p of 0.6 and 1, the spruce and polyurethane fires typically had temperatures of 850 K and lower compared to temperatures of 920 K and higher for hexane and PMMA. The modeling work indicated that upper layer temperatures of 875 K were needed to oxidize all CO to CO_2. Based on the average layer temperatures, the higher spruce and polyurethane CO yield data agrees very well with this theory. The temperatures above 900 K for PMMA and most hexane resulted in near complete CO oxidation as indicated by the low yields.

Considering that the effect of the layer temperature could be removed and the CO yields appropriately readjusted, the generation of CO, which is a product of incomplete combustion, does not appear to be strongly governed by fuel composition. As a matter of

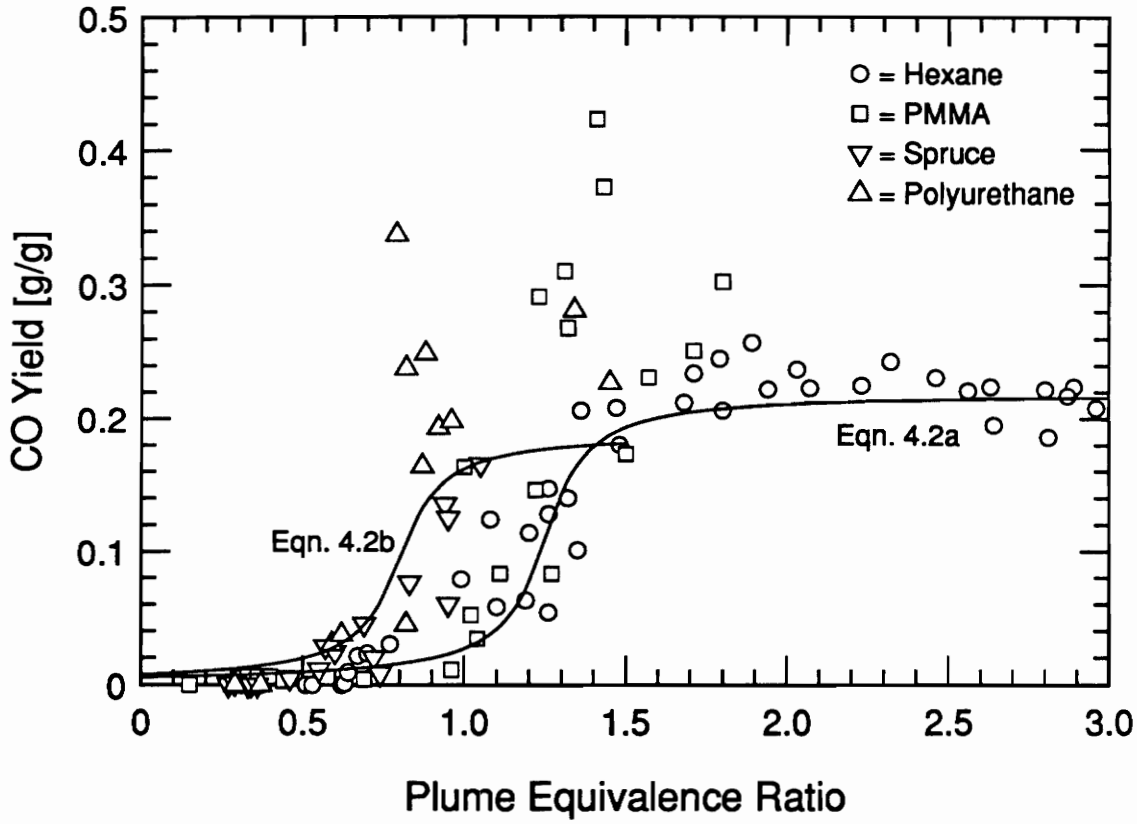

Figure 4.44 Comparison of unnormalized CO yield correlations for all fuels tested in the compartment fires.

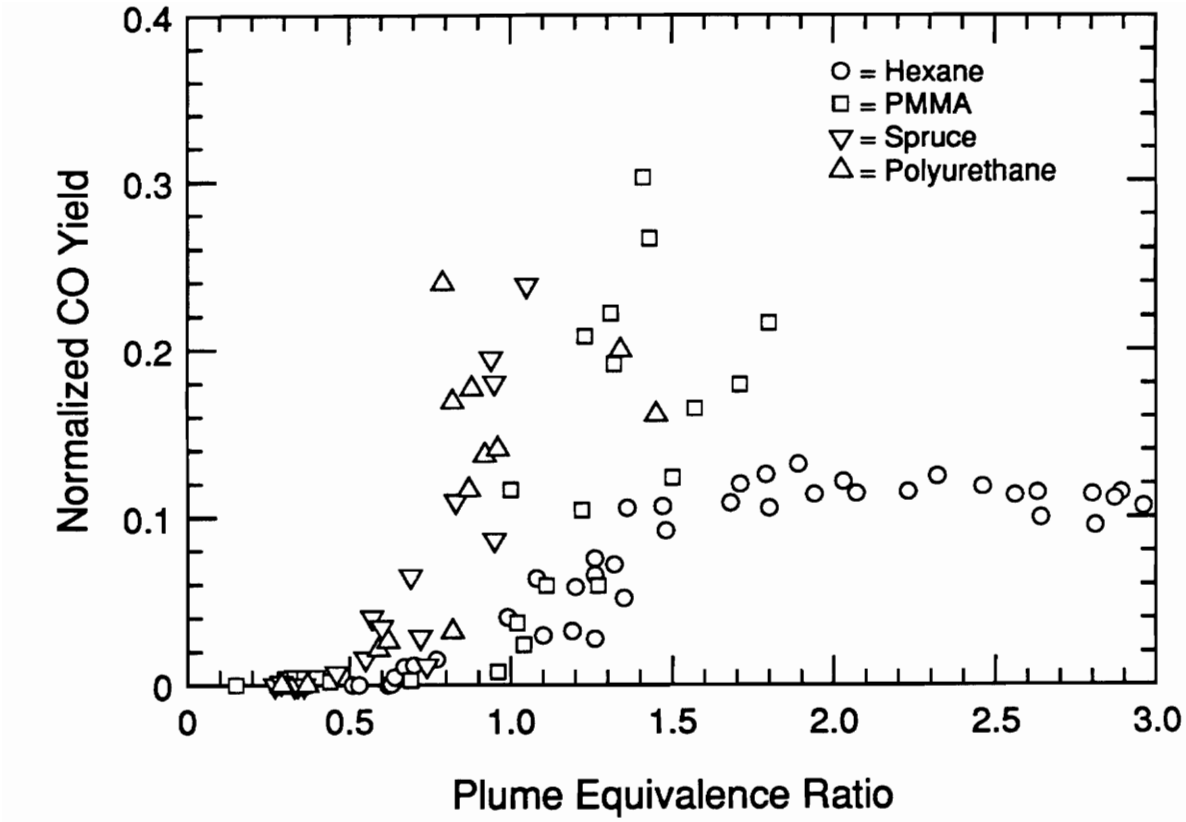

Figure 4.45 Comparison of normalized CO yield correlations for all fuels tested in the compartment fires.

fact, closer agreement is observed between fuels for unnormalized yields than normalized yields. This is believed to be due to the fact that CO is effectively an "intermediate" product which depends more on the elementary chemistry than on fuel composition which determines products of complete combustion.

Figure 4.45 shows the normalized CO yield correlations for all fuels tested. The general trends between fuels are the same as for the unnormalized CO correlations except that the normalized data for all fuels does not agree as well as the unnormalized data. The normalized hexane yields level out to an average of 0.11 and the PMMA and polyurethane yields appear to level out to 0.19, 73 percent higher than hexane. Thus, the unnormalized yields show closer agreement between fuels as they differ by less than 20 percent. A study of Beyler's data reveals the same general conclusion. This trend is advantageous in terms of fire analysis, because the use of the unnormalized yield correlation is preferred since no knowledge of the fuel composition is needed.

Only the hexane data shows a distinct leveling off of the CO yield for highly underventilated conditions. The average unnormalized CO yield for underventilated hexane fires was 0.22. Polyurethane and PMMA unnormalized CO yield data suggest a leveling off is starting to occur at a value of about 0.26, less than 20 percent higher than the hexane result. However, any global conclusion about CO yields leveling off during underventilated conditions is restricted by the limited equivalence ratios obtained for the fuels. Based on the kinetic modeling and the leveling off of hexane yields above ϕ_p equal to 1.5, CO is expected to level out for non-oxygenated fuels when layer O_2 concentrations go to zero with increasing equivalence ratio. The burning of oxygenated fuels, such as PMMA, may continue to increase CO levels with increasing equivalence ratio since the additional fuel carries its on oxygen to at least partially oxidize to CO.

Although relatively insensitive to fuel, the CO yield does depend on fuel composition. Beyler observed that different fuels had basically the same normalized CO yield correlations up to an equivalence ratio of 0.9, and that above 0.9, the yields leveled out to different average values for the different fuels: 0.09 for hexane, 0.13 for PMMA and 0.15 for pine. Beyler's average yields were taken for fires with equivalence ratios greater than 1.2. Beyler observed that CO yields are higher for fuels with higher oxygen-to-carbon ratios. The hexane and PMMA studied in the compartment fires show the same ranking. This trend is consistent with the chemical kinetics results, presented in section 4.3, that hydrocarbon oxidation is faster than CO oxidation. Thus, the oxygenated fuels, which can be considered already partially oxidized, produce more CO faster than the CO can oxidize to CO_2.

As can be seen in Figure 4.44, the hexane data can be viewed as a lower limit of CO yield observed for all fuels tested. Except for toluene, this is also true for all fuels that Beyler studied. An approximate fit of the hexane data is proposed as a lower boundary of the unnormalized CO yield in a compartment fire:

$$Y_{CO} = (0.22/180) * \tan^{-1}[10*(\phi-1.25)] + 0.11 \qquad [4.2a]$$

where the result of the inverse tangent function is in degrees. This equation is representative of fires with upper layer temperatures greater than 875 K. The effect of temperature on the hexane CO yields is shown in Figure 4.44 as equation [4.2b], which is a fit to Beyler's hood data for hexane fires.

$$Y_{CO} = (0.19/180) * \tan^{-1}[10*(\phi_p-0.8)] + 0.095 \qquad [4.2b]$$

Consistent with the temperature theory, equation (2) brackets the rise of CO yield at low ϕ_p for spruce and polyurethane burned in the compartment as both had upper layer

temperatures below 875 K. However, higher CO yields are observed for polyurethane than for hexane at low temperatures (i.e., as represented by equation (2)). This is attributed to polyurethane being an oxygenated fuel.

4.4.2 Carbon Dioxide and Oxygen

The CO_2 and O_2 unnormalized yields correlate well with respect to equivalence ratio for each fuel. However, the correlations are quantitatively different and cannot be described by a single curve. For example, the overventilated CO_2 yield for hexane is 3.1 and only 1.1 for spruce. For different fuels, the CO_2 and O_2 yield to equivalence ratio correlations only collapse down to a single curve when the yields are normalized by the maximum possible yield for the given fuel. Although complete combustion does not always occur, combustion efficiencies are similar enough between fuels that a fuel's particular stoichiometry will dictate the generation of CO_2 and the depletion of O_2. Therefore, the species associated with near complete combustion are not expected to have equal yields for different fuels since varying fuel compositions will dictate different limits of CO_2 that can be generated and O_2 that can be consumed per a gram of fuel burned. By normalizing the yields, the variability of fuel composition is removed.

Figures 4.46 and 4.47 show the normalized CO_2 and O_2 yield correlations for all fuels tested. As can be seen, there is very good agreement between all fuels and the data is well described by the simple model. The CO_2 data deviates from the model as is expected to account for the unburned hydrocarbons and production of CO and smoke.

4.4.3 Smoke

The yield of smoke appeared to be governed by the chemical nature of the fuel. Soot is formed in a flame where concentration gradients produce low oxygen levels. In

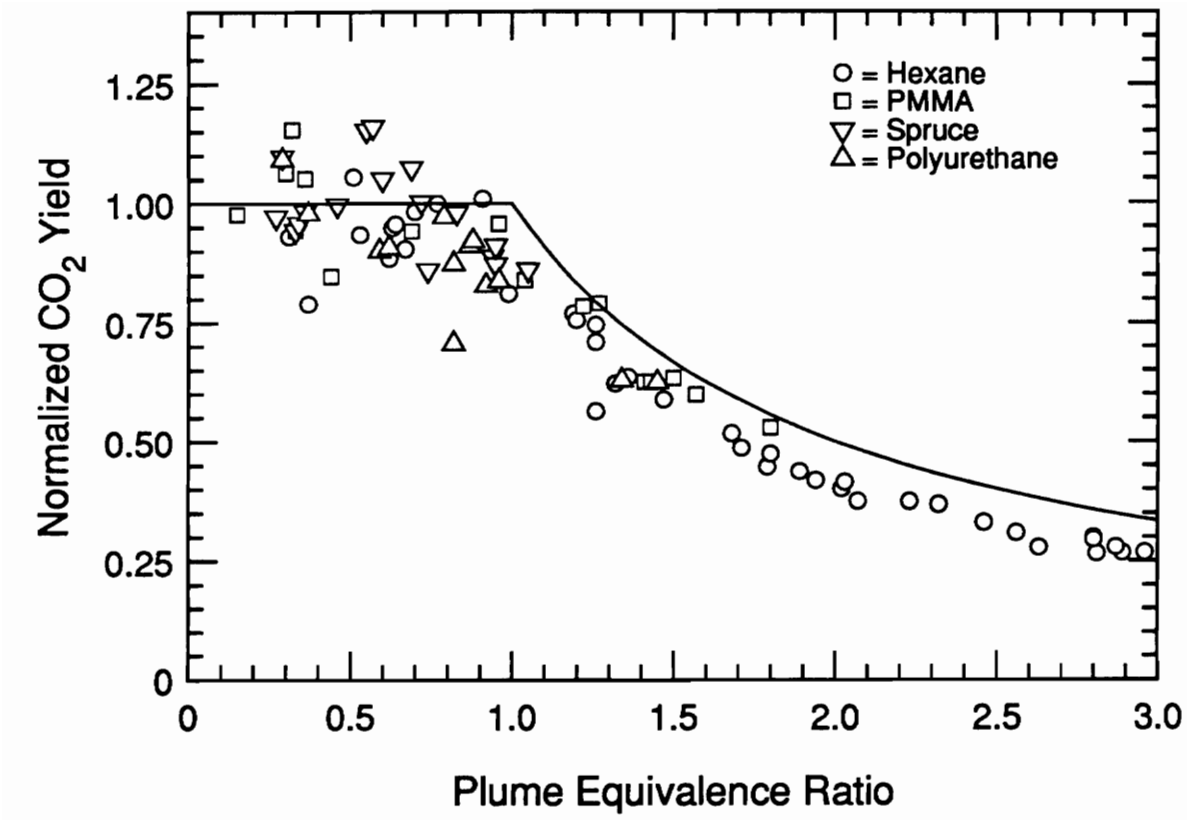

Figure 4.46 Comparison of normalized CO_2 yield correlations for all fuels tested in the compartment fires.

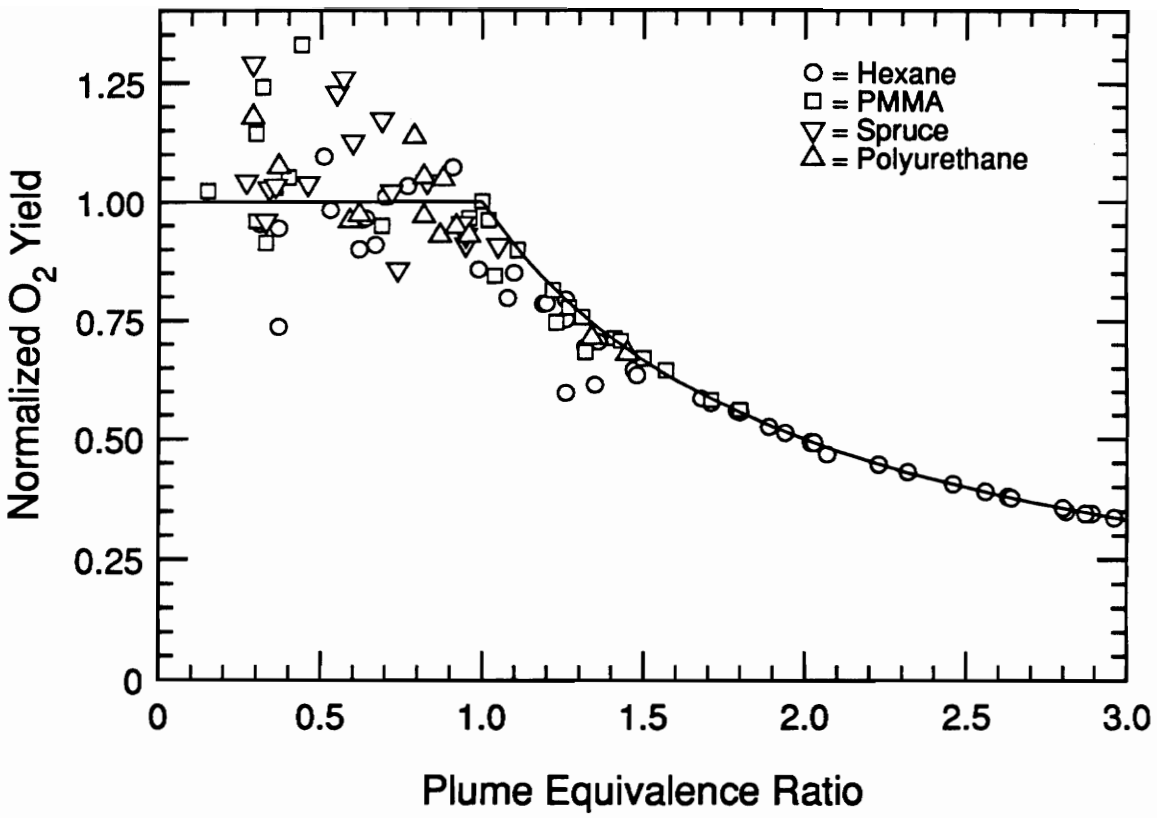

Figure 4.47 Comparison of normalized O_2 yield correlations for all fuels tested in the compartment fires.

these regions, pyrolysis of the fuel leads to the formation of species, such as polycyclic aromatic hydrocarbons and polyacetylenes, which are considered precursors to soot [46]. Depending on localized temperatures and oxygen concentrations, soot may either burn in the flame or grow, leading to the emission of smoke from the flame. Fuels with higher oxygen-to-carbon, O/C, ratios tend to produce less smoke, and the data bears this out. Hexane produced the highest average overventilated smoke yield (0.016) compared to the oxygenated fuels. Additionally, polyurethane, which has an O/C ratio of 0.3, produced over twice as much smoke as spruce, which has an O/C ratio of 1.5. Polyurethane fires had an average yield of 0.013 and spruce fires had an average of 0.046 for ϕ_p between 0.5 and 1.

Fuels with higher O/C ratios effectively have more oxygen readily available to, one, oxidize the fuel to CO and, two, reduce the probability of regions of low oxygen concentrations in the flame. Thus, fuel pyrolysis, which is needed for soot initiation, is reduced. Due to the effect of higher O/C ratios, it is then consistent to state that fuels with higher tendencies to soot produce less CO for underventilated conditions. As earlier discussed, increasing the fuel O/C ratio increases the CO yield at high equivalence ratios. This is because the oxidation of hydrocarbons occurs faster than the oxidation of CO. Thus, extra oxygen available in more oxygenated fuels results in hydrocarbons oxidizing to CO faster than CO can oxidize to CO_2.

4.4.4 Combustion Efficiency

Figure 4.48 shows the combustion efficiency plotted against the equivalence ratio for all fuels. The maximum possible heat release rate, Xc_{max}, is also plotted for comparison. The over- and underventilated average ratio of Xc/Xc_{max} is presented along

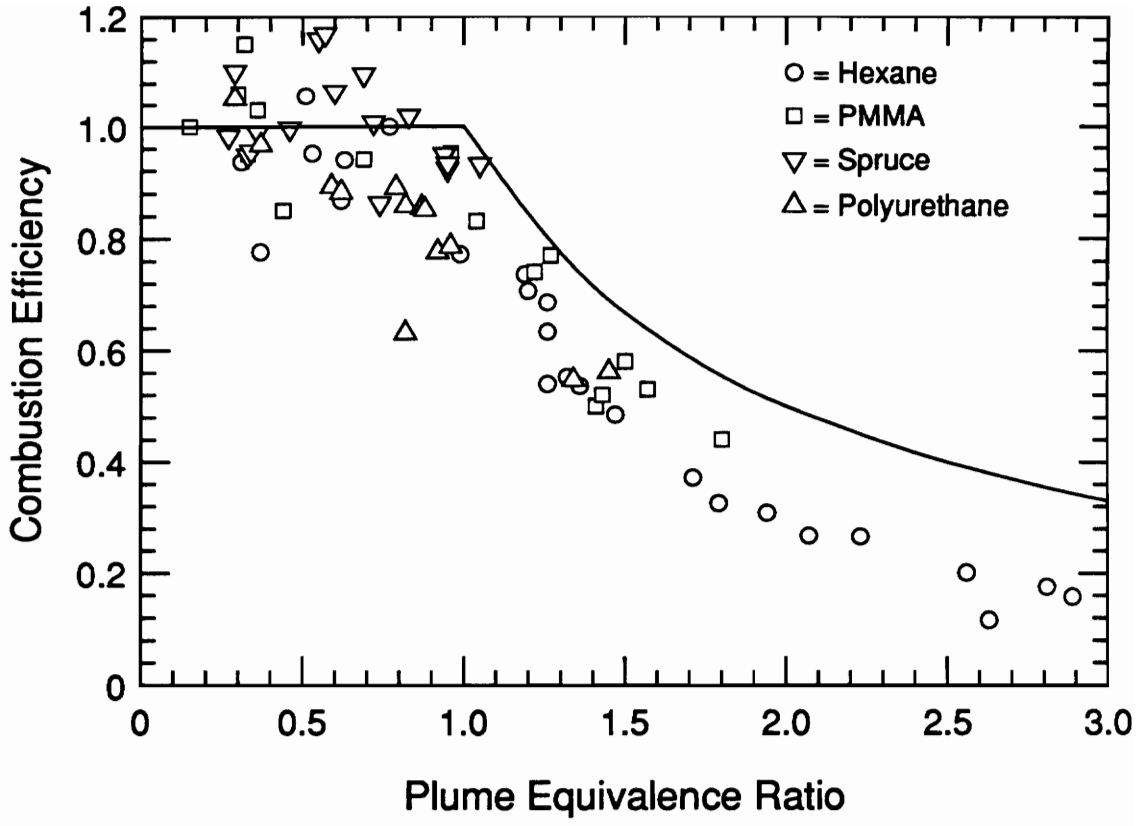

Figure 4.48 Comparison of combustion efficiency for all fuels tested in the compartment fires.

with the average combustion efficiencies in Table 4.3 for all the fuels tested, including Beyler's data. The correlations for each fuel agree reasonably well. The combustion efficiency is relatively constant for overventilated fires and decreases with increasing equivalence ratio for highly underventilated fires. Tewarson reported similar results for wood crib enclosure fires except that quite low combustion efficiencies of about 0.7 for overventilated fires were observed and the combustion efficiency did not decrease until an equivalence ratio of about 1.4 [17]. As discussed in chapter 1, it is important to note that the equivalence ratio data presented by Tewarson, was not measured directly but calculated from the ventilation parameter, $Ah^{1/2}$, and, therefore is suspect. Moreover, the elemental compositions used for the wood studies reported by Tewarson were not corrected for char yield. A correction of this sort would tend to decrease the equivalence ratio and increase the calculated combustion efficiency, more consistent with the compartment fires studied in this work.

As can be seen in Figure 4.48, the combustion efficiency for compartment fires can be predicted as a simple function of the equivalence ratio and represented by the following equation:

Equation (4)

$$X_c = A \qquad \phi < 1 \qquad [4.3a]$$

$$X_c = A / \phi \qquad \phi > 1 \qquad [4.3b]$$

where A is an experimentally determined value for the ratio of Xc/Xc_{max}, the combustion efficiency to the maximum possible combustion efficiency, for a given fuel and burning mode (over- or underventilated). Based on the four fuels tested, an average value of 0.81

Table 4.3 Average combustion efficiency and average ratio of combustion efficiency to maximum possible efficiency for all the fuels tested in compartment fires and for the similar fuels tested by Beyler.

FUEL	Xc_{AVG}		Xc/Xc_{max}	
	$\phi<1$	$\phi>1$	$\phi<1$	$\phi>1$
Hexane	0.91	0.42	0.91	0.65
PMMA	0.99	0.61	0.99	0.84
Spruce	1.01	0.93	1.01	0.98
Polyurethane	0.86	0.55	0.86	0.77
BEYLER:				
Hexane	0.77	0.40	0.77	0.50
PMMA	0.82	0.57	0.82	0.71
Ponderosa Pine	0.92	0.65	0.92	0.87

is suggested for a first estimate for underventilated compartment fires. The ratio of Xc/Xc_{max} is not a constant with increasing equivalence ratio. Therefore, the above estimate for A is just that; for example, values as low as 0.65 are observed for very underventilated hexane fires. Based on work by Toner and by Morehart, a value of 0.9 is suggested for gaseous fuels which, by nature, will burn more completely than solid and liquid fuels. From Beyler's data an average value of 0.96 is obtained for propane and an average value of 0.90 is obtained for propene.

CHAPTER 5

CARBON MONOXIDE PRODUCTION DOWNSTREAM OF THE COMPARTMENT

5.1 Introduction

Due to the flow of fire gases through a building, many people die in rooms that are remote from the source of the fire. Therefore, it is important to be able to predict the composition of gases leaving a compartment fire. The correlations presented in Chapter 3 provide a means to predict the major species yields in an upper layer. However, it was not previously known what the yields of these species are outside of the compartment, especially with the presence of external combustion. This chapter presents and discusses the results of the study of carbon monoxide production downstream of a compartment fire. The different modes of external burning observed are characterized and the effect of external burning on CO and smoke yields downstream of hexane-fueled compartment fires is examined.

5.2 Experiments

Downstream-sampled experiments were conducted to study the effect of external burning on the levels of CO leaving the compartment. The experimental procedure and apparatus were described in Chapter 2 and are essentially the same as used for the upper layer-sampled tests. Basically, the downstream-sampled tests consisted of burning hexane-fueled fires under the same conditions as the hexane-fueled upper layer-sampled tests. Sampling downstream of the compartment in the exhaust duct provided measurements of the effect of external burning on the yields of CO and CO_2 exiting the compartment compared to the initial yields in the upper layer. Smoke measurements

during the periods of external burning were compared to smoke levels just prior to the phenomenon.

5.3 Results and Discussion

Two distinctly different types of external combustion phenomena were observed during the compartment fires: 1) external flames jets and 2) flames due to external ignition and burning of fuel-rich exhaust gases (referred to as external burning). External flame jets were a result of large ceiling and wall jets that wrapped around the soffit and out the vent and, in the case of large vent sizes, from the extension of the main compartment fire out the ventilation opening. In general, external flame jets preceded external burning and were red/orange in color extending up to 0.75 m outside of the exhaust vent. External burning was characterized by large turbulent diffusion flames that were orange/yellow in color and extended up to 1.5 m outside of the vent. For underventilated (plume equivalence ratio greater than one) compartment fires with external combustion, the usual sequence of events, as the plume equivalence ratio became richer, was as follows: A) the appearance of external flame jets, B) quick flashes of external burning, C) significant bursts of external burning lasting a second or longer, D) sustained external burning that usually encompassed the entire exhaust vent, E) external burning ended and F) external flame jets retreated into the compartment. It should be noted that every event did not occur for all underventilated fires.

Table 5.1 presents a list of the underventilated fires that were studied and shows, for each fire, the average quasi-steady-state equivalence ratio along with the instantaneous equivalence ratio at the time that the first initial flashes and sustained external burning were visually observed to have started. Overventilated fires are not included since, as was expected, none were observed to have external burning.

Table 5.1 Underventilated hexane compartment fires. ϕ_{ss} is the average steady-state equivalence ratio. ϕ_{flash} and ϕ_{sus} are the instantaneously measured equivalence ratio at the time of initial flashes and at the beginning of sustained external burning, respectively. $\phi_{50\%}$ is the instantaneous equivalence ratio at which a 50% reduction in downstream yield occurs due to external burning. UL designates upper layer-sampled test and * designates that no reduction in CO yield was observed.

Entry #	ϕ_{ss}	ϕ_{flash}	ϕ_{sus}	$\phi_{50\%}$	Vent (cm^2)
1	1.0			UL	400
2	1.0			*	400
3	1.1	1.1		UL	1600
4	1.1			UL	400
5	1.2	1.0		*	400
6	1.2	1.0		UL	400
7	1.2			UL	400
8	1.3			UL	400
9	1.3	0.9		UL	1600
10	1.3			UL	400
11	1.3			*	400
12	1.3	0.8		UL	1200
13	1.4	1.1		UL	1600
14	1.4	1.1		*	1200
15	1.4	1.2		*	1200
16	1.5	1.2		UL	1200
17	1.5	1.0		UL	800
18	1.5			*	400
19	1.7	1.4		UL	400
20	1.7	1.0	1.6	UL	1600
21	1.7	1.8	1.5	1.9	800
22	1.8	1.8	2.0	2.2	400
23	1.8	1.6	1.7	1.7	400
24	1.8	1.7	1.7	1.7	400
25	1.9	0.8	1.8	UL	800
26	1.9	0.9	1.7	1.8	800
27	1.9	0.8	1.8	1.8	1200
28	2.0	1.9	1.7	1.8	400
29	2.0	1.8	2.1	UL	800

Table 5.1 (CON'T)

Entry #	Φ_{ss}	Φ_{flash}	Φ_{sus}	$\Phi_{50\%}$	Vent (cm^2)
30	2.0	1.6	2.0	UL	800
31	2.0	1.7	2.0	2.0	400
32	2.2	2.2	2.2	2.3	400
33	2.2	1.7	2.0	UL	400
34	2.3	1.4	2.2	2.1	400
35	2.3	1.5	2.1	1.9	400
36	2.4	2.3	2.3	UL	400
37	2.4	0.9	1.8	1.7	800
38	2.5	0.9	1.6	1.6	800
39	2.5	1.3	1.7	UL	800
40	2.5	2.4	2.4	UL	400
41	2.6	1.5	1.8	UL	800
42	2.6	1.6	1.7	UL	800
43	2.8	1.2	2.2	UL	800
44	2.8	1.3	2.8	UL	400
45	2.9	1.2	1.5	UL	800
46	3.0	1.0	1.9	UL	800
	AVG:	1.4	1.9	1.9	
	STD:	±0.4	±0.3	±0.2	

Instantaneous equivalence ratios were determined by noting, from video tape, the time that the given mode of burning occurred and then identifying the instantaneously measured equivalence ratio from the data files. Column 5 of Table 5.1, discussed below, shows the instantaneous equivalence ratio at which a 50 percent reduction in downstream CO yield was reached due to external burning. Column 6 is the exhaust vent size.

As can be seen from Table 5.1, a different equivalence ratio characterizes the onset of each mode of external burning. The progression of one mode of external burning to another, i.e. from flashes to sustained burning, is in general a function of increasing equivalence ratio; initial flashes occurred at an average ϕ of 1.4 ± 0.4 and sustained external burning occurred at an average ϕ of 1.9 ± 0.3. The fairly large standard deviations, particularly for initial flashes, are primarily due to the fact that initial flashes typically occurred during a very transient stage of the fire. Thus, the equivalence ratio was changing very rapidly over a small range of sampling time intervals leading to higher uncertainty in correlating it with the time of external burning.

The data also suggests that a relationship exists between the exhaust vent geometry and the instantaneous equivalence ratio at which external burning occurs. The onset of sustained external burning occurred at higher instantaneous equivalence ratios, ϕ_{sus}, for the fires with the smaller ventilation areas (400 cm^2). The average ϕ_{sus} is 2.1 ± 0.3 for fires with 400 cm^2 vents and 1.8 ± 0.2 for fires with 800 to 1600 cm^2 vents. It was observed that the larger ventilation openings (800, 1200 and 1600 cm^2) had substantially larger external flame jets which provided more of an ignition source for external burning to occur. Fires with the same equivalence ratio but with the smaller ventilation opening (400 cm^2) were observed to have substantially smaller external flame jets or none at all.

An example of this can be seen in Table 5.1 between entries 19 and 20 which were for fires that had similar steady-state equivalence ratios and CO yields but different ventilation sizes. The fire with the 400 cm^2 vent was a smaller fire with only small (less than 15 cm extension out of the vent) intermittent external flame jets and only one flash of external burning that lasted for a few seconds. Whereas, the fire with the 1600 cm^2 vent had steady external flame jets about 60 cm out of the vent and had sustained external burning. Therefore, even though the potential for external burning is governed by the equivalence ratio, the exhaust vent geometry appears to be a factor since the presence of an ignition source (i.e. external flame jets) is more probable with a larger ventilation opening.

The downstream-sampled burning experiments clearly showed a substantial reduction in CO and smoke yields when sustained external burning occurred. Figures 5.1 and 5.2 shows the CO yield and equivalence ratio time histories of a typical upper layer-sampled hexane fire and a downstream-sampled fire with the same initial conditions (i.e., same fuel source, vent size and initial compartment temperature). As both fires became underventilated, the CO yield rose quickly approaching a value of 0.22. For the upper layer-sampled test, Figure 5.1 (entry 29 in Table 5.1), initial flashes of external burning occurred at 219 seconds (ϕ = 1.7). Sustained external burning started at 228 seconds (ϕ = 2.0) and external burning fully encompassed the vent at 241 seconds (ϕ = 2.1). Sustained external burning lasted until the end of the fire (330 seconds) when the fuel rapidly burned out. During the transition to and during sustained external burning the CO yield obtained a value of 0.2 in the upper layer.

For the downstream-sampled fire, Figure 5.2 (entry 31 in Table 5.1), the initial flashes of external burning appeared at 175 seconds (ϕ = 1.5) which also marked the time

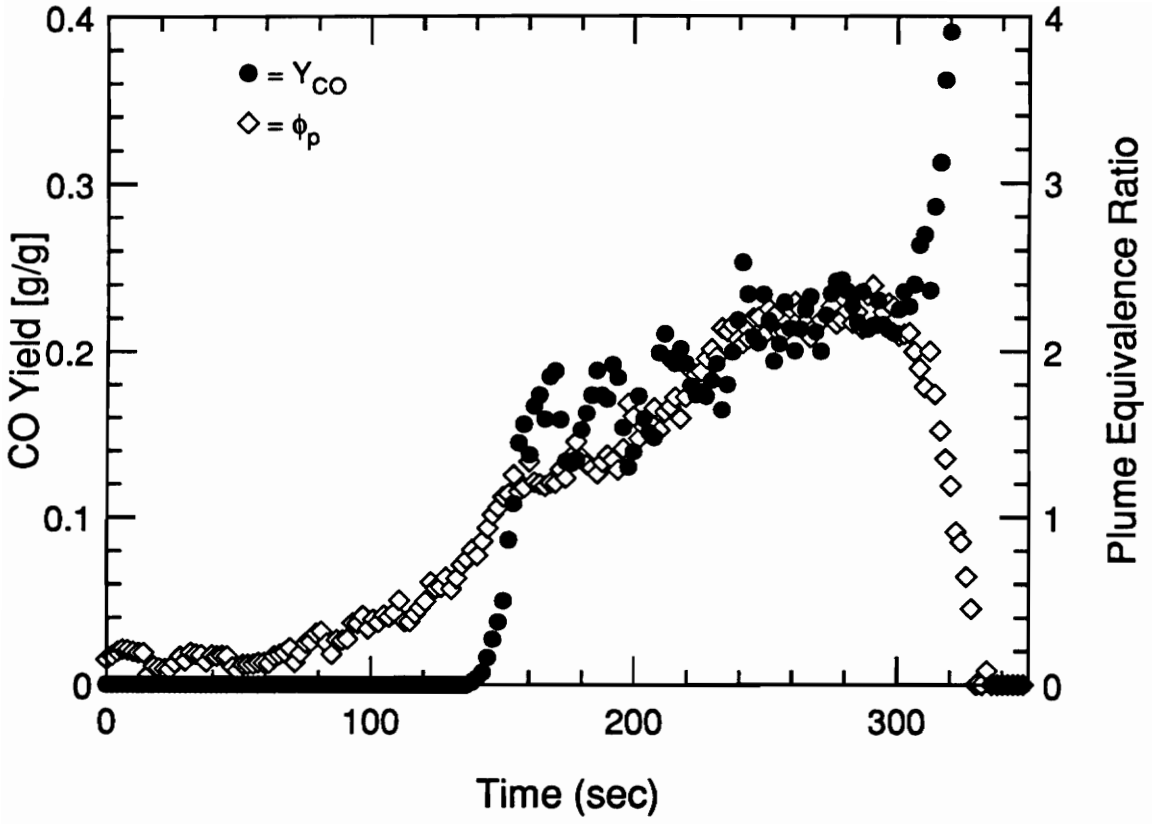

Figure 5.1 Typical time histories of upper layer CO yield and plume equivalence ratio for an underventilated hexane fire with external burning.

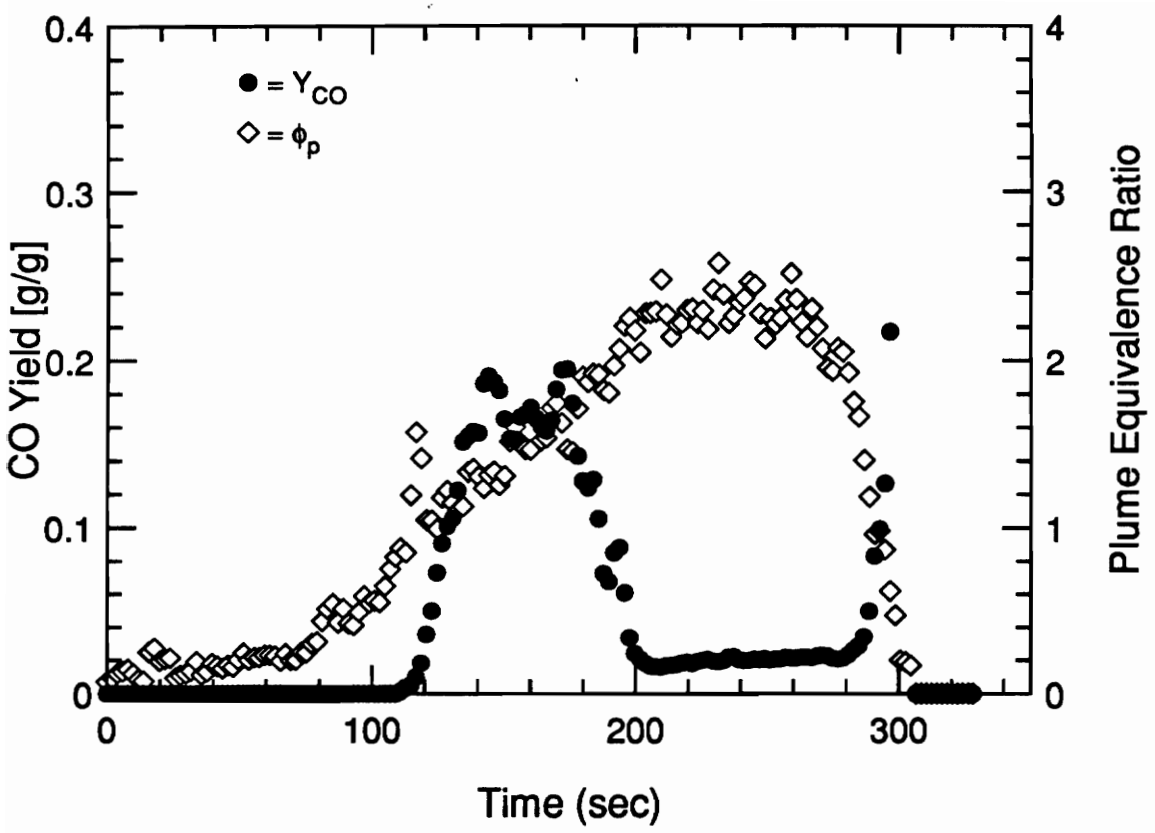

Figure 5.2 Typical time histories of downstream CO yield and plume equivalence ratio for an underventilated hexane fire with external burning. This fire had essentially the same initial conditions as the fire in Figure 5.1.

at which the CO yield had attained a value of 0.2. At 194 seconds (ϕ = 2.1) sustained external burning started. The external flame encompassed the vent at 202 seconds (ϕ = 2.2) and lasted until 298 seconds when the fire burned out. During the transition from initial flashes to attached sustained burning, the CO yield decreased rapidly reaching a steady average of 0.02 which was a reduction to 10 percent of the CO level leaving the compartment upper layer. Also, during the period of sustained external burning, the CO_2 yield approached the theoretical maximum, thus, indicating near complete combustion of all carbon leaving the compartment.

The quasi-steady-state average unnormalized CO yield versus average equivalence ratio for each fire is plotted in Figure 5.3. For equivalence ratios less than 1.7, the CO yield in the upper layer agrees well with the CO yield observed downstream of the compartment for similar fires. However, for fires reaching quasi-steady-state equivalence ratios of 1.7 or greater, the downstream measured CO yield was typically 10 to 25 percent of the CO yield in the upper layer for similar fires. All of the fires with reduced downstream CO yields had sustained external burning. Whereas, all fires which had downstream CO yields comparable to upper layer yields had no sustained burning, but, in some cases, did have flashes and/or bursts of external flames. It can also be seen from Figure 5.3 that the transition region exists about an equivalence ratio of 1.7 as illustrated by the fire with a yield of 0.12. For this fire, sustained burning did not last the entire steady-state period as reflected in the higher average CO yield.

These averaged steady-state results suggest that a compartment fire reaching an instantaneous equivalence ratio greater than 1.7 would have sustained external burning and a substantial reduction in CO yield. To investigate this point, the instantaneous equivalence ratio at which a 50 percent reduction in the downstream CO yield occurred

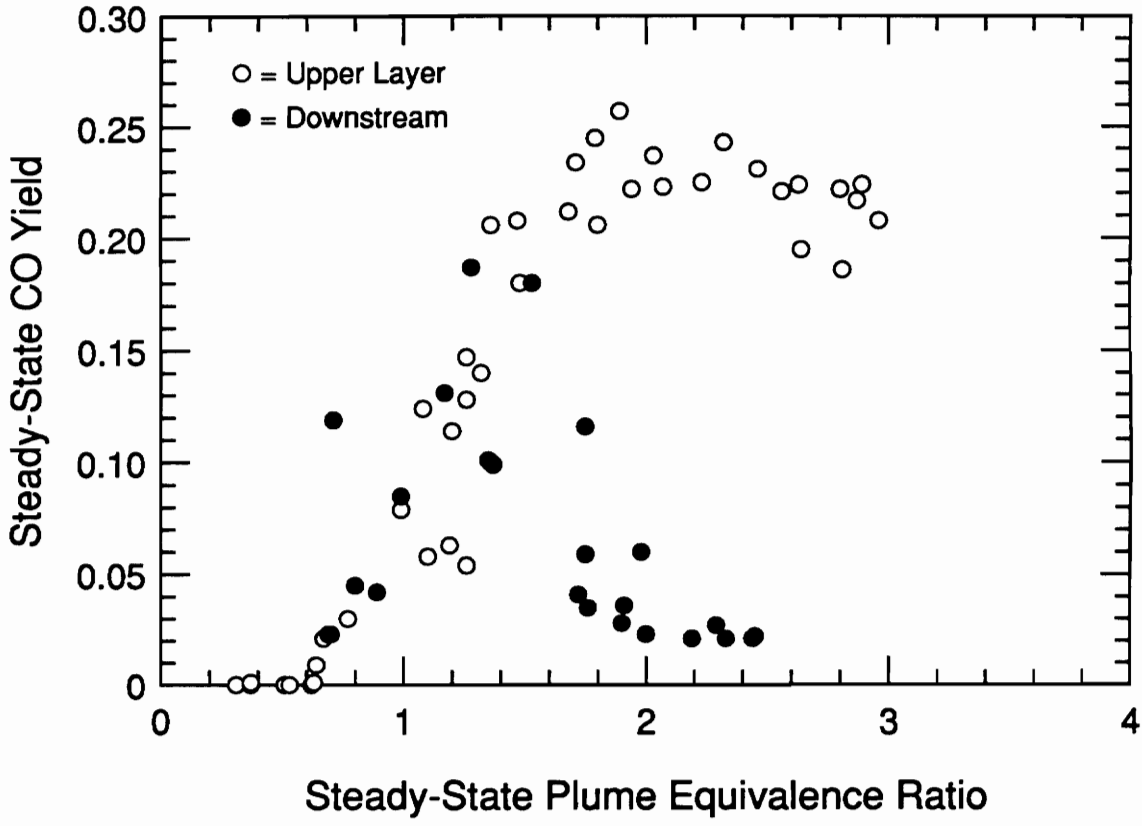

Figure 5.3 The averaged steady-state CO yield plotted against the averaged steady-state plume equivalence ratio for upper layer-sampled fires and for downstream-sampled fires.

was evaluated for all the downstream-sampled tests and the results are presented in column 5 of Table 5.1. The average equivalence ratio at which a 50 percent CO yield reduction is obtained is 1.9 ± 0.2 which agrees with the average equivalence ratio for which sustained burning occurs. Also, the time at which a 50 percent CO yield reduction is obtained corresponds to within 10 seconds of the onset of sustained external burning, therefore, showing that sustained external burning is the important mode in terms of hazard reduction of compartment effluent.

The effect of external burning on the smoke yield was also investigated and found to qualitatively follow the effect on CO yield discussed above. Figure 5.4 shows the smoke and CO yield plotted with respect to time for a fire with external burning. As the fire became underventilated, before any external burning, both the smoke and the CO started to rise. The first flashes of external burning appeared at 305 seconds (ϕ = 1.7). As sustained external burning started at 336 seconds (ϕ = 1.7), both the smoke and CO yields decreased dramatically. For this particular fire, the smoke yield was reduced from 0.15 by essentially 100 percent during sustained external burning. However, in general the reduction in smoke ranged from 50 to 100 percent for the fires investigated. A plot of the quasi-steady-state average smoke yield versus the average equivalence ratio for each fire shows the same general trend as seen for the CO yield in Figure 5.3, except with a larger amount of scatter in the smoke data. The average smoke yields for fires with and without sustained external burning were 0.015 and 0.007, respectively. Visual observation also confirmed that a substantial reduction of smoke occurred with sustained external burning.

In a hood apparatus, Beyler was able to successfully predict the occurrence of burning along the interface between the hot upper layer of combustion products and the

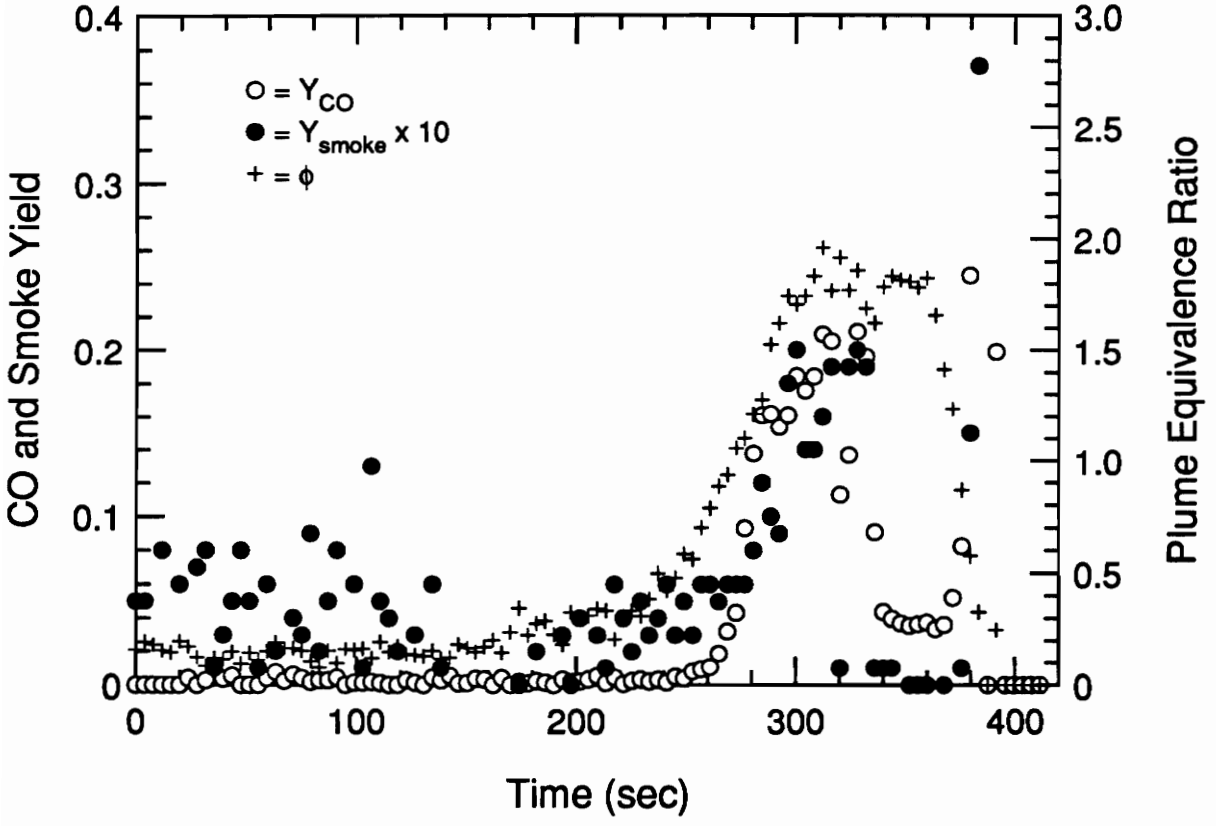

Figure 5.4 Typical time history of smoke yield, CO yield and plume equivalence ratio for an underventilated hexane fire with external burning.

lower layer of ambient air [47]. Based on classical empirical relations for lean premixed flammability limits, an ignition index was developed such that a value greater than one indicates that the upper layer has the potential to burn along the interface if an ignition source is present. For hexane fires with upper layer temperatures between 500 to 600 K, Beyler predicted that layer burning would occur at plume equivalence ratios of 1.7 or greater, and he was able to show that the prediction agreed well with experimental results [48].

Since the proposed ignition criterion is quite general for any fuel/oxidant stream pairs, it is of interest to evaluate its usefulness in predicting the occurrence of any or all modes of external burning resulting from a jet of hot, fuel-rich upper layer gases issuing from the compartment into relatively quiescent air. Therefore, the ignition index was evaluated for each upper layer-sampled fire.

In calculating the index, the composition of the upper layer needed to be specified beyond the CO, CO_2 and O_2 mole fractions that were measured. The mole fraction of H_2O was calculated as the CO_2 mole fraction times the molar ratio of H_2O to CO_2 at stoichiometric conditions. This was the same assumption used to correct the gas concentration measurements for water removal (section 2.2.4.1). Where measurements were not available, the mole fraction of unburned hydrocarbons (represented as C_2H_4) was estimated from the relationship that the fraction of unburned carbon equals $1-1/\phi$. Work by Beyler [14] and by Tewarson [27] has shown this relationship to be representative for compartment fire environments. Nitrogen was calculated from a mole balance once H_2 was determined.

The ignition index was calculated using several different methods of estimating the H_2 mole fraction. Based on Beyler's hexane data [48], the ratio of H_2 to CO concentrations range from 0.26 to 0.67 for underventilated conditions up to an equivalence ratio of 1.6. The hydrogen mole fraction was calculated from the CO measurement using both extremes of the H_2-to-CO ratio observed. A third method estimated the H_2 mole fraction from a mole balance. This method predicted H_2 concentrations approximately 3 times those observed by Beyler. Since the results of Chapter 3 indicate more complete combustion in the compartment fires, H_2 concentrations are expected to be less than those observed by Beyler; therefore, this method was considered unreasonable. Using a H_2-to-CO ratio of 0.5 to calculate the H_2 mole fraction was deemed most representative of the expected measurements and resulted in ignition index values that agreed within 10 percent of using a ratio of 0.26.

The ignition index was calculated using the steady-state average measurements for the upper layer-sampled hexane fires. Table 5.2 shows the calculated ignition index for the underventilated fires. The results indicate that for fires obtaining steady-state equivalence ratios approximately equal to or greater than 1.3, the upper layer had the potential to burn if an ignition source was present. This is in agreement with the experimental results, presented in Table 5.1, that showed initial flashes of external burning occurring for fires with equivalence ratios of 1.3 and higher, generally the fires with vents larger than 400 cm^2. As was discussed above, the fires with larger vents had larger external flame jets. Therefore, the ignition index can be used to predict the potential for external burning, but the occurrence of external burning is dependent on the presence of an ignition source (i.e. flame jets) which is dictated by the vent geometry and fire size.

Table 5.2 Calculated ignition index for underventilated hexane compartment fires.

	ϕ_{ss}	Ignition Index
	1.0	0.6
	1.1	0.8
	1.1	0.5
	1.2	0.7
	1.2	0.8
	1.3	0.8
	1.3	1.0
	1.3	0.9
	1.3	1.0
	1.4	1.1
	1.4	1.1
	1.5	1.2
	1.5	1.2
*	1.7	1.1
	1.7	1.3
	1.8	1.3
*	1.9	1.4
	1.9	1.4
*	2.0	1.4
	2.1	1.5
	2.2	1.5
*	2.3	1.3
*	2.5	1.4
	2.6	1.6
	2.6	1.5
	2.6	1.6
*	2.8	1.5
	2.8	1.6
*	2.9	1.5
	2.9	1.6
*	3.0	1.5

* indicates that hydrocarbons were measured.

Since these underventilated compartment fires had upper layer temperatures of 900 to 1100 K (300 to 600 K higher than Beyler observed), the ignition criteria predicts the potential for external burning to occur at equivalence ratios of about 1.3, which is lower than 1.7 predicted for layer burning in Beyler's experiments. This is to be expected since the lean flammability limit decreases as the temperature of the mixture increases.

It was shown above that the occurrence of sustained external burning was a function of the equivalence ratio, for which the upper layer composition can be correlated. Since the ignition index is primarily a function of the upper layer composition and temperature, it is expected that the onset of sustained external burning is characterized by a distinct ignition index value that is greater than one. In order to determine if a unique value exists, the ignition index was calculated as a function of time for each upper layer-sampled, underventilated fire. For each fire, the ignition index was then evaluated at the time when sustained external burning occurred. The results, presented in Table 5.3, show that when sustained external burning started, the average ignition index for all fires examined was 1.3 ± 0.08. In a consistent manner, fires that did not have sustained external burning had index values less than 1.2. The results demonstrate that the ignition criterion can be quite useful in identifying when the potential for external burning exists and more importantly the time at which sustained external burning occurs, and thus, a decrease in the CO hazard. As the upper layer composition is correlated with ϕ_p, the ignition index can be said to be a funtion of the equivalence ratio. Since the index is a function of upper layer temperature also, it is a better means than the equivalence ratio of predicting external burning. This is because the yield-equivalence ratio correlations are dependent on temperature.

Table 5.3 Instantaneous Ignition Index at time which sustained external burning started.

	ϕ_{ss}	Ignition Index
	1.7	1.2
*	1.9	1.2
*	2.0	1.3
	2.2	1.3
*	2.4	1.4
*	2.5	1.3
	2.6	1.2
	2.6	1.3
*	2.8	1.4
*	2.9	1.4
*	3.0	1.3
	AVG:	1.3
	STD:	±0.08

* indicates that hydrocarbons were measured.

For completeness, the occurrence of layer burning was examined in light of the ignition index and the occurrence of external burning. Generally, layer burning was observed to occur prior to the initial flashes of external burning, but always occurred before sustained external burning. The time at which the ignition index obtained a value of 1 was typically within 10 seconds of the time at which layer burning occurred.

Further compartment fire studies with full layer composition measurements are needed to verify the actual index values calculated here, due to the number of assumptions involved with calculating the ignition index and limited data. However, the results are very encouraging in indicating that the ignition criterion is a useful tool for predicting compartment fire behavior.

5.4 Summary and Conclusions

The ignition and burning of fuel-rich upper layer gases outside of the fire compartment (external burning) was observed experimentally. Hexane fires were burned in the 2.2 m^3 compartment with a window-style exhaust vent to study the effects of external burning on carbon monoxide and smoke yields downstream of the fire compartment. External burning was observed to occur in several modes: 1) intermittent flashes, 2) bursts that lasted for only a few seconds and 3) sustained external burning. Results showed that the flammability of the compartment fire effluent was a function of the equivalence ratio and that distinguishable equivalence ratios exist that determine which mode of external burning can be obtained for a given compartment fire. Results also showed that the reduction of carbon monoxide and smoke only occurs when sustained external burning occurs. For fires which obtained steady-state, plume equivalence ratios above 1.7, sustained external burning occurred and downstream

carbon monoxide yields were reduced to 10 to 25 percent of the upper layer yields. For equivalence ratios below 1.7, carbon monoxide yields downstream of a compartment fire were the same as upper layer yields even when flashes or short bursts of external burning occurred. During the course of a fire, including times with and without external burning, the production and consumption of smoke downstream of a fire compartment qualitatively followed that of carbon monoxide. For plume equivalence ratios above 1.7, the downstream smoke yield was reduced to 0 to 50 percent of the level observed prior to sustained external burning.

A study of the transient history of each fire indicated that sustained external burning occurred at an instantaneous ϕ_p of 1.8 for fires with large vents and at ϕ of 2.1 for fires with smaller vents of 400 cm^2. This was consistent with the observation that the fires with the larger vents had substantial external flame jets which provided an ignition source for external burning to more readily occur.

Lastly, Beyler's ignition criterion for layer burning was applied to the mixing of the hot fuel-rich, upper layer gases and ambient air outside of the fire compartment. The results show that the ignition index predicts the potential for external burning at equivalence ratios of 1.3 which is in reasonable agreement with the experimental observatory. Of more importance, a unique ignition index value (1.3) was identified when sustained external burning started to occur for the hexane fires. This provides a means, which is a function of both the equivalence ratio and upper layer temperature, of predicting when the CO hazard is reduced outside of a compartment fire.

CHAPTER 6

CONCLUSIONS AND RECOMMENDATIONS

6.1 Summary and Conclusions

Experiments were performed to examine the species production rates for four fuels (hexane, PMMA, spruce and flexible polyurethane foam) burning in a 2.2 m^3 compartment. The compartment was specially designed to separate the entrained air flow from the outflow of upper layer gases. This allowed direct measurement of the entrained air rate and, thus, the plume equivalence ratio. Therefore, this test facility allowed the study of realistic compartment fire behavior while eliminating the large uncertainty associated with calculating the plume equivalence ratio from the ventilation parameter, $Ah^{1/2}$, as had been done in the past.

Well-defined, empirical correlations between the upper layer yield of major species and the plume equivalence ratio were shown to exist for these compartment fires. The results reveal that the production of CO is strongly dependent on the compartment flow dynamics and upper layer temperature and less sensitive to the fuel type. However, the production of CO_2 and O_2 are dependent on all three parameters but can be represented as normalized yields which remove the fuel dependence.

The comparison between correlations obtained in the current work and those developed in simplified upper layer environments (hood experiments) show qualitatively similar curves but quantitatively different production rates for the same equivalence ratio. A comparison between the hood and compartment fire experiments indicated that the main difference between fire environments was a substantial increase in layer temperature for the enclosure fires. A chemical kinetics analysis of the upper layer was

successful in explaining the differences between correlations and revealing the temperature effect.

The effect of temperatures on compartment fire upper layer compositions appears to be two-fold; 1) the generation of species in the plume is changed and 2) oxidation of post flame gases in the layer is affected. Elevated compartment temperatures correlate to increased plume temperatures and more complete oxidation of the fuel to CO_2 and H_2O within the plume. The layer temperature dictates post flame oxidation in the layer. Temperatures above 875 K allow nearly complete oxidation of CO to CO_2 for overventilated and slightly underventilated conditions. Layer temperatures below 875 K result in freezing out the CO to CO_2 reaction, leaving high CO concentrations. During underventilated conditions, two mechanisms affecting net CO formation compete (CO and hydrocarbon oxidation). Increasing temperature over 875 K depletes CO by accelerating the CO to CO_2 conversion. However, with increasing equivalence ratios, incomplete oxidation of unburned hydrocarbons increases the CO level. Since hydrocarbon oxidation is much faster than CO oxidation, net CO levels in the layer increase with equivalence ratio as unburned hydrocarbon yield from the plume increases.

The carbon monoxide yield correlations obtained for the different fuels appear to be less sensitive to the fuel composition than to temperature. This is indicated by the better agreement between fuels for correlations of CO yield rather than normalized CO yield, which is dependent on the fuel. However, a tendency for oxygenated fuels to produce more CO was observed.

Although the compartment fires were shown to be quasi-steady in nature, correlations between transient CO yield and equivalence ratio showed very good agreement to the correlations obtained from the quasi-steady-state data of all fires. The

results suggest that for very transient conditions, the yield correlations can be used as long as the yields are adjusted for the effective dilution that occurs as ϕ_{ul} lags behind ϕ_p.

The CO yields downstream of hexane compartment fires were investigated and compared to the upper layer yields. Results showed that downstream CO levels can be correlated to the plume equivalence ratio when taking in account the occurrence of external burning.

External burning was observed to occur in several modes: 1) initial intermittent flashes, 2) bursts that lasted for only a few seconds and 3) sustained external burning. Results showed that the flammability of the compartment fire effluent was a function of the equivalence ratio and that distinguishable equivalence ratios exist that determine which mode of external burning can be obtained for a given compartment fire. Results also showed that the reduction of carbon monoxide and smoke only occurred when sustained external burning occurred. Typically, fires obtaining average steady-state equivalence ratios of 1.7 or higher, were observed to have sustained external burning and a reduction of downstream CO to 10 to 25 percent of the upper layer yield. For fires with no sustained external burning, carbon monoxide yields downstream of a compartment fire were the same as upper layer yields even when flashes or short bursts of external burning occurred.

During the course of a fire, including times with and without external burning, the production and consumption of smoke downstream of a fire compartment qualitatively followed that of carbon monoxide. For plume equivalence ratios above 1.7, the downstream smoke yield was reduced to 0 to 50 percent of the level observed prior to sustained external burning.

The use of an ignition criterion, which depends primarily on the upper layer composition and temperature, developed by Beyler appears to be a useful tool in predicting when external burning can occur and, more importantly, when sustained external burning occurs (i.e., a reduction in downstream CO hazard). A unique ignition index value of 1.3 was identified at which sustained external burning started to occur for all hexane fires studied.

6.2 Recommendations for Future Work

The yield correlations were obtained for compartment fires in which well defined two layer systems developed. Ventilation systems in buildings may cause the two layer environment to break down due to enhanced mixing. Flow dynamics in the compartment would, therefore, be significantly altered; possibly approaching a situation similar to a well-stirred reactor in extreme cases. Experiments need to be performed to determine the effect on species correlations when the two layer environment is destroyed.

Application of the correlations to actual fires is also limited by the inability to define a global equivalence ratio. Calculation of the equivalence ratio requires that the fuel volatile composition be known. This can prove to be a difficult task due to the wide variety of fuel items that can be found in a room. In the case of multiple fuels burning, the problem becomes more complex. Even if the overall volatile composition can be determined for a multiple fuel fire, the effect on the net upper layer yield correlations due to multiple plumes in the compartment is not certain. This becomes more complicated to analyze as plumes are immersed deeper in the upper layer where feed-back mechanisms between plumes and upper layer gases becomes important. Further work in this area is clearly needed.

Due to the number of assumptions involved with calculating the ignition index for external burning and the limited data available, further compartment fire studies with detailed layer composition measurements are needed to verify the actual index values calculated. However, the results are very encouraging in indicating that the ignition criterion is a useful tool for predicting compartment fire behavior.

Further work also needs to be done in examining different geometries outside of the compartment on fire. The window-style exhaust vent used in this study allows sufficient air entrainment for near complete combustion of CO to CO_2 under external burning conditions. Geometries such as a ceiling outside the exhaust vent may reduce air entrainment and the efficiency of external flames to destroy CO. It must also be noted that the geometry of a window-style vent is not a typical ventilation opening for inside a building. The result of a having a doorway opening is that the layer interface extends out of the room on fire to the adjacent room. Therefore, it is expected that external burning would occur at the same time as layer burning due to the extension of the layer interface out of the room.

Lastly, further testing should be done for other fuels. The burning of oxygenated fuels, which tend to produce more CO, may result in sustained external burning occurring at lower equivalence ratios due to increased ignition potential.

REFERENCES

1. Hall, J. R., Jr. and A. E Cote, "America's Fire Problem and Fire Protection," in Fire Protection Handbook, (Ed. A. E. Cote) National Fire Protection Association, Quincy, Mass. (1991).

2. Anderson, R. A., A. A. Watson, and W. A. Harland, "Fire Deaths in Glasgow Area: II The Role of Carbon Monoxide," Med. Sci. Law, 21, 289-294 (1981).

3. Harland, W. A. and Anderson, R. A., "Causes of Death in Fires," Proceedings, Smoke and Toxic Gases from Burning Plastics, 15/1-15/19, London England, Jan 6-7, (1982).

4. Harwood, B. and Hall, J. R., "What Kills in Fires: smoke inhalation or burns?" Fire Journal, 83, 29-34, May/June (1989).

5. Braker, W. and A. L. Mossman, Matheson Gas Data Book, sixth edition, Matheson, Lyndhurst, NJ (1980).

6. Budnick, E. K., "Mobile Home Living Room Fire Studies: The Role of Interior Finish," NBSIR 78-1530, National Bureau of Standards, Gaithersburg, MD (1978).

7. Budnick, E. K., D. P. Klein and R. J. O'Laughlin, "Mobile Home Bedroom Fire Studies: The Role of Interior Finish," NBSIR 78-1531, National Bureau of Standards, Gaithersburg, MD (1978).

8. Kisko, T. M. and D. W. Stroup, "EVACNET+: A Computer Program to Determine Optimal Building Evacuation Plans," Fire Safety Journal, 9, 211-220 (1985).

9. Nelson, H. E., "FPETOOL: Fire Protection Engineering Tools for Fire Estimation," NISTIR 4380, National Institute of Standards and Technology, Gaithersburg, MD (1989).

10. Cooper, L. Y., " Estimating the Environment and the Response of Sprinkler Links in Compartment Fires with Draft Curtains and Fusible-Link-Actuated Ceiling Vents Theory," Fire Safety Journal, 16, 137-163 (1990).

11. Walton, W. D. and Budnick, E. K., "Deterministic Computer Fire Models" in Fire Protection Handbook, (Ed. A. E. Cote) National Fire Protection Association, Quincy, Mass. (1991).

12. Emmons, H. W., "The Needed Fire Science," in Fire Safety Science - Proceedings of First International Symposium, (Eds. Grant, C. E. and P. J. Pagni) Hemisphere, Washington, D.C. 33-53 (1986).

13. Toner S. J., E. E. Zukoski, and T. Kubota, "Entrainment, Chemistry, and Structure of Fire Plumes," National Institute of Standards and Technology, Center for Fire Research, Report NBS-GCR-87-528 (1987).

14. Beyler, C. L., "Major Species Production by Diffusion Flames in a Two Layer Compartment Fire Environment," Fire Safety Journal, **10**, 47-56 (1986).

15. Beyler, C. L., "Major Species Production by Solid Fuels in a Two Layer Compartment Fire Environment," in Fire Safety Science - Proceedings of First International Symposium, (Eds. Grant, C. E. and P. J. Pagni) Hemisphere, Washington, D.C. 431-430 (1986).

16. Morehart, J. H., E. E. Zukoski, and T. Kubota, "Species Produced in Fires Burning in Two-Layered and Homogeneous Vitiated Environments," National Institute of Standards and Technology, Center for Fire Research, Report NBS-GCR-90-585 (1990).

17. Tewarson, A., Twentieth Symposium (International) on Combustion, The Combustion Institute, Pittsburgh, PA, 1555-1566 (1984).

18. Zukoski, E.E., S. J. Toner, J. H. Morehart and T. Kubota, "Combustion Processes in Two-Layer Configurations," in Fire Safety Science - Proceedings of Second International Symposium, (Ed. Wakamatsu, T.) Hemisphere, Washington, D.C. 295-304 (1989).

19. Zukoski, E.E., J. H. Morehart, T. Kubota and S. J. Toner, "Species Production and Heat Release Rates in Two-Layer Natural Gas Fires," Combustion and Flame 83, 324-332 (1991).

20. Yokoi, S.: Building Research Institute, Report No. 34, Tokyo (1960).

21. Seigel, L. G.: Fire Technology, **5**, 43 (1969).

22. Thomas, P. H. and Law, M.: Fire Research Note, No. 921 (1972).

23. Thomas, P. H. and Heselden, A. J. M.: Conseil Internationale du Batiment Report No. 20, Fire Research Note, No. 923 (1972).

24. Bullen, M. L. and Thomas, P. H.: Seventeenth Symposium (International) on Combustion, p. 1139, The Combustion Institute (1978).

25. Skelly, M. J., "An Experimental Investigation of Glass Breakage in Compartment Fires," Masters Thesis, Virginia Polytechnic Institute and State University (1990).

26. Fluid Meters: Their Theory and Application, Report of A.S.M.E Research Committee on Fluid Meters, Sixth edition (Ed. Bean, H. S.), ASME, NY (1971).

27. Tewarson, A., "Generation of Heat and Chemical Compounds in Fires" in The SFPE Handbook of Fire Protection Engineering (P. J. DiNenno, Ed), National Fire Protection Association, Quincy, MA, (1988).

28. "Special Reference Material Report GM 25 and GM 26," Materials Bank Compendium of Fire Property Data, Product Research Committee (1976).

29. Babrauskas, V., "Burning Rates" in The SFPE Handbook of Fire Protection Engineering (P. J. DiNenno, Ed), National Fire Protection Association, Quincy, MA, (1988).

30. Tewarson, A., Combustion and Flame, 19, 101-111 (1972).

31. Quintiere, J. G., B. J. McCaffrey and K. Den Braven, Seventeenth Symposium (International) on Combustion, The Combustion Institute, Pittsburgh, PA, 1125-1137 (1978).

32. Gross, D and Robertson, A. F., Tenth Symposium (International) on Combustion, The Combustion Institute, Pittsburgh, PA, 931-942 (1965).

33. Tewarson, A., Flame Retardant Polymeric Materials, Vol 3 (M. Lewin, S. M. Atlas and E. M. Pearce, Eds.), Plenum Press, New York, p 97 (1982).

34. Kee, R. J., F. M. Rupley and J. A. Miller, Sandia Report SAND89-8009 (December 1990).

35. Lutz, A. E., R. J. Kee and J. A. Miller, Sandia Report SAND87-8248 (February 1991).

36. Pitts, W. M., Twenty-Fourth Symposium (International) on Combustion, The Combustion Institute, Pittsburgh, PA, (1992).

37. Miller, J. A. and Bowman, C. T., "Mechanism and Modeling of Nitrogen Chemistry in Combustion," Prog. Energy Combustion Science, 15, 287-338 (1989).

38. Chakir, A., M. Bellimam, J C. Boettner and M Cathonnet, International Journal of Chemical Kinetics, 24, 385-410 (1992).

39. Dagaut, P., J C. Boettner and M Cathonnet, International Journal of Chemical Kinetics, 22, 641-664 (1990).

40. Yetter, R. A. and F. L. Dryer, Combust. Sci. and Tech., 79, 97-128, (1991).

41. Yetter, R. A. and F. L. Dryer, Combust. Sci. and Tech., 79, 129-140, (1991).

42. Dagaut, J C. Boettner and M Cathonnet, Combust. Sci. Tech., 77, 127-148 (1991).

43. Vaughn, C. B., W. H. Sun, J. B. Howard and J. P. Longwell, Combustion and Flame, 84, 38-46 (1991).

44. Dagaut, M Cathonnet and J C. Boettner, International Journal of Chemical Kinetics, 23, 437-455 (1991).

45. Norton, T. S. and F. L. Dryer, International Journal of Chemical Kinetics, 24, 319-344 (1992).

46. Drysdale, D., Fire Dynamics, John Wiley and Sons, New York (1985).

47. Beyler, C. L.: Combustion Science and Technology 39, 287 (1984).

48. Beyler, C. L.: Ph.D. Thesis, Harvard University (1983).

49. Newman, J. S. and J Steciak, Combustion and Flame, 67, 55-64 (1987).

APPENDIX A

CALIBRATION OF THE VELOCITY PROBE

The entrained air rate into the compartment was measured with a hot film, 0-2m/s linear velocity probe (Kurz model 415) with an accuracy of ±2.5 percent of the reading. The probe was positioned at the point of mean velocity based on measured velocity profiles. The flow was turbulent and, thus, the velocity profile was quite flat. The probe was calibrated in the experimental setup using a CO gas tracer method.

The general concept of the gas tracer method is to measure the total volumetric flow rate of gas through a duct by introducing a known flow rate of gas A, different from the primary gas, at the upstream end of the duct and measuring the concentration of gas A at the opposite end. Assuming no concentration gradients in the flow, the total flow rate through the duct is equal to the flow rate of gas A divided by the measured mole fraction of gas A.

Carbon monoxide was chosen as a suitable tracer gas since it is not found, in measurable quantities, in air and since it could be measured with the already available NDIR CO analyzer. Due to the fact that the gas tracer method provides volumetric flow rate measurements, the velocity probe was calibrated in terms of the same measurement. This was appropriate since the inlet duct was a fixed area and also, since the final quantity desired was the mass entrainment rate of air, which equals the volumetric flow rate multiplied by the density.

The calibration setup consisted of using a variable speed fan, just inside the exhaust vent, to produce a range of flows through the compartment. The fan simulated the fire plume in drawing air through the inlet duct, into the test compartment and out the

exhaust vent. Carbon monoxide was introduced into the air stream 15 cm in from the upstream end of the inlet duct and the concentration of CO was measured downstream in the air plenum. To insure the CO and air were well mixed prior to entering the plenum, the CO was supplied by four parallel tubes evenly distributed in the duct. The end of each tube was capped and four perpendicular holes were drilled around the periphery of the tube near the end. Therefore, the CO was injected into the air stream at 16 points across the area of the duct. The flow of CO to the duct was measured before and after each run using a dry gas test meter (Singer, model DTM-115). The measured supplied CO flow rate was accurate to within 2 percent of the value and the CO analyzer was accurate to within 10 ppm on a 1000 ppm range. Typical CO concentrations measured in the calibration procedure were 500 to 700 ppm.

The procedure for calibration was to establish a steady flow of air and the CO tracer through the compartment, and then record the CO concentration and the velocity probe output for 120 seconds. Both values were then averaged over time to obtain one data set. The velocity probe was calibrated by the manufacturer to have a linear output of 0 to 5 volts corresponding to 0 to 2 m/s. The velocity was multiplied by the duct area to yield the volumetric flow rate. Figure A.1 shows the volumetric flow rate measured by the CO tracer method plotted versus the measurement calculated from the velocity probe. A linear fit to the data is also shown in Figure A.1. The sum of the absolute value of the residuals is 0.0376 for 20 data points (i.e., a maximum of 6 percent uncertainty associated with the linear fit for the range of flows measured). The equation for the fit follows:

$$Q = 1.235E\text{-}2 + 0.9395 * Q_V \qquad [A.1]$$

where Q is the volumetric flow rate through the duct and Q_V is the measurement from the velocity probe. Using this equation to calculate the entrained air flow rate eliminated the

combined uncertainties of correct probe placement and any questions of relying on the manufacturer's calibration. As long as the probe location remained the same, the measured air entrainment rate was not affected by changes in the location of the mean velocity due to varying flow conditions.

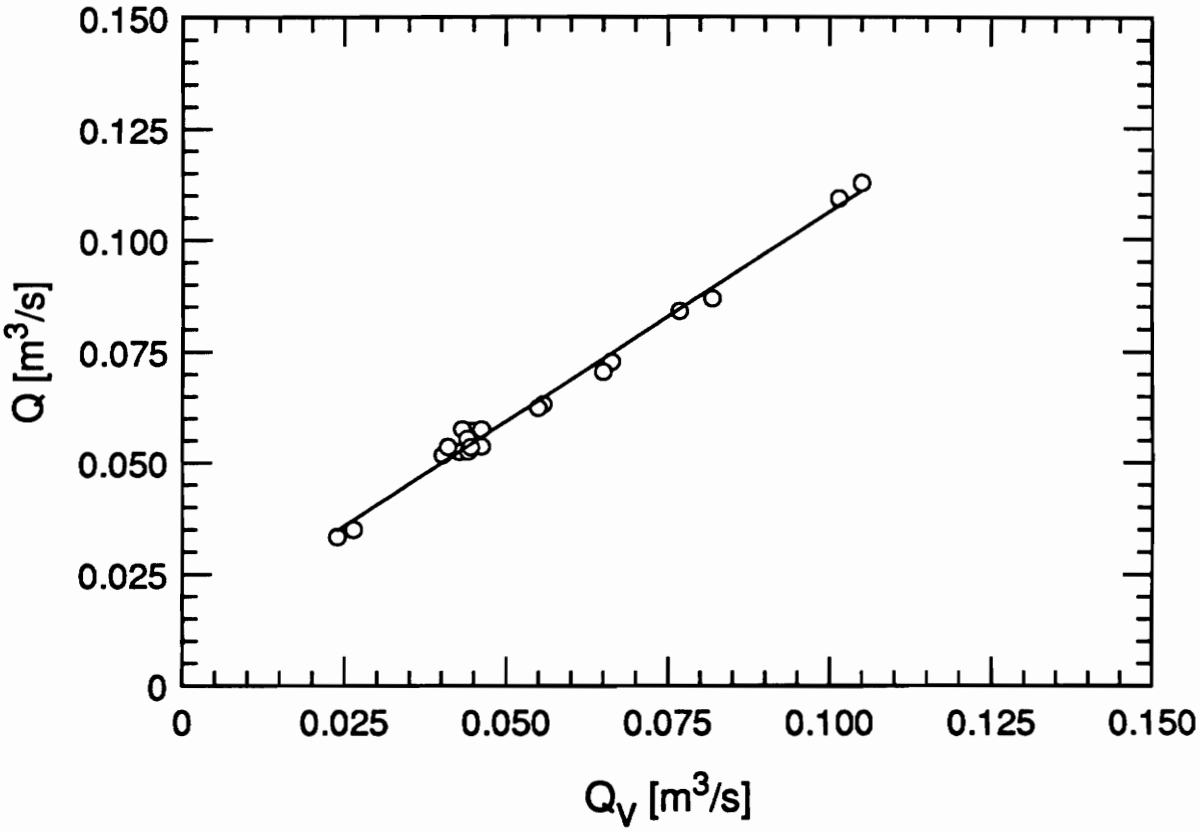

Figure A.1 The volumetric flow rate through the inlet duct based on the CO tracer method versus the calculated flow rate based on the velocity probe output. The data is represented with a least-squares linear fit.

APPENDIX B

DATA REDUCTION PROGRAM

The program used to reduce the data obtained from the data acquisition system is shown below. The data acquisition system stores all data sequentially in a single array file. The reduction program first reads in the raw data and stores each measured value in a seperate array before further calculations are performed.

```
C   PROGRAM REDUCE.FOR
C
$LARGE
    IMPLICIT REAL*8(A-H,O-Z)
    DIMENSION TIME(1300),DRYCO(1300),DRYCO2(1300),DRYO2(1300)
    DIMENSION FUEL(1300), AIRVEL(1300),TC(14,1300)
    DIMENSION FTOA(1300),UTC(14),SUTC(14)
    DIMENSION FUELRATE(1300), AIRRATE(1300)
    DIMENSION RAWFUEL(1300),RESTIME(1300),Q(1300)
    DIMENSION DEL2FUEL(1300),SMOKE1(1300),SMOKE0(1300)
    DIMENSION FID(1300)
    INTEGER PTSTART, PTSPAST, CONSTANT,I,K,IFUELTYPE,TFLAG
    INTEGER DUCT,AVGFLAG,TIMEFLAG
    PARAMETER (VOLC=1.137, PRESS=15.8, AREA = 0.0699573)
    REAL*8 IGNITION,LAYER,MASSODL,NP,NPCP,N2MOLES,NTOTST
    CHARACTER*7 FNAME,RUN
C
C ---------------------------------------------------------------------
C
C       INITIALIZE VARIABLES
C
    FIDSPAN = 1.
    FIDRANGE = 0.
    FIDZERO = 0.
    FIDCAL = 1.
    TOTDUCTMOLES = 0.0
    EXMOLES  = 1.0
    SMOKED = 0.0
    SMOKEVF = 0.0
    EXTCOEFF =0.0
    SRATIO = 0.0
    DO 200 N=1,1000
        SMOKE0(N) = 0.0
        SMOKE1(N) = 0.0
        FID(N) = 0.0
        FUELRATE(N) = 0.0
        RESTIME(N) = 0.0
 200 CONTINUE
C ---------------------------------------------------------------------
C
C   INPUT RUN PARAMETERS
```

```
C
    WRITE(*,*) 'ENTER FILE NAME'
    READ(*,15) FNAME
   15 FORMAT(A7)
    WRITE(*,*) 'ENTER RUN #'
    READ(*,*) IRUNNUMBER
    WRITE(*,*) 'ENTER CO RANGE 1, 2 or 3'
    READ(*,*) ICORANGE
    WRITE(*,*) 'ENTER CO2 RANGE 1, 2 or 3'
    READ(*,*) ICO2RANGE
    WRITE(*,*) 'ENTER THE RUN TIME PAST END OF FIRE (sec)'
    READ(*,*) TIMEPAST
    WRITE(*,*) 'COMPARTMENT (1) OR EXHAUST (2) RUN, ENTER 1 or 2'
    READ(*,*) IPROBE
    IF (IPROBE.EQ.1) THEN
     PROBE='COMPARTMENT'
    ELSE
     PROBE='EXHAUST'
    ENDIF
    IF (IRUNNUMBER.GE.86.AND.IRUNNUMBER.LE.113) THEN
     WRITE(*,*)'ENTER AMBIENT TEMPERATURE (C)'
     READ(*,*) TAMB
     TAMB = TAMB+273.15
    ENDIF
    IF (IRUNNUMBER.GE.86.AND.IRUNNUMBER.LE.105) THEN
     WRITE(*,*)'ENTER UPPER LAYER TEMPERATURE (K)'
     READ(*,*) TEMPUL
    END IF
    WRITE(*,*) 'ENTER AMBIENT PRESSURE'
    READ(*,*) PA
    WRITE(*,*) 'HEXANE (1), PMMA (2), WOOD (3) OR POLYURETHANE (4) FIR
   $E?'
    READ(*,*)IFUELTYPE
    IF (IFUELTYPE .EQ. 1) THEN
      TFUEL = 'HEXANE'
    ELSE IF (IFUELTYPE .EQ. 2) THEN
      TFUEL = 'PMMA'
    ELSE IF (IFUELTYPE .EQ. 3) THEN
      TFUEL = 'WOOD'
    ELSE IF (IFUELTYPE .EQ. 4) THEN
      TFUEL = 'POLYURETHANE'
    END IF
    IF (IRUNNUMBER.GE.203) THEN
    WRITE(*,*) 'ENTER THE FID SPAN GAS CONCENTRATION (ppm C2)'
    READ(*,*) FIDSPAN
    WRITE(*,*) 'ENTER THE FID OPERATING RANGE (eg. 1e-9)'
    READ(*,*) FIDRANGE
    WRITE(*,*) 'ENTER THE FID ZERO GAS READING AS mv times the range'
    READ(*,*) FIDZERO
    WRITE(*,*) 'ENTER THE FID SPAN GAS READING AS mv times the range'
    READ(*,*) FIDCAL
```

```
      ENDIF
      IF(IPROBE.EQ.1) THEN
           PTSTART=9
      ELSE
           PTSTART=6
      ENDIF
      IF(IRUNNUMBER.LE.136) THEN
           PTSTART=6
      ENDIF

C     SET VALUES FOR HEXANE FIRE
C
      IF(IFUELTYPE .EQ. 1) THEN
           DELHC = 44735.0
      END IF
C
C     SET VALUES FOR PMMA FIRE
C
      IF (IFUELTYPE .EQ. 2) THEN
           DELHC = 25200.0
      END IF
C
C     SET VALUES FOR WOOD FIRE
C
      IF (IFUELTYPE .EQ. 3) THEN
           DELHC = 17900.0
      END IF

C
C     SET VALUES FOR POLYURETHANE FIRE
C
      IF (IFUELTYPE .EQ. 4) THEN
           DELHC = 26570.0
      END IF


C
C     ASSIGN THE APPROPRIATE MAXIMUM VALUE FOR CHOSEN ANALYZER RANGE
C
      O2CONSTANT=100.0
      O2GAS=.02*4.74
      IF(ICORANGE.EQ.1) THEN
           CORANGE=1000.0
           COCONSTANT=1000000.0
      ENDIF
      IF(ICORANGE.EQ.2) THEN
           CORANGE=1.
           COCONSTANT=100.
      ENDIF
      IF(ICORANGE.EQ.3) THEN
           CORANGE=10.
```

```
        COCONSTANT=100.
    ENDIF
    IF(ICO2RANGE.EQ.1) THEN
        CO2RANGE=2.
        CO2CONSTANT=100.
    ENDIF
    IF(ICO2RANGE.EQ.2) THEN
        CO2RANGE=15.
        CO2CONSTANT=100.
    ENDIF
    IF(ICO2RANGE.EQ.3) THEN
        CO2RANGE=20.
        CO2CONSTANT=100.
    ENDIF
C
C
C ---------------------------------------------------------------------
C
C   INPUT FILE AND CREATE AN ARRAY FOR EACH CHANNEL
C
C
C   I IS THE NUMBER OF DATA POINTS PER CHANNEL
    I=1
    OPEN(5,FILE=FNAME)
    IF (IRUNNUMBER.GE.137) THEN
 10     READ(5,*,END=20) TIME(I)
        READ(5,*) DRYCO(I)
        READ(5,*) DRYCO2(I)
        READ(5,*) DRYO2(I)
        READ(5,*) FUEL(I)
        READ(5,*) AIRVEL(I)
        READ(5,*) FID(I)
        READ(5,*) SMOKE0(I)
        READ(5,*) SMOKE1(I)
        READ(5,*) TC(1,I)
        READ(5,*) TC(2,I)
        READ(5,*) TC(3,I)
        READ(5,*) TC(4,I)
        READ(5,*) TC(5,I)
        READ(5,*) TC(6,I)
        READ(5,*) TC(7,I)
        READ(5,*) TC(8,I)
        READ(5,*) TC(9,I)
        READ(5,*) TC(10,I)
        READ(5,*) TC(11,I)
        READ(5,*) TC(12,I)
        READ(5,*) TC(13,I)
        READ(5,*) TC(14,I)
        I=I+1
        GOTO 10
 20     I=I-1
```

```
  ELSE IF(IRUNNUMBER.LT.137) THEN
   IF(IRUNNUMBER.GE.106.AND.IRUNNUMBER.LE.113)THEN
12              READ(5,*,END=23) TIME(I)
                        READ(5,*) DRYCO(I)
                        READ(5,*) DRYCO2(I)
                        READ(5,*) DRYO2(I)
                        READ(5,*) FUEL(I)
                        READ(5,*) AIRVEL(I)
                        READ(5,*) DUMPRESS
                        READ(5,*) TCJ1
                        READ(5,*) TCJ2
                        READ(5,*) TCJ3
                        READ(5,*) TCJ4
                        READ(5,*) TCJ5
                        READ(5,*) TCJ6
                        READ(5,*) TCJ7
                        READ(5,*) TCJ8
                        READ(5,*) TCJ9
                        READ(5,*) TCJ10
                        READ(5,*) TCJ11
                        READ(5,*) TCJ12

          IF(IRUNNUMBER.EQ.106.OR.IRUNNUMBER.EQ.107)THEN
                        TC(1,J)=TCJ2
                        TC(2,J)=TCJ3
                        TC(3,J)=TCJ4
                        TC(4,J)=TCJ5
                        TC(5,J)=TCJ6
                        TC(6,J)=TCJ7
                        TC(7,J)=TCJ8
                        TC(8,J)=TCJ9
                        TC(9,J)=TCJ10
                        TC(10,J)=0.
                        TC(11,J)=TCJ11
                        TC(12,J)=TCJ12
          ENDIF

          IF(IRUNNUMBER.EQ.108.OR.IRUNNUMBER.EQ.109)THEN
                        TC(1,J)=TCJ3
                        TC(2,J)=TCJ4
                        TC(3,J)=TCJ2
                        TC(4,J)=TCJ5
                        TC(5,J)=TCJ6
                        TC(6,J)=TCJ7
                        TC(7,J)=TCJ8
                        TC(8,J)=TCJ9
                        TC(9,J)=TCJ10
                        TC(10,J)=0.0
                        TC(11,J)=TCJ12
                        TC(12,J)=TCJ11
          ENDIF
```

```
            IF(IRUNNUMBER.GE.110.AND.IRUNNUMBER.LE.113)THEN
                        TC(1,J)=TCJ2
                        TC(2,J)=TCJ3
                        TC(3,J)=TCJ4
                        TC(4,J)=TCJ5
                        TC(5,J)=TCJ6
                        TC(6,J)=TCJ7
                        TC(7,J)=TCJ8
                        TC(8,J)=TCJ9
                        TC(9,J)=TCJ10
                        TC(10,J)=0.0
                        TC(11,J)=TCJ12
                        TC(12,J)=TCJ11
            ENDIF

                        I=I+1
                        GOTO 12
 23             I=I-1
    ELSE

 11             READ(5,*,END=21) TIME(I)
                        READ(5,*) DRYCO(I)
                        READ(5,*) DRYCO2(I)
                        READ(5,*) DRYO2(I)
                        READ(5,*) FUEL(I)
                        READ(5,*) AIRVEL(I)
                        READ(5,*) DUMPRESS
                        READ(5,*) TC(1,I)
                        READ(5,*) TC(2,I)
                        READ(5,*) TC(3,I)
                        READ(5,*) TC(4,I)
                        READ(5,*) TC(5,I)
                        READ(5,*) TC(6,I)
                        READ(5,*) TC(7,I)
                        READ(5,*) TC(8,I)
                        READ(5,*) TC(9,I)
                        READ(5,*) TC(10,I)
                        READ(5,*) TC(11,I)
                        READ(5,*) TC(12,I)
                        I=I+1
                        GOTO 11
 21             I=I-1
    ENDIF
   ENDIF
   CLOSE (5)

C
C ---------------------------------------------------------------------
C
```

```
C    DATA MANIPULATION FOR EACH CHANNEL  LOOP J=1 to I
C
C
     PTSPAST=NINT(TIMEPAST/1.97)
C
     K=PTSTART
     DO 30 J=1,I



     TC(1,J)=TC(1,J)+273.15
     TC(2,J)=TC(2,J)+273.15
     TC(3,J)=TC(3,J)+273.15
     TC(4,J)=TC(4,J)+273.15
     TC(5,J)=TC(5,J)+273.15
     TC(6,J)=TC(6,J)+273.15
     TC(7,J)=TC(7,J)+273.15
     TC(8,J)=TC(8,J)+273.15
     TC(9,J)=TC(9,J)+273.15
     TC(10,J)=TC(10,J)+273.15
     TC(11,J)=TC(11,J)+273.15
     TC(12,J)=TC(12,J)+273.15
     TC(13,J)=TC(13,J)+273.15
     TC(14,J)=TC(14,J)+273.15

C
C    CO ANALZER
C
          IF(DRYCO(K).LT.0.0)THEN
           DRYCO(K)=0.0
          ENDIF
          DRYCO(J)=(DRYCO(K)/5.0)*CORANGE/COCONSTANT
C
C    CO2 ANALZER
C
          DRYCO2(K)=DRYCO2(K)
          IF(DRYCO2(K).LT.0.0)THEN
           DRYCO2(K)=0.0
          ENDIF
          DRYCO2(J)=(DRYCO2(K)/5.0)*CO2RANGE/CO2CONSTANT
C
C    O2 ANALZER
C
          O2=DRYO2(K)
          IF(DRYO2(K).LT.0.0)THEN
           DRYO2(K)=0.0
          ENDIF
          IF(IRUNNUMBER.LE.52.OR.IRUNNUMBER.EQ.211)THEN
           O2RANGE=0.5
          ELSE
           O2RANGE=22.0
```

```
          ENDIF
          DRYO2(J)=(DRYO2(K)/5.08)*O2RANGE/O2CONSTANT
C
C    FUEL WEIGHT (kg)
C
          FUEL(J)=(FUEL(J)-1.0)*10.0/4.0
          RAWFUEL(J) = FUEL(J)
C
C    INLET AIR VELOCITY (m/s)
C
          IF (IRUNNUMBER.GE.86.AND.IRUNNUMBER.LE.113) THEN
           AIRVEL(J)=(AIRVEL(J)/5.0)*5.1*TAMB/PA
          ELSE
           AIRVEL(J)=(AIRVEL(J)/5.0)*5.1*TC(12,J)/PA
          END IF
C
C
C    ADJUST THC MEASUREMENTS FOR THE ANALYZER DELAY TIME
C
C
     IF (IPROBE.EQ.1) THEN
          FID(J)=FID(K-3)
     ELSE
          FID(J)=FID(K)
     ENDIF
     IF (IRUNNUMBER.GE.220.AND.IRUNNUMBER.LE.223) THEN
      FID(J)=FID(K+2)
     ENDIF
C
C
     K=K+1
  30 CONTINUE
C
C    ELIMINATE INCORRECT FUEL DATA POINTS
C
     DO 65 J=2,I
          IF(FUEL(J+1).GT.FUEL(J)) THEN
           FUEL(J)=(FUEL(J-1)+FUEL(J+1))/2.0
           GOTO 65
          ENDIF
  65 CONTINUE
C
C ---------------------------------------------------------------------
C    CALCULATE FUEL BURN RATE (kg/sec)
C
     DO 90 J=8,(I-PTSPAST-5)
          FUELRATE(J)=(FUEL(J-5)-FUEL(J+5))/(TIME(J+5)-TIME(J-5))
  90 CONTINUE
C

     DO 95 J=1,7
```

```
        FUELRATE(J)=FUELRATE(8)
  95 CONTINUE
C
    DO 97 J=(I-PTSPAST-4),(I-PTSPAST-2)
        FUELRATE(J)=(FUEL(J-2)-FUEL(J+2))/(TIME(J+2)-TIME(J-2))
  97 CONTINUE
C
    DELTIME=TIME(I-PTSPAST)-TIME(I-PTSPAST-2)
    FUELRATE(I-PTSPAST-1)=(FUEL(I-PTSPAST-2)-FUEL(I-PTSPAST))/DELTIME
    DELTIME2=TIME(I-PTSPAST)-TIME(I-PTSPAST-1)
    FUELRATE(I-PTSPAST)=(FUEL(I-PTSPAST-1)-FUEL(I-PTSPAST))/DELTIME2
    DO 100 J=(I-PTSPAST+1),I
        FUELRATE(J)=0.0
  100 CONTINUE
    IF (IRUNNUMBER .GE. 137) THEN
        SRATIO = 0.0
        DO 110 J=1,5
          SRATIO = SRATIO + SMOKE1(J)
  110   CONTINUE
        SRATIO = SRATIO/5.
    END IF
C
C
C ---------------------------------------------------------------------
C    CREATE OUTPUT FILES

    DO 140 J=1,5
        FNAME(7:7) = CHAR(64+J)
      OPEN(UNIT=J, FILE = FNAME, STATUS='NEW')
  140 CONTINUE

    DIV    = 0.0
    TIMEFLAG = 2
    SMKMAX = 0.0

    DO 150  K=1,I

    IF (AVGFLAG .EQ. 1) THEN
        IF (TIME(K) .GE. START-1. .AND. TIME(K) .LE. END+1.) THEN
          TIMEFLAG = 1
        ELSE
          TIMEFLAG = 2
        END IF
    END IF
C
C    CALCULATE HEAT RELEASE RATE (kW)
C
        Q(K) = FUELRATE(K)*DELHC
C
C---------------------------------------------------------------------
C    CALCULATE AIR FLOWRATE (kg/sec)
```

```
C                AND RESIDENCE TIME (sec)
C
      IF (IRUNNUMBER.GE.86.AND.IRUNNUMBER.LE.113) THEN
            DENSITY=(PA/TAMB/0.287)*0.1333
       ELSE
            DENSITY=(PA/TC(12,K)/0.287)*0.1333
      END IF
      IF (AIRVEL(K).LE. 0.0) THEN
       RESTIME(K) = 999.
      ELSE
       IF (IRUNNUMBER.GE.86.AND.IRUNNUMBER.LE.105) THEN
         RESTIME(K) = VOLC/(AIRVEL(K)*AREA*TEMPUL/TAMB)
        ELSE
         RESTIME(K) = VOLC/(AIRVEL(K)*AREA*TC(3,K)/TC(12,K))
       ENDIF
       IF (IRUNNUMBER.GE.106.AND.IRUNNUMBER.LE.113) THEN
         RESTIME(K) = VOLC/(AIRVEL(K)*AREA*TC(3,K)/TAMB)
       ENDIF
      ENDIF

      AIRVOLRATE=AIRVEL(K)*AREA
      CORRAIRVOLRATE=0.0123508+AIRVOLRATE*0.939457
      AIRRATE(K)=CORRAIRVOLRATE*DENSITY
C     AIRRATE(K)=AIRVEL(K)*DENSITY*AREA
C
C   CALCULATE FUEL/AIR RATIO
C
      IF (AIRVEL(K).LE. 0.0) THEN
       FTOA(K) = 0.0
      ELSE
       FTOA(K)=FUELRATE(K)/AIRRATE(K)
      ENDIF
C
C
C ---------------------------------------------------------------------
C
C   VOLUMETRIC FLOWRATE (m^3/s) IN EXHAUST DUCT
C
       EXMOLES = (AIRRATE(K)+FUELRATE(K))/28.97
       DUCTFLOW = 1.95147*0.62*DSQRT(PRESS*TC(10,K)/PA)
       TOTDUCTMOLES = DUCTFLOW*PA*0.1333/28.97/.287/TC(10,K)

C   CALCULATE WET CONCENTRATIONS and YIELDS

       IF (IPROBE.EQ.1) THEN
       IF (IFUELTYPE.EQ.1) THEN
        DENOM=1.0+(1.167*DRYCO2(K))
        IF(IRUNNUMBER.EQ.55.OR.IRUNNUMBER.EQ.59)THEN
         DENOM=1.0+(1.167*0.10)
        ENDIF
        IF(IRUNNUMBER.EQ.55.OR.IRUNNUMBER.EQ.55)THEN
```

```
            DENOM=1.0+(1.167*0.10)
           ENDIF
           IF(IRUNNUMBER.EQ.65)THEN
            DENOM=1.0+(1.167*0.085)
           ENDIF
          ELSE IF (IFUELTYPE.EQ.2) THEN
           DENOM=1.0+(0.8*DRYCO2(K))
           IF(IRUNNUMBER.GE.106.AND.IRUNNUMBER.LE.114)THEN
            DENOM=1.11111
           ENDIF
          ELSE IF (IFUELTYPE.EQ.3) THEN
           DENOM =1.0+(1.792*DRYCO2(K))
          ELSE
           DENOM = 1.0+((0.87)*DRYCO2(K))
          ENDIF

          WETCO=DRYCO(K)/DENOM
          WETCO2=DRYCO2(K)/DENOM
          WETO2=DRYO2(K)/DENOM

         ELSE

          WETCO=DRYCO(K)
          WETCO2=DRYCO2(K)
          WETO2=DRYO2(K)
         ENDIF

         IF(FUELRATE(K).EQ.0) THEN
          COYIELD=0
          CO2YIELD=0
          O2YIELD=0
         ELSE
          IF (IPROBE.EQ.1) THEN
C         upper layer-sampled
    COYIELD=WETCO*EXMOLES*28./FUELRATE(K)
    CO2YIELD=WETCO2*EXMOLES*44./FUELRATE(K)
    O2YIELD=((.21*AIRRATE(K)*32./28.97)-(WETO2*EXMOLES*32.))
   $       /FUELRATE(K)

          ELSE
C         downstream-sampled
         COYIELD=(WETCO*(TOTDUCTMOLES)*(28.))/FUELRATE(K)
         CO2YIELD=((WETCO2-.00035)*(TOTDUCTMOLES)*(44.))/FUELRATE(K)
         O2YIELD=0.0
          ENDIF
         ENDIF

    IF (CO2YIELD .GT. 100) THEN
          CO2YIELD = 999.
    END IF
    IF (COYIELD .GT. 100) THEN
```

```
          COYIELD = 999.
      END IF
      IF (O2YIELD .GT. 100) THEN
          O2YIELD = 999.
      END IF

C-----------------------------------------------------------------------
C
C   CALCULATE SMOKE VOLUME FRACTION  for runs 137 on
C    smoke vol fraction is in ppb
C
          IF (IRUNNUMBER.GE.137) THEN

            IF(SMOKE1(K).EQ.0.)THEN
             EXTCOEFF= 999.
             SMOKEVF = 999.
            ELSE
             EXTCOEFF = 2.18723*DLOG(SRATIO/SMOKE1(K))
             SMOKEVF = 1.3697E-07*EXTCOEFF*1.0E+9
             IF(SMOKEVF.LE.0.)THEN
              SMOKEVF = 0.0
             ENDIF
             IF(SMOKEVF.GT.SMKMAX.AND.TIME(K).LE. END+1.)THEN
                    SMKMAX = SMOKEVF
                    IF (FUELRATE(K).NE.0) THEN
                     CINSMOKE = 4282.8*SMKMAX/FUELRATE(K)/1.E+9
                    ENDIF
             ENDIF
C
C
C   CALCULATE SMOKE YIELD ACCORDING TO TEWARSON
C
             IF(FUELRATE(K).EQ.0.)THEN
              SMKYIELD = 999.
             ELSE
              ODL = EXTCOEFF/2.303
              MASSODL = ODL * DUCTFLOW / (FUELRATE(K)*1000.)
              SEC = 3.213/(0.67*1.1)
              CS  = ODL/SEC
              GF  = FUELRATE(K)*1000.
              SMKYIELD = CS * DUCTFLOW/GF
             ENDIF
            ENDIF
          ENDIF

C
C   EQUIVALENCE RATIO FOR HEXANE
C
    IF (IFUELTYPE.EQ.1) THEN
          EQUIVALENCE=FTOA(K)*15.2222
C
```

```
C    EQUIVALENCE RATIO FOR PMMA
C
          ELSE IF (IFUELTYPE.EQ.2) THEN
           EQUIVALENCE=FTOA(K)*8.2824
C
C    EQUIVALENCE RATIO FOR WOOD - ASSUMES 15% CHAR
C
          ELSE IF (IFUELTYPE.EQ.3) THEN
           EQUIVALENCE=FTOA(K)*3.823

C
C    EQUIVALENCE RATIO FOR POLYURETHANE - ASSUMES NO CHAR
C
          ELSE IF (IFUELTYPE.EQ.4)THEN
           EQUIVALENCE=FTOA(K)*8.83

      ENDIF


      IF(EQUIVALENCE .LT.0.0) THEN
           EQUIVALENCE = 0.0
      END IF

C
C-----------------------------------------------------------------
C     CALCULATE DERIVATIVE OF FUEL BURNING RATE
C
      IF (K.LE.7) THEN
           DEL2FUEL(K)=0.0
      ENDIF
      IF (K.GE.I-PTSPAST-4) THEN
           DEL2FUEL(K)=0.0
       ELSE
           DEL2FUEL(K)=(FUELRATE(K+5)-FUELRATE(K-5))/(TIME(J+5)-TIME(J-5))
      ENDIF


C
C-----------------------------------------------------------------
C     STEADY STATE TIME RATIO
C
      IF (FUELRATE(K) .EQ. 0.0) THEN
           FUELRATE(K) = 0.00001
      END IF
      SSTIME=RESTIME(K)*DEL2FUEL(K)/FUELRATE(K)
      IF (ABS(SSTIME) .GT. 10.) THEN
           SSTIME = 10.
      END IF


C-----------------------------------------------------------------
```

```
C  CALCULATE UNBURNED HYDROCARBONS (mole fraction) and YIELD

    IF (IRUNNUMBER.LT.203) THEN
          THC=0.0
          THCYIELD=0.0
          GOTO 13
    ENDIF
    IF (IRUNNUMBER.GE.203) THEN
     IF(FID(K).EQ.0.0)THEN
          THC=0.0
          THCYIELD=0.0
          GOTO 13
     ENDIF
     THC=(FIDSPAN/(FIDCAL-FIDZERO))*((FID(K)*1000.*FIDRANGE)-FIDZERO)/
    $         1000000.0

     THCYIELD=(THC*(AIRRATE(K)+FUELRATE(K))*(28.05/28.97))/FUELRATE(K)
    ENDIF

C-----------------------------------------------------------------
C  CARBON BALANCE CHECK
C
C
  13      IF(FUELRATE(K).EQ.0) THEN
           CERROR=999.
           GOTO 9
          ENDIF
C
C    MOLES OF CARBON ORIGINATING FROM FUEL
C
C     for Hexane
          IF (IFUELTYPE.EQ.1) THEN
           CMOLIN=6.0*FUELRATE(K)/86.0
C     for PMMA
          ELSE IF (IFUELTYPE .EQ. 2) THEN
           CMOLIN=5.0*FUELRATE(K)/100.0
C     for Wood
          ELSE IF (IFUELTYPE .EQ. 3) THEN
           CMOLIN=FUELRATE(K)/40.428
C     for Polyurethane
          ELSE
           CMOLIN=FUELRATE(K)/19.91
          ENDIF
          IF(CMOLIN.EQ.0.)THEN
           CERROR=999
           GOTO 9
          ENDIF

C    MOLES ACCOUNTED FOR BY MEASUREMENTS
C         if compartment sampled
          IF (IPROBE .EQ. 1) THEN
```

```
          CMOLOUT=(WETCO + WETCO2 + 2.*THC)*EXMOLES
        ELSE
C       if exhaust sampled
          CMOLOUT =(WETCO + WETCO2-0.00035 + 2.*THC)*TOTDUCTMOLES
        END IF
        CERROR=(CMOLOUT-CMOLIN)*100.0/CMOLIN
        IF (ABS(CERROR) .GT. 999) THEN
          CERROR = 999
        END IF
  9 CONTINUE

C-----------------------------------------------------------------
C  IGNITION INDEX CALCULATION for Hexane fires
C
        IF (IPROBE .EQ. 1) THEN
         WETH2O = 1.167*WETCO2
         H2OMOLES = WETH2O*EXMOLES
         COMOLES = WETCO*EXMOLES
         CO2MOLES = WETCO2*EXMOLES
         O2MOLES = WETO2*EXMOLES

         IF(IRUNNUMBER.GE.203)THEN
           THCMOLES = THC*EXMOLES
         ELSE
          IF(EQUIVALENCE.LE.1.)THEN
            THCMOLES = 0.
            THC = 0.0
          ELSE
            THCMOLES = 3.0*FUELRATE(K)*(1.-(1./EQUIVALENCE))/86.
            THC = THCMOLES/EXMOLES
          ENDIF
         ENDIF

         H2MOLES = 0.5 * COMOLES
         WETH2 = H2MOLES/EXMOLES
         N2MOLES = EXMOLES-(COMOLES+CO2MOLES+O2MOLES+H2OMOLES+THCMOLES
     $                    +H2MOLES)
           WETN2 = N2MOLES/EXMOLES

         ALPHA = 0.5*(WETCO+WETH2)+3.*THC-WETO2
         NTOTST = 1.+ALPHA*4.76
         XCOST = WETCO/NTOTST
         XH2ST = WETH2/NTOTST
         XTHCST = THC/NTOTST
         NP = (WETCO+WETCO2+4.*THC+WETH2O+WETH2+WETN2+ALPHA*3.76)/NTOTST
         NPCP =( (WETCO+WETCO2+2.*THC)*54.3+(2.*THC+WETH2O+WETH2)*
     $        41.2+(WETN2+ALPHA*3.76)*32.7)*NP/NTOTST

         IF (IRUNNUMBER.GE.86.AND.IRUNNUMBER.LE.105) THEN
          T0 = (TEMPUL+ALPHA*4.76*320.)/NTOTST
         ELSE
```

```
          TEMPUL = (TC(1,K)+TC(2,K)+TC(3,K)+TC(4,K))/4.
          T0 = (TEMPUL+ALPHA*4.76*320.)/NTOTST
         ENDIF

         IGNITION = XCOST*283000/NPCP/(1450-T0) +
     $              XTHCST*1411000/NPCP/(1700-T0) +
     $              XH2ST*242000/NPCP/(1080-T0)
        ELSE
         IGNITION = 0.0
        ENDIF


C-----------------------------------------------------------------------
C  STORE DATA

    WRITE(1,1000)TIME(K),WETCO,WETCO2,WETO2,COYIELD,CO2YIELD,O2YIELD,
   $EQUIVALENCE,SMKYIELD,THCYIELD
    WRITE(2,1100)TIME(K),FUEL(K),FUELRATE(K),AIRVEL(K),AIRRATE(K),
   $DEL2FUEL(K),CERROR,Q(K)
    WRITE(3,1200)TIME(K),TC(1,K),TC(2,K),TC(3,K),TC(4,K),TC(5,K),
   $      TC(6,K),TC(7,K),TC(8,K),TC(9,K),TC(10,K),TC(11,K),TC(12,K)
    WRITE(4,1300)TIME(K),RESTIME(K),SSTIME,
   $DRYCO(K),DRYCO2(K),DRYO2(K),TC(13,K),TC(14,K),THC,SMOKEVF,
   $TOTDUCTMOLES/EXMOLES
    WRITE(5,1400)TIME(K),SMOKE0(K),SMOKE1(K),EXTCOEFF,WETH2O,WETH2,
   $          IGNITION


 1000 FORMAT(F7.1,3E9.3,F6.4,2F9.4,F7.3,F8.3,F6.4)
 1100 FORMAT(F7.1,F9.3,F9.4,F9.2,F9.3,F8.5,F10.2,F9.2)
 1200 FORMAT(F7.1,12F6.0)
 1300 FORMAT(F7.1,F5.1,F6.2,3E9.3,2F6.0,F9.6,F7.2,F5.1)
 1400 FORMAT(F7.1,6F10.3)
  150 CONTINUE

    CLOSE (1)
    CLOSE (2)
    CLOSE (3)
    CLOSE (4)
    CLOSE (5)

    WRITE(*,*)'DATA MANIPULATION COMPLETED'
    END
```

APPENDIX C

Reaction Mechanism

The reaction mechanism used for the chemical kinetics study presented in Chapter 4 is shown below. The mechanism is a subset of the one used by Miller and Bowman [37], and reactions are numbered according to this reference.

Reaction Mechanism Rate Coefficients

$k_f = AT^{\beta}\exp(-E/RT)$

Units: moles, cm3, s, K, cal/mole

	Reaction	A	β	E
1.	$2CH_3 + M = C_2H_6 + M$ H_2/2.0/ CO/2.0/ CO_2/3.0/ H_2O/5.0/	9.03E+16	-1.180	654.
2.	$CH_3 + H + M = CH_4 + M$ H_2/2.0/ CO/2.0/ CO_2/3.0/ H_2O/5.0/	6.00E+16	-1.000	0.
3.	$CH_4 + O2 = CH_3 + HO_2$	7.90E+13	0.000	56000.
4.	$CH_4 + H = CH_3 + H_2$	2.20E+04	3.000	8750.
5.	$CH_4 + OH = CH_3 + H_2O$	1.60E+06	2.100	2460.
5a.	$CH_4 + O = CH_3 + OH$	1.02E+09	1.500	8604.
6.	$CH_4 + HO_2 = CH_3 + H_2O_2$	1.80E+11	0.000	18700.
7.	$CH_3 + HO_2 = CH_3O + OH$	2.00E+13	0.000	0.
8.	$CH_3 + O_2 = CH_3O + O$	2.05E+19	-1.570	29229.
9.	$CH_3 + O = CH_2O + H$	8.00E+13	0.000	0.
10.	$CH_2OH + H = CH_3 + OH$	1.00E+14	0.000	0.
11.	$CH_3O + H = CH_3 + OH$	1.00E+14	0.000	0.
12.	$CH_3 + OH = CH_2 + H2O$	7.50E+06	2.000	5000.
13.	$CH_3 + H = CH_2 + H_2$	9.00E+13	0.000	15100.
14.	$CH_3O + M = CH_2O + H + M$	1.00E+14	0.000	25000.
15.	$CH_2OH + M = CH_2O + H + M$	1.00E+14	0.000	25000.
16.	$CH_3O + H = CH_2O + H_2$	2.00E+13	0.000	0.
17.	$CH_2OH + H = CH_2O + H_2$	2.00E+13	0.000	0.
18.	$CH_3O + OH = CH_2O + H_2O$	1.00E+13	0.000	0.
19.	$CH_2OH + OH = CH_2O + H_2O$	1.00E+13	0.000	0.
20.	$CH_3O + O = CH_2O + OH$	1.00E+13	0.000	0.
21.	$CH_2OH + O = CH_2O + OH$	1.00E+13	0.000	0.
22.	$CH_3O + O_2 = CH_2O + HO_2$	6.30E+10	0.000	2600.
23.	$CH_2OH + O_2 = CH_2O + HO_2$	1.48E+13	0.000	1500.
24.	$CH_2 + H = CH + H_2$	1.00E+18	-1.560	0.
25.	$CH_2 + OH = CH + H_2O$	1.13E+07	2.000	3000.
26.	$CH_2 + OH = CH_2O + H$	2.50E+13	0.000	0.
27.	$CH + O_2 = HCO + O$	3.30E+13	0.000	0.
28.	$CH + O = CO + H$	5.70E+13	0.000	0.
29.	$CH + OH = HCO + H$	3.00E+13	0.000	0.
30.	$CH + CO_2 = HCO + CO$	3.40E+12	0.000	690.
31.	$CH + H = C + H_2$	1.50E+14	0.000	0.
32.	$CH + H_2O = CH_2O + H$	1.17E+15	-0.750	0.
33.	$CH + CH_2O = CH_2CO + H$	9.46E+13	0.000	-515.
34.	$CH + C_2H_2 = C_3H_2 + H$	1.00E+14	0.000	0.
35.	$CH + CH_2 = C_2H_2 + H$	4.00E+13	0.000	0.
36.	$CH + CH_3 = C_2H_3 + H$	3.00E+13	0.000	0.
37.	$CH + CH_4 = C_2H_4 + H$	6.00E+13	0.000	0.
38.	$C + O_2 = CO + O$	2.00E+13	0.000	0.
39.	$C + OH = CO + H$	5.00E+13	0.000	0.
40.	$C + CH_3 = C_2H_2 + H$	5.00E+13	0.000	0.
41.	$C + CH_2 = C_2H + H$	5.00E+13	0.000	0.
42.	$CH_2 + CO_2 = CH_2O + CO$	1.10E+11	0.000	1000.

43.	$CH_2 + O = CO + {}_2H$	5.00E+13	0.000	0.
44.	$CH_2 + O = CO + H_2$	3.00E+13	0.000	0.
45.	$CH_2 + O_2 = CO_2 + 2H$	1.60E+12	0.000	1000.
46.	$CH_2 + O_2 = CH_2O + O$	5.00E+13	0.000	9000.
47.	$CH_2 + O_2 = CO_2 + H_2$	6.90E+11	0.000	500.
48.	$CH_2 + O_2 = CO + H_2O$	1.90E+10	0.000	-1000.
49.	$CH_2 + O_2 = CO + OH + H$	8.60E+10	0.000	-500.
50.	$CH_2 + O_2 = HCO + OH$	4.30E+10	0.000	-500.
51.	$CH_2O + OH = HCO + H_2O$	3.43E+09	1.180	-447.
52.	$CH_2O + H = HCO + H_2$	2.19E+08	1.770	3000.
53.	$CH_2O + M = HCO + H + M$	3.31E + 16	0.000	81000.
54.	$CH_2O + O = HCO + OH$	1.80E+13	0.000	3080.
55.	$HCO + OH = H_2O + CO$	1.00E+14	0.000	0.
56.	$HCO + M = H + CO + M$	2.50E+14	0.000	16802.
	$O/1.9/\ H_2/1.9/\ CH_4/2.8/\ CO_2/3.0/\ H_2O/5.0/$			
57.	$HCO + H = CO + H_2$	1.19E+13	0.250	0.
58.	$HCO + O = CO + OH$	3.00E+13	0.000	0.
59.	$HCO + O = CO_2 + H$	3.00E+13	0.000	0.
60.	$HCO + O_2 = HO_2 + CO$	3.30E+13	-0.400	0.
61.	$CO + O + M = CO_2 + M$	6.17E+14	0.000	3000.
62.	$CO + OH = CO_2 + H$	1.51E+07	1.300	-758.
63.	$CO + O_2 = CO_2 + O$	1.60E+13	0.000	41000.
64.	$HO_2 + CO = CO_2 + OH$	5.80E+13	0.000	22934.
65.	$C_2H_6 + CH_3 = C_2H_5 + CH_4$	5.50E-01	4.000	8300.
66.	$C_2H_6 + H = C_2H_5 + H_2$	5.40E+02	3.500	5210.
67.	$C_2H_6 + O = C_2H_5 + OH$	3.00E+07	2.000	5115.
68.	$C_2H_6 + OH = C_2H_5 + H_2O$	8.70E+09	1.050	1810.
69.	$C_2H_4 + H = C_2H_3 + H_2$	1.10E+14	0.000	8500.
70.	$C_2H_4 + O = CH_3 + HCO$	1.60E+09	1.200	746.
71.	$C_2H_4 + OH = C_2H_3 + H_2O$	2.02E+13	0.000	5955.
72.	$CH_2 + CH_3 = C_2H_4 + H$	3.00E+13	0.000	0.
73.	$H + C_2H_4 + M = C_2H_5 + M$	2.21E+13	0.000	2066.
	$H_2/2.0/\ CO/2.0/\ CO_2/3.0/\ H_2O/5.0/$			
74.	$C_2H_5 + H = {}_2CH_3$	1.00E+14	0.000	0.
75.	$C_2H_5 + O2 = C_2H_4 + HO_2$	8.43E+11	0.000	3875.
76.	$C_2H_2{+}O = CH_2 + CO$	1.02E+07	2.000	1900.
77.	$C_2H_2 + O = HCCO + H$	1.02E+07	2.000	1900.
78.	$H_2 + C_2H = C_2H_2 + H$	4.09E+05	2.390	864.
79.	$H + C_2H_2 + M = C_2H_3 + M$	5.54E+12	0.000	2410.
	$H_2/2.0/\ CO/2.0/\ CO_2/3.0/\ H_2O/5.0/$			
80.	$C_2H_3 + H = C_2H_2 + H_2$	4.00E+13	0.000	0.
81.	$C_2H_3 + O = CH_2CO + H$	3.00E+13	0.000	0.
82.	$C_2H_3 + O_2 = CH_2O + HCO$	4.00E+12	0.000	-250.
83.	$C_2H_3 + OH = C_2H_2 + H_2O$	5.00E+12	0.000	0.
84.	$C_2H_3 + CH_2 = C_2H_2 + CH_3$	3.00E+13	0.000	0.
85.	$C_2H_3 + C_2H = 2C_2H_2$	3.00E+13	0.000	0.
86.	$C_2H_3 + CH = CH_2 + C_2H_2$	5.00E+13	0.000	0.
87.	$OH + C_2H_2 = C_2H + H_2O$	3.37E+07	2.000	14000.
88.	$OH + C_2H_2 = HCCOH + H$	5.04E+05	2.300	13500.
89.	$OH + C_2H_2 = CH_2CO + H$	0.218E-03	4.500	-1000.
90.	$OH + C_2H_2 = CH_3 + CO$	0.483E-03	4.000	-2000.
91.	$HCCOH + H = CH_2CO + H$	1.000E+13	0.000	0.
92.	$C_2H_2 + O = C_2H + OH$	3.16E+15	-0.600	15000.
93.	$CH_2CO + H = CH_3 + CO$	1.13E+13	0.000	3428.
94.	$CH_2CO + O = CO_2 + CH_2$	1.75E+12	0.000	1350.

95.	$CH_2CO + H = HCCO + H_2$	5.00E+13	0.000	8000.
96.	$CH_2CO + O = HCCO + OH$	1.00E+13	0.000	8000.
97.	$CH_2CO + OH = HCCO + H_2O$	7.50E+12	0.000	2000.
98.	$CH_2CO + M = CH_2 + CO + M$	3.00E+14	0.000	70980.
99.	$C_2H + O_2 = 2CO + H$	5.00E+13	0.000	1500.
100.	$C_2H + C_2H_2 = C_4H_2 + H$	0.300E+14	0.000	0.
101.	$H + HCCO = CH_2 + CO$	1.00E+14	0.000	0.
102.	$O + HCCO = H + 2CO$	1.00E+14	0.000	0.
103.	$HCCO + O_2 = 2CO + OH$	1.60E+12	0.000	854.
104.	$CH + HCCO = C_2H_2 + CO$	5.00E+13	0.000	0.
105.	$2HCCO = C_2H_2 + 2CO$	1.00E+13	0.000	0.
106.	$CH_2 + M = CH_2 + M$	1.00E+13	0.000	0.
107.	$CH_2 + CH_4 = 2CH_3$	4.00E+13	0.000	0.
108.	$CH_2 + C_2H_6 = CH_3 + C_2H_5$	1.20E+14	0.000	0.
109.	$CH_2 + O2 = CO + OH + H$	3.00E+13	0.000	0.
110.	$CH_2 + H_2 = CH_3 + H$	7.00E+13	0.000	0.
111.	$CH_2 + H = CH_2 + H$	2.00E+14	0.000	0.
112.	$C_2H + O = CH + CO$	5.00E+13	0.000	0.
113.	$C_2H + OH = HCCO + H$	2.00E+13	0.000	0.
114.	$2CH_2 = C_2H_2 + H_2$	4.00E+13	0.000	0.
115.	$CH_2 + HCCO = C_2H_3 + CO$	3.00E+13	0.000	0.
116.	$CH_2 + C_2H_2 = C_3H_3 + H$	0.120E+14	0.000	6600.
117.	$C_4H_2 + OH = C_3H_2 + HCO$	0.666E+13	0.000	-410.
118.	$C_3H_2 + O_2 = HCO + HCCO$	0.100E+14	0.000	0.
119.	$C_3H_3 + O_2 = CH_2CO + HCO$	0.300E+11	0.000	2868.
120.	$C_3H_3 + O = CH_2O + C_2H$	0.200E+14	0.000	0.
121.	$C_3H_3 + OH = C_3H_2 + H_2O$	0.200E+14	0.000	0.
122.	$C_2H_2 + C_2H_2 = C_4H_3 + H$	0.200E+13	0.000	45900.
123.	$C_4H_3 + M = C_4H_2 + H + M$	0.100E+17	0.000	59700.
124.	$CH_2 + C_2H_2 = C_3H_3 + H$	3.000E+13	0.000	0.
125.	$C_4H_2 + O = C_3H_2 + CO$	1.200E+12	0.000	0.
126.	$C_2H_2 + O_2 = HCCO + OH$	2.00E+08	1.500	30100.
127.	$C_2H_2 + M = C_2H + H + M$	4.20E+16	0.000	107000.
128.	$C_2H_4 + M = C_2H_2 + H_2 + M$	1.50E+15	0.000	55800.
129.	$C_2H_4 + M = C_2H_3 + H + M$	1.40E+16	0.000	82360.
130.	$H_2 + O_2 = 2OH$	1.70E+13	0.000	47780.
131.	$OH + H_2 = H_2O + H$	1.17E+09	1.300	3626.
132.	$O + OH = O_2 + H$	4.00E+14	-0.500	0.
133.	$O + H_2 = OH + H$	5.06E+04	2.670	6290.
134.	$H + O_2 + M = HO_2 + M$	3.61E+17	-0.720	0.
	H_2O/18.6/ CO_2/4.2/ H_2/2.9/ CO/2.1/ N_2/1.3/			
135.	$OH + HO_2 = H_2O + O_2$	7.50E+12	0.000	0.
136.	$H + HO_2 = 2OH$	1.40E+14	0.000	1073.
137.	$O + HO_2 = O_2 + OH$	1.40E+13	0.000	1073.
138.	$2OH = O + H_2O$	6.00E+08	1.300	0.
139.	$2H + M = H_2 + M$	1.00E+18	-1.000	0.
140.	$2H + H_2 = 2H_2$	9.20E+16	-0.600	0.
141.	$2H + H_2O = H_2 + H_2O$	6.00E+19	-1.250	0.
142.	$2H + CO_2 = H_2 + CO_2$	5.49E+20	-2.000	0.
143.	$H + OH + M = H_2O + M$	1.60E+22	-2.000	0.
	H_2O/5.0/			
144.	$H + O + M = OH + M$	6.20E+16	-0.600	0.
	H_2O/5.0/			
145.	$2O + M = O_2 + M$	1.89E+13	0.000	-1788.
146.	$H + HO_2 = H_2 + O_2$	1.25E+13	0.000	0.

147.	$2HO_2 = H_2O_2 + O_2$	2.00E+12	0.000	0.
148.	$H_2O_2 + M = 2OH + M$	1.30E+17	0.000	45500.
149.	$H_2O_2 + H = HO_2 + H_2$	1.60E+12	0.000	3800.
150.	$H_2O_2 + OH = H_2O + HO_2$	1.00E+13	0.000	1800.
232.	$N + NO = N_2 + O$	0.327E+13	0.300	0.
233.	$N + O_2 = NO + O$	0.640E+10	1.000	6280.
234.	$N + OH = NO + H$	0.380E+14	0.000	0.
235.	$H + O_2 + O_2 = HO_2 + O_2$	0.670E+20	-1.420	0.0

VITA

Daniel T. Gottuk was born on April 20, 1967 in Redbank, New Jersey. He graduated from Rumson-Fair Haven Regional High School in 1985 and moved South to attend Virginia Polytechnic Institute and State University. Dan graduated Magna Cum Laude in 1989 with a B.S. in Mechanical Engineering. The same year he married Ruth E. Cooper.

As an undergraduate Dan worked on a flame diagnostic graduate research project, which sparked his interest in combustion. So, in August of 1989, he began his graduate work in the area of fire science at Virginia Polytechnic Institute and State University. Dan graduated with a Ph.D. in Mechanical Engineering in 1992.

After graduation, Dan is moving to Columbia, Maryland to work as a combustion research engineer for Hughes Associates, Inc. He is also eagerly awaiting the arrival of his first child in January 1993.

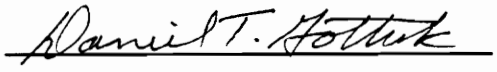

Daniel T. Gottuk